Donor-emitter Fluorophore Pairs in Luminescent Solar Concentrators: from Material Synthesis to Device Fabrication

Bolong Zhang

Submitted in total fulfilment of the requirements of the degree of Doctor of Philosophy

School of Chemistry

University of Melbourne

September 2019

Produced on archival quality paper.

Declaration

This thesis is comprised of the candidate's publications, which are {ACS Energy Lett. 2019, 4, 1839-1844; Chem. Mater. 2019, 31, 8, 3001-3008; Mater. Chem. Front., 2018, 2, 615-619; Chem. Mater. 2017, 29, 19, 8395-8403 and Aggregation-Induced Emitters in Light Harvesting. In: Principles and Applications of Aggregation-Induced Emission. Springer, Cham. 2019}, as sections of Chapters. Co-authors included in the publications have signed agreement forms that certify the following:

- the candidate has contributed more than 50% to the content of the manuscripts including planning, preparation, and execution of the work described in each manuscript
- the candidate is the "primary" or "first" author of the manuscripts
- the manuscripts can be included in the candidate's thesis in its published form without redactions or omissions

These agreement forms are found in the Appendices section of this thesis.

Acknowledgements

I wish to thank my supervisors Dr. Wallace W.H. Wong, Dr. David J. Jones and Prof. Kenneth P. Ghiggino for allowing me to work independently. I appreciate their constructive guidance and critical thinking on my projects. I wish to thank my supervisors for their help in improving my English writing skills.

I thank my thesis advisory committee chair, Prof. Paul Mulvaney for providing constructive feedback and suggestions for my projects and allowing me to do experiments in his lab. I thank Prof. Jonathan M. White for analysis of crystallographic data. I thank Assoc. Prof. Trevor A. Smith, Dr. James A. Hutchison, Dr. Hamid Soleimaninejad, Dr. Christopher R. Hall and Dr. Siobhan J. Bradley for their advice on laser instrumentation and spectroscopy measurements. I thank Dr. Pengjun Zhao and Dr. Jegadesan Subbiah for photovoltaic device fabrication and characterization. I thank Dr. James L. Banal for providing me priceless suggestions and his excellent work on LSCs. I thank my colleagues, Dr. Can Gao, Dr. Nicolau Saker Neto and Mr. Lachlan J. Wilson for their help and contribution to my work. I thank all members from Wong/Jones Lab and UML group.

I thank my parents who support me, mentally and financially, all the way regardless about what I am doing. In the end, I thank my wife, Liying Cai. She is the lighthouse in my life.

List of Publications and Conferences

Several publications were produced during the duration of the PhD candidature. These include peer-reviewed journal articles and a book chapter. The results described in this thesis have also been presented at both local and international conferences. These are listed herein for reference:

Journal Papers

1. Bolong Zhang, Pengjun Zhao, Lachlan J. Wilson, Jegadesan Subbiah, Hanbo Yang, Paul Mulvaney, David J. Jones, Kenneth P. Ghiggino and Wallace W.H. Wong. A High-Performance Large-Area Luminescence Solar Concentrator Incorporating a Donor-Emitter Fluorophore System. ACS Energy Lett. 2019, 4, 1839-1844. DOI: 10.1021/acsenergylett.9b01224

2. Bolong Zhang, Can Gao, Hamid Soleimaninejad, Jonathan M. White, Trevor A. Smith, David J. Jones, Kenneth P. Ghiggino, Wallace W.H. Wong. Highly Efficient Luminescent Solar Concentrators by Selective Alignment of Donor-Emitter Fluorophores. Chem. Mater. 2019, 31, 8, 3001-3008. DOI: 10.1021/acs.chemmater.9b00647

3. Bolong Zhang, James L. Banal, David J. Jones, Ben Zhong Tang, Kenneth P. Ghiggino, Wallace W.H. Wong. Aggregation-induced Emission-mediated Spectral Downconversion in Luminescent Solar Concentrators. Mater. Chem. Front., 2018, 2, 615-619. DOI: 10.1039/C7QM00598A

4. Bolong Zhang, Hamid Soleimaninejad, David J. Jones, Jonathan M. White, Kenneth P. Ghiggino, Trevor A. Smith, Wallace W.H. Wong. Highly Fluorescent Molecularly Insulated Perylene Diimides: Effect of Concentration on Photophysical Properties. Chem. Mater. 2017, 29, 19, 8395-8403. DOI: 10.1021/acs.chemmater.7b02968

5. Can Gao, Jia Yi Seow, Bolong Zhang, Christopher Hall, Andrew J. Tilley, Jonathan M.

White, Trevor A. Smith, Wallace W.H. Wong. Tetraphenylethene 9,10-Diphenylanthracene Derivatives-Synthesis and Photophysical Properties. ChemPlusChem, 2019, 84, 1-9. DOI: 10.1002/cplu.201900100

6. Randy P. Sabatini, Bolong Zhang, Akhil Gupta, Julien Leoni, Wallace W.H. Wong, Girish Lakhwani. Molecularly isolated perylene diimides enable both strong exciton–photon coupling and high photoluminescence quantum yield. J. Mater. Chem. C, 2019, 7, 2954-2960. DOI: 10.1039/C9TC00093C

7. Mark A. Gregory, Bolong Zhang, Andrew J. Tilley, Tamika Scheerlinck, Jonathan M. White, Wallace W.H. Wong. Amine-Substituted Diazocine Derivatives-Synthesis, Structure, and Photophysical Properties. Helv. Chim. Acta., 2018, 11, e1800146. DOI: 10.1002/hlca.201800146

8. Yinan Wang, Hongming Yao, Jian Zhou, Yuning Hong, Bin Chen, Bolong Zhang, Trevor A. Smith, Wallace W.H. Wong, Zujin Zhao. A Water-soluble, AIE-active Polyelectrolyte for Conventional and Fluorescence Lifetime Imaging of Mouse Neuroblastoma Neuro-2A Cells. J. Polym. Sci. A, 2018, 56, 672-680. DOI: 10.1002/pola.28943

9. Jingjing Xu, Bolong Zhang, Marina Jansen, Lars Goerigk, Wallace W.H. Wong, Chris Ritchie. Highly Fluorescent Pyridinium Betaines for Light Harvesting. Angew. Chem. Int. Ed., 2017, 56,13882–13886. DOI: 10.1002/anie.201704832

10. James L. Banal, Bolong Zhang, David J. Jones, Kenneth P. Ghiggino, Wallace W.H. Wong. Emissive Molecular Aggregates and Energy Migration in Luminescent Solar Concentrators. Acc. Chem. Res. 2017, 50, 1, 49-57. DOI: 10.1021/acs.accounts.6b00432

Book Chapter

1. Bolong Zhang, Can Gao, Nicolau Saker Neto, Wallace W.H. Wong. Aggregation-Induced Emitters in Light Harvesting. In: Principles and Applications of Aggregation-Induced Emission.

Springer, Cham. 2019. (book chapter) DOI: 10.1007/978-3-319-99037-8_20

Conference Talks and Posters

1. MEI Symposium 2018, Melbourne Energy Institute, AU, 2018

Oral: Luminescence Solar Concentrator: Colorful and Transparent ‘Solar Panel’.

2. 10th Asian Photochemistry Conference, National Taiwan University, TW, 2018

Poster: Selectively Aligning Donor-Emitter Fluorophore Pairs in a Luminescent Solar Concentrator.

3. 256th ACS National Meeting, Boston, US, 2018

Poster: Selectively Aligning Donor-Emitter Fluorophore Pairs in a Luminescent Solar Concentrator.

4. ARC Centre of Excellence in Exciton Science annual workshop, AU, 2017.

Poster: Aggregation-induced emission-mediated spectral downconversion in luminescent solar concentrators.

5. ISNA 2017 Conference, Stony Brook University, US, 2017.

Poster: Highly Fluorescent Molecularly Insulated Perylene Diimides (PDI) and Applications in Luminescent Solar Concentrator.

6. ACAP and AUSIAPV Annual Conference, AU, 2016.

Poster: Highly Fluorescent Molecularly Insulated Perylene Diimides (PDI) and Applications in Luminescent Solar Concentrator.

Abstract

A luminescent solar concentrator (LSC) is a type of light harvesting device, showing potential as an alternative to the traditional photovoltaics (PV). A typical LSC consists of a planar waveguide system embedded with fluorophores, which absorb light incident on the surface and confines the emission to the edges. As the surface area of the LSC is much bigger than the edge area, the incident light can be concentrated. A PV cell attached to the edge will convert the output light into electricity. Although there are many advantages of LSCs, the unsatisfactory efficiency of LSCs still limits their wide applications. There are four major energy loss pathways of LSCs, which are 1. the photoluminescence quantum efficiency (ϕ_{PL}) loss, 2. the escape cone loss, 3. the re-absorption effect and 4. the transmittance loss.

The donor-emitter fluorophore pair system can potentially improve the performance of LSCs via multiple aspects, in particular, reducing the re-absorption effect. The donor-emitter fluorophore pair is a biomimetic system inspired by the light-harvesting antenna from the natural photosynthesis where a light absorbing donor harvests the incident light and transfers the energy to the acceptor (or emitter), via mainly the Förster resonance energy transfer (FRET) process. By carefully tuning the concentration ratio of the donor and the emitter, one can achieve a fluorophore pair system that is mainly comprised of the donor's absorption spectrum and the emitter's emission spectrum. Consequently, the spectral overlap between the absorption and emission spectra of the fluorophore pair can be minimized, leading to a reduction of the re-absorption effect. By using specially engineered donor-emitter pairs one can reduce not only the re-absorption effect but also the escape cone loss and the ϕ_{PL} loss.

To build a highly efficient donor-emitter fluorophore pair system, the concentration of both the donor and the emitter are required to be high enough to fulfill the requirement of the FRET process. However, this may lead to the aggregation caused quenching (ACQ) of the fluorophores, resulting in reduced ϕ_{PL}. Aggregation induced emission (AIE) is one approach to neutralize the ACQ in the donor-emitter fluorophore pair system. The AIE effect allows the ϕ_{PL} of fluorophores to remain at a

reasonable level in high concentration or in solid state. By replacing the common fluorophores by AIE type of fluorophores in the donor-emitter fluorophore pair system, one can expect a better overall ϕ_{PL} of the fluorophore pair in the required concentration. The photophysics of an AIE donor-emitter pair was characterized in this thesis and the performance in an LSC evaluated.

The other approach to avoid the ACQ effect is to stop the intermolecular interaction of the fluorophores by installing some bulky substituents to keep the fluorophores apart in aggregates. Perylene diimide (PDI) derivatives are a class of molecules that show excellent photophysical properties, but often affected by the ACQ effect. When the bulky substituents are added through the imide position on PDI, the resulting molecule should show a better tolerance to the ACQ effect and leave the photophysical properties untouched. In the thesis, a series of PDI donors with bulky substituents were designed and synthesized and paired with a PDI emitter. The performance of a LSC based on the PDI donor-emitter showed considerable improvement due to the increased ϕ_{PL} and the reduced re-absorption.

Inspired by the success of the PDI donor-emitter pair, a large area LSC device was fabricated based on the same materials. To ensure efficient FRET, the fluorophore concentration of a donor-emitter pair is required to be high. Therefore, a thin layer of the fluorophore coated on a transparent substrate was the chosen device structure for the large-area LSC. Doctor blading thin film deposition was applied to print the dye layer on the surface of the substrate. Two different types of substrate materials and three types of solar cells were investigated to reveal the effects on LSC performance. By optimizing the substrate materials and the attached solar cells, the performance of the resulting large-area LSC was among the best LSCs reported in the literature.

The escape cone loss is the last major energy loss pathway in LSCs, which can be also eliminated by using donor-emitter fluorophore pair system. The escape cone loss can be minimized by aligning the transition-dipole of the emitter perpendicular to the surface of the waveguide. However, the absorbance of the LSC with the aligned fluorophore will be reduced, because the transition dipole of the fluorophore is then parallel to the direction of the incident light. One way to avoid the absorption reduction in the emitter-aligned LSC is to introduce a donor fluorophore that is isotropically oriented. The isotropic donors will harvest incident light as normal, but the energy will be transported to the perpendicularly aligned emitter. The emitters then emit light in parallel to the surface of the waveguide, leading to a reduced escape cone loss. A prototype LSC was prepared based on the selectively aligned donor-emitter pair and fully characterized in the thesis.

Content

Chapter I

Introduction

1.1 Solar energy

To some extent, human history is a history of how efficiently our society uses solar energy.

In very early ages, sunlight provided warmth and provided food for survival through the natural photosynthesis process in plants. Later, wood was burned to release the chemical energy that had been transformed from sunlight. Since the industrial revolution, coal and oil have provided fuel, also products of natural photosynthesis. However, the direct manipulation and application of sunlight can be traced back to the Romans and Greeks in the 3rd century B.C. who used mirrors to concentrate solar energy to light torches.[1-2] The first solar collector, the 'hot box', was invented by Swiss scientist Horace de Saussure in 1767 and then later was improved and used for practical food cooking in 1803.[3] In 1816, Robert Stirling invented a heat engine that concentrated solar thermal energy and generated electricity.[4] French scientist Edmond Becquerel discovered the photovoltaic effect in 1839[5] and American inventor Charles Fritts made the first solar cells from selenium wafers in 1883.[6] In 1954, Daryl Chapin, Calvin Fuller, and Gerald Pearson developed the silicon photovoltaic (PV) cell at Bell Labs.[7] The development of humankind is strongly tied to the use of solar energy with the continuous development of technologies for solar light harvesting.

1.1.1 The solar spectrum

The solar spectrum refers to the distribution of wavelengths of the electromagnetic radiation emitted

from the sun. As the Earth's atmosphere can block or absorb some radiation from the sun, the spectrum of the solar radiation reaching the surface of Earth is different from the solar spectrum in space. The air mass (AM) is a unit of the sunlight path distance in the Earth's atmosphere (Figure 1.1a). The spectra designated AM0 and AM1 refer to the solar spectrum recorded in space and at the normal incident angle to the ground respectively. The solar spectrum of AM1.5 is the most commonly used spectrum for terrestrial research and applications of solar radiation and refers to the spectrum of sunlight passing through the Earth's atmosphere at an angle of 41.81° to the horizon line. The wavelength range of the AM1.5 solar spectrum is from 250 nm to 2500 nm, with the total solar energy consisting of 2% ultraviolet light, 47% visible light and 51% infrared light. There are two types of the AM1.5 spectrum being widely used, namely the global (AM1.5G, 100 mW/cm^2) and direct (AM1.5D, 90 mW/cm^2) spectra (Figure 1.1b). The spectrum of AM1.5G is a combination of both the direct and the diffused sunlight, which has been most commonly used in PV research.

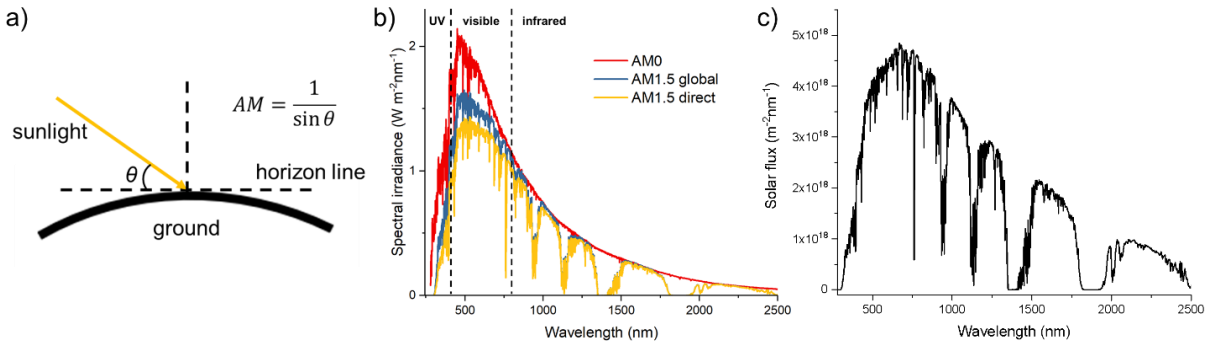

Figure 1.1 a) the definition of air mass, b) the reference AM1.5 solar spectrum and c) the solar flux spectrum at AM1.5G. The AM0 spectrum refers to the solar spectrum outside the Earth's atmosphere. The global spectrum refers to the sum of the direct solar irradiance and the diffused solar irradiance.

1.1.2 Photon refining and solar concentrators

To date, there are already many approaches that can directly convert solar energy to other forms of energy, for example, solar panels, solar water-heaters and artificial photosynthesis. However, besides direct solar energy conversion, photon refining is another important aspect of solar energy

harvesting. Photon refining can be defined as a process in which photons are manipulated for the desired application. Light concentration, spectral wavelength tuning, photon energy fusion, and photon energy fission are all processes of photon refinement.[8] In the context of light harvesting, photon refining is used to improve energy conversion efficiency which has a direct impact on reducing the cost of energy generation.

For photovoltaics, photon refining provides approaches to overcome the Shockley-Queisser efficiency limit (SQ limit), which refers to the maximum theoretical efficiency of a single p-n junction photovoltaic cell under one sun irradiation.[9-10] A single p-n junction photovoltaic cell has a fundamental efficiency limit because of the amount of light energy that can be converted given the bandgap of the semiconductor (Figure 1.2). For photons of short wavelength, the photon energy is much higher than the bandgap of the material, which leads to energy loss by thermal relaxation. On the other hand, photons at long wavelength go unused because the photon energy is less than the bandgap of the photovoltaic material. Last but not least, there are other energy loss pathways, mainly related to the electron-hole recombination behavior of the solar cells. In the SQ limit model, the recombination rate of a solar cell is a constant for a given cell, therefore, the fraction of loss from recombination is inversely proportional to the incident light intensity. According to the SQ limit, the power conversion efficiency for single junction solar cells cannot exceed 33.7% under the one sun AM1.5G spectrum. To date, many photon refining techniques have been studied and applied to photovoltaics to overcome the SQ limitation. Examples include multi-exciton generation, photon upconversion and solar light concentration, which can be applied to make better use of high energy, below-bandgap photons and reduce the recombination loss fraction respectively and improve the total power conversion efficiency of photovoltaic devices.

A solar concentrator is a method to refine sunlight by focusing the incident sunlight from a large area to a smaller area and thus increase the intensity. In comparison with the approaches of multi-exciton generation and photon upconversion, the solar light concentration can be easily achieved by focusing light into a small area typically through the use of mirrors. While it is clear how light

concentration works in solar thermal applications, its effect on photovoltaics is less obvious at first glance. The first effect of solar light concentration on photovoltaic efficiency comes from increases in the device voltage with increasing light intensity,[11] thereby exceeding the SQ limit in standard sunlight condition. However, the level of efficiency improvement is modulated by power losses to heat stemming from the series resistance of the device. The other aspect of the efficiency benefit from the solar light concentration is the so-called photovoltaic/thermal hybrid solar technology[12-14], which can effectively bypass the SQ limit by recycling the waste heat from a photovoltaic device into thermal energy and cooling the solar cell at the same time. The second benefit of solar light concentration is to reduce the overall cost of the photovoltaic system.[15-17] The economic benefit of solar light concentration comes from different aspects. Firstly, the size of the solar cells can be reduced when coupling with a relatively cheaper solar concentrator, leading to a reduced price of the overall photovoltaic system, as the solar concentrator is usually made of glass, plastic or mirrors. The economic benefit is more considerable for a system using high efficiency but more expensive solar cells, such as gallium arsenide (GaAs) cells. Secondly, solar concentrators are usually also cheaper in transportation, installation, and maintenance in comparison with solar cells, which indirectly reduces the cost of concentrated photovoltaics.

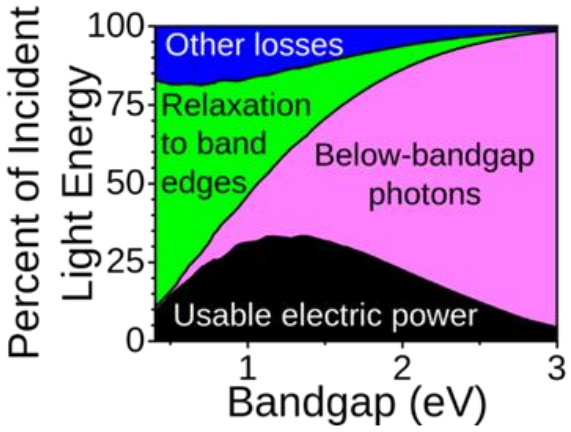

Figure 1.2 A diagram illustrating the Shockley-Queisser limit. The maximum efficiency of a traditional solar cell (black) under one-sun conditions (AM 1.5G) and the percentage losses of the incident light energy against the bandgap (or energy gap) of the solar cell materials.[9, 18]

There are two major types of the traditional solar concentrator system[19], i.e. the Fresnel-lens concentrator and the reflector concentrator. The Fresnel-lens concentrator can focus the incident light to a smaller solar cell behind it, which is often used in small-scale applications, where the weight and space are limited. The reflector concentrator usually consists of a matrix of mirrors that are reflecting the sunlight to a receptor. This concentrator is usually used in solar thermoelectricity or photovoltaic/thermal hybrid systems on a large scale.

The traditional solar concentrators are usually very bulky instruments that require major construction and a large area of ground to set up. As the structure of the traditional solar concentrator can only focus light onto one point, they only work under direct incident conditions but not diffuse light. In addition, the mirrors that are used by the traditional solar concentrator do not usually have selectivity to remove unfavorable wavelengths, which may lead to overheating of the PV cells and usually requires an active cooling system. To overcome the above-mentioned disadvantages of the traditional solar concentrators, a different form of solar concentrator has been designed and reported, i.e. the luminescence solar concentrator.

1.2 Luminescent solar concentrator (LSC)

1.2.1 What is a LSC?

A luminescent solar concentrator (LSC) is a device that can harvest solar light in a large area and concentrate the re-emitted light to a relatively smaller area.[2, 20-21] A typical LSC device consists of a planar transparent waveguide, made of glass or plastic, containing photoluminescent materials. The photoluminescent materials capture the incident photons and the re-emitted photons are trapped in the waveguide by total internal reflection. In this way, light is waveguided to the edge of the device leading to the concentration of light at the edge. This concentrated light can then be converted to electric current by photovoltaic cells attached on the LSC device edge.[22] The performance of a LSC is defined by the energy loss mechanisms in the device which can be divided into two main categories: losses stemming from the photophysical properties of the chromophore (to be discussed

in detail in the following sections); and waveguide losses which include reflection, scattering and escape cone loss (Figure 1.3a).

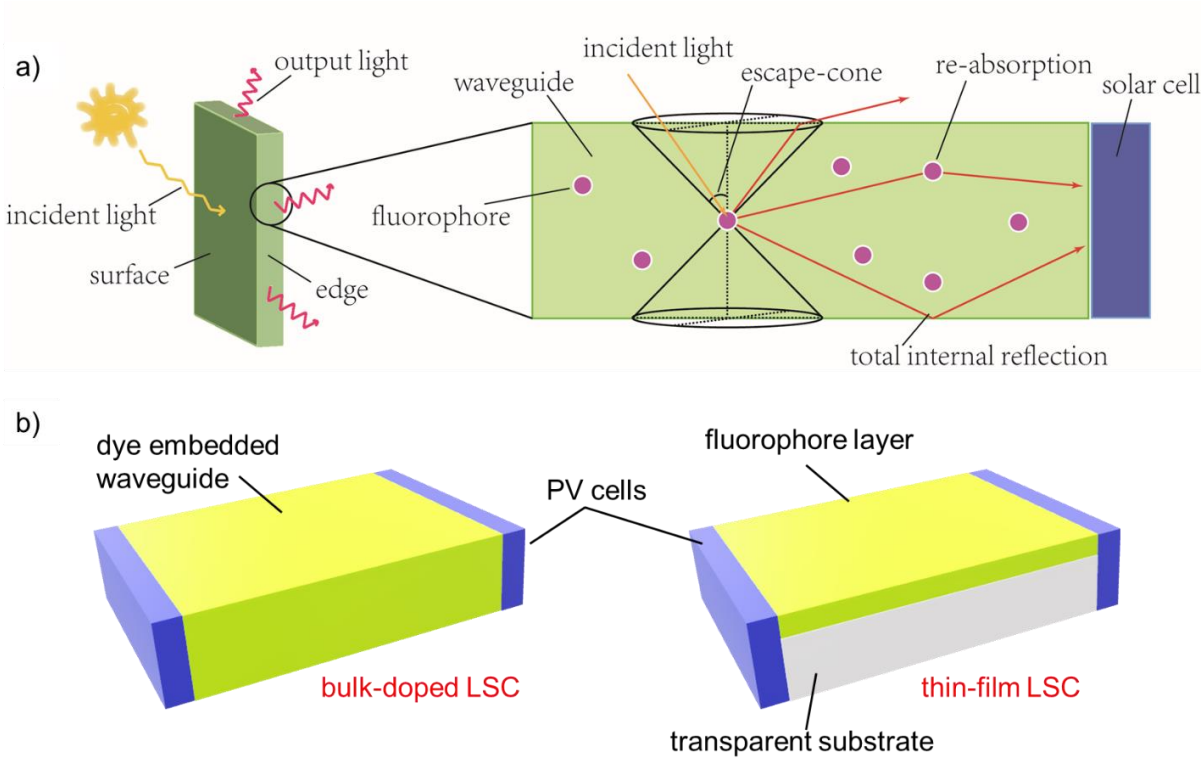

Figure 1.3 a) A schematic diagram of a typical LSC device and b) the general structures of bulk-doped LSC and thin-film LSC devices. The waveguide matrix of bulk-doped LSC is usually made of plastics, so the chromophores can be pre-blended into the matrix materials and dispersed homogeneously in the waveguide system. The thin-film LSC is usually made of glass plates which are coated with a thin chromophore-embedded plastic membrane.

A variety of LSC device geometries exists especially when one includes devices integrated with photovoltaics.[20] Here, two basic LSC geometries are presented with relevance to the following discussion.[20, 23] One is the bulk-doped LSC, which consists of a single piece of waveguide (usually a polymer matrix) with luminescent dyes dispersed homogeneously inside the matrix. The other is the thin-film LSC, which is made of a clear waveguide with a thin layer of dye-containing plastic matrix cast on the surface (Figure 1.3b). The key difference between these two LSC device

geometries is the concentration of chromophore required to achieve the desired level of light harvesting. Thin-film LSCs require a higher concentration of the chromophore to achieve the same absorbance compared to thick bulk-doped devices, but they have some advantages in device fabrication. Depending on the chromophore, it is sometimes a challenge to fabricate bulk-doped LSCs with uniform dye dispersion.

There are several advantages of using LSCs as a light harvesting device:

1. LSCs are excellent at harvesting diffuse light.
2. The materials used to construct a LSC can be very cheap, reducing the cost of photovoltaics by reducing the required photovoltaic cell area.
3. The planar and potentially light-weight device geometry allows easy integration in applications, such as building-integrated photovoltaics.
4. The device geometry is such that the photovoltaic cells are unlikely to suffer from overheating, as can be the case in mirror-type concentrators.
5. LSC devices are less bulky compared to mirror-type concentrators.

1.2.2 Terms and definitions in the LSC area

The performance of LSC devices can be defined by several different parameters and each of the parameters can be related to the others. The geometric gain (G) of LSCs refers to the amplification resulting from the large light harvesting area and small edge area of a waveguide system. For a planar waveguide, G is defined as:

$$G = \frac{A_{surface}}{A_{edges}} \tag{1-1}$$

where the $A_{surface}$ and A_{edges} are the area of the surface and the edges of the waveguide system respectively. Consider a 5 m × 5 m × 0.05 m LSC device with all four edges covered by PV cells for example, the G of the device is 25 and the area of PV cells is 1 m^2, indicating the PV cells can

harvest light from the surface of 25 m^2.

The flux gain (F) refers to the amplification of the photon intensity from the incident light to the output light from the edges of LSC:

$$F = \frac{D_{out}}{D_{in}} \tag{1-2}$$

where the D_{in} andD_{out} are the density of incident and output photons respectively. However, in practice, F reported in the literature can be classified into two types depending on the measurement approaches chosen, namely the optical flux gain (F_{opt}) and the photo-current flux gain (F_{pc}). F_{opt} is usually obtained by directly measuring the D_{out} to D_{in} respectively via a calibrated photo-diode or an integrating sphere:

$$F_{opt} = \frac{D_{out}}{D_{in}} \tag{1-3}$$

Therefore, F_{opt} is an absolute property of a LSC device which is only dependent on the incident light source, for example, one-sun AM1.5G condition or single wavelength. However, the measurement of F_{opt} is not practical when the responsivity of the detector is unknown or difficult to obtain under the experimental conditions. F_{pc}, usually measured by PV cells, refers to the photon-current density gain of a PV cell when coupled with a LSC device:

$$F_{pc} = \frac{J_{out}}{J_{in}} \tag{1-4}$$

where the J_{out} and J_{in} are the observed photocurrent density of a PV cell with and without coupling to a LSC respectively. F_{pc} is relative to the performance of the PV cell when it is directly excited by the light source without coupling to the LSC, thus the value of F_{pc} can vary with different PV cells. Furthermore, the overall PCE of the LSC device (PCE_{LCS}) should also be reported along with F_{pc} to reveal the absolute performance of the LSC device when coupled with the particular types of PV cells.

The fraction of photons trapped by the waveguide (η_{trap}) refers to the ratio of the edge output photons (N_{out}) to the sum of photons released from all faces (N_{all}):

$$\eta_{trap} = \frac{N_{out}}{N_{all}} \tag{1-5}$$

The optical quantum efficiency (OQE), or internal quantum efficiency (IQE), is defined as the fraction of the N_{out} to the absorbed photons (N_{abs}):

$$OQE = \frac{N_{out}}{N_{abs}} = 1.602 \times 10^{19} \frac{I_{out}}{N_{abs}} \tag{1-6}$$

The external quantum efficiency (EQE) of a LSC is defined as the fraction of the edge output photons (N_{out}) to the incident photons (N_{in}):

$$EQE = \frac{N_{out}}{N_{in}} = 1.602 \times 10^{19} \frac{I_{out}}{N_{\mathrm{in}}} = \frac{F}{G} = OQE \times Abs\% \tag{1-7}$$

where *Abs%* is the absorptance of the waveguide system and I_{out} is the current output of the LSC.

As the LSC is mainly used for converting light into electricity, the power conversion efficiency (PCE_{LCS}) is also frequently used to describe the performance:

$$PCE_{LCS} = \frac{P_{out}}{P_{in}} = \frac{V_{oc}\, J_{sc}\, FF}{P_{in}} \tag{1-8}$$

where P_{in} and P_{out} are the incident luminous power and the output electric power respectively, while J_{sc}, V_{oc}, and FF refer to the short circuit current density, open-circuit voltage and fill factor that is measured from the J-V curves.

1.2.3 The photoluminescence quantum yield (ϕ_{PL})

The ϕ_{PL} is a factor to describe how well a fluorophore can emit photons after being excited, and is defined as the fraction of the emitted (N_{emi}) photons per absorbed photons (N_{abs}) of a fluorophore:

$$\phi_{PL} = \frac{N_{emi}}{N_{abs}} \tag{1-9}$$

As a LSC requires high efficiency in photon-to-photon conversion, the ϕ_{PL} is the most essential criterion for choosing fluorophore candidates. In general, the ϕ_{PL} decreases as the fluorophore emission wavelength increases, due to the narrowing of the energy gap between the ground state and the excited-state increases the non-radiative decay rate.[24-26] This phenomenon has been described as the Energy Gap Law. Taking the rylene family, for example, the perylene or terylene derivatives are usually very emissive, but the quaterrylene derivatives only show modest ϕ_{PL}, while the derivatives of pentarylene and hexarylene are essentially non-emissive.[27-28]

The ϕ_{PL} also depends on the rigidity of both the fluorophores and the surrounding environment because a fluorophore system with higher rigidity will have less chance to lose the energy by vibration. In addition, the concentration also shows a significant influence on the ϕ_{PL} for most organic fluorophores due to the aggregation caused quenching (ACQ) effect. With aggregation, some fluorophores will undergo π-π stacking, which affects the energy levels of the aggregates and often leads to additional non-radiative pathways. However, many fluorophores can give close to unity ϕ_{PL} in certain conditions. By choosing the fluorophore carefully, one can minimize the losses in ϕ_{PL} in a LSC waveguide system.

1.2.4 The escape cone loss

The escape cone loss refers to the portion of emitted light that is released from the top and bottom surfaces of a waveguide (see Figure 1.4), and is considered to be one of the primary energy (or photon) losses of LSCs.[20, 29-30] As mentioned previously, the emitted light inside the waveguide can be transported to the edges via total internal reflection. According to Snell's Law, there is a limitation of the internal total reflection process that only emitted rays within the range of the critical angle (θ_c) can be trapped in the waveguide:[31]

$$\theta_c = sin^{-1}\left\{\left(\frac{n_{out}}{n_{in}}\right\}\right) \quad (1\text{-}10)$$

where n_{in} is the refractive index of the waveguide matrix and n_{out} is the refractive index of the surrounding environment which is generally considered to be air (n_{air} = 1). Therefore, for each

fluorophore, the escape cone refers to the angle of θ_c at the top and bottom surfaces of the waveguide. Since the emission rays are either located inside or outside the two conical volumes, the fraction of the escaped photons (η_{escape}) can be described as the ratio of the area of the two spherical crowns extended from the escape cone to the area of the sphere with the same radius (see Figure 1.4). The area of the spherical crown ($A_{spherical\,crown}$) and the area of sphere A_{sphere} are given by

$$A_{spherical\,crown} = 2\pi r^2(1 - \cos\theta_c) \tag{1-11}$$

$$A_{sphere} = 4\pi r^2 \tag{1-12}$$

The fraction of the escaped photons can be described as

$$\eta_{escape} = \frac{2A_{spherical\,crown}}{A_{sphere}} = \frac{4\pi r^2(1-\cos\theta_c)}{4\pi r^2} = 1 - \cos\theta_c \tag{1-13}$$

while the fraction of the trapped photons can be simply described as

$$\eta_{trap} = 1 - \eta_{escape} = \cos\theta_c \tag{1-14}$$

According to the equation (1-10), the η_{trap} can be represented as

$$\eta_{trap} = \cos\left[\sin^{-1}\left(\frac{n_{out}}{n_{in}}\right)\right] = \sqrt{1 - \left(\frac{n_{out}}{n_{in}}\right)^2} \tag{1-15}$$

According to the above-mentioned equations, the trapping efficiency of a waveguide made by glass (n = 1.5) will be around 75%.

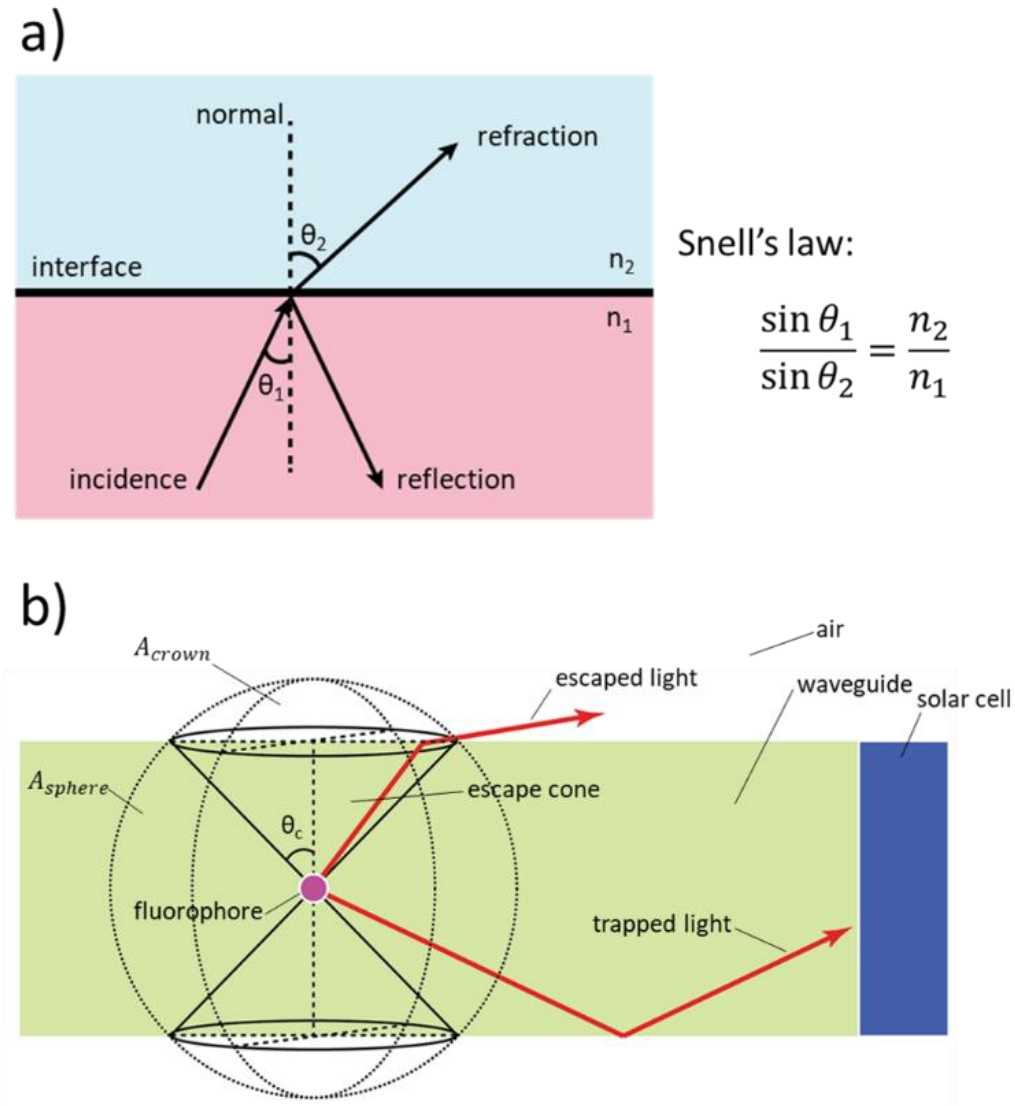

Figure 1.4 a) According to Snell's law, the critical angle of the total internal reflection θ_c is equal to the incident angle θ_1 when the refraction angle θ_2 is 90° and b) The escape cone loss of LSCs depends on the ratio of A_{crown} to A_{sphere}.

1.2.5 The re-absorption effect

The re-absorption effect of LSCs refers to the process where the emitted light from one fluorophore is absorbed by other fluorophores and is one of the main factors affecting the collection efficiency of the waveguide ($\eta_{waveguide}$). The $\eta_{waveguide}$ is the probability that a photon generated inside a waveguide is released from the edges. The value of $\eta_{waveguide}$ is decided by multiple factors

including the escape cone loss (η_{esc}), the average number of re-absorption events (n), the scattering loss (η_{sca}) and the matrix loss (η_{mat}). The η_{sca} refers to the light loss from the waveguide defects, such as micro-bubbles and a heterogeneous matrix, that lead to scattering, while the η_{mat} relates to the absorption from impurities in the matrix:

$$\eta_{waveguide} = (\phi_{PL}\eta_{esc}\eta_{sca}\eta_{mat})^n \quad (1\text{-}16)$$

Normally, η_{sca} and η_{mat} are often ignored. Therefore, according to the equation 1-16, the losses contributing to $\eta_{waveguide}$ caused by the re-absorption effect only occurs when the absorbed photons are lost due to non-radiative decay or the emitted light is released from the escape cone (see Figure 1.5).

The likelihood that a waveguide will exhibit the re-absorption effect depends on three factors, namely the overlap of the absorption and emission spectra of the fluorophores, the concentration of fluorophores and also the geometrical size of the waveguide. In most of the cases, the concentration of fluorophores and the size of the waveguide are determined by other design criteria of a LSC device. Therefore, eliminating the absorption/emission spectral overlap of the fluorophores becomes the major approach to minimize the re-absorption effect.

Using fluorophores with a large Stokes shift is one way to eliminate the spectral overlap. The Stokes shift is the difference in wavelength (or frequency) between the absorption and emission maximum for a fluorophore. By using fluorophores with a large Stokes shift, one can reduce the extent of spectral overlap of the absorption and emission and thus decrease the re-absorption of emission by the fluorophores. A donor-acceptor fluorophore system can also increase the total Stokes shift of the LSC devices. In a donor-acceptor fluorophore system, intermolecular non-radiative energy transfer depends on the extent of spectral overlap of the donor's emission and acceptor's absorption leading to a large Stokes shift of the mixture based on the donor's absorption and the acceptor's emission spectrum.

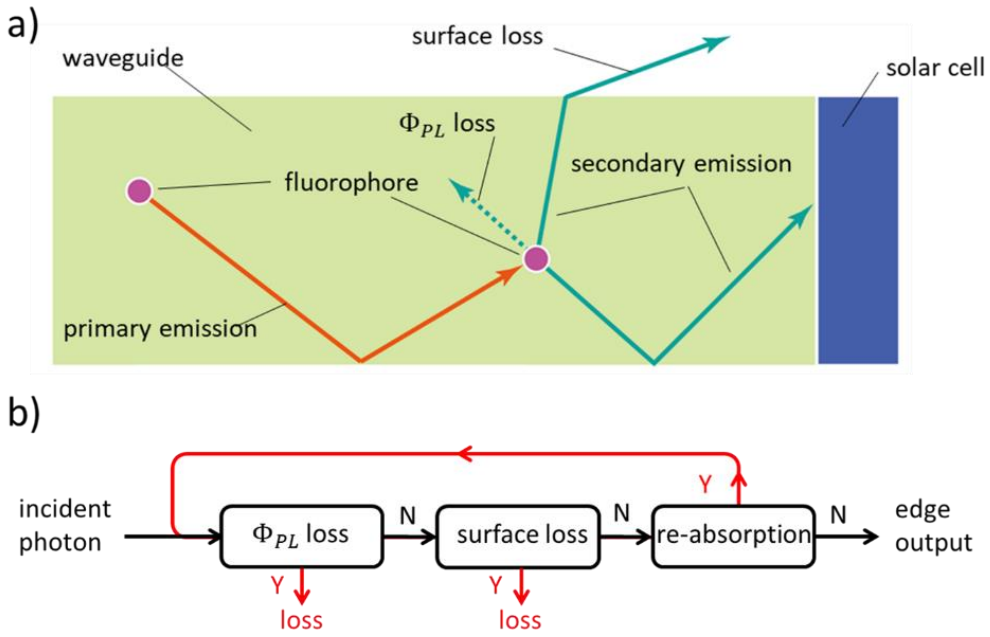

Figure 1.5 a) The re-absorption effect in a LSC waveguide and b) the energy losses caused by the re-absorption effect.

Besides modifying the Stokes shift, one can also reduce the losses arising from the re-absorption effect by increasing the ϕ_{PL} of the fluorophores. From equation 1-16, the influence of ϕ_{PL} is raised to the power of the number of re-absorption events (n). For example, if the ϕ_{PL} of a LSC fluorophore system increases from 80% to 90%, for n = 2, the improvement in the $\eta_{waveguide}$ will increase by approximately 26% (assume no other losses, $(0.9^2\text{-}0.8^2)/\ 0.8^2 = 0.26$). The escape cone loss also influences the $\eta_{waveguide}$ significantly in the presence of large re-absorption effects. It is difficult to modify the η_{esc} of a LSC device unless one changes the matrix material of the waveguide system or aligns the fluorophore orientation. Further discussion about the fluorophore alignment in LSCs can be found in later sections of the Introduction and **Chapter VI**.

1.3 Past research on LSCs

1.3.1 The history of LSCs

The prototype of LSCs can be traced back to as early as 1951 with a report of a planar fluorescence collecting system designed for radiance amplification (a γ −radiation sensor).[32] In this work, the author made a three-junction light concentrator that can down-convert γ -radiation to red emission at around 600 nm. In Figure 1.6, an anthracene-naphthalene-benzene solution in Box 1 will absorb the γ -radiation and Box 1 will concentrate the re-emission at 400 nm to Box 2. By the same process, Box 2 and Box 3 will down-convert the light to 600 nm and focus the output light at the tip of Box 3, where the detector lays. The flux gain of this prototype device was estimated to be around 10-100. However, the paper did not specify the materials used in Box 2 and Box 3.

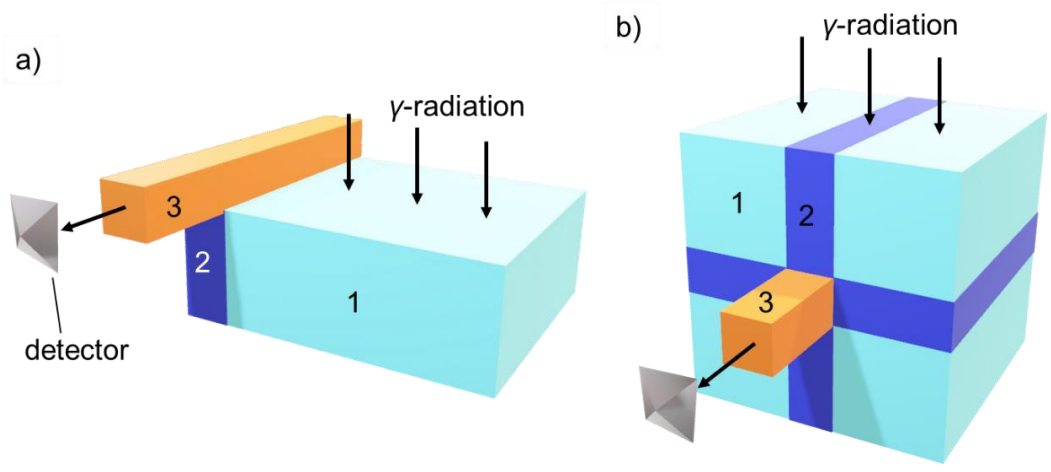

Figure 1.6 The γ -radiation signal concentrator, the prototype of LSC in 1951. a) the three junction waveguide system can absorb γ -radiation from Box 1 and emit at 600 nm from Box 3. b) the demonstrated device can amplify the light intensity 100 times.

In 1976,[33] a planar solar collector was reported by Weber et.al. using a medium containing

chromophore to harvest light and a solar cell to collect the emission via total internal reflection. This was the first report to apply the luminescent concentrator in the field of solar light harvesting. Subsequent improvements on this prototype include a multi-dye planar solar concentrator.[34] In the latter work, a donor dye (Coumarin 6) was used to harvest light and transfer the energy to an acceptor dye (Rhodamine 6G) which had an emission window matched to the absorbance spectrum of the photovoltaic cell. In 1981, Goetzberger et. al.[35] suggested to stack multi-layers of LSCs with different absorption bands for harvesting sunlight over a wider spectral range. As the SQ limit also applies to LSCs, there is relaxation loss for light with energy higher than the bandgap and transmittance loss for light with energy lower than the bandgap. However, one can overcome the SQ limit, by stacking LSCs with different bandgaps of fluorophores and solar cells. This approach is a prototype for tandem LSCs.

Since the price reduction of Si solar cells after 2007, LSCs lost some advantages in competing with Si PV cells. As a consequence, new applications for LSCs have been investigated. The idea of visibly transparent LSCs[36-37] was mentioned by Lunt et. al. in 2013.[38] Visibly transparent LSCs only absorb light in the UV or rear-IR range, thus leaving the LSC transparent in the visible range (400nm-800nm). As the colour, transparency, shape and flexibility can be easily tuned, LSCs are also suitable for the building-integrated photovoltaics.[39] So far, LSCs have been reported in applications of building windows[40], noise barriers[41-43] and bus stops[44] in the past few years.

To date, many organic small molecule fluorophores have been used in LSCs. A large proportion of chromophores reported in LSC devices are commercially available dyes, though there is an increasing number of reports of new organic dye structures, luminescent polymers, and quantum dots.[20, 45-47]

1.3.2 The traditional molecular fluorophore

Traditional molecular organic fluorophores, such as rhodamine, coumarin, etc., have been

reported for use in LSCs since 1976.[33] The benefits of the molecular fluorophores include low-cost, high absorption coefficient, great quantum efficiency and convenience in device fabrication. However, the drawbacks of the molecular organic fluorophores are also very obvious, as they are often affected by either the ACQ effect or poor stability.

So far, the most widely used small-molecular organic fluorophores in LSCs are the perylene diimide (PDI) derivatives, due to their close-to-unit ϕ_{PL} and good photostability. Among the perylene diimide derivatives, Lumogen® F Red 305 (LR305) from BASF has been most extensively reported in the literature.[20, 48] In 2008, Sloof et. al. demonstrated the benchmarked PCE (7.1%) of a small-scale LSC (5 cm × 5 cm, G = 2.5) using LR305 as the fluorophore. Three different solar cells were examined, which were multi-crystal Si solar cell, InGaP solar cell and GaAs solar cell. The LSC coupled with GaAs solar cell showed the benchmark result, due to a better spectral matching of the emission of LR305 and the absorbance of the solar cell. As the optical properties of the PDI derivatives can be dramatically affected by the ACQ effect, several studies were focusing on the influence of the fluorophore aggregation to the performance of LSCs. In 2012, Haines et. al. reported the photophysical property variation of a PDI derivative against an increasing fluorophore concentration.[49] As the concentration increased, the absorbance of the PDI blue-shifted and the ϕ_{PL} rapidly decreased, indicating the formation of H-aggregates. Both the simulated and the experimental EQE of LSC improved with the increasing fluorophore concentration until 10 mg/g of the PDI derivative in the PMMA matrix. Thereafter, the EQE of the LSC started to decrease when the concentration was above 10 mg/g in PMMA, mainly due to the ϕ_{PL} reduction of the fluorophore aggregates. In 2014, Gilbertson et. al. investigated a series of sterically hindered PDIs (derivatives of Lumogen F Orange 240) and their solubility in a liquid crystal matrix.[50] By modifying the bulky-substituents on the PDIs, the solubility of the PDI varied from 0.13 mg/L to 22 mg/L, due to a stronger interaction with liquid crystal material. The resulting small scale LSC showed a 74% OQE.

4-Dicyanomethylene-2-methyl-6-(p-dimethylaminostyryl)-4H-pyran (DCM) is another molecular organic fluorophore that has been extensively used in LSCs. The earliest record can be traced back to 1982, when Thomas et. al. prepared a LSC of DCM in PMMA substrate.[51] In the following year, Lesiecki et al. studied the re-absorption effect of DCM based LSCs, due to its relatively large Stokes shift.[52] By 1987, DCM and Rhodamine 640 was considered as the benchmark fluorophores in the field of LSCs, and scientists compared newly developed fluorophores with them as reference.[53] In 2010, Baldo et. al. reported a horizontally aligned LSC fabricated by DCM and coumarin 6 in a liquid crystal polymer substrate (Figure 1.7).[54] The liquid crystal polymer matrix was aligned parallel to two edges of a square LSC, leading to the transition dipoles of DCM and coumarin 6 being also aligned parallel to the edges. As a consequence, the EQE measured from the parallel edges was much higher than from the perpendicular edges, resulting in a better concentration rate in the favoured edges of the LSCs. The same group also reported a tandem LSC based-on DCJTB, rubrene and Pt(TPBP) as fluorophores (Figure 1.7), which will be discussed later on in **Chapter I**.[55] In the same year, Debije reported a comparison of the alignment phenomenon of three commonly used small molecular organic fluorophores, which were LR305, DCM and K160 (a coumarin derivative), in LSCs of liquid crystal matrix.[56] In this case, the LSC was assembled by sandwiching a fluorophore-embedded liquid crystal layer in-between two transparent electrode layers. When voltage bias was applied on the electrodes, the liquid crystal layer was aligned perpendicular to the surface of the electrodes, leading to the fluorophores being aligned in the same direction. The alignment behavior was different among the tested fluorophores, due to the different molecular shape and dichroism parameter of the fluorophores.[57] In 2013, Rogers et. al. assembled GaAs solar cells on the surface of a DCM embedded LSC.[58] The resulting device increased the power output of the GaAs solar cell more than one fold, and considerably decreased the cost-per-watt by increasing G of the LSC.

Besides the traditional molecular organic dyes, polymer fluorophores have also been used in

LSCs. In 2016, Swager et. al. reported a down-converting tri-fluorophore system that consisted of two π-conjugated polymer donors (P1 and P2) and LR305 as the emitter.[45] The absorption spectrum of P2 is red-shifted about 80 nm to the absorption of P1, leading to an overall absorption band of the donors covering the 400 nm to 540 nm range. The energy absorbed by both the donors was then transferred to LR305 and emitted efficiently. By reducing the absorbance of the emitter, the spectrum overlap was minimized, and the re-absorption effect was reduced in the tri-fluorophore system. The simulation suggested the F of the resulting LSC can remain > 80 at G = 400, mainly due to the reduced re-absorption. There are more examples of polymeric and dendritic fluorophores being used in LSCs.[59-61] More about the down-conversion and re-absorption reduction will be discussed later in the thesis.

Phosphors and rare earth metal complexes were also options for LSCs. In 2010, Zhang et al. reported a LSC embedded with a rare earth complex, $Eu(TTA)_3(TPPO)_2$, the structure is shown in Figure 1.7.[62] The rare earth complex shows maximum absorbance at 350 nm and emits in a very narrow emission band at 613 nm with the ϕ_{PL} of 73%.[63] Unlike other organic fluorophores, the ligands of the complex absorb the light, being excited to S_1, converting to T_1 via the intersystem crossing process and then transferring the energy to Eu^{3+} by the non-radiative path. The Eu^{3+} core then emits ($^5D_j \rightarrow {}^7F_j$). Due to the large Stokes shift and the narrow emission band the re-absorption was minimized. In 2013, Lunt et al. reported the use of nanocluster phosphors, in particular, $K_2Mo_6Cl_{14}$ and $(TBA)_2Mo_6Cl_{14}$, for the application of visibly transparent LSCs.[38] The nanocluster phosphors absorb at 350 nm and emit at 750 nm, with the ϕ_{PL} > 75%. The resulting LSC provided PCE = 0.44% at G = 6.

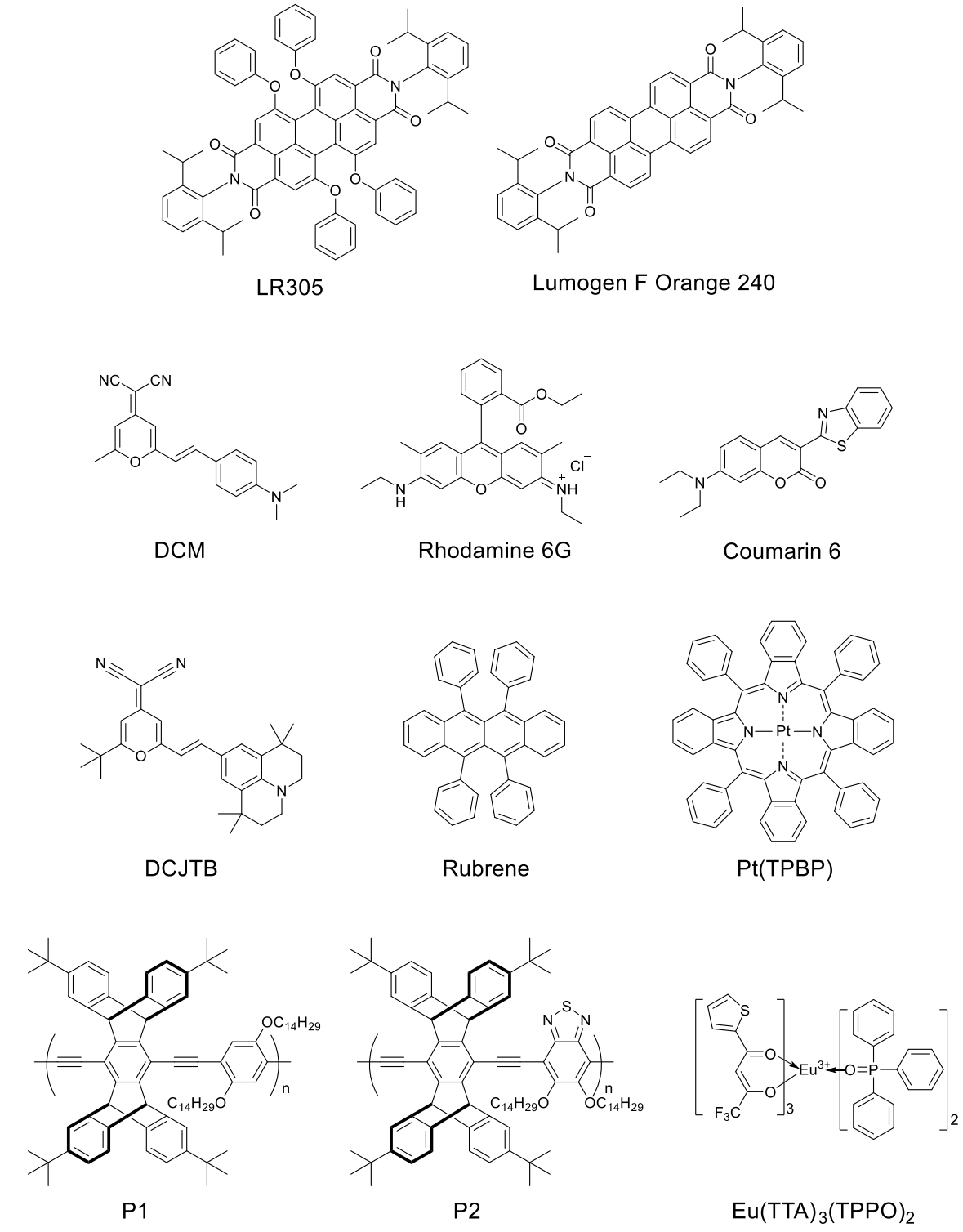

Figure 1.7 Chemical structures of the small molecular organic fluorophores that are widely used in LSCs.

1.3.3 Aggregation-induced emission (AIE)*

Typical luminescent organic dyes (e.g. coumarins, rhodamines, perylenes, etc.) have planar aromatic structures and are prone to self-aggregation, resulting in the aggregation-caused quenching (ACQ) of photoluminescence. Although dyes are dispersed in polymer matrices in LSC devices, these organic dyes will still aggregate with increasing concentration as they do in solution. This means dye concentration must remain low to maintain high ϕ_{PL} and, consequently, thicker devices are necessary to maintain useful absorbance values.

Aggregation-induced emission (AIE) materials are a subclass of fluorophores that can provide high ϕ_{PL} in aggregated states, leading to a clear advantage over typical organic dyes in this application. In addition, AIE chromophores are not only emissive in their aggregated state but also when dispersed in a solid-state matrix.[64-67] Tetraphenylethene (TPE) and its derivatives are a family of well-known AIE materials that have been used in many applications. It has been demonstrated that TPE is highly photoluminescent in a polystyrene matrix.[68] Interestingly, TPE was more emissive in glassy polystyrene compared to poly(styrene-butadiene) copolymer. It was suggested that the rotational motion of the phenyl groups of the TPE was more restricted in the rigid glassy matrix making the sample more emissive. TPE has also been examined in LSC devices.[69] In a proof-of-concept study, a series of phenyl-substituted alkene compounds were investigated as potential LSC chromophores. While all compounds in the study showed AIE behavior, their ϕ_{PL} was lower than the simple TPE structure. Subsequently, the performance of TPE in LSCs was tested as a thin film on glass showing ϕ_{PL} of 49.5% and the simulated n_{edge} of 13.7% at *G* = 50. The large 1.1 eV Stokes shift of TPE meant that re-absorption of emission was small and the performance of TPE devices scaled well with the area. The topics of Stokes shift and re-absorption are discussed in greater detail in the next section. One problem identified with

* This section has been published elsewhere by the author.[2] Reprinted with permission from Ref [2], copyright © 2019 Springer Nature.

TPE was its crystallinity as opaque light-scattering films were obtained when TPE was used in high concentration in PMMA. This highlights the importance of physical compatibility of the dye with the waveguiding matrix. TPE is a UV-absorbing material with emission in the blue spectral region. While suitable for transparent device applications such as smart windows, LSC devices containing TPE have limited power output as it does not harvest any visible light.

A red-emitting AIE-type chromophore, TPE-AC, has been reported for a visible light harvesting LSC.[70] The LSC devices were fabricated by dispersing TPE-AC in PMMA in chloroform solution and coated on top of glass substrates. Evaporation of the solvent resulted in PMMA thin films 25±5 μm thick embedded with TPE-AC. The prepared TPE-AC films had a wavelength of maximum emission in the 600 - 620 nm range and the maximum ϕ_{PL} was 50% with 0.1 wt% of dye in the polymer matrix. The ϕ_{PL} decreased to 30% with 1.2 wt% of TPE-AC in PMMA. Interestingly, polycarbonate films containing TPE-AC showed higher ϕ_{PL} at greater dye concentration. The ϕ_{PL} of the TPE-AC/polymer film at the highest chromophore content was comparable to benchmark materials in the long-wavelength range.[71-72] The observed optical quantum efficiency maximum of TPE-AC LSC devices was 6.7%, comparable to other reported LSCs with red-emitting chromophores.[73-74] Following this research, the same group reported a TPE-substituted red-emitting ATRP initiator that can be used in PMMA-based LSC devices.[75] The TPE-substituted chromophore shows excellent photostability but the ϕ_{PL} requires improvement to increase LSC performance.

As described earlier, the classic AIE chromophore, TPE, has been reported in a proof-of-principle LSC device.[69] While TPE shows a high Stokes shift of 130 nm, the lower ϕ_{PL} results in LSC devices with moderate performance. An advancement on this work was reported with two gem-pyrene ethene derivatives providing even larger Stokes shifts (Figure 9).[76] Both molecules showed the AIE effect in solution and a polystyrene matrix, but gem-1-pyrene ethene showed higher ϕ_{PL} up to 64%. Interestingly, the Stokes shift of gem-2-pyrene ethene ($\lambda_{abs} = 340\,nm,$

$\lambda_{em} = 420\ nm$) was about 80 nm, while the Stokes shift of gem-1-pyrene ethene ($\lambda_{abs} = 360\ nm$, $\lambda_{em} = 540\ nm$) was significantly increased to 180 nm. The emission spectrum of gem-1-pyrene ethene was significantly redshifted and was indicative of excimer formation and emission. Crystallographic data for gem-1-pyrene ethene showed crystal packing of pyrene dimers that are well-known to form excimers on photoexcitation. The combination of good ϕ_{PL} and large Stokes shift for gem-1-pyrene ethene makes it an appropriate chromophore for a transparent LSC device. Another reason for using AIE fluorophores in LSCs is to reduce the re-absorption effect, due to their relatively large Stokes shift. [77-79]

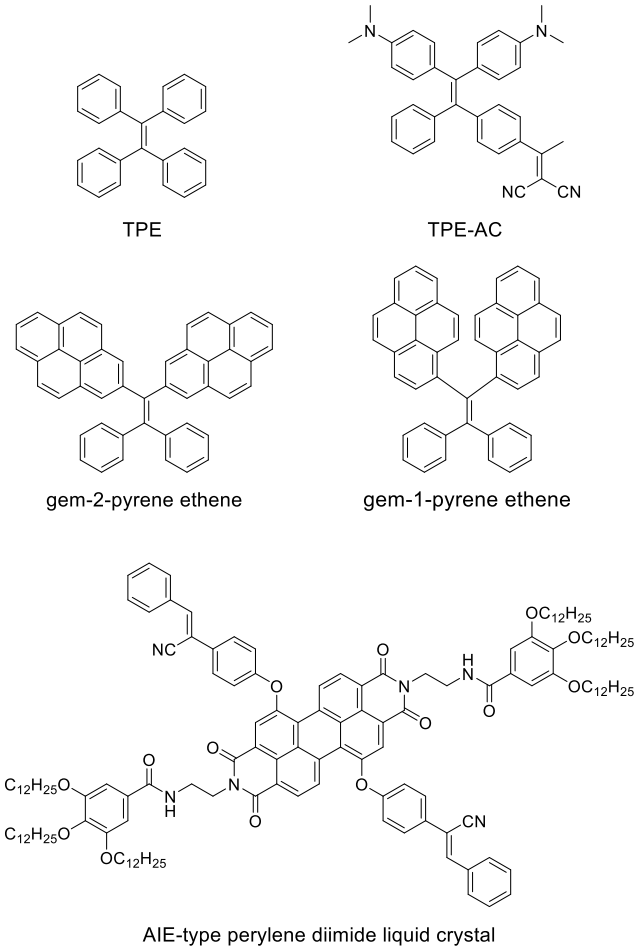

Figure 1.8 The chemical structures of AIE-type chromophores used in LSC devices. Reprinted with permission from Ref [2], copyright © 2019 Springer Nature.

Although not specifically designed for LSC application, another example of an AIE-type material showing a large Stokes shift is an intramolecular energy donor-acceptor system (Figure 1.8).[80] The molecule consisted of cyanoethene groups attached to the bay position of a liquid crystalline perylene diimide. When excited at 330 nm, where the cyanoethene substituent absorbs, the energy transferred to the perylene core and the molecule emitted with the maximum at 575 nm, resulting in a large Stokes shift of 251 nm. Notably, the ϕ_{PL} of the material increased as a function of the increasing ratio of H_2O in THF/H_2O solution, which indicated the AIE effect. Further research regarding intramolecular donor-acceptor systems based on AIE-type functional substituents has been reported in recent years.[81-82]

1.3.4 Quantum dots

Besides the traditional organic fluorophores, many inorganic materials have also been used in LSCs. Quantum dots (QDs) are a subclass of fluorophores that have been widely used in LSCs since 2000.[83-84]

In 2014, Klimov et. al. reported a large-area LSC fabricated based-on 'Stokes-shift-engineered' core-shell CdSe/CdS QDs.[85] According to the article, both the absorption and the emission of the QD can be tuned by changing the number of the CdS monolayers in the shell structure of the QD (Figure 1.9). By adding 14 monolayers into the shell, they obtained the core-shell QDs showing a red-shift of 80 nm in emission in comparison with the core-only CdSe QD, leading to the Stokes-shift of more than 400 meV. The core-shell QDs were then blended with MMA, the monomer of PMMA, and poured into a module to form the waveguide via bulk-polymerization. The QDs with 14 monolayers in the shell showed no significant decrease in PLQY after incorporation into PMMA, while the QDs with a thinner shell suffered severe photoluminescent quenching. The Monte-Carlo ray simulation suggested that about 14% of the emitted photons were lost via the non-radiative pathways (re-absorbed but not re-emitted) for the core-shell CdSe/CdS QD based LSC, while the non-radiative loss was 83% for the core-only CdSe QD counterpart.

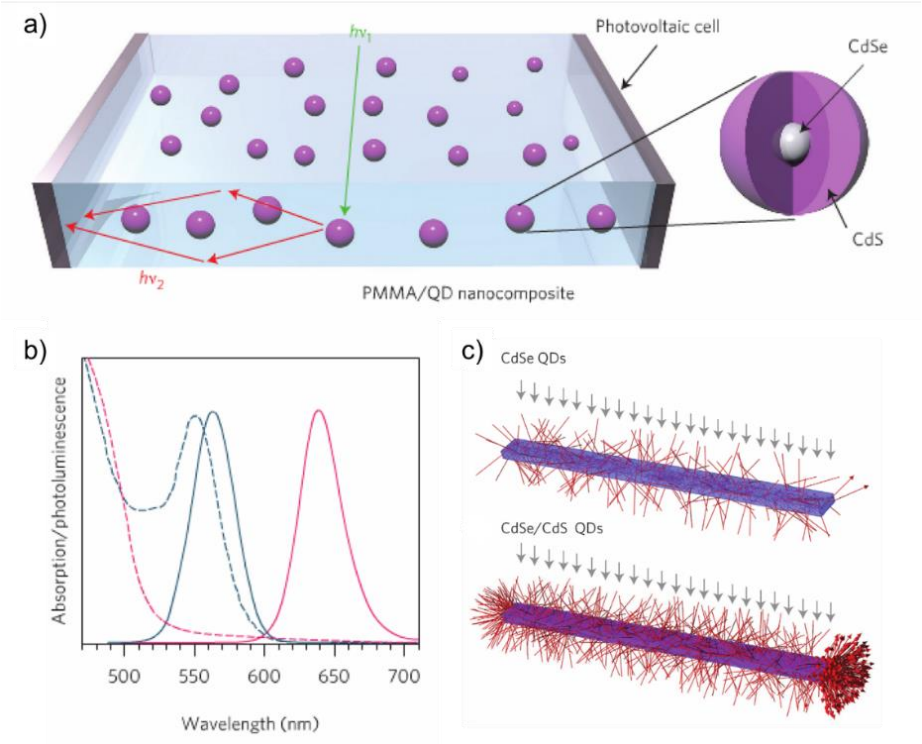

Figure 1.9 a) the core-shell CdSe/CdS QDs embedded in the PMMA matrix, fabricated by the approach of bulk-polymerization; b) the absorption (dash line) and emission (solid line) spectra of the core-only CdSe QDs (green) and the core-shell CdSe/CdS QDs with 14 monolayers in the shell (red); c) the visualized Monte-Carlo ray simulation of LSCs based one the core-only CdSe QD and the core-shell CdSe/CdS QDs. Reprinted with permission from Ref [85], copyright 2014 © Springer Nature.

In 2015, Brovelli et. al. reported a large-area colourless LSC using heavy-metal-free QDs of ternary I-III-VI_2 semiconductors(Figure 1.11).[46] In comparison with other types of QDs, the ternary QD was less toxic, inexpensive in preparation and can provide a large Stokes shift of hundreds meV. They used the core-shell CuInSeS/ZnS QDs in this work, which had the ϕ_{PL} of above 40% and the Stokes shift of 0.53 eV. The large-area LSC was fabricated by the bulk-polymerization of a blend of the ternary QD and lauryl methacrylate. The resulting LSC had the absorption onset at the near-infrared range and was strongly emitting at around 900 nm, leading to the EQE of 3.27 %

over the 20% absorption of the AM1.5G spectrum. At the end of the work, they further proposed that the large Stokes shift of the ternary QD was due to the intragap state associated with the native defect of the QDs. Thus, the observed red-shifting of the emission was due to the 'true' Stokes shift. It is worth to mention, as the Stokes shift may not be well defined for some materials, the overlap integral is suggested to be used instead.[86]

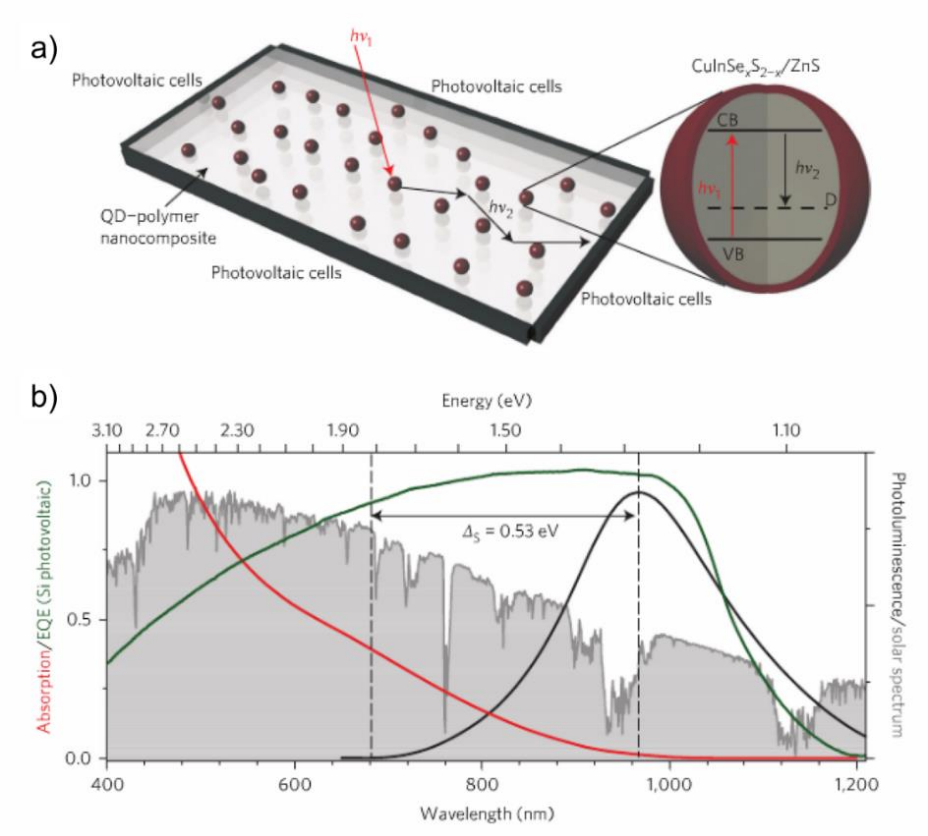

Figure 1.10 a) the scheme of the LSC waveguide embedded with the core-shell CuInSeS/ZnS QDs and b) the absorption, emission spectra of the QD, the EQE spectrum of the Si photovoltaic and the AM1.5G solar spectrum. Reprinted with permission from Ref [46], copyright 2015 © Springer Nature.

However, the application of quantum-cutting nanocrystals may improve the performance of LSCs to the next level. Quantum-cutting refers to the phenomenon of two photons re-emission per

absorption, in which the re-emitting photons has less than half the energy of the absorbed photon. In consequence, a quantum-cutting system will have the maximum ϕ_{PL} as 200% and massive Stokes shift, which is ideal for the waveguide of LSCs. In 2019, Gamelin et. al. reported an Yb^{3+}-doped perovskite nanocrystal quantum-cutting system and its application in LSCs.[87] The quantum-cutting perovskite nanocrystal strongly absorbs at 400 nm and emits at 1000 nm with the experimental ϕ_{PL} around 170% (Figure 1.11).[88] A monolithic bilayer waveguide was prepared with the front layer of the quantum-cutting perovskite nanocrystal and the back layer of a red-emitting $CuInS_2$/ZnS QD. The simulation suggested the F of the quantum-cutting perovskite nanocrystal bilayer LSC can reach to around 50 at G = 150.

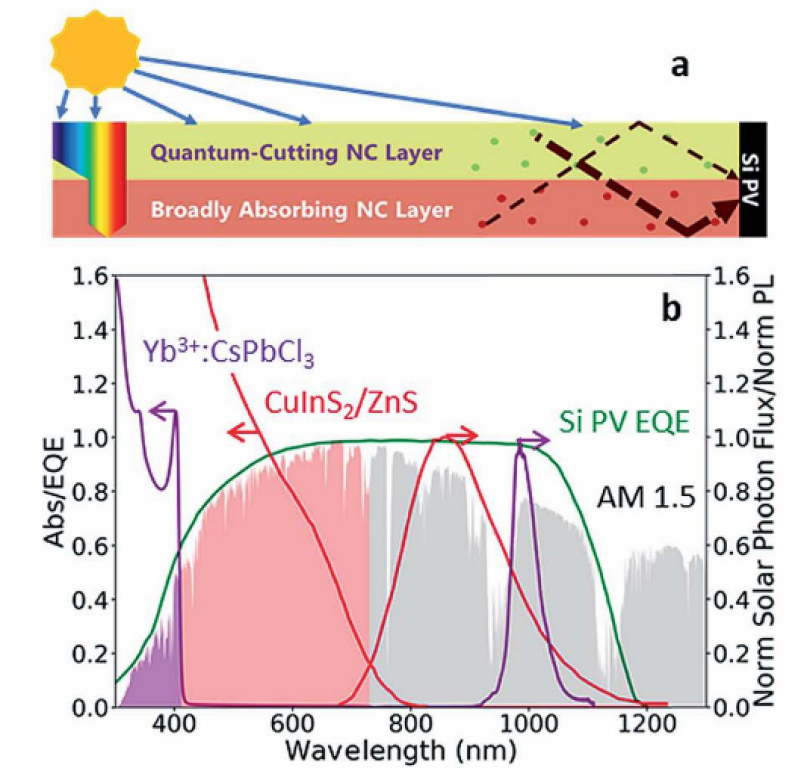

Figure 1.11 a) the device structure of the monolithic bilayer LSC based-on the Yb^{3+}-doped perovskite nanocrystals, and b) the spectra of the Yb^{3+}-doped perovskite nanocrystal layer and the $CuInS_2$/ZnS QD layer. Reprinted with permission from Ref [87], copyright © 2019 Royal Society of Chemistry.

1.3.5 Development of the waveguide and device geometry of LSC.

Other than developing the fluorophores, the research in the design and fabrication of the waveguide system of LSCs has also progressed. Many techniques, such as the liquid-crystal, multi-junction tandem device structures and a variety of shapes and matrices of the waveguide, have been investigated for enhancing LSC performance.

Liquid media, for example, a container full with fluorescent solution, has been used as the waveguide since the very first prototype of LSCs.[32] In 2007, Carter et. al. built a planar glass container that consisted of a square glass rod frame sandwiched by two pieces of glass sheets.[89] A liquid solution can be injected into the container as both the solution of the fluorophores and waveguiding media. This design can simplify the LSC device assembling, allowing one to study multiple devices with moderate effort. In their research, 7 fluorophore systems at a variety of concentrations were studied.

Plastics, such as PS and PMMA, and glass are the most common waveguide substrate materials for LSCs. However, there is an emergence of new waveguide materials. In 2016, Papakonstantinou et. al. reported a flexible LSC made by fluorophore-doped polydimethylsiloxane.[90] In the work, they investigated the influence of the waveguide curvature radius on the performance of the resulting LSCs. In the same year, Evans et. al. also reported a flexible LSC based on the organic-inorganic hybrid ureasil polymer substrate.[59, 91]

In 2009, Debije et. al. first reported the concept of enhancing the light-concentrating effect of LSCs by aligning the fluorophores in the waveguide.[57] In their approach, a dichroic dye was embedded in a liquid crystal matrix layer. By rubbing the liquid crystal layer, the liquid crystal molecules were aligned in parallel to the direction of the shear force, leading to the dye molecules being aligned in the same direction. The resulting LSC was focusing more light on two opposite edges and reducing intensity on the other two edges.

In 2014, Schenning et. al. reported a switchable LSC[92] where the transparency of the device can be tuned by the alignment direction of a liquid crystal (Figure 1.12). In that work, the author sandwiched a liquid-crystal layer in-between two ITO coated glass sheets. A dichroic perylene diimide (PDI) fluorophore was embedded in the liquid crystal layer. In the normal situation, the liquid-crystal molecules were naturally aligned in parallel to the glass surfaces, leading to the dichroic PDI also laying parallel to the glass surface. In this case, the absorbance of the waveguide was strong as the transition dipole of the PDI was oriented in the favored direction to harvest the incident light. When a voltage of 10 V was applied across the top and bottom glass sheets, the liquid-crystal matrix was then aligned perpendicular to the glass sheet surface, leading to the PDI molecules also being aligned in the perpendicular direction. The LSC became colourless and both the absorption and emission intensity decreased, due to the unfavored transition dipole orientation of the PDI to the incident light.

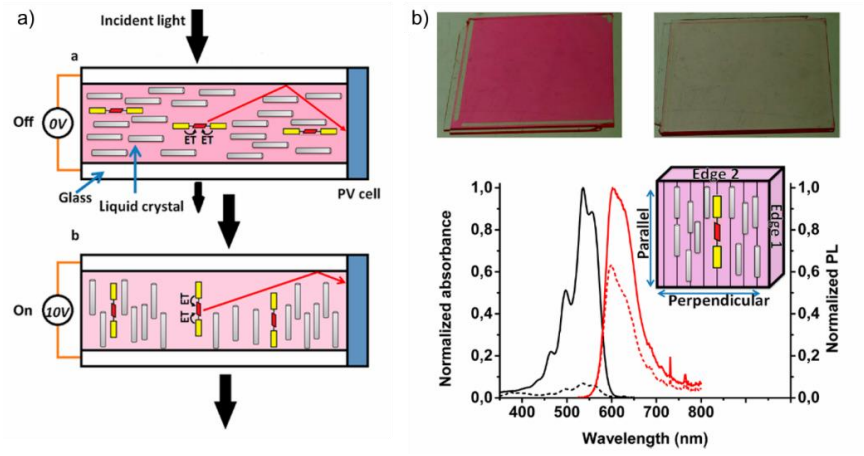

Figure 1.12 a) When a voltage of 10 V was applied across the top and bottom glass sheets, the alignment direction of the liquid-crystal matrix and the transition dipole of the fluorophore molecules can be switched from parallel to perpendicular to the waveguide surface; b) the intensity change of the absorption and emission spectra of the waveguide in the 'off' (solid line) and 'on' (dash line) conditions. The LSC was switched from deep pink to colourless. Reprinted with permission from Ref [92], copyright 2014 © by American Chemical Society.

The tandem waveguiding system is another approach to enhance the performance of LSCs, by broadening the absorption band of the waveguide. A three-junction tandem LSC[93] was reported in 2004 that consisted of a violet, a green and a pink waveguide layer. However, the design of the tandem LSC was not aimed at generating electricity, but to provide white-light output from the edges of the LSC. The three layers of waveguides were stacked on each other with their edges joined to a PMMA luminaire to mix the emission of the three colours into white light. A white diffuser layer was added to the PMMA luminaire to maximize the edge output. The concept of generating white light via a LSC is not widely adopted yet, but this work did provide some guidance about designing tandem LSCs.

In 2018, Klimov et. al. had reported a tandem LSC[94] that consisted of two waveguide layers. The top layer was embedded with CuInSe/ZnS QDs, which strongly absorbs light below 440 nm and emits at 600 nm with a very small spectral overlap. The bottom layer consists of CuInSeS QDs, absorbs up to 800 nm and emits (maximum) at 800 nm (Figure 1.13). Although the ϕ_{PL} of CuInSeS QDs was lower than CuInSe/ZnS QDs, the bottom layer can still recover a considerable amount of transmittance loss from the top layer waveguide. The tandem LSC showed 3.1% PCE over a ~232 cm^2 working area, with the top and bottom waveguides contributed 1.3% and 1.8% PCE respectively.

Other examples of developing the device geometry of LSCs include changing the shape of the waveguide. In 2007, Mcintosh et. al. reported a theoretical comparison of the performance between cylindrical LSCs and traditional planar LSCs.[95] Another set of solid and hollow cylindrical LSCs were reported by Ghosh et. al in 2011, using near-infrared quantum dots as fluorophores.[96] In 2010, Zhang et. al. reported two polymer optical fibers doped with either $Eu(TTA)_3Phen$ or Rhodamine 6G as the fluorophores.[97] They attached two solar cells at the cross profiles of the optical fiber to convert it into LSCs, but no experimental performance of the device was given. The same group also demonstrated a theoretical model of a cylindrical LSC in 2013.[98] Other than

cylindric and planar square, there were also examples of using dish-shaped waveguides in LSCs.[99]

Besides the development of fluorophores and waveguides in the field of LSCs, one can also improve the LSC performance via the energy transfer process. This is also the main focus of this thesis, which will be further discussed in the following section.

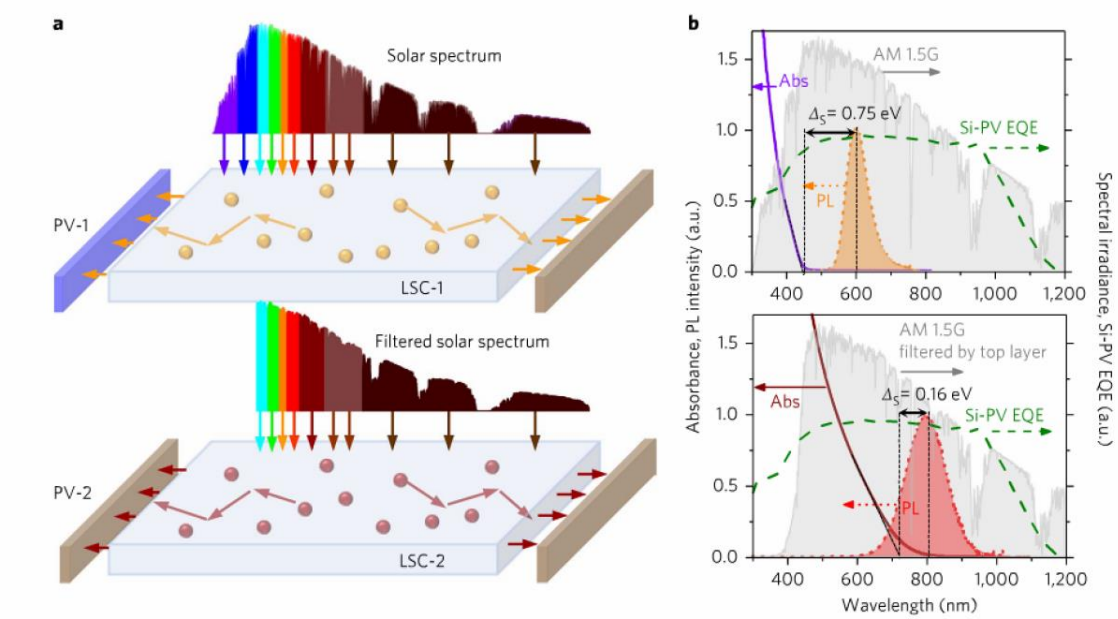

Figure 1.13 a) The QD doped tandem LSC and b) the spectra of QDs used in each layer. Reprinted with permission from Ref [94], copyright © 2018 Springer Nature.

1.4 The donor-emitter fluorophore pair system

The donor-emitter fluorophore pair system in LSCs has been considered as an effective approach to reduce photon losses via the re-absorption effect.[45, 55, 100-101] The energy donor can harvest sunlight and transfer the energy to the emitter, the emitter then emits the light into the waveguide of the LSC. This is a biomimetic process inspired by the light-harvesting antenna of natural photosynthesis.

1.4.1 Artificial photosynthesis and light-harvesting antenna*

Photosynthesis refers to the process in which the sunlight is captured and stored by an organism, and the stored energy can be used to drive energy-requiring cellular processes.[102-104] Photosynthesis can convert solar energy to chemical energy (Figure 1.14a). There are four steps in a typical natural photosynthetic process, which are the energy collection, primary photochemistry, stabilization by secondary reactions and the synthesis of stable products. Although the detailed photosynthetic mechanism is different between species, most of the process starts with the solar light being absorbed by a type of protein complex called the light-harvesting antenna complex.[105] This complex usually consists of proteins and light-harvesting pigments that surround the photosynthetic reaction center (Figure 1.14b).[106] The entire system is called the photosynthetic unit. The light-harvesting antenna increases the absorption cross section of the reaction center. When the light is absorbed by the pigments located on the antenna complex, the energy transfers through different pigment molecules, in a process called energy migration, to the photosynthetic reaction center, where the primary photochemical reaction steps occur. Ultimately the chemical energy produced is temporarily stored in adenosine triphosphate (ATP) and later in glucose.

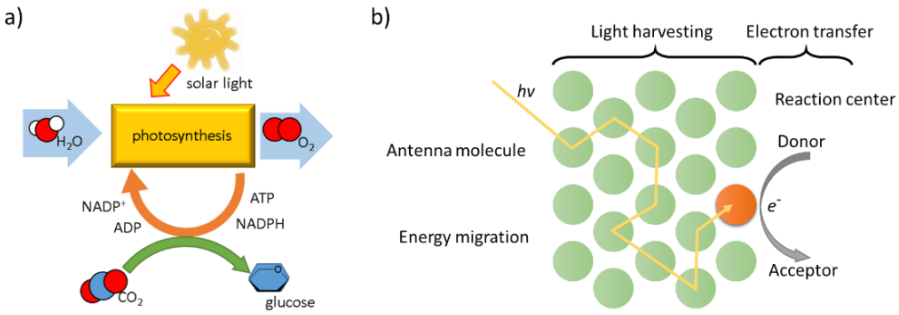

Figure 1.14 The illustration of a) photosynthetic process and b) energy migration in a light-harvesting antenna. Reprinted with permission from Ref [2], copyright © 2019 Springer Nature.

* This section has been published elsewhere by the author.[2] Reprinted with permission from Ref [2], copyright © 2019 Springer Nature.

The light-harvesting antenna component of photosynthesis is remarkably efficient given the number of pigments involved. Both the energy cascade and the spatial arrangement of the chromophores are established to allow energy to funnel efficiently to the reaction center. Therefore, it is a great challenge to mimic photosynthesis in artificial photosynthetic systems. To better understand how to design new light-harvesting materials, a critical aspect to consider is the mechanism of energy transfer in light-harvesting arrays.

Looking more closely at the energy transfer processes in natural photosynthesis, the light-harvesting antenna system containing many chromophore molecules surrounds the reaction center acting as an energy funnel. Once a photon is absorbed, the energy has to be transferred via a large number of chromophores before reaching the reaction center. This energy transfer process can proceed through a variety and combination of mechanisms, including Förster resonance energy transfer (FRET), Dexter energy transfer, exciton coupling, and quantum coherence, depending on the molecular distance, orientations and the photophysical properties of the chromophores. Among the possible mechanisms, the FRET process has been well studied from many aspects in both natural and synthetic systems.[103, 107] In general, to allow exciton hopping, the FRET process requires the appropriate alignment of energy levels of the energy-donating and the energy-accepting molecules. A resonance interaction of transition dipoles of the molecules is also necessary for energy transfer via FRET. However, with correct energy level alignment and relative molecular orientation, FRET allows relatively long through-space energy transfer distances in the nanometer range. The FRET critical radius (R_0, nm) refers to the molecular distance where the efficiency of FRET is 50%. R_0 is defined via the following Förster equation:[108-109]

$$R_0 = 0.02108 \times \left(\frac{\kappa^2 \Phi_{PL} J}{n^4}\right)^{\frac{1}{6}} \quad (1\text{-}17)$$

$$J = \int \varepsilon_A(\lambda) F_D(\lambda) \lambda^4 \, d\lambda \quad (1\text{-}18)$$

where κ^2 is the orientation factor (κ^2 = 2/3 for a randomly-oriented long lifetime donor-acceptor system), Φ_{PL} refers to the photoluminescence quantum efficiency of the donor chromophore in the absence of the acceptor, J(nm^{4}M^{-1}cm^{-1}) is the overlap integral which can be calculated from the overlap between the normalized (area) emission spectrum (F_D) of the donor and the acceptor absorption spectrum expressed as the extinction coefficient (ε_A), λ is the wavelength over the full spectrum, and n is the refractive index of the matrix material. It is worth mentioning that this equation can describe both single and multi-chromophore systems. According to the above equation, the FRET process is highly dependent on the donor-to-acceptor energy levels overlap (J), ϕ_{PL} of chromophores and the concentration of the chromophores (average molecular distance should be smaller than R_0 for efficient transfer). The overlap of the energy levels can be easily tuned by varying the donor or acceptor chromophores.

1.4.2 The donor-emitter fluorophore pairs in LSCs

Combinations of dyes with the appropriate alignment of the absorption and emission energies have been used to improve LSC performance.[110] Using multiple chromophores can increase spectral coverage of LSCs as well as reduce emission re-absorption.[111] To reduce re-absorption, the approach is to use a blend of at least two chromophores that can form a donor-emitter FRET pair. The donor dye molecules are usually the dominant species to capture the incident light, while the emitters are used in a much smaller amount to ensure there is only minimal reabsorption by the acceptor molecules (Figure 1.15a). Once the incident light is absorbed by the donor, the excited molecules transfer the energy to the acceptors via the FRET process and the acceptors re-emit the light. Therefore, the overall spectrum of the blend reveals mainly the donor's absorption and the emitter's emission spectra and leads to an increased total Stokes shift. This donor-emitter blend approach provides a constructive method to modify both the absorption and emission spectra of LSC devices. However, it requires a high concentration of the chromophores to provide efficient energy transfer with an average intermolecular distance of no more than a few

nanometers for efficient FRET. Therefore, this approach should only be used in thin-film LSC devices and most chromophores which undergo ACQ are not suitable (Figure 1.15b).

Besides the donor-to-emitter FRET, the energy transfer within the donor materials, the so-called energy migration, is another important criterion of the donor-emitter fluorophore pair system (Figure 1.15b). The FRET efficiency highly depends on the distance between the donor and the emitter. If the FRET occurs among the highly concentrated donors, the exciton diffusion length can be greatly increased, leading to a better chance for the donor exciton to meet the emitters. In short, via the energy migration process, the emission from the donor can be quenched by less of the emitter, further reducing the over-all re-absorption.

It should be noted that the FRET pathway from the donor to the emitter is a competitive process to other non-radiative pathways of the donor material. As a consequence, the energy losses from the donors can be efficiently reduced by adding the emitters, which can increase the over-all Φ_{PL} in comparison to the donor-only samples.

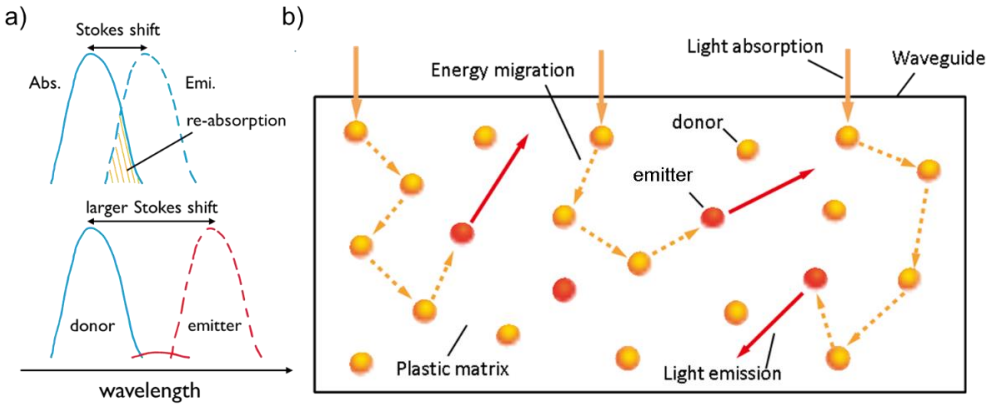

Figure 1.15 a) the spectral overlap in a single-fluorophore system can be reduced by a donor-emitter fluorophore pair system, resulting in a reduced re-absorption effect. The solid curve and dash curve represent the absorption and emission respectively. b) an example of the donor-emitter fluorophore pair with a higher concentration of the donor and a lower concentration of the emitter in a plastic matrix.

There have been already several examples of successfully using a donor-emitter fluorophore pair in LSCs. In 2007, Wittmershaus et. al. reported a LSC based on a three-dye system.[112] In their devices, the three fluorophores all absorbed light strongly, but the energy was ultimately emitted by the fluorophore with the lowest energy gap. Although the three-dye system was not designed for reducing the re-absorption effect, the absorbed light did downshift from the two donors to the emitter via FRET very efficiently. The current output of the reported LSC based-on the three-dye system was much higher in comparison to the single-dye LSCs, due to the broader absorption of the dye mixture. In 2008, Baldo et.al. reported a tandem LSC,[55] showing 6.1% PCE at G = 45, which was a benchmarked record at the time. A molecular donor-emitter fluorophore pair, rubrene and DCJTB respectively (Figure 1.7), was used in the top layer to provide a large over-all Stokes shift via the FRET process (Figure 1.16). In the bottom layer, a phosphorescent emitter, Pt(TPBP) (Figure 1.7), was used, which also showed a large Stokes shift due to the intersystem crossing. Consequently, the energy losses via the re-absorption effect were minimized from both layers of the tandem LSC, leading to less PCE reduction with increasing G. In 2017, Greenham et. al. reported a star-shaped donor-emitter fluorophore system[113] consisting of three oligofluorene side chains linked to a boron-dipyrromethene core (Figure 1.17). Working as light harvesting antennas, the oligofluorenes can absorb the incident light from different directions and transfer the energy to the boron-dipyrromethene core. By changing the number of the repeating units in the oligofluorene side chain, they can tune the donor-to-emitter ratio that kept the supramolecule with low overlap between the absorption and emission spectra. In their hypothesis, if the boron-dipyrromethene complex can be coupled to a deep red emitter, the emission of the over-all fluorophore can be red-shifted from 600 nm to 750 nm, further reducing the re-absorption effect.

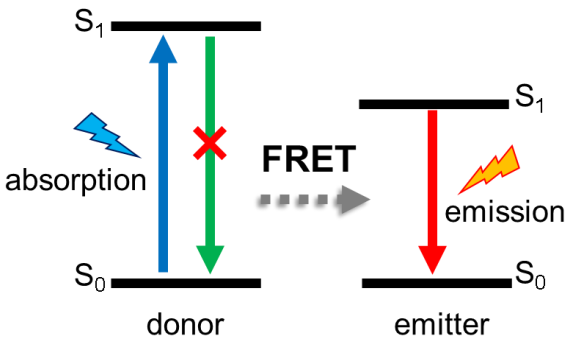

Figure 1.16 A scheme of the FRET between the donor and the emitter leading to a large Stokes shift. The donor absorbs light, while the emitter quenches the fluorescence from the donor and re-emits the light.

Previous studies by our research group also suggested that the donor-emitter fluorophore pair system can efficiently enhance the performance of LSCs.[2]* In 2014, the photophysical properties of a pair of small-molecule fluorophores[114] were first characterized in our lab as a donor-emitter pair system and the performance of a LSC based on this fluorophore pair was further examined. An AIE energy donor, DPATPAN, was used with a commercially available laser dye, DCJTB, as the energy acceptor and emitter in LSC devices (Figure 1.17).[67] DPATPAN ($\lambda_{abs} = 390\,nm$, $\lambda_{em} = 550\,nm$) is a typical AIE material which showed >90% ϕ_{PL} in PMMA matrix when dilute (less than 10% w/w) and still maintained close to 90% Φ_{PL} at high concentration (50% w/w). On the other hand, the acceptor DCJTB ($\lambda_{abs} = 500\,nm,\ \lambda_{em} = 610\,nm$) is a typical organic dye that shows the ACQ effect, with unity ϕ_{PL} at low concentration and rapidly decreasing ϕ_{PL} at increasing concentration (80% ϕ_{PL} at 1% w/w in PMMA). It was demonstrated that at the donor-acceptor molar ratio of 99:1, the emission of the donor was fully quenched by the acceptor. The overall ϕ_{PL} of the chromophore blend remained at above 90% while the Stokes shift increased

* This section has been published elsewhere by the author.[2] Reprinted with permission from Ref [2], copyright © 2019 Springer Nature.

from about 50 nm to 190 nm, leading to the simulated OQE of the LSC reaching 50% at G = 50. Extensive studies of an AIE FRET pair is described in **Chapter III** of the thesis.

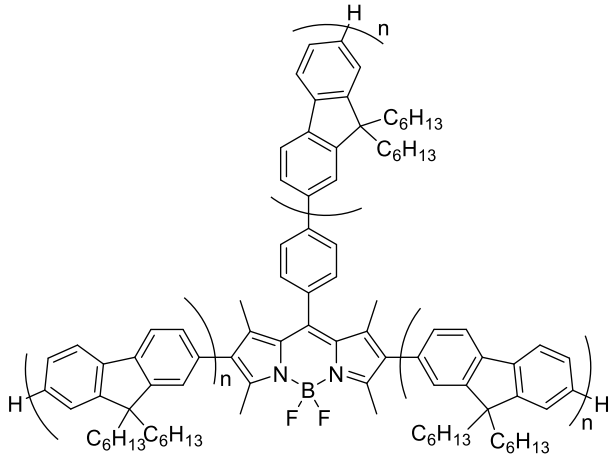

borondipyrromethene with three oligofluorenes

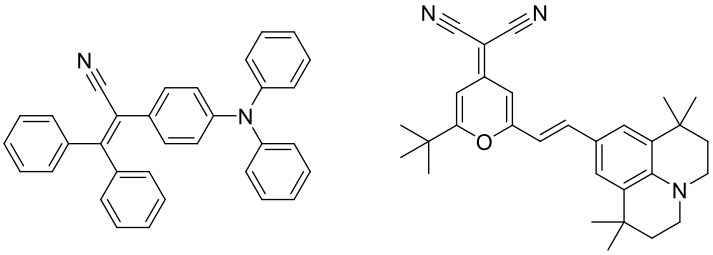

DPATPAN DCJTB

Figure 1.17 The chemical structure of the boron-dipyrromethene with three oligofluorenes, the AIE fluorophore DPATPAN and the commercial laser-dye DCJTB.

Another donor-emitter fluorophore pair system was reported by our group in 2016. In this work, a molecular insulated PDI was designed and synthesized as the energy donor, and paired with a commercial PDI fluorophore for the FRET pair.[115] The molecular insulation increased the ϕ_{PL} of the donor PDI in high fluorophore concentration, leading to an improved overall ϕ_{PL} of the donor-emitter pair. The resulting LSC showed remarkable performance due to the high ϕ_{PL} and reduced re-absorption effect. An extensive study of a molecularly insulated PDI as a donor in a FRET pair is described in **Chapter IV**.

The above-mentioned research strongly suggested that the donor-emitter fluorophore pair system can help to enhance ϕ_{PL} and reduce the re-absorption of the LSCs. However, there are limitations of the donor-emitter fluorophore pair system, such as the ACQ effect and the escape cone loss that requires further research to solve.

1.5 Thesis outline

The research in this thesis mainly focuses on studies of donor-emitter fluorophore pair systems and their applications in LSCs. The advantages of donor-emitter fluorophore pair systems are discussed in detail through the following chapters which cover aspects of materials design and synthesis, photophysical properties characterization and device fabrication.

The overall question addressed in this thesis is: **'How can the performance of a LSC be improved by using a donor-emitter fluorophore pair system?**'. The overall thesis question can be sub-divided into three secondary thesis questions, namely:

1. What makes a good LSC?

2. How can materials be optimized to produce an efficient donor-emitter fluorophore system?

3. What is the optimum device design for a LSC based on a donor-emitter fluorophore pair system?

The three sub-thesis questions are addressed sequentially. The targets of this thesis are to understand the parameters controlling the light harvesting performance of LSCs, to understand the donor-emitter fluorophore pair system, and to fabricate LSCs with a donor-emitter pair. The first thesis question is addressed in **Chapter I**.

In **Chapter II**, the general methodology and experimental approaches used/developed in the thesis are described, and includes information on fluorophore synthesis, device fabrication and spectroscopy analysis.

In **Chapter III**, a donor-emitter fluorophore pair consisting of two AIE materials were fully studied to overcome the re-absorption effects typically found for single fluorophore LSCs. As the FRET process usually requires the fluorophores in a high concentration, the AIE materials can provide some resistance to the ACQ effect and allowed the overall ϕ_{PL} of the donor-emitter pair to remain high at high concentration. This chapter focuses on the influence of the AIE effect on re-absorption and the overall ϕ_{PL} of the fluorophore pairs, and their overall impact on LSC performance. The second thesis question is addressed in this chapter.

In **Chapter IV**, a series of molecularly insulated PDI derivatives were designed and synthesized to further reduce the ACQ effect on the donor-emitter fluorophore pair system. The bulky-substituents were installed at the imide-position of the perylene core to introduce steric-hindrance but leaving the photophysical properties of the PDI unaffected. The ACQ tolerance of the PDIs was enhanced by increasing the bulkiness of the substituents, leading to above 90% ϕ_{PL} of the PDIs at 120 mM in a PMMA matrix. The champion PDI was blended with a commercial PDI fluorophore to form the donor-emitter pair. The OQE of the resulting LSC was very promising, due to the low-level re-absorption effect and the very high overall ϕ_{PL} of the PDI fluorophore pair. The second thesis question is addressed in this chapter.

Inspired by the outcomes of Chapter IV, a large-area printed LSC based on the PDI fluorophore pair is described in **Chapter V**. The re-optimized PDI donor-emitter fluorophore pair system was used to print a 20 cm × 20 cm area LSC via the doctor blading process. The effects of the waveguide matrix materials and coupled solar cells were also examined. By optimizing the choice of the donor-emitter pair, the matrix material, the solar cells and the printing process, a benchmark large-area LSC is described in this chapter. The third thesis question is addressed in this chapter.

In **Chapter VI**, diphenyl anthracene derivatives were designed and synthesized to investigate the concept of selective alignment of a donor-emitter fluorophore pair on improving the collection

efficiency of LSCs. A liquid crystal polymer matrix was used to align the rod-shaped emitter perpendicular to the waveguide surface via the self-assembling process to confine the re-emitted light in the preferred angle for light collection. By tuning the substituents, the ellipsoid-shaped donor remained in a random orientation in the liquid crystal polymer matrix to avoid any decrease in light absorption. The selectively aligned donor-emitter system allowed the LSC to harvest light normally but emitted light parallel to the waveguide, leading to reduced escape cone losses and a higher OQE. The second thesis question is addressed in this chapter.

Chapter VII summarizes the key achievements of the thesis and provides some guidance for future work.

Reference:

1. Pieper, A.; Hohgardt, M.; Willich, M.; Gacek, D. A.; Hafi, N.; Pfennig, D.; Albrecht, A.; Walla, P. J., Biomimetic Light-Harvesting Funnels for Re-Directioning of Diffuse Light. *Nat. Comm.* **2018,** *9* (1), 666.
2. Zhang, B.; Gao, C.; Saker Neto, N.; Wong, W. W. H., Aggregation-Induced Emitters in Light Harvesting. In *Principles and Applications of Aggregation-Induced Emission*, Tang, Y.; Tang, B. Z., Eds. Springer International Publishing: Cham, 2019; pp 479-504.
3. Horace De Saussure and His Hot Boxes of the 1700's. http://www.solarcooking.org/saussure.htm (accessed 27 February 2018).
4. Medintz, I.; Hildebrandt, N., *Fret-Förster Resonance Energy Transfer: From Theory to Applications*. John Wiley & Sons: Hoboken, 2013.
5. Becquerel, A.-E., Recherches Sur Les Effets De La Radiation Chimique De La Lumiere Solaire Au Moyen Des Courants Electriques. *CR Acad. Sci.* **1839,** *9* (145), 1.
6. Fritts, C. E., On a New Form of Selenium Cell, and Some Electrical Discoveries Made by Its Use. *Am. J. Sci.* **1883,** (156), 465-472.
7. Chapin, D. M.; Fuller, C. S.; Pearson, G. L. Solar Energy Converting Apparatus. US Patent 2780765A, 1957.
8. McKenna, B.; Evans, R. C., Towards Efficient Spectral Converters through Materials Design for Luminescent Solar Devices. *Adv. Mater.* **2017,** *29* (28), 1606491.
9. Shockley, W.; Queisser, H. J., Detailed Balance Limit of Efficiency of P-N Junction Solar Cells. *J. Appl. Phys.* **1961,** *32* (3), 510-519.
10. Rühle, S., Tabulated Values of the Shockley–Queisser Limit for Single Junction Solar Cells. *Solar Energy* **2016,** *130*, 139-147.
11. Würfel, P., Limitations on Energy Conversion in Solar Cells. In *Physics of Solar Cells*, Wiley-VCH Verlag GmbH: 2005; pp 137-153.
12. Powell, K. M.; Rashid, K.; Ellingwood, K.; Tuttle, J.; Iverson, B. D., Hybrid Concentrated Solar Thermal Power Systems: A Review. *Renew. Sust. Energy Rev.* **2017,** *80*, 215-237.
13. Chow, T. T., A Review on Photovoltaic/Thermal Hybrid Solar Technology. *Appl. Energy* **2010,** *87* (2), 365-379.
14. Lamba, R.; Kaushik, S. C., Modeling and Performance Analysis of a Concentrated Photovoltaic–

Thermoelectric Hybrid Power Generation System. *Energy Convers. Manage.* **2016,** *115*, 288-298.
15. Sharaf, O. Z.; Orhan, M. F., Concentrated Photovoltaic Thermal (Cpvt) Solar Collector Systems: Part I – Fundamentals, Design Considerations and Current Technologies. *Renew. Sust. Energy Rev.* **2015,** *50*, 1500-1565.
16. Chemisana, D., Building Integrated Concentrating Photovoltaics: A Review. *Renew. Sust. Energy Rev.* **2011,** *15* (1), 603-611.
17. Kong, C.; Xu, Z.; Yao, Q., Outdoor Performance of a Low-Concentrated Photovoltaic–Thermal Hybrid System with Crystalline Silicon Solar Cells. *Appl. Energy* **2013,** *112*, 618-625.
18. Rühle, S., Tabulated Values of the Shockley–Queisser Limit for Single Junction Solar Cells. *Sol. Energy* **2016,** *130* (Phys. E 14 2002), 139-147.
19. Xie, W. T.; Dai, Y. J.; Wang, R. Z.; Sumathy, K., Concentrated Solar Energy Applications Using Fresnel Lenses: A Review. *Renew. Sust. Energy Rev.* **2011,** *15* (6), 2588-2606.
20. Debije, M. G.; Verbunt, P. P. C., Thirty Years of Luminescent Solar Concentrator Research: Solar Energy for the Built Environment. *Adv. Energy Mater.* **2012,** *2* (1), 12-35.
21. Klampaftis, E.; Ross, D.; McIntosh, K. R.; Richards, B. S., Enhancing the Performance of Solar Cells Via Luminescent Down-Shifting of the Incident Spectrum: A Review. *Sol. Energy Mater. Sol. Cells* **2009,** *93* (8), 1182-1194.
22. van Sark, W. G.; Barnham, K. W. J.; Slooff, L. H., Luminescent Solar Concentrators-a Review of Recent Results. *Opt. Express* **2008,** *16* (26), 21773-21792.
23. Banal, J. L.; Zhang, B.; Jones, D. J.; Ghiggino, K. P.; Wong, W. W., Emissive Molecular Aggregates and Energy Migration in Luminescent Solar Concentrators. *Acc. Chem. Res.* **2017,** *50* (1), 49-57.
24. Caspar, J. V.; Meyer, T. J., Application of the Energy-Gap Law to Nonradiative, Excited-State Decay. *J. Phys. Chem.* **1983,** *87* (6), 952-957.
25. Lin, S. H., Energy Gap Law and Franck–Condon Factor in Radiationless Transitions. *J. Chem. Phys.* **1970,** *53* (9), 3766-3767.
26. Englman, R.; Jortner, J., The Energy Gap Law for Radiationless Transitions in Large Molecules. *Mol. Phys.* **1970,** *18* (2), 145-164.
27. Herrmann, A.; Müllen, K., From Industrial Colorants to Single Photon Sources and Biolabels: The Fascination and Function of Rylene Dyes. *Chem. Lett.* **2006,** *35* (9), 978-985.
28. Zhao, X.; Xiong, Y.; Ma, J.; Yuan, Z., Rylene and Rylene Diimides: Comparison of Theoretical and Experimental Results and Prediction for High-Rylene Derivatives. *J. Phys. Chem. A* **2016,** *120* (38), 7554-7560.
29. Tummeltshammer, C.; Taylor, A.; Kenyon, A. J.; Papakonstantinou, I., Losses in Luminescent Solar Concentrators Unveiled. *Sol. Energy Mater. Sol. Cells* **2016,** *144*, 40-47.
30. Debije, M. G.; Verbunt, P. P.; Rowan, B. C.; Richards, B. S.; Hoeks, T. L., Measured Surface Loss from Luminescent Solar Concentrator Waveguides. *Appl. Opt.* **2008,** *47* (36), 6763-8.
31. McDowall, S.; Butler, T.; Bain, E.; Scharnhorst, K.; Patrick, D., Comprehensive Analysis of Escape-Cone Losses from Luminescent Waveguides. *Appl. Opt.* **2013,** *52* (6), 1230-1239.
32. Shurcliff, W. A., Radiance Amplification by Multi-Stage Fluorescence System. *J. Opt. Soc. Am.* **1951,** *41* (3), 209.
33. Weber, W. H.; Lambe, J., Luminescent Greenhouse Collector for Solar Radiation. *Appl. Opt.* **1976,** *15* (10), 2299-300.
34. Swartz, B. A.; Cole, T.; Zewail, A. H., Photon Trapping and Energy Transfer in Multiple-Dye Plastic Matrices: An Efficient Solar-Energy Concentrator. *Opt. Lett.* **1977,** *1* (2), 73-5.
35. Goetzberger, A.; Wittwer, V., Fluorescent Planar Collector-Concentrators: A Review. *Solar Cells* **1981,** *4* (1), 3-23.
36. Banal, J. L.; White, J. M.; Lam, T.; Blakers, A. W.; Ghiggino, K. P.; Wong, W. W. H., A Transparent Planar Concentrator Using Aggregates of Gem‐Pyrene Ethenes. *Adv. Energy Mater.* **2015,** *5* (19), 1500818.
37. Zhao, Y.; Meek, G. A.; Levine, B. G.; Lunt, R. R., Near‐Infrared Harvesting Transparent Luminescent Solar Concentrators. *Adv. Opt. Mater.* **2014,** *2* (7), 606-611.
38. Zhao, Y.; Lunt, R. R., Transparent Luminescent Solar Concentrators for Large-Area Solar Windows Enabled by Massive Stokes-Shift Nanocluster Phosphors. *Adv. Energy Mater.* **2013,** *3* (9), 1143-1148.

39. Meinardi, F.; Bruni, F.; Brovelli, S., Luminescent Solar Concentrators for Building-Integrated Photovoltaics. *Nat. Rev. Mater.* **2017,** *2*, 17072.
40. Aste, N.; Buzzetti, M.; Pero, D. C.; Fusco, R.; Testa, D.; Leonforte, F., Visual Performance of Yellow, Orange and Red Lscs Integrated in a Smart Window. *Energy Procedia* **2017,** *105*, 967-972.
41. Kanellis, M.; de Jong, M. M.; Slooff, L.; Debije, M. G., The Solar Noise Barrier Project: 1. Effect of Incident Light Orientation on the Performance of a Large-Scale Luminescent Solar Concentrator Noise Barrier. *Renew. Energy* **2017,** *103*, 647-652.
42. Debije, M. G.; Tzikas, C.; Rajkumar, V. A.; de Jong, M. M., The Solar Noise Barrier Project: 2. The Effect of Street Art on Performance of a Large Scale Luminescent Solar Concentrator Prototype. *Renew. Energy* **2017,** *113*, 1288-1292.
43. Debije, M. G.; Tzikas, C.; de Jong, M. M.; Kanellis, M.; Slooff, L. H., The Solar Noise Barrier Project: 3. The Effects of Seasonal Spectral Variation, Cloud Cover and Heat Distribution on the Performance of Full-Scale Luminescent Solar Concentrator Panels. *Renew. Energy* **2018,** *116*, 335-343.
44. Vasiliev, M.; Alameh, K.; Nur-E-Alam, M., Spectrally-Selective Energy-Harvesting Solar Windows for Public Infrastructure Applications. *Appl. Sci.* **2018,** *8* (6), 849.
45. Gutierrez, G. D.; Coropceanu, I.; Bawendi, M. G.; Swager, T. M., A Low Reabsorbing Luminescent Solar Concentrator Employing Π-Conjugated Polymers. *Adv. Mater.* **2016,** *28* (3), 497-501.
46. Meinardi, F.; McDaniel, H.; Carulli, F.; Colombo, A.; Velizhanin, K. A.; Makarov, N. S.; Simonutti, R.; Klimov, V. I.; Brovelli, S., Highly Efficient Large-Area Colourless Luminescent Solar Concentrators Using Heavy-Metal-Free Colloidal Quantum Dots. *Nat. Nanotechnol.* **2015,** *10* (10), 878-885.
47. Xu, J.; Zhang, B.; Jansen, M.; Goerigk, L.; Wong, W. W. H.; Ritchie, C., Highly Fluorescent Pyridinium Betaines for Light Harvesting. *Angew. Chem. Int. Ed.* **2017,** *56* (44), 13882-13886.
48. McKenna, B.; Evans, R. C., Towards Efficient Spectral Converters through Materials Design for Luminescent Solar Devices. *Adv. Mater.* **2017,** *29* (28), 1606491.
49. Haines, C.; Chen, M.; Ghiggino, K. P., The Effect of Perylene Diimide Aggregation on the Light Collection Efficiency of Luminescent Concentrators. *Sol. Energy Mater. Sol. Cells* **2012,** *105*, 287-292.
50. Benjamin, W. E.; Veit, D. R.; Perkins, M. J.; Bain, E.; Scharnhorst, K.; McDowall, S.; Patrick, D. L.; Gilbertson, J. D., Sterically Engineered Perylene Dyes for High Efficiency Oriented Fluorophore Luminescent Solar Concentrators. *Chem. Mater.* **2014,** *26* (3), 1291-1293.
51. Drake, J. M.; Lesiecki, M. L.; Sansregret, J.; Thomas, W. R. L., Organic Dyes in Pmma in a Planar Luminescent Solar Collector: A Performance Evaluation. *Appl. Opt.* **1982,** *21* (16), 2945-2952.
52. Sansregret, J.; Drake, J. M.; Thomas, W. R. L.; Lesiecki, M. L., Light Transport in Planar Luminescent Solar Concentrators: The Role of Dcm Self-Absorption. *Appl. Opt.* **1983,** *22* (4), 573-577.
53. Mugnier, J.; Dordet, Y.; Pouget, J.; Le Bris, M. T.; Valeur, B., Performances of Fluorescent Solar Concentrators Doped with a New Dye (Benzoxazinone Derivative). *Sol. Energy Mater.* **1987,** *15* (2), 65-75.
54. Mulder, C. L.; Reusswig, P. D.; Beyler, A. P.; Kim, H.; Rotschild, C.; Baldo, M. A., Dye Alignment in Luminescent Solar Concentrators: Ii. Horizontal Alignment for Energy Harvesting in Linear Polarizers. *Opt. Express* **2010,** *18* (9), 9.
55. Currie, M. J.; Mapel, J. K.; Heidel, T. D.; Goffri, S.; Baldo, M. A., High-Efficiency Organic Solar Concentrators for Photovoltaics. *Science* **2008,** *321* (5886), 226-228.
56. Debije, M. G., Solar Energy Collectors with Tunable Transmission. *Adv. Funct. Mater.* **2010,** *20* (9), 1498-1502.
57. Verbunt, P. P. C.; Kaiser, A.; Hermans, K.; Bastiaansen, C. W. M.; Broer, D. J.; Debije, M. G., Controlling Light Emission in Luminescent Solar Concentrators through Use of Dye Molecules Aligned in a Planar Manner by Liquid Crystals. *Adv. Funct. Mater.* **2009,** *19* (17), 2714-2719.
58. Sheng, X.; Shen, L.; Kim, T.; Li, L.; Wang, X.; Dowdy, R.; Froeter, P.; Shigeta, K.; Li, X.; Nuzzo, R. G.; Giebink, N. C.; Rogers, J. A., Doubling the Power Output of Bifacial Thin-Film Gaas Solar Cells by Embedding Them in Luminescent Waveguides. *Adv. Energy Mater.* **2013,** *3* (8), 991-996.
59. Meazzini, I.; Blayo, C.; Arlt, J.; Marques, A.-T.; Scherf, U.; Burrows, H. D.; Evans, R. C., Ureasil

Organic–Inorganic Hybrids as Photoactive Waveguides for Conjugated Polyelectrolyte Luminescent Solar Concentrators. *Mater. Chem. Front.* **2017,** *1* (11), 2271-2282.
60. Nolasco, M. M.; Vaz, P. M.; Freitas, V. T.; Lima, P. P.; Andre, P. S.; Ferreira, R. A. S.; Vaz, P. D.; Ribeiro-Claro, P.; Carlos, L. D., Engineering Highly Efficient Eu(Iii)-Based Tri-Ureasil Hybrids toward Luminescent Solar Concentrators. *J. Mater. Chem. A* **2013,** *1* (25), 7339-7350.
61. Altan Bozdemir, O.; Erbas‐Cakmak, S.; Ekiz, O. O.; Dana, A.; Akkaya, E. U., Towards Unimolecular Luminescent Solar Concentrators: Bodipy‐Based Dendritic Energy‐Transfer Cascade with Panchromatic Absorption and Monochromatized Emission. *Angew. Chem. Int. Ed.* **2011,** *50* (46), 10907-10912.
62. Wang, T.; Zhang, J.; Ma, W.; Luo, Y.; Wang, L.; Hu, Z.; Wu, W.; Wang, X.; Zou, G.; Zhang, Q., Luminescent Solar Concentrator Employing Rare Earth Complex with Zero Self-Absorption Loss. *Sol. Energy* **2011,** *85* (11), 2571-2579.
63. Teotonio, E. E. S.; Fett, G. M.; Brito, H. F.; Faustino, W. M.; de Sa, G. F.; Felinto, M. C. F. C.; Santos, R. H. A., Evaluation of Intramolecular Energy Transfer Process in the Lanthanide(Iii) Bis- and Tris-(Tta) Complexes: Photoluminescent and Triboluminescent Behavior. *J. Lumin.* **2008,** *128* (2), 190-198.
64. Mei, J.; Hong, Y.; Lam, J. W.; Qin, A.; Tang, Y.; Tang, B. Z., Aggregation-Induced Emission: The Whole Is More Brilliant Than the Parts. *Adv. Mater.* **2014,** *26* (31), 5429-79.
65. Mei, J.; Leung, N. L.; Kwok, R. T.; Lam, J. W.; Tang, B. Z., Aggregation-Induced Emission: Together We Shine, United We Soar! *Chem. Rev.* **2015,** *115* (21), 11718-940.
66. Shi, J.; Chang, N.; Li, C.; Mei, J.; Deng, C.; Luo, X.; Liu, Z.; Bo, Z.; Dong, Y. Q.; Tang, B. Z., Locking the Phenyl Rings of Tetraphenylethene Step by Step: Understanding the Mechanism of Aggregation-Induced Emission. *Chem. Commun.* **2012,** *48* (86), 10675-7.
67. Banal, J. L.; Ghiggino, K. P.; Wong, W. W., Efficient Light Harvesting of a Luminescent Solar Concentrator Using Excitation Energy Transfer from an Aggregation-Induced Emitter. *Phys. Chem. Chem. Phys.* **2014,** *16* (46), 25358-63.
68. Iasilli, G.; Battisti, A.; Tantussi, F.; Fuso, F.; Allegrini, M.; Ruggeri, G.; Pucci, A., Aggregation-Induced Emission of Tetraphenylethylene in Styrene-Based Polymers. *Macromol. Chem. Phys.* **2014,** *215* (6), 499-506.
69. Banal, J. L.; White, J. M.; Ghiggino, K. P.; Wong, W. W., Concentrating Aggregation-Induced Fluorescence in Planar Waveguides: A Proof-of-Principle. *Sci. Rep.* **2014,** *4*, 4635.
70. De Nisi, F.; Francischello, R.; Battisti, A.; Panniello, A.; Fanizza, E.; Striccoli, M.; Gu, X.; Leung, N. L. C.; Tang, B. Z.; Pucci, A., Red-Emitting Aiegen for Luminescent Solar Concentrators. *Mater. Chem. Front.* **2017,** *1* (7), 1406-1412.
71. Valeur, B.; Berberan-Santos, M., *Molecular Fluorescence: Principles and Applications*. John Wiley & Sons: 2012.
72. Minei, P.; Fanizza, E.; Rodríguez, A. M.; Muñoz-García, A. B.; Cimino, P.; Pavone, M.; Pucci, A., Cost-Effective Solar Concentrators Based on Red Fluorescent Zn(Ii)–Salicylaldiminato Complex. *RSC Adv.* **2016,** *6* (21), 17474-17482.
73. Lucarelli, J.; Lessi, M.; Manzini, C.; Minei, P.; Bellina, F.; Pucci, A., "N-Alkyl Diketopyrrolopyrrole-Based Fluorophores for Luminescent Solar Concentrators: Effect of the Alkyl Chain on Dye Efficiency". *Dyes Pigm.* **2016,** *135*, 154-162.
74. Carlotti, M.; Fanizza, E.; Panniello, A.; Pucci, A., A Fast and Effective Procedure for the Optical Efficiency Determination of Luminescent Solar Concentrators. *Solar Energy* **2015,** *119*, 452-460.
75. Mori, R.; Iasilli, G.; Lessi, M.; Muñoz-García, A. B.; Pavone, M.; Bellina, F.; Pucci, A., Luminescent Solar Concentrators Based on Pmma Films Obtained from a Red-Emitting Atrp Initiator. *Polym. Chem.* **2018**.
76. Banal, J. L.; White, J. M.; Lam, T. W.; Blakers, A. W.; Ghiggino, K. P.; Wong, W. W. H., A Transparent Planar Concentrator Using Aggregates Ofgem-Pyrene Ethenes. *Adv. Energy Mater.* **2015,** *5* (19), 1500818.
77. Hu, R.; Gomez-Duran, C. F.; Lam, J. W.; Belmonte-Vazquez, J. L.; Deng, C.; Chen, S.; Ye, R.; Pena-Cabrera, E.; Zhong, Y.; Wong, K. S.; Tang, B. Z., Synthesis, Solvatochromism, Aggregation-Induced Emission and Cell Imaging of Tetraphenylethene-Containing Bodipy Derivatives with Large Stokes Shifts. *Chem. Commun.* **2012,** *48* (81), 10099-101.
78. Chen, S.; Liu, J.; Liu, Y.; Su, H.; Hong, Y.; Jim, C. K. W.; Kwok, R. T. K.; Zhao, N.; Qin, W.; Lam,

J. W. Y.; Wong, K. S.; Tang, B. Z., An Aie-Active Hemicyanine Fluorogen with Stimuli-Responsive Red/Blue Emission: Extending the Ph Sensing Range by “Switch + Knob” Effect. *Chem. Sci.* **2012,** *3* (6), 1804-1809.

79. Zhang, J.; Chen, R.; Zhu, Z.; Adachi, C.; Zhang, X.; Lee, C. S., Highly Stable near-Infrared Fluorescent Organic Nanoparticles with a Large Stokes Shift for Noninvasive Long-Term Cellular Imaging. *ACS Appl. Mater. Interfaces* **2015,** *7* (47), 26266-74.
80. Zhu, M.; Zhuo, Y.; Cai, K.; Guo, H.; Yang, F., Novel Fluorescent Perylene Liquid Crystal with Diphenylacrylonitrile Groups: Observation of a Large Pseudo Stokes Shift Based on Aie and Fret Effects. *Dyes Pigm.* **2017,** *147*, 343-349.
81. Zhao, Q.; Zhang, X. A.; Wei, Q.; Wang, J.; Shen, X. Y.; Qin, A.; Sun, J. Z.; Tang, B. Z., Tetraphenylethene Modified Perylene Bisimide: Effect of the Number of Substituents on Aie Performance. *Chem. Commun.* **2012,** *48* (95), 11671-3.
82. Zhao, Q.; Zhang, S.; Liu, Y.; Mei, J.; Chen, S.; Lu, P.; Qin, A.; Ma, Y.; Sun, J. Z.; Tang, B. Z., Tetraphenylethenyl-Modified Perylene Bisimide: Aggregation-Induced Red Emission, Electrochemical Properties and Ordered Microstructures. *J. Mater. Chem.* **2012,** *22* (15), 7387-7394.
83. Moraitis, P.; Schropp, R. E. I.; van Sark, W. G. J. H. M., Nanoparticles for Luminescent Solar Concentrators - a Review. *Opt. Mater.* **2018,** *84*, 636-645.
84. Barnham, K.; Marques, J.; Hassard, J.; O’Brien, P., Quantum-Dot Concentrator and Thermodynamic Model for the Global Redshift. *Appl. Phys. Lett.* **2000,** *76* (9), 1197-1199.
85. Meinardi, F.; Colombo, A.; Velizhanin, K. A.; Simonutti, R.; Lorenzon, M.; Beverina, L.; Viswanatha, R.; Klimov, V. I.; Brovelli, S., Large-Area Luminescent Solar Concentrators Based on ‘Stokes-Shift-Engineered’ Nanocrystals in a Mass-Polymerized Pmma Matrix. *Nat. Photonics* **2014,** *8* (5).
86. Yang, C.; Zhang, J.; Peng, W.-T.; Sheng, W.; Liu, D.; Kuttipillai, P. S.; Young, M.; Donahue, M. R.; Levine, B. G.; Borhan, B.; Lunt, R. R., Impact of Stokes Shift on the Performance of near-Infrared Harvesting Transparent Luminescent Solar Concentrators. *Scientific Reports* **2018,** *8* (1), 16359.
87. Cohen, T. A.; Milstein, T. J.; Kroupa, D. M.; MacKenzie, D. J.; Luscombe, C. K.; Gamelin, D. R., Quantum-Cutting Yb 3+ -Doped Perovskite Nanocrystals for Monolithic Bilayer Luminescent Solar Concentrators. *J. Mater. Chem. A* **2019,** *7* (15), 9279-9288.
88. Milstein, T. J.; Kroupa, D. M.; Gamelin, D. R., Picosecond Quantum Cutting Generates Photoluminescence Quantum Yields over 100% in Ytterbium-Doped Cspbcl 3 Nanocrystals. *Nano Lett.* **2018,** *18* (6), 3792-3799.
89. Sholin, V.; Olson, J. D.; Carter, S. A., Semiconducting Polymers and Quantum Dots in Luminescent Solar Concentrators for Solar Energy Harvesting. *J. Appl. Phys.* **2007,** *101* (12), 123114.
90. Tummeltshammer, C.; Taylor, A.; Kenyon, A. J.; Papakonstantinou, I., Flexible and Fluorophore-Doped Luminescent Solar Concentrators Based on Polydimethylsiloxane. *Opt. Lett.* **2016,** *41* (4), 713-716.
91. Kaniyoor, A.; McKenna, B.; Comby, S.; Evans, R. C., Design and Response of High‐Efficiency, Planar, Doped Luminescent Solar Concentrators Using Organic–Inorganic Di ‐ Ureasil Waveguides. *Adv. Opt. Mater.* **2016**.
92. ter Schiphorst, J.; Kendhale, A. M.; Debije, M. G.; Menelaou, C.; Herz, L. M.; Schenning, A. P. H. J., Dichroic Perylene Bisimide Triad Displaying Energy Transfer in Switchable Luminescent Solar Concentrators. *Chem. Mater.* **2014,** *26* (13), 3876-3878.
93. Earp, A. A.; Smith, G. B.; Franklin, J.; Swift, P., Optimisation of a Three-Colour Luminescent Solar Concentrator Daylighting System. *Sol. Energy Mater. Sol. Cells* **2004,** *84* (1-4), 411-426.
94. Wu, K.; Li, H.; Klimov, V. I., Tandem Luminescent Solar Concentrators Based on Engineered Quantum Dots. *Nat. Photonics* **2018,** *12* (2), 105-110.
95. McIntosh, K. R.; Yamada, N.; Richards, B. S., Theoretical Comparison of Cylindrical and Square-Planar Luminescent Solar Concentrators. *Appl. Phys. B* **2007,** *88* (2), 285-290.
96. Inman, R. H.; Shcherbatyuk, G. V.; Medvedko, D.; Gopinathan, A.; Ghosh, S., Cylindrical Luminescent Solar Concentrators with near-Infrared Quantum Dots. *Opt. Express* **2011,** *19* (24), 24308-24313.

97. Wu, W.; Wang, T.; Wang, X.; Wu, S.; Luo, Y.; Tian, X.; Zhang, Q., Hybrid Solar Concentrator with Zero Self-Absorption Loss. *Sol. Energy* **2010,** *84* (12), 2140-2145.
98. Wang, T.; Yu, B.; Chen, B.; Hu, Z.; Luo, Y.; Zou, G.; Zhang, Q., A Theoretical Model of a Cylindrical Luminescent Solar Concentrator with a Dye-Doping Coating. *J. Opt.* **2013,** *15* (5), 55709.
99. Gajic, M.; Lisi, F.; Kirkwood, N.; Smith, T. A.; Mulvaney, P.; Rosengarten, G., Circular Luminescent Solar Concentrators. *Sol. Energy* **2017,** *150* (Sol. Energy 126 2016), 30-37.
100. Swartz; Cole, T.; Zewail, A. H., Photon Trapping and Energy Transfer in Multiple-Dye Plastic Matrices: An Efficient Solar-Energy Concentrator. *Photon trapping and energy transfer in multiple-dye plastic matrices: an efficient solar-energy concentrator* **1977**.
101. Balaban, B.; Doshay, S.; Osborn, M.; Rodriguez, Y.; Carter, S. A., The Role of Fret in Solar Concentrator Efficiency and Color Tunability. *J. Lumin.* **2014,** *146*, 256-262.
102. Lambers, H.; Chapin, F. S.; Pons, T. L., Photosynthesis. In *Plant Physiological Ecology*, Springer New York: New York, NY, 2008; pp 11-99.
103. Blankenship, R. E., *Molecular Mechanisms of Photosynthesis*. John Wiley & Sons: 2014.
104. Scholes, G. D.; Fleming, G. R.; Olaya-Castro, A.; van Grondelle, R., Lessons from Nature About Solar Light Harvesting. *Nat. Chem.* **2011,** *3* (10), 763-74.
105. Herek, J. L.; Wohlleben, W.; Cogdell, R. J.; Zeidler, D.; Motzkus, M., Quantum Control of Energy Flow in Light Harvesting. *Nature* **2002,** *417* (6888), 533-5.
106. Mirkovic, T.; Ostroumov, E. E.; Anna, J. M.; van Grondelle, R.; Govindjee; Scholes, G. D., Light Absorption and Energy Transfer in the Antenna Complexes of Photosynthetic Organisms. *Chem. Rev.* **2017,** *117* (2), 249-293.
107. Frischmann, P. D.; Mahata, K.; Wurthner, F., Powering the Future of Molecular Artificial Photosynthesis with Light-Harvesting Metallosupramolecular Dye Assemblies. *Chem. Soc. Rev.* **2013,** *42* (4), 1847-70.
108. Demchenko, A. P., Fluorescence Detection Techniques. In *Introduction to Fluorescence Sensing*, 2009; pp 65-118.
109. Medintz, I.; Hildebrandt, N., Fret-Förster Resonance Energy Transfer: From Theory to Applications. *FRET-Förster resonance energy transfer: from theory to applications* **2013**.
110. Currie, M. J.; Mapel, J. K.; Heidel, T. D.; Goffri, S.; Baldo, M. A., High-Efficiency Organic Solar Concentrators for Photovoltaics. *Science* **2008,** *321* (5886), 226-8.
111. Zhang, B.; Soleimaninejad, H.; Jones, D. J.; White, J. M.; Ghiggino, K. P.; Smith, T. A.; Wong, W. W. H., Highly Fluorescent Molecularly Insulated Perylene Diimides: Effect of Concentration on Photophysical Properties. *Chem. Mater.* **2017,** *29* (19), 8395-8403.
112. Bailey, S. T.; Lokey, G. E.; Hanes, M. S.; Shearer, J.; McLafferty, J. B.; Beaumont, G. T.; Baseler, T. T.; Layhue, J. M.; Broussard, D. R.; Zhang, Y.-Z.; Wittmershaus, B. P., Optimized Excitation Energy Transfer in a Three-Dye Luminescent Solar Concentrator. *Sol. Energy Mater. Sol. Cells* **2007,** *91* (1), 67-75.
113. Davis, N. J. L. K.; MacQueen, R. W.; Jones, S. T. E.; Orofino-Pena, C.; Cortizo-Lacalle, D.; Taylor, R. G. D.; Credgington, D.; Skabara, P. J.; Greenham, N. C., Star-Shaped Fluorene–Bodipy Oligomers: Versatile Donor–Acceptor Systems for Luminescent Solar Concentrators. *J. Mater. Chem. C* **2017,** *5* (8), 1952-1962.
114. Banal, J. L.; Ghiggino, K. P.; Wong, W. W. H., Efficient Light Harvesting of a Luminescent Solar Concentrator Using Excitation Energy Transfer from an Aggregation-Induced Emitter. *Phys. Chem. Chem. Phys.* **2014,** *16* (46), 25358-25363.
115. Banal, J. L.; Soleimaninejad, H.; Jradi, F. M.; Liu, M.; White, J. M.; Blakers, A. W.; Cooper, M. W.; Jones, D. J.; Ghiggino, K. P.; Marder, S. R.; Smith, T. A.; Wong, W. W. H., Energy Migration in Organic Solar Concentrators with a Molecularly Insulated Perylene Diimide. *J. Phys. Chem. C* **2016,** *120* (24), 12952-12958.

Chapter II

Methods

The general experimental approaches used in the thesis are provided in this chapter. Any specific approaches that are different from the general approach are discussed separately in the Supporting Information section of each of the following chapters. The information from this chapter has been also used in other published work.[1]

2.1 General information on materials synthesis and characterization

All commercial reagents were used in the synthesis as received (unless otherwise indicated). Dry solvents were obtained either from activated neutral alumina columns under argon atmosphere or passing through 4Å molecular sieves. Air sensitive reactions were performed under N_2 atmosphere. Oxygen-free solvents were obtained by N_2 purging for at least 20 minutes.

Flash chromatography purification was performed using standard methods on silica gel (Merck Silica Gel 60, 0.040-0.063 mm, 230-400 mesh ASTM). All reactions were monitored by thin-layer chromatography using silica gel (Merck, Silica Gel 60 F254) coated glass sheets, either examined under UV lamps (254 nm and 365 nm) in a black box or stained by $KMnO_4$/ethanol solution with heat treatment.

The ^{1}H, ^{13}C and COSY NMR spectroscopy presented in this thesis were collected by using the

Agilent MR400 (400 MHz), Oxford 500 (500 MHz) or Varian Inova 600 (600 MHz). All NMR spectra unless specified were measured under room temperature (25 ℃) and internally calibrated against residual undeuterated solvent as reference. All HPLC-based analysis and purification were carried out using a standard HPLC system with a UV-Vis detector. FT-IR spectra were obtained by a Perkin Elmer Spectrum One FT-IR spectrometer. All high-resolution mass spectrometry (HRMS) experiments were conducted with the use of a commercially available hybrid orbital-trap and Fourier-transform ion cyclotron resonance mass spectrometer, equipped with electrospray ionization (ESI). Electrochemical measurements were recorded on a Solartron 1287A Potentiostat/Galvanostat. UV-Vis spectra were recorded using a Cary UV-Vis spectrometer. The photoluminescence measurements of both solution and thin-film samples are conducted on a Fluorolog®-3 fluorimeter.

The X-ray crystallography data reported in this thesis were collected and solved by Prof. Jonathan White, University of Melbourne. The data were either collected at 100 K on the MX1 beamline at the Australian Synchrotron[2] or collected on an Oxford SuperNova CCD diffractometer at 130 K. The structures were resolved by direct methods and difference Fourier synthesis. Thermal ellipsoid plots were generated using the program ORTEP-3 integrated within the WINGX suite of programs.

2.2 Approaches for device fabrication and characterization

2.2.1 Thin-film sample fabrication

All the glass (MENZEL-GLÄSER Microscope Slides, 76 × 26 mm) and quartz (PST Quartz slide, 76 mm × 25 mm) slides used in casting the thin-film samples were cleaned by ultrasonicating sequentially in $CHCl_3$, acetone, NaOH (a.q.), distilled water isopropanol and dried using a strong flow of N_2.

All the glass and quartz slides used for absolute ϕ_{PL} measurement were cut into the size of 1.25 cm × 1.25 cm × 0.1 cm, cleaned by ultrasonicating sequentially in $CHCl_3$, acetone, NaOH (a.q.), distilled water and isopropanol and dried using a strong flow of N_2. All the thin film samples for the absolute ϕ_{PL} measurement was prepared by either drop-casting or spin-coating processes.

To the drop-casting process, a fixed amount of the casting solution was added to the matrix surface until all the surface area was covered. The remaining air bubbles were always removed. After drop-casting, the samples were sitting in a Petri dish for 30 min to evaporate the solvent slowly and heated for 30 min at 100 ℃ to further remove the solvent residue.

In the spin-coating process, a fixed amount of the casting solution was added to the matrix surface until all the surface area was covered. The remaining air bubbles were always removed. The spin coating speed was from 500 to 2000 rpm depending on the absorbance requirement of the sample and the acceleration was around 1000 rpm/s. After spin coating, the samples were baked at 100 ℃ for 30 min to evaporate the solvent.

The casting solution is prepared by the dissolving the dye in a PMMA solution (1% w/w in chloroform). The concentration of the dye is determined by the molar concentration to the volume of the PMMA solid, assuming the volume of the dye can be neglectable.

2.2.2 In-situ polymerization

The bulk-LSC can be made by the in-situ polymerization (so-called bulk-polymerization or plastics casting) process. The general procedure of in-situ polymerization used in the thesis is described as follows:

1. Cutting a piece of Teflon® sheet (1 to 10 mm thickness) into a U (or O) shape, sandwich it in between two pieces of glass and clamped tight by clips. The resulting device will be used as the mould of the polymerization (Figure 2.1a).

2. The inhibitor in the monomer of the plastic will be removed by flash chromatography on silica gel. The monomer, initiator (around 0.1% w/w) and the dye are heated to 60℃ and stirred around 20 minutes.

3. The mixture is then poured directly into the glass mold. Place the mold in an oven, bake at 50 ℃ for 24h.

4. Once the polymerization is complete, place the mold in an ice-bath to allow the plastic sheet to shrink and then peeled from the mold. Cut the resulting plastic sheet into the desired shape (Figure 2.1b).

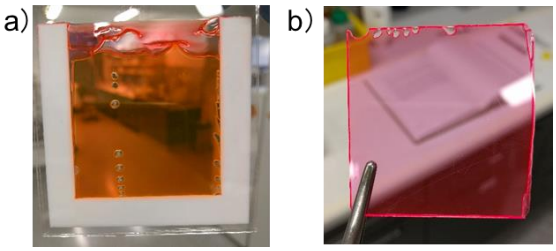

Figure 2.1 a) the waveguide mold for the U-shape Teflon sandwiched by two pieces of glass. When the sealing is not tight, it can cause bubbles in the product. b) the LSC was taken from the mold after the in-situ polymerization.

2.2.3 Doctor blading film deposition

The large-area thin-film LSC was prepared by the doctor blade film deposition process (Figure 2.2a).[3] A solution of PMMA (100,000 Mw, Sigma Aldrich, 3% w/w in chlorobenzene) was prepared beforehand and the fluorophore was dissolved in the solution. The doctor blade was sitting on the surface of the waveguide substrate. The height of the blade to the substrate was pre-judged (10-1000 μm) to allow depositing the desired film thickness. The PMMA solution was then deposited along the gap in-between the blade and the waveguide surface. A robot-arm was used to drive the blade to move forward at a steady speed (10-20 cm/s), pushing the PMMA solution and

leaving a homogenous wet PMMA film (Figure 2.2b). The chlorobenzene was allowed to evaporate in the air for 1 minute and then the substrate baked at 100 ℃ for 1h to further remove the solvent residue. The resulting LSC was then cut into the desired shape.

Figure 2.2 a) the scheme of the doctor blading film deposition process and b) the doctor blade used and the robot-arm driving the blade on a waveguide surface.

2.2.4 LSC demonstrator assembly

A window-size LSC display was assembled by the author for the university outreach activities (Figure 2.3). A commercial Perspex® (600 mm × 800 mm × 8 mm) was used as the waveguide. An aluminum frame was assembled in the desired size beforehand. 20 pieces of solar cells (ANYANG CITY SUNSHINE SCIENCE AND EDUCATION ENERGY LIMITED, amorphous silica, 7.5 cm × 1.0 cm) were attached inside the slot of the two longer edges on the aluminium frame. The solar cells were connected by copper wires in series to accumulate the current output. The wires from two edges were combined and linked to a USB adaptor. The Perspex was inserted into the frame, with the long edges attached to the solar cells. Several drops of optical oil (Olympus) was deposited in-between the Perspex edges and the solar cell surface to reduce the interface scattering loss. The top frame was assembled to lock the Perspex and the frames on the long edges in place. The resulting LSC display provided a power output of 7.7 V and 55 mA outdoor on a sunny day. It was able to charge cellphones or other small electronics.

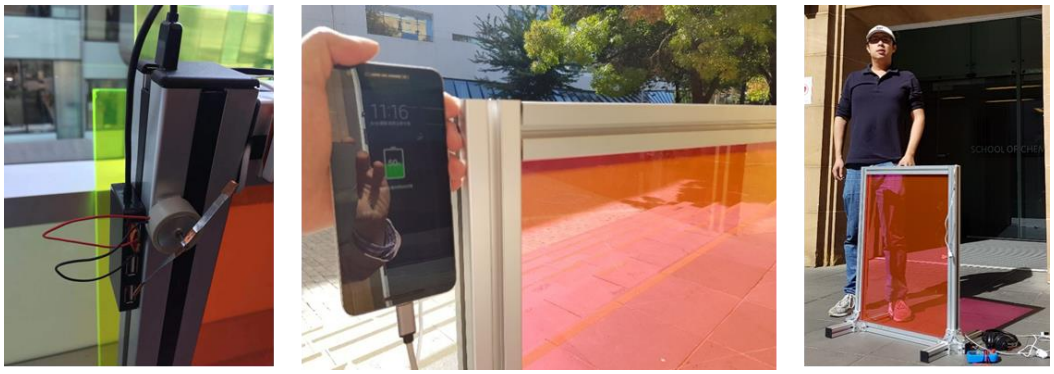

Figure 2.3 The window-size LSC display has a USB adapter for power output. It can charge a cellphone on a sunny day.

2.2.5 Distance dependent external quantum efficiency (EQE) measurements

The LSC device for the EQE measurement was prepared by drop-casting on top of a 2.5 cm × 3.75 cm × 0.1 cm glass slide. After drop-casting, the device was left in a Petri dish for 30 min to allow complete solvent evaporation followed by heating at 100 ℃ for 30 minutes.

The EQE of the thin-film LSC device was measured by an EQE Measurement Kit (Newport). The LSC was clamped by a Teflon sample holder and placed on top of a calibrated solar cell. The short bottom edge of the LSC was just attached to the active area of the solar cell and a drop of optical oil was added to avoid the interface scattering loss. The LSC device was excited by a 325 W Hg Arc light source. The size of the excitation beam spot on the LSC device was kept at 0.5 cm to match the same condition in the calibration. The EQE was measured several times with the excitation spot at a different distance to the solar cell (see Figure 2.4).

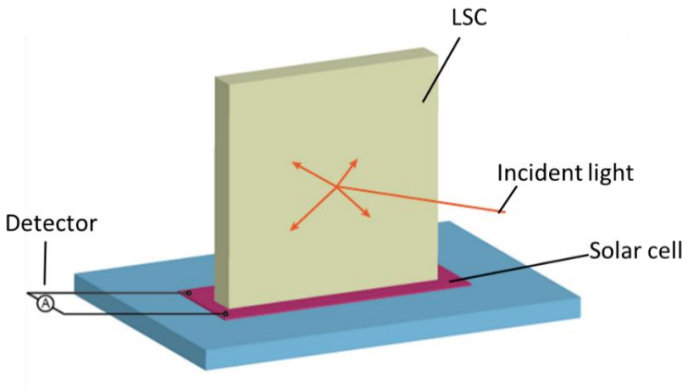

Figure 2.4 Setup of distance dependent EQE measurement

2.3 Approaches of spectroscopy analysis

2.3.1 Absolute photoluminescence quantum yield measurement:

The absolute photoluminescence (PL) quantum yield (QY) measurements of both solution and thin-film samples are conducted using an integrating sphere (F3018, Horiba Jobin Yvon) on a Fluorolog®-3 fluorimeter. Figure 2.5 reveals the typical construction of an integrating sphere for the thin film sample measurement. The angle of the excitation beamline to the normal of the sample surface can be modified by the tunable sample holder. All spectra for the absolute quantum yield measurement were recorded with correction for the light source noise, wavelength sensitivity and the transmittance of the filters. The photon counts of all the measurements on the Fluorolog®-3 fluorimeter were within the linear response range of the detector (less than 2×10^6 cps).

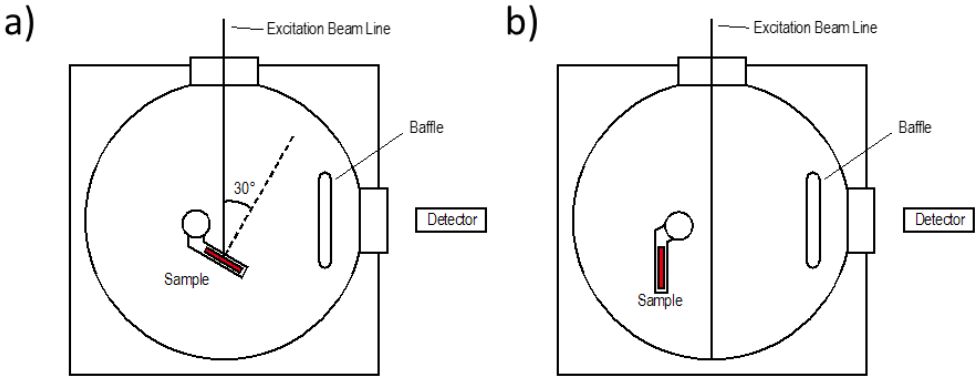

Figure 2.5 The position of thin-film sample in the integrating sphere: a) sample in the excitation beamline; b) sample out of beamline.

In general, the absolute PL quantum yield (ϕ_{PL}) can be defined as the quotient of the emission photon flux ($F_{emission}$) of the sample to the absorption photon flux ($F_{absorption}$) of the sample:

$$F_{emission} = \int_{\lambda_{em1}}^{\lambda_{em2}} \frac{I_x(\lambda_{em}) - I_b(\lambda_{em})}{s(\lambda_{em})} \lambda_{em} d\lambda_{em} \quad (2\text{-}1)$$

$$F_{absorption} = \int_{\lambda_{ex1}}^{\lambda_{ex2}} \frac{I_b(\lambda_{ex}) - I_x(\lambda_{ex})}{s(\lambda_{ex})} \lambda_{ex} d\lambda_{ex} \quad (2\text{-}2)$$

$$\Phi_{PL} = \frac{F_{emission}}{F_{absorption}} \quad (2\text{-}3)$$

where the I_x and I_b is the intensity of the spectra from the sample and the blank respectively, s is the spectral responsivity. [4-5]

The absolute PLQY of all samples described in this article was measured and calculated according to the experimental approach described by Porres et al.[6] Accordingly, the PLQY measured using an integrating sphere can be defined by the following formula[7-8]:

$$\Phi_{PL} = \frac{E_{x,in} - (1-A)E_{x,out}}{AL_{b,in}} \quad (2\text{-}4)$$

where *A* is the percentage of the photons absorbed directly by the sample corrected by removing

the secondary absorption from the sphere-reflected photons:

$$A = \frac{L_{x,out} - L_{x,in}}{L_{x,out}} \quad (2\text{-}5)$$

In the above formulas, E is the number of photon counts from the emission spectra and L is the number of photon counts from the scattering spectra. The index x and b are the samples and the blank. The subscripts in and out reveal whether the sample holder is in the excitation beamline or out of the excitation beamline (see Figure 2.5).

2.3.2 Re-absorption correction:

The re-absorption correction was considered in some ϕ_{PL} measurements when the overlap of absorption and emission spectrum of the fluorophore was significant.[9-10] To conduct the re-absorption correction, a diluted sample was prepared and its emission spectrum was measured by a fluorimeter in the absence of the integrating sphere (F_{true}). The observed emission spectrum of the sample (F_{obs}) then was tail matched with (F_{true}) to give the enhanced observed emission spectrum (F'_{obs}). (See Figure 2.6)

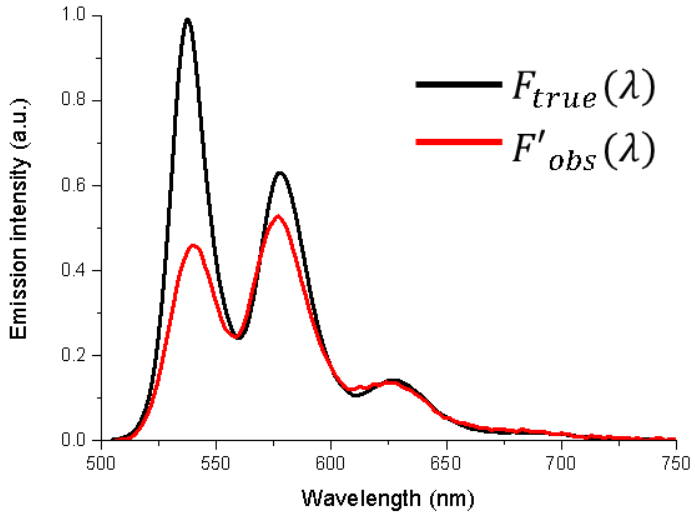

Figure 2.6 An example of the enhanced observed emission spectrum of $F'_{obs}(\lambda)$ tail matched with the emission spectrum of a dilute sample $F_{true}(\lambda)$.

The re-absorption corrected quantum yield ($\phi_{PL,cor}$) is given by

$$\Phi_{\mathrm{PL,cor}} = \frac{\Phi_{\mathrm{PL,\,obs}}}{1 - a + a \times \Phi_{\mathrm{PL,\,obs}}}$$

$$a = 1 - \frac{\int_0^\infty F'_{obs}(\lambda)\, d\lambda}{\int_0^\infty F_{true}(\lambda)\, d\lambda}$$

where $\phi_{PL,obs}$ is the observed PLQY of the sample, a refers to the probability for an emitted photon being re-absorbed, $F_{true}(\lambda)$ is the emission spectrum of a dilute sample in which the re-absorption effect is eliminated, $F'_{obs}(\lambda)$ is the enhanced observed emission spectrum.

2.3.3 Time-correlated single photon counting

Time-correlated single photon counting (TCSPC) is an optical spectroscopy technique used to measure the fluorescence lifetime of an excited state. There is a certain probability for a photon to be emitted following photo-excitation of a molecule. In TCSPC, the time delay is measured between the exposure of the sample to a short laser pulse and a fluorescence photon being detected. The experiment is repeated many times to provide a distribution of the emission decay probability. The resulting decay curve can be fitted to an appropriate kinetic model (usually a first order decay) to extract the fluorescence lifetime (Figure 2.7).

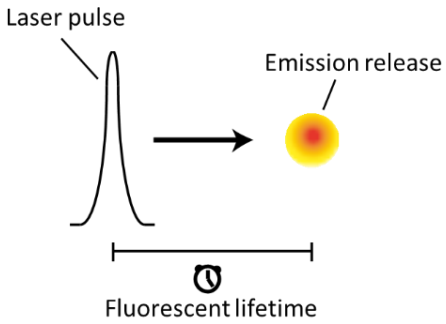

Figure 2.7 Time-correlated single photon counting records the time delay from the laser pulse to the emission photon detection for multiple excitation events.

All the TCSPC measurements described in this thesis were conducted by Dr. Hamid Soleimaninejad, University of Melbourne.[11-12] The excitation source was a mode-locked and cavity dumped Ti:Sapphire laser (Coherent Mira 900F/APE PulseSwitch) pumped by a Coherent Verdi-10 DPSS Nd:YVO_4 laser. The laser output (880 nm wavelength, 5.4 MHz repetition rate) was frequency doubled to provide an excitation wavelength of 440 nm. The individual fluorescence decay curves were collected using the time-correlated single photon counting technique.[7] Synchronization of the laser pulses was achieved using a fast photodiode (Becker & Hickl, PHD-400-N) fed through a nanosecond delay box and constant fraction discriminator (Tennelec TC455) as the stop signal for the time-to-amplitude converter (Ortec model 457). The emission spectrum was generated by a monochromator (JOBIN YVON) and detected by a single photon counting photomultiplier tube (XP2020Q). Fluorescent decays were fit with exponential decays using iterative reconvolution with the instrument response function to extract the fluorescence lifetime using the FAST (Edinburgh Instrument) software package with χ^2 as fitting criteria for the goodness of fit. Fluorescence lifetime derived from decay fits have uncertainties of ~0.1 ns.

2.3.4 Time-resolved fluorescence anisotropy

When a material is excited by polarized light, the polarization level of the emitted light may be decreased as a function against time. The anisotropy (r) stands for the extent of the polarization reduction of the emitted light. There are two main reasons for the dropping of the anisotropy, namely the rotation diffusion effect and the energy migration effect. The rotation diffusion refers to the depolarization of the emitted light caused by the rotational motion of the emission transition dipole during the fluorescence lifetime. The energy migration effect refers to the depolarization caused by the energy transfer process among the molecules in an anisotropic system during the fluorescence lifetime. The concept of time-resolved fluorescence anisotropy can be described based on the following equations:

$$r(t) = \frac{I_{\parallel}(t) - GI_{\perp}(t)}{I_{\parallel}(t) + 2GI_{\perp}(t)} \tag{2-6}$$

$$= \frac{I_{VV}(t) - GI_{VH}(t)}{I_{VV}(t) + 2GI_{VH}(t)}$$

$$G = \frac{I_{HV}}{I_{HH}} \tag{2-7}$$

where $I_{\parallel}(t)$ and $I_{\perp}(t)$ are the components of the time-dependent fluorescence intensity parallel and perpendicular to the polarization of the excitation laser pulse and G is a factor for correcting the polarization bias of the detector, the indices V and H refer to the direction of the polarizers used in the measurement.

All the measurements of time-resolved fluorescence anisotropy described in this report were conducted by Dr. Hamid Soleimaninejad, University of Melbourne.[11-12] The excitation source was a mode-locked and cavity dumped Ti:Sapphire laser (Coherent Mira 900F/APE PulseSwitch) pumped by a Coherent Verdi-10 DPSS Nd:YVO_4 laser. The laser output (880 nm wavelength, 5.4 MHz repetition rate) was frequency doubled to provide an excitation wavelength of 440 nm. The individual fluorescence decay curves were collected using the time-correlated single photon counting technique.[7] Synchronization of the laser pulses was achieved using a fast photodiode (Becker & Hickl, PHD-400-N) fed through a nanosecond delay box and constant fraction discriminator (Tennelec TC455) as the stop signal for the time-to-amplitude converter (Ortec model 457). The excitation beam passed through a silica double rhomb to select the input (vertical) excitation polarization. The emission was collected at right angles relative to the excitation, first passing through a polarization analyzer mounted on a stage that rotates both the polarizer and collection lens to collect vertically and horizontally polarized emission. The analyzer orientation was driven by a computer-controlled stepper motor board (Phidgets 1067). The emission was then passed through a polarization scrambler (ThorLabs DPU-25), spectrally selected using a monochromator (Jobin Yvon, H20), and detected using a single photon counting photomultiplier

tube (XP2020Q). The memory of the multichannel analyser (MCA-p7882, Fastcom Tech) was divided into segments in which the various I_{ij} components (i and j are the polarization of the excitation and detection respectively), generated following control of the stepper motors, are saved during each acquisition sequence. Decay profiles were acquired by sequentially toggling between the respective polarisation orientations/memory locations to achieve equal collection conditions for each orientation. The correction for the polarization bias of detection system (G factor) was determined to be very close to unity by both tail-matching the I_{VV} and I_{VH} profiles and the I_{HV}/I_{HH} ratio from the time-resolved fluorescence decay of Coumarin 153 in solution.[11-12]

2.4 Calculation and Simulation

To predict the edge output performance of LSC devices, Monte-Carlo ray-tracing simulation[13-15] was performed in this thesis. The code of the Monte-Carlo ray-tracing program used in this thesis was developed by Mr. Chris Haines on MATLAB®. The author, Dr. James Banal and Ms. Hanbo Yang made some modification to the original code to add more functions.

The flow chart of the simulation process is demonstrated in Figure 2.8. At the beginning of a calculation cycle, one photon will be generated based on the spectrum of the light source. The code then decides whether the photon is absorbed or transmitted via the system according to the absorbance of the waveguide. The absorbed photon then either emits at a new wavelength depending on the emission spectrum or is lost via a non-radiative decay based on the PLQY of the fluorophores. The emitted photon will be given a random path, which determines whether the photon is lost through the escape cone or trapped by the waveguide. The trapped photon will be either released from one edge based on the refractive index of the waveguide matrix or be absorbed again. Once the photon is lost or collected, a new cycle will start until the counting of trapped photons reaches a limit value. During the simulation process, all of the events, for example, the re-absorption, reflection, escape cone loss, PLQY loss or release from edges, are

recorded for assessing the performance of the waveguide system. The scattering caused loss is not considered in the simulation.

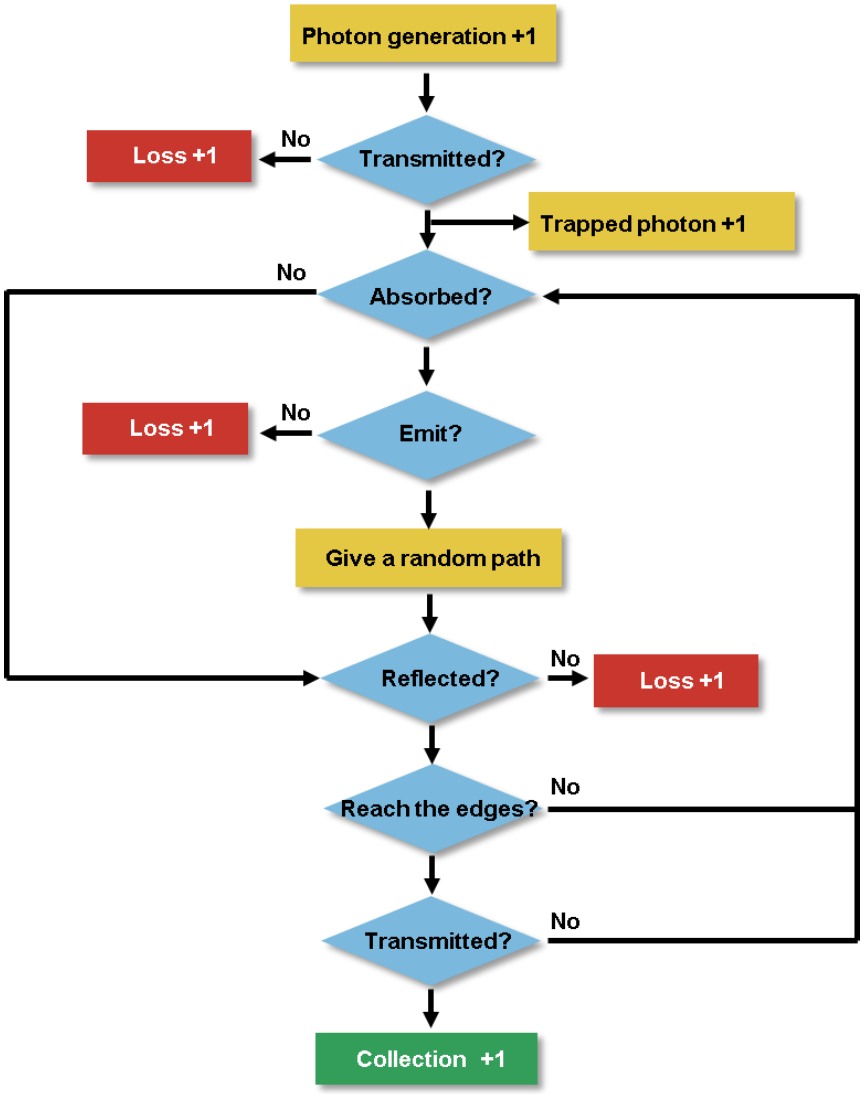

Figure 2.8 Flow chart of the Monte-Carlo ray-tracing simulation process.

Reference:

1. Xu, J.; Zhang, B.; Jansen, M.; Goerigk, L.; Wong, W. W. H.; Ritchie, C., Highly Fluorescent Pyridinium Betaines for Light Harvesting. *Angew. Chem. Int. Ed.* **2017,** *56* (44), 13882-13886.
2. Cowieson, N.; Aragao, D.; Clift, M.; Ericsson, D. J.; Gee, C.; Harrop, S. J.; Mudie, N.; Panjikar, S.; Price, J. R.; Riboldi-Tunnicliffe, A., Mx1: A Bending-Magnet Crystallography Beamline Serving

Both Chemical and Macromolecular Crystallography Communities at the Australian Synchrotron. *J. Synchrotron Radiat.* **2015,** *22* (1), 187-190.

3. Zhang, B.; Zhao, P.; Wilson, L. J.; Subbiah, J.; Yang, H.; Mulvaney, P.; Jones, D. J.; Ghiggino, K. P.; Wong, W. W. H., High-Performance Large-Area Luminescence Solar Concentrator Incorporating a Donor–Emitter Fluorophore System. *ACS Energy Lett.* **2019**, 1839-1844.
4. Würth, C.; Grabolle, M.; Pauli, J.; Spieles, M.; Resch-Genger, U., Comparison of Methods and Achievable Uncertainties for the Relative and Absolute Measurement of Photoluminescence Quantum Yields. *Anal. Chem.* **2011,** *83* (9), 3431-3439.
5. Würth, C.; Grabolle, M.; Pauli, J.; Spieles, M.; Resch-Genger, U., Relative and Absolute Determination of Fluorescence Quantum Yields of Transparent Samples. *Nature protocols* **2013,** *8* (8), 1535-1550.
6. Porrès, L.; Holland, A.; Pålsson, L.-O.; Monkman, A. P.; Kemp, C.; Beeby, A., Absolute Measurements of Photoluminescence Quantum Yields of Solutions Using an Integrating Sphere. *J. Fluoresc.* **2006,** *16* (2), 267-273.
7. Pålsson, L. O.; Monkman, A. P., Measurements of Solid-State Photoluminescence Quantum Yields of Films Using a Fluorimeter. *Adv. Mater.* **2002**.
8. de Mello, J. C.; Wittmann, H. F.; Friend, R. H., An Improved Experimental Determination of External Photoluminescence Quantum Efficiency. *Adv. Mater.* **1997**.
9. Würth, C.; Lochmann, C.; Spieles, M.; Pauli, J.; Hoffmann, K.; Schüttrigkeit, T.; Franzl, T.; Resch-Genger, U., Evaluation of a Commercial Integrating Sphere Setup for the Determination of Absolute Photoluminescence Quantum Yields of Dilute Dye Solutions. *Appl. Spectrosc.* **2010,** *64* (7), 733-741.
10. Ahn, T.-S.; Al-Kaysi, R. O.; Müller, A. M.; Wentz, K. M.; Bardeen, C. J., Self-Absorption Correction for Solid-State Photoluminescence Quantum Yields Obtained from Integrating Sphere Measurements. *Rev. Sci. Instrum.* **2007,** *78* (8), 86105.
11. Banal, J. L.; Soleimaninejad, H.; Jradi, F. M.; Liu, M.; White, J. M.; Blakers, A. W.; Cooper, M. W.; Jones, D. J.; Ghiggino, K. P.; Marder, S. R.; Smith, T. A.; Wong, W. W. H., Energy Migration in Organic Solar Concentrators with a Molecularly Insulated Perylene Diimide. *J. Phys. Chem. C* **2016,** *120* (24), 12952-12958.
12. Zhang, B. L.; Soleimaninejad, H.; Jones, D. J.; White, J. M.; Ghiggino, K. P.; Smith, T. A.; Wong, W. W. H., Highly Fluorescent Molecularly Insulated Perylene Diimides: Effect of Concentration on Photophysical Properties. *Chem. Mater.* **2017,** *29* (19), 8395-8403.
13. Hernandez-Noyola, H.; Potterveld, D. H.; Holt, R. J.; Darling, S. B., Optimizing Luminescent Solar Concentrator Design. *Energy Environ. Sci.* **2012,** *5* (2), 5798-5802.
14. Carrascosa, M.; Unamuno, S.; Agullo-Lopez, F., Monte Carlo Simulation of the Performance of Pmma Luminescent Solar Collectors. *Appl. Opt.* **1983**.
15. Şahin, D.; Ilan, B.; Kelley, D. F., Monte-Carlo Simulations of Light Propagation in Luminescent Solar Concentrators Based on Semiconductor Nanoparticles. *J. Appl. Phys.* **2011,** *110* (3), 33108.

Chapter III

An AIE Donor-emitter Fluorophore Pair for LSCs

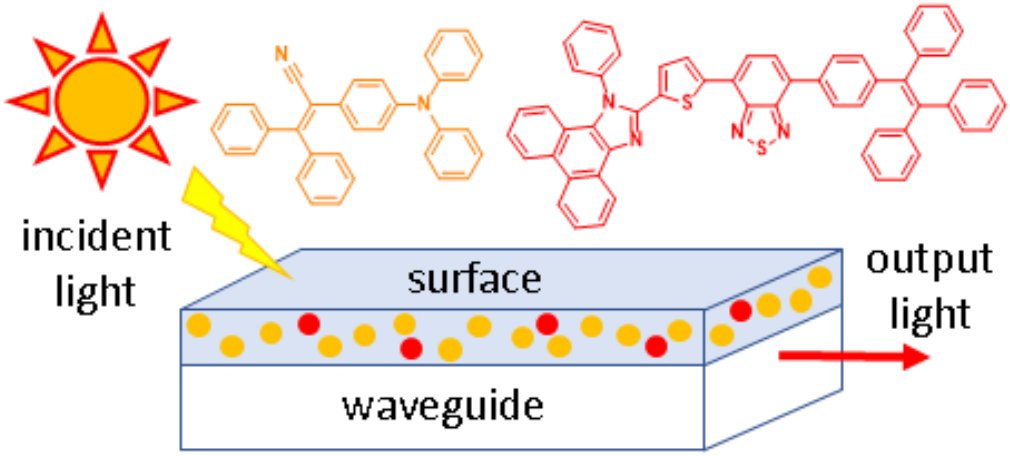

Reprinted with the permission from Ref [5], copyright © 2018 Royal Society of Chemistry.

3.1 Preface

As discussed in **Chapter I**, a highly efficient LSC requires the embedded fluorophore system to have high ϕ_{PL} and small spectral overlap in-between the absorption and emission. The donor-emitter fluorophore pair system can benefit the LSCs by improving the ϕ_{PL} and reducing the spectral overlap. In this chapter, a donor-emitter fluorophore pair system was introduced and characterized, and the performance of a LSC based-on the donor-emitter pair was examined. The

experimental result revealed information in two aspects: 1. How to improve the performance of a LSC and 2. How to design the donor-emitter pairs.

A highly efficient donor-emitter fluorophore pair system usually requires both the donor and the emitter to be in a high concentration to meet the close donor-acceptor distance requirements imposed by the Förster resonance energy transfer (FRET) mechanism. However, most organic fluorophores are affected by aggregation caused quenching (ACQ), meaning the ϕ_{PL} decreases with increasing fluorophore concentration. To achieve high fluorophore concentrations of the donor and the emitter for efficient energy transfer one needs to find a way to avoid the ACQ effect.

As discussed in **Chapter I**, aggregation induced emission (AIE) fluorophores are organic fluorophores that emit more intensely in aggregates than in dilute solution. Some of AIE fluorophores can even achieve close to unity ϕ_{PL} in the solid-state. Therefore, one may consider AIE fluorophores suitable candidates for the donor-emitter fluorophore pairs in the LSC waveguide system. As summarized in **Chapter I**, there are already many examples of LSCs using AIE materials as fluorophores.[1-3] Previous studies by our research group also suggested that the donor-emitter fluorophore pair system based-on some AIE materials can efficiently enhance the performance of LSCs.[4]

In this chapter, a donor-emitter fluorophore pair system that consists of two AIE fluorophores was studied to address the question 'How can materials be optimized to produce an efficient donor-emitter fluorophore system?'. The photophysical properties of the AIE fluorophore pair were fully characterized. Furthermore, the concentrations and ratios of the AIE donor-emitter fluorophore pair were optimized and the performance of LSC devices based on this AIE fluorophore pair were also examined via the Monte-Carlo ray-tracing simulation. The research results have been published in the following article[5]:

Bolong Zhang, James L. Banal, David J. Jones, Ben Zhong Tang, Kenneth P. Ghiggino, Wallace

W.H. Wong. Aggregation-induced Emission-mediated Spectral Downconversion in Luminescent Solar Concentrators. *Mater. Chem. Front.*, **2018**, 2, 615-619. DOI: 10.1039/C7QM00598A

The experimental details are included in the Supporting Information section following the main manuscript. Reprinted with the permission from Ref [5], copyright © 2018 Royal Society of Chemistry.

Contribution of the candidate:

- All spectroscopy measurements.
- Photoluminescent quantum yield measurements.
- Monte-Carlo ray tracing simulations.
- Fabrication of the LSC devices.
- Writing drafts of the manuscript.

Reference:

1. Banal, J. L.; White, J. M.; Ghiggino, K. P.; Wong, W. W. H., Concentrating Aggregation-Induced Fluorescence in Planar Waveguides: A Proof-of-Principle. Sci. Rep. 2014, 4, 4635.
2. Banal, J. L.; White, J. M.; Lam, T.; Blakers, A. W.; Ghiggino, K. P.; Wong, W. W. H., A Transparent Planar Concentrator Using Aggregates of Gem-Pyrene Ethenes. Adv. Energy Mater. 2015, 5 (19), 1500818.
3. De Nisi, F.; Francischello, R.; Battisti, A.; Panniello, A.; Fanizza, E.; Striccoli, M.; Gu, X.; Leung, N. L. C.; Tang, B. Z.; Pucci, A., Red-Emitting Aiegen for Luminescent Solar Concentrators. Mater. Chem. Front. 2017, 1 (7), 1406-1412.
4. Banal, J. L.; Ghiggino, K. P.; Wong, W. W. H., Efficient Light Harvesting of a Luminescent Solar Concentrator Using Excitation Energy Transfer from an Aggregation-Induced Emitter. Phys. Chem. Chem. Phys. 2014, 16 (46), 25358-25363.
5. Zhang, B.; Banal, J. L.; Jones, D. J.; Tang, B.; Ghiggino, K. P.; Wong, W. W. H., Aggregation-Induced Emission-Mediated Spectral Downconversion in Luminescent Solar Concentrators. Mater. Chem. Front. 2018, 2 (3), 615-619.

MATERIALS CHEMISTRY
FRONTIERS

RESEARCH ARTICLE

View Article Online
View Journal | View Issue

Cite this: *Mater. Chem. Front.*, 2018, **2**, 615

Aggregation-induced emission-mediated spectral downconversion in luminescent solar concentrators†

Bolong Zhang, [a] James L. Banal, [b] David J. Jones, [a] Ben Zhong Tang, [c] Kenneth P. Ghiggino [a] and Wallace W. H. Wong *[a]

Received 19th December 2017,
Accepted 24th January 2018

DOI: 10.1039/c7qm00598a

rsc.li/frontiers-materials

The light-harvesting efficiency of luminescent solar concentrators (LSCs) is encumbered by reabsorption of emission and concentration quenching. Energy transfer from a high-concentration donor to a low-concentration energy trap can reduce reabsorption losses while maintaining efficient light collection. Emissive aggregates enable this approach by reducing the impact of concentration quenching, which is detrimental to the entire energy transfer process. Here we describe a LSC that utilizes emissive aggregates as energy-transfer pairs for downconversion. We characterize the photophysics of a benzothiadiazole-based emissive aggregate, PITBT-TPE, that complements a highly emissive donor, DPATPAN, and functions as a highly emissive energy-transfer acceptor even at high concentrations in excess of 180 mM in the PMMA matrix. Monte Carlo simulations of LSCs that leverage these emissive aggregates as energy-transfer pairs predicted notable optical efficiencies at large concentrator dimensions. We demonstrate for the first time a LSC that utilizes donor and acceptor AIE chromophores to reduce reabsorption.

Widespread utility of solar technologies requires lowering the cost of highly-efficient photovoltaics devices while also ensuring compatibility and integration with urban infrastructures, such as buildings, houses, or noise-barriers.[1–4] Luminescent solar concentrators (LSCs) are large-area and planar spectral down-converting devices that function as a light-harvesting accessory to small-area photovoltaic cells.[5] A typical LSC consists of a planar glass or plastic waveguide with chromophores dispersed on the surface of a waveguide or embedded within a high refractive index matrix for waveguiding (Fig. 1a). The chromophores absorb incident photons and subsequent emitted photons can be trapped in the waveguide by total internal reflection. The emitted photons are concentrated to the edge of the waveguide where a photovoltaic cell is attached.[5,6] As the emitted photons traverse through the waveguide, the probability of reabsorption by other chromophores increases due to multiple total internal reflection events. These reabsorbed photons can be lost by non-radiative decay, if the photoluminescence quantum yield (ϕ_{PL}) of the chromophore is less than unity, and by emission into the escape cone of the waveguide. Chromophores that have innately large Stokes shifts have been proposed to circumvent the reabsorption.[7,8] However, further increasing the Stokes shift by introducing electron donating/withdrawing substituents to the chromophore often leads to a compromise with quantum yields.[8] A large Stokes shift can also be achieved using a Förster resonance energy transfer (FRET) donor–acceptor pair. An emissive donor of significantly high concentration within the LSC matrix absorbs light and transfers

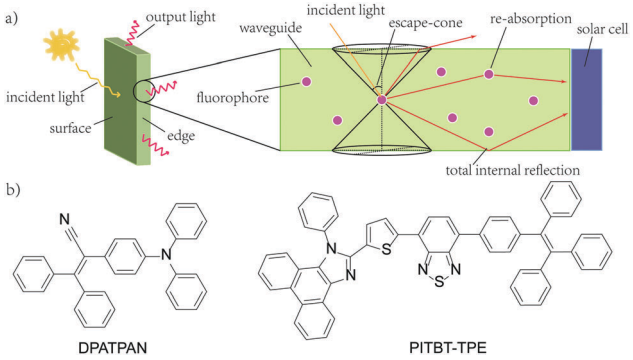

Fig. 1 (a) A typical structure of a LSC with attached solar cell (b) the chemical structures of DPATPAN and PITBT-TPE.

[a] School of Chemistry, Bio21 Institute, The University of Melbourne, Parkville, Victoria, 3010, Australia. E-mail: wwhwong@unimelb.edu.au
[b] Department of Biological Engineering, Massachusetts Institute of Technology, Cambridge, Massachusetts, 02139, USA
[c] Hong Kong Branch of Chinese National Engineering Research Centre for Tissue Restoration and Reconstruction, Department of Chemistry, The Hong Kong University of Science & Technology (HKUST), Clear Water Bay, Kowloon, Hong Kong

† Electronic supplementary information (ESI) available. See DOI: 10.1039/c7qm00598a

its energy non-radiatively *via* Förster mechanism to an acceptor that has a comparatively lower concentration in the film.[9–12] The acceptor then emits at longer wavelengths compared to the incident light. By optimizing the concentration and ratio of donor and acceptor chromophores in the LSC, reabsorption from the acceptor can be mitigated while maintaining efficient light-harvesting.[9–11,13] Using this energy migration and trapping approach for LSCs provides broad tunability in the emission wavelengths and absorption bandwidth of LSCs.

Our group recently reported the use of FRET donor chromophores that showed high ϕ_{PL} at high concentration in poly(methyl methacrylate) (PMMA).[9] Previously, we have identified a chromophore, DPATPAN that has aggregation-induced emission (AIE) characteristics[14] and was used as the FRET donor with a laser dye, DCJTB, as the FRET acceptor (structure of DPATPAN shown in Fig. 1b).[9] While this FRET system showed enhanced LSC performance relative to DCJTB alone, DCJTB underwent fast photobleaching in ambient experimental conditions, in addition to concentration quenching, which limits its long-term utility for LSCs. We identified benzothiadiazole-based PITBT-TPE, a recently synthesized AIE chromophore,[15] as a potential acceptor candidate to replace DCJTB. Apart from being an appropriate FRET acceptor for DPATPAN, we observed that PITBT-TPE is still highly emissive even at very high concentrations in PMMA. Here, we investigated the photophysical properties and LSC performance of the DPATPAN/PITBT-TPE donor–acceptor pair. A high quantum yield was observed for PITBT-TPE and its blends with DPATPAN even at very high concentrations. Monte Carlo ray tracing simulations were used to predict the possible performance of a LSC that uses the DPATPAN/PITBT-TPE energy-transfer pair. We demonstrate for the first time LSC devices that utilize a FRET pair with both chromophores showing AIE characteristics.

All thin-film samples in this work were PMMA films containing chromophores which were deposited on glass slides by spin-coating from chloroform solutions (see ESI† for sample preparation details). The absorption spectrum of PITBT-TPE overlaps well with the emission spectrum of DPATPAN (Fig. 2a). In addition, the emission onset for PITBT-TPE in PMMA is significantly shifted to longer wavelengths relative to the absorption tail of DPATPAN, similar to DCJTB. This spectral separation between the donor absorbance and acceptor emission spectra is key to avoid reabsorption of acceptor emission by the donor, particularly for the energy migration and trapping approach wherein the tail optical density of the donor can be significant to maintain efficient light-harvesting. Significant tail absorption, as demonstrated by us[16] and others,[17] can lead to considerable reabsorption losses in LSCs.

The ϕ_{PL} measurements of chromophore thin-films were carried out using the integrating sphere method (see ESI† for details).[13] The quantum yield of PITBT-TPE in a PMMA thin-film matrix decreased as a function of concentration, from 93% at 9 mM to 45% at 225 mM (Fig. 2b). This suggested that PITBT-TPE, despite being an AIE chromophore, was susceptible to concentration quenching in a PMMA matrix. In contrast, DPATPAN, also an AIE chromophore, showed much higher

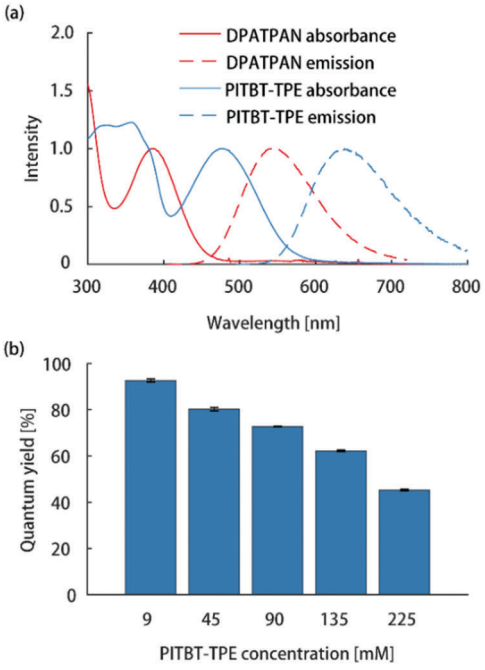

Fig. 2 (a) Normalized absorption and emission spectra of DPATPAN (250 mM in PMMA) and PITBT-TPE (200 mM in PMMA). (b) Emission quantum yield of PITBT-TPE at different concentrations in PMMA.

concentration quenching tolerance compared to PITBT-TPE. The ϕ_{PL} of DPATPAN was ~98% even at 250 mM in PMMA.

Using a constant DPATPAN concentration of 250 mM in PMMA, the ϕ_{PL} of films containing different DPATPAN and PITBT-TPE ratios was measured (Fig. 3a). The emission spectra of the blends systematically shifted to longer wavelengths with increasing amounts PITBT-TPE in the film (Fig. 3b). When the concentration of PITBT-TPE was higher than 22.5 mM, the emission spectrum of the DPATPAN/PITBT-TPE blends were identical to PITBT-TPE alone and full quenching of DPATPAN emission was observed (Fig. S1b, ESI†). At 250 mM in PMMA, the energy migration process between DPATPAN molecules has been previously identified to occur *via* a FRET mechanism using time-resolved fluorescence anisotropy experiments.[11] In this work, PITBT-TPE molecules act as energy traps. The FRET critical distance (R_0) between DPATPAN and PITBT-TPE molecules, at 250 mM and 22.5 mM in PMMA respectively, was 4.49 nm as calculated from the UV-Vis absorption and PL emission data. The mean inter-molecular distance between DPATPAN and PITBT-TPE was calculated to be 1.63 nm at these concentrations. This distance was within the R_0 value but larger than typical distances required for a Dexter transfer mechanism to be operative (see ESI† for calculation details).

We also observe consistently higher ϕ_{PL} of DPATPAN/PITBT-TPE blends when excited in the region where the donor strongly absorbs (390 nm) compared to direct excitation of the acceptor alone (Fig. 2b, 490 nm). We initially hypothesized that this observation was a result of a shift in dielectric environment from the addition of DPATPAN. The quantum yield was then measured by exciting the donor–acceptor blend at the acceptor's

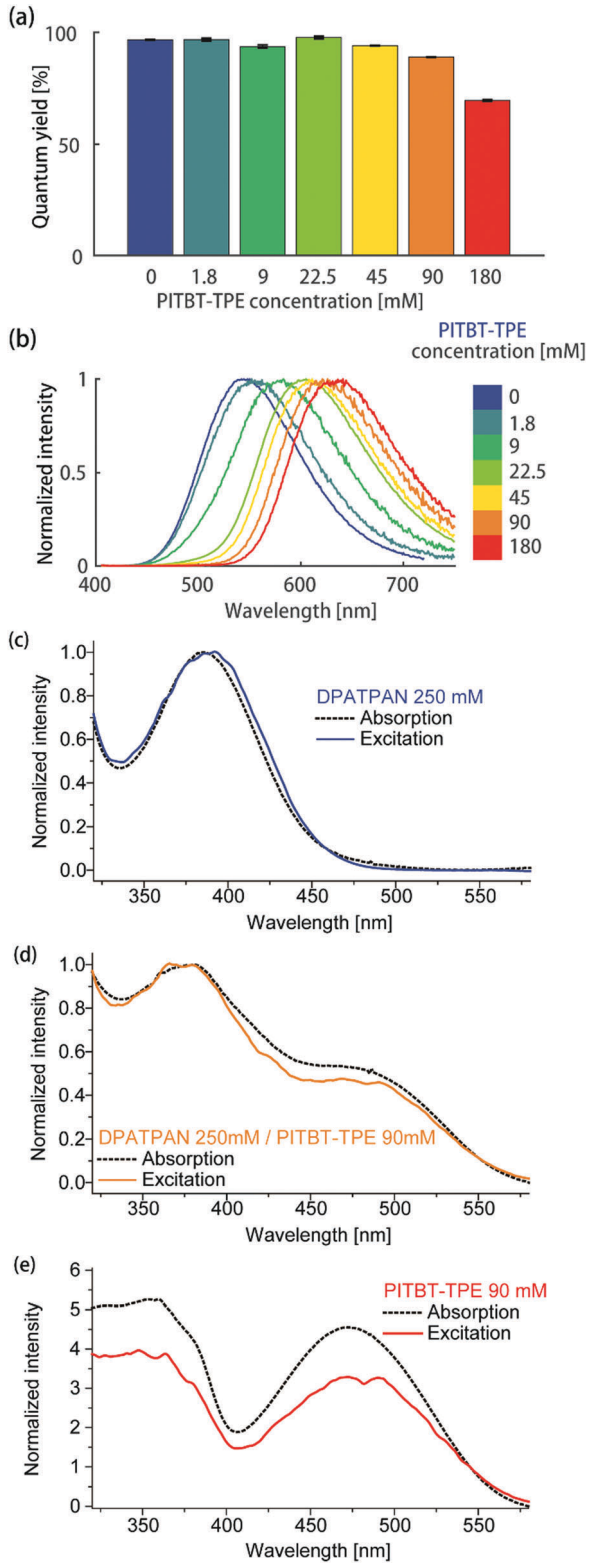

Fig. 3 (a) ϕ_{PL} and (b) emission spectrum of DPATPAN/PITBT-TPE blends in PMMA. The concentration of DPATPAN in all mixtures was 250 mM while the concentration of PITBT-TPE was varied. The ϕ_{PL} of all samples were measured by an integrating sphere (see ESI† for details). Comparison of the normalized absorption and excitation spectra of (c) DPATPAN (250 mM), (d) DPATPAN (250 mM)/PITBT-TPE (90 mM) blend and (e) PITBT-TPE (90 mM) in PMMA. Spectra in (c and d) were normalized at maximum intensity, while spectra in (e) were normalized at 540 nm.

absorption maximum. In this case, the quantum yield (ϕ_{PL} = 57.8 ± 0.5%, PITBT-TPE 180 mM, 490 nm) returned to the same level of the acceptor alone at the same concentration (Fig. 2b), which suggested a quantum yield variation of the donor–acceptor blends against the excitation wavelength, rather than a variation in dielectric environment with increasing chromophore concentration. The ϕ_{PL} of the DPATPAN/PITBT-TPE blends in the PMMA matrix decreased gradually with increasing concentration of PITBT-TPE. We ascribed the decrease in the quantum yield of the DPATPAN/PITBT-TPE blends with increasing concentration of PITBT-TPE to concentration quenching of PITBT-TPE. Considering the emission of DPATPAN was fully quenched at 22.5 mM of PITBT-TPE and the ϕ_{PL} of the DPATPAN/PITBT-TPE blends were all higher than PITBT-TPE alone, the FRET efficiency from DPATPAN to PITBT-TPE should be close to unity. The difference between the absorption and excitation spectra measured from the DPATPAN (250 mM)/PITBT-TPE (90 mM) blend films can be ascribed to ϕ_{PL} variation with excitation wavelength in the DPATPAN/PITBT-TPE blends. The excitation and absorption spectra of the sample with DPATPAN only matched very well from 320 nm to 550 nm, which suggested that there was little variation in the ϕ_{PL} of DPATPAN in this wavelength range (Fig. 3c).

On the other hand, the excitation spectrum of the DPATPAN/PITBT-TPE blend was lower than its absorption spectrum from 400 nm to 540 nm, which suggested the ϕ_{PL} of the blend excited in this range was lower than at other wavelengths (Fig. 3d, spectra normalised at 540 nm). In addition, the excitation spectrum of PITBT-TPE was much lower than its absorption spectrum below 540 nm, which indicated the ϕ_{PL} of PITBT-TPE decreased when excited at wavelengths shorter than 540 nm (Fig. 3e, spectra normalised at 540 nm). These absorption and excitation spectra comparisons and the quantum yield data suggested a possible whereby resonance energy transfer from DPATPAN to PITBT-TPE avoids higher excitation energy loss in PITBT-TPE (see ESI† for an illustration of one possible mechanism, Fig. S3). Further studies are required to fully examine this effect and elucidate the mechanism.

The Monte Carlo ray tracing simulation (see ESI† for details) was carried out to further examine the optical properties of LSC devices based on a series of DPATPAN/PITBT-TPE fluorophore samples.[18] In the simulation, the concentration of DPATPAN was maintained at 250 mM while the concentration of PITBT-TPE was at 22.5 mM, the minimum PITBT-TPE concentration at which the emission of DPATPAN was already fully quenched by FRET (Fig. 3b). As a reference, we also simulated the performance of an LSC that only contained 250 mM DPATPAN. The ϕ_{PL} of 250 mM DPATPAN in the presence or absence of 22.5 mM of PITBT-TPE were comparable (Fig. 3a). To compare the re-absorption effect of the DPATPAN-only and DPATPAN/PiTBT-TPE in a LSC device, we define the re-absorption value, F_R, as:

$$F_R = \frac{N_{Re}}{N_{absorbed}}$$

where N_{Re} is the number of photons that were counted as re-absorbed photons by the Monte Carlo ray trace simulation

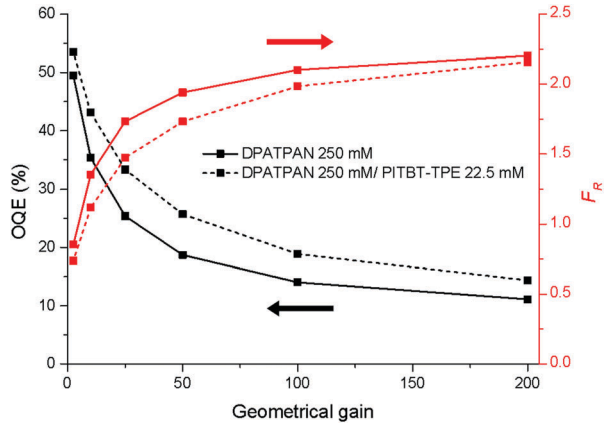

Fig. 4 Simulated OQE (black curves) and re-absorption number (red curves) of the LSC devices as a function of the geometric gain. The devices were based on 250 mM DPATPAN with (dashed line) or without (continuous line) PITBT-TPE in a PMMA thin-film matrix casted on a 1 mm thick square glass waveguide. The absorbance of all samples was set to 1.0 at 390 nm. All samples were excited at 390 nm and a total of 100 000 photons were traced in each simulation.

and $N_{absorbed}$ is the number of surface incident photons absorbed by the LSC ($N_{absorbed}$ = 100 000). As shown in Fig. 4, the simulated F_R of the LSC that contained the DPATPAN/PITBT-TPE blend was lower than the LSC that only contained DPATPAN over the range of geometric gains that were simulated. This result shows that re-absorption was reduced in the DPATPAN/PITBT-TPE blend.

The performance of the LSC devices was further characterised using optical quantum efficiency (OQE) as a comparison metric, define as:[19]

$$\mathrm{OQE} = \frac{N_{edge}}{N_{absorbed}}$$

where N_{edge} is the number of photons that are emitted only from all the edges of the LSC device. From the Monte Carlo analysis, the OQE of LSC devices that incorporated the DPATPAN/PITBT-TPE blend were all higher compared to LSC devices that contained only DPATPAN in the range of geometric gains simulated. We observed an OQE improvement of ~8%, at an LSC geometric gain of 25. Given the high ϕ_{PL} values of both DPATPAN only and DPATPAN/PITBT-TPE thin-films (Fig. 2b and 3a), the improvement in the simulated OQE could be ascribed to the reduction of re-absorption within the LSC. Further examination of the Monte Carlo data showed the external quantum efficiency (EQE) at 390 nm excitation and the flux gain of LSC devices based on the donor–acceptor blends were all higher than the devices of DPATPAN in the examined geometrical gain range (Fig. S4 and S5, ESI†). At a geometrical gain of 50, the flux gain of a LSC based on the DPATPAN (250 mM)/PITBT-TPE (22.5 mM) blend was 11.6. This flux gain value is comparable to reported benchmark LSC devices(flux gain = 11 flux gain at G = 45).[19] On increasing the concentration of PITBT-TPE to 180 mM, both the OQE and EQE of the LSC devices decreased due to lower ϕ_{PL} of PITBT-TPE at this concentration (Fig. S6, ESI†).

In conclusion, we have investigated the photophysics of PITBT-TPE in PMMA and its potential as an acceptor for LSCs that leverages energy migration and trapping to reduce reabsorption. It was observed that the quantum yield of PITBT-TPE can be sustained at high concentrations in PMMA. The blend composition of the DPATPAN/PITBT-TPE pair in thin-films has been optimised to maximize both the energy-transfer efficiency and emission quantum yield. Monte Carlo simulations of a LSC with optimal DPATPAN/PITBT-TPE composition predicted a reduction of re-absorption compared to LSCs with only DPATPAN. Our results provide insight and motivation into the development of AIE-based LSCs that can maximize light-harvesting as well as reduce reabsorption simultaneously.

Future work may additionally seek to broaden the absorption bandwidth of LSCs by using different AIE chromophores that will harvest most of the visible region of the solar spectrum and trap the absorbed energy to a low concentration, near-infrared emitter.[20,21] Designing highly emissive dyes that can absorb most of the red region of the solar spectrum and also sustain high concentrations in thin-films[22,23] are then desirable to achieve broadband light collection for LSCs.

Conflicts of interest

There are no conflicts to declare.

Acknowledgements

This work was made possible by support from the Australian Renewable Energy Agency which funds the project grants within the Australian Centre for Advanced Photovoltaics (ACAP). JLB was supported by an Australian Postgraduate Award and Eugen Singer Award during the period of this work. Responsibility for the views, information or advice expressed herein is not accepted by the Australian Government. WWHW is supported by an ARC Future Fellowship (FT130100500). KPG and WWHW are also supported by the ARC Centre of Excellence in Exciton Science (CE170100026). BZT acknowledges the Innovation and Technology Commission (ITC-CNERC14SC01) for support.

References

1 M. G. Debije, C. Tzikas, M. M. de Jong, M. Kanellis and L. H. Slooff, *Renewable Energy*, 2018, **116**, 335–343.
2 M. G. Debije, C. Tzikas, V. A. Rajkumar and M. M. de Jong, *Renewable Energy*, 2017, **113**, 1288–1292.
3 M. G. Debije and P. P. C. Verbunt, *Adv. Energy Mater.*, 2012, **2**, 12–35.
4 M. Kanellis, M. M. de Jong, L. Slooff and M. G. Debije, *Renewable Energy*, 2017, **103**, 647–652.
5 B. McKenna and R. C. Evans, *Adv. Mater.*, 2017, **29**, 1606491.
6 C. J. Traverse, R. Pandey, M. C. Barr and R. R. Lunt, *Nat. Energy*, 2017, **2**, 849–860.

7 A. Sanguineti, M. Sassi, R. Turrisi, R. Ruffo, G. Vaccaro, F. Meinardi and L. Beverina, *Chem. Commun.*, 2013, **49**, 1618–1620.
8 R. Turrisi, A. Sanguineti, M. Sassi, B. Savoie, A. Takai, G. E. Patriarca, M. M. Salamone, R. Ruffo, G. Vaccaro, F. Meinardi, T. J. Marks, A. Facchetti and L. Beverina, *J. Mater. Chem. A*, 2015, **3**, 8045–8054.
9 J. L. Banal, K. P. Ghiggino and W. W. H. Wong, *Phys. Chem. Chem. Phys.*, 2014, **16**, 25358–25363.
10 J. L. Banal, H. Soleimaninejad, F. M. Jradi, M. Liu, J. M. White, A. W. Blakers, M. W. Cooper, D. J. Jones, K. P. Ghiggino, S. R. Marder, T. A. Smith and W. W. H. Wong, *J. Phys. Chem. C*, 2016, **120**, 12952–12958.
11 J. L. Banal, B. Zhang, D. J. Jones, K. P. Ghiggino and W. W. H. Wong, *Acc. Chem. Res.*, 2017, **50**, 49–57.
12 G. D. Gutierrez, I. Coropceanu, M. G. Bawendi and T. M. Swager, *Adv. Mater.*, 2016, **28**, 497–501.
13 B. Zhang, H. Soleimaninejad, D. J. Jones, J. M. White, K. P. Ghiggino, T. A. Smith and W. W. H. Wong, *Chem. Mater.*, 2017, **29**, 8395–8403.
14 Y. Gong, Y. Tan, J. Liu, P. Lu, C. Feng, W. Z. Yuan, Y. Lu, J. Z. Sun, G. He and Y. Zhang, *Chem. Commun.*, 2013, **49**, 4009–4011.
15 J. Zhou, B. He, J. Xiang, B. Chen, G. Lin, W. Luo, X. Lou, S. Chen, Z. Zhao and B. Z. Tang, *ChemistrySelect*, 2016, **1**, 812–818.
16 J. L. Banal, J. M. White, K. P. Ghiggino and W. W. H. Wong, *Sci. Rep.*, 2014, **4**, 4635.
17 L. R. Wilson, B. C. Rowan, N. Robertson, O. Moudam, A. C. Jones and B. S. Richards, *Appl. Opt.*, 2010, **49**, 1651–1661.
18 C. Haines, M. Chen and K. P. Ghiggino, *Sol. Energy Mater. Sol. Cells*, 2012, **105**, 287–292.
19 M. J. Currie, J. K. Mapel, T. D. Heidel, S. Goffri and M. A. Baldo, *Science*, 2008, **321**, 226–228.
20 R. Rondão, A. R. Frias, S. F. H. Correia, L. Fu, V. de Zea Bermudez, P. S. André, R. A. S. Ferreira and L. D. Carlos, *ACS Appl. Mater. Interfaces*, 2017, **9**, 12540–12546.
21 Y. Zhao, G. A. Meek, B. G. Levine and R. R. Lunt, *Adv. Opt. Mater.*, 2014, **2**, 606–611.
22 F. De Nisi, R. Francischello, A. Battisti, A. Panniello, E. Fanizza, M. Striccoli, X. Gu, N. L. C. Leung, B. Z. Tang and A. Pucci, *Mater. Chem. Front.*, 2017, **1**, 1406–1412.
23 F. Gianfaldoni, F. De Nisi, G. Iasilli, A. Panniello, E. Fanizza, M. Striccoli, D. Ryuse, M. Shimizu, T. Biver and A. Pucci, *RSC Adv.*, 2017, **7**, 37302–37309.

The electronic supporting information of

Aggregation-induced emission-mediated spectral downconversion in luminescent solar concentrators

Bolong Zhang, James L. Banal, David J. Jones, Ben Zhong Tang, Kenneth P. Ghiggino, and Wallace W. H. Wong*

General experimental details

All commercial reagents and solvents were used in the paper as received from suppliers. DPATPAN[1] and PITBT-TPE[2] have been reported previously and they were synthesized using procedures as described.

Supporting figures

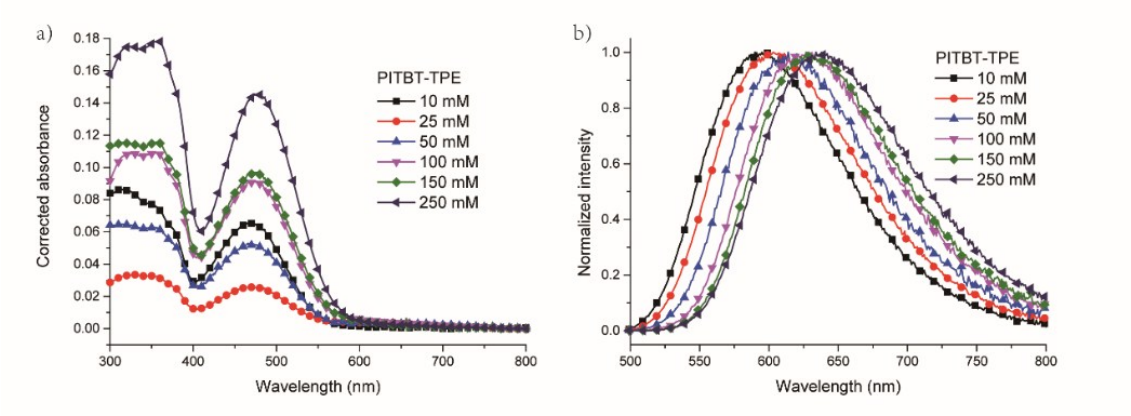

Figure S1. a) The corrected absorbance spectra and b) the normalized emission spectra of PITBT-TPE alone in PMMA thin-film matrix.

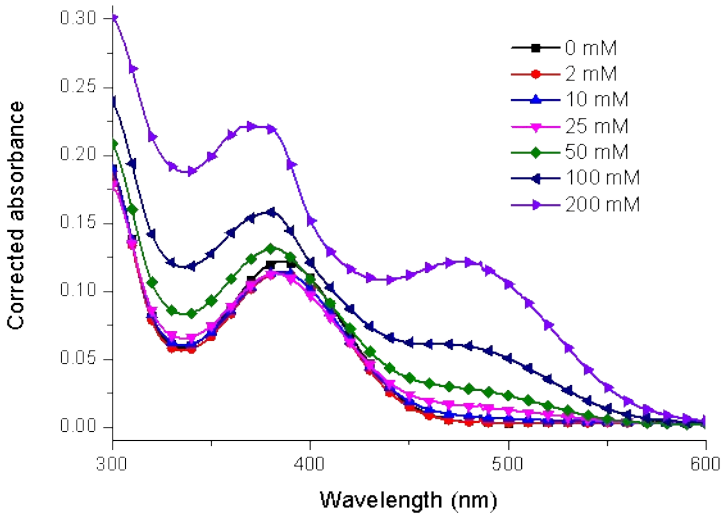

Figure S2. a) The absorbance spectra of DPATPAN/PITBT-TPE blend in PMMA thin-film matrix, where DPATPAN concentration is 250 mM for all samples.

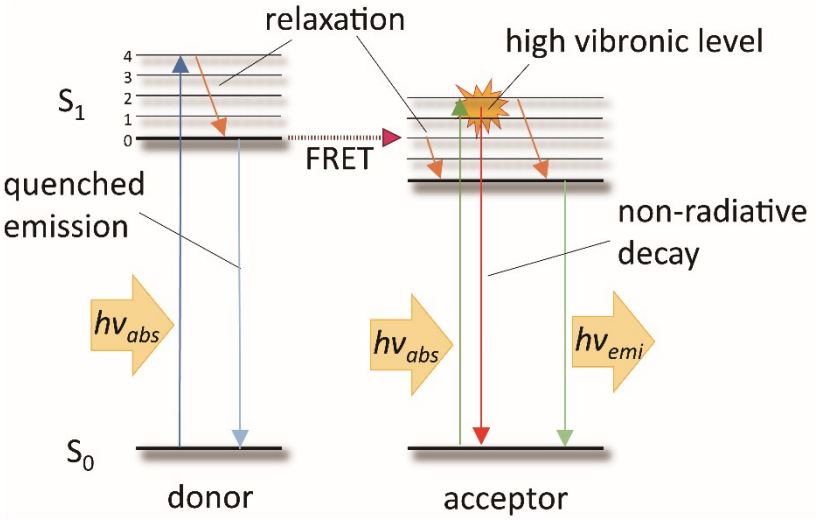

Figure S3. A Jablonski diagram illustrating a possible mechanism of energy transfer from DPATPAN donor to PITBT-TPE acceptor that may lead to the higher photoluminescence quantum yield observed in the donor-acceptor blend film. A potential hypothesis is PITBT-TPE prepared in a high S_1 vibronic state undergoes an additional non-radiative process resulting in a reduced φ_{PL}. By exciting the absorption maximum of DPATPAN in the DPATPAN/PITBT-TPE blend, this additional non-radiative process can be by-passed through energy transfer to a lower vibronic states in PITBT-TPE, resulting in a higher φ_{PL}.

Thin film sample preparation

All the glass (MENZEL-GLÄSER Microscope Slides, 76 × 26 mm) and quartz (PST Quartz slide, 76 × 25mm) slides used in the absolute quantum yield measurements were cut to 1.25 cm × 1.25 cm × 0.1 cm, cleaned by sonicating sequentially in $CHCl_3$, acetone, NaOH (a.q.), distilled water and isopropanol and dried using a strong flow of N_2.

All the thin film samples for the absolute quantum yield measurement were prepared by spin coating 80 µL of a casting solution of the dyes and PMMA (Sigma-Aldrich, Mw ~996,000) on top of the above-mentioned glass or quartz slides. The spin coating speed was from 500 to 800 rpm depending on the absorbance required for the sample and the acceleration was 400 rpm/s. The casting solutions of the dyes and PMMA were prepared by diluting the mixture of the prototypical solution of each dye (5 mM in $CHCl_3$) and the PMMA solution (0.05 g/ml in $CHCl_3$) with $CHCl_3$ to reduce the concentration of PMMA to 1% w/w. The concentration of the dyes in the casting solutions were calculated based on the volume of the solid-state PMMA. After spin coating, the samples were baked at 100°C for 10 min to evaporate the solvent.

Absolute quantum yield measurements and re-absorption correction

Absolute quantum yield measurements of all samples were performed according to the experimental approach described elsewhere[3] using an integrating sphere accessory (F3018, Horiba Jobin Yvon) on a Fluorolog®-3 fluorimeter. The angle of the excitation beam to the normal of the sample surface can be modified using the variable angle sample holder. All spectra for the absolute quantum yield measurements were corrected for the light source noise, wavelength sensitivity

and the transmittance of the filters. The photon counts of all the measurements on the Fluorolog®-3 fluorimeter were within the linear response range of the detector (less than 2×10^6 cps). The re-absorption correction[4] was used on all measurement. The reference emission spectrum for re-absorption correction was recorded from the samples in the absence of the integrating sphere.

Calculation of Förster critical distance (R_0)

The Förster resonance energy transfer (FRET) critical radius (R_0, nm) from DPATPAN to PITBT-TPE is defined via the following Förster equation[5]:

$$R_0 = 0.02108 \times \left(\frac{\kappa^2 \Phi_{PL} J}{n^4}\right)^{\frac{1}{6}}$$

$$J = \int \varepsilon_A(\lambda) F_D(\lambda) \lambda^4 d\lambda$$

where κ^2 is the orientation factor (κ^2=2/3 for random orientation, long lifetime donor and acceptor system), Φ_{PL} refers to the PLQY of the donor fluorophore in the absence of the acceptor, J (nm^4, M^{-1}, cm^{-1}) is a coefficient related to the overlap between the normalized (area) emission spectrum (F_D) of the donor and the absorption extinction coefficient (ε_A) of the acceptor, λ is the wavelength over the full spectrum, and n is the refractive index of the matrix material (n=1.49 for PMMA matrix). The calculated R_0 of DPATPAN (250 mM) to PITBT-TPE (22.5 mM) is 4.49 nm.

The mean inter-particle distance of DPATPAN (d_D) is defined by the following equation:

$$d_D = \left(c \times N_A \times 1000\right)^{-\frac{1}{3}}$$

where, c is the molar concentration of the material (M) and N_A is the Avogadro's constant.

Then the mean inter-particle distance of between DPATPAN to PITBT-TPE (d_{D-A}) is defined by the following equation:

$$d_{D-A} = \frac{\sqrt{3}}{2} d_D$$

Performance of LSC devices

All performance results of LSC devices were calculated by Monte-Carlo tracing simulation, the details can be found in publish reports.[6] The inputs of the simulation is based on experimental data that measured from real samples, which includes the absorption spectrum , emission spectrum and the photoluminescent quantum yield.

The external quantum efficiency (EQE), and G (geometrical gain) can be defined as:

$$EQE = \frac{n_{edge}}{n_{incident}}$$

$$G = \frac{S_{surface}}{S_{edge}}$$

where n_{edge} is the number of the total edge output photon, $n_{incident}$ is number of the incident photon to the surface. S_{edge} and $S_{surface}$ are the area of the edges and surface of the waveguide respectively.

The flux gain (F) can be defined as:

$$F = \frac{I_{edge}}{I_{surface}} = EQE \times G$$

where the I_{edge} refers to the intensity of one edge output and $I_{surface}$ is the intensity of the light absorbed.

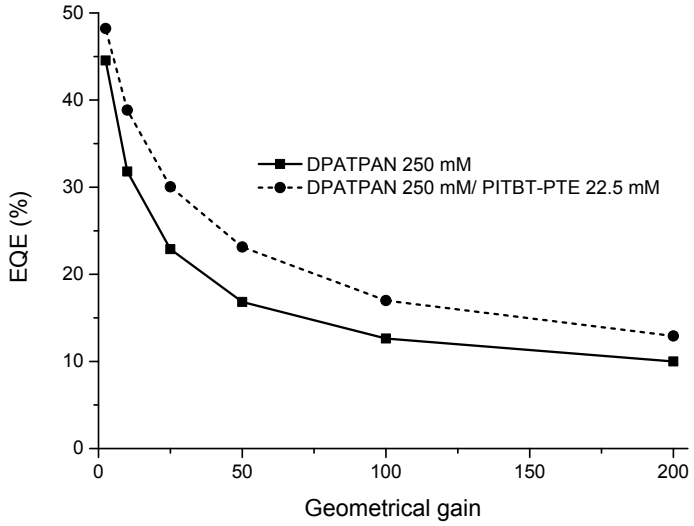

Figure S4 Simulated EQE of the LSC devices as a function of the geometric gain at 390 nm excitation.

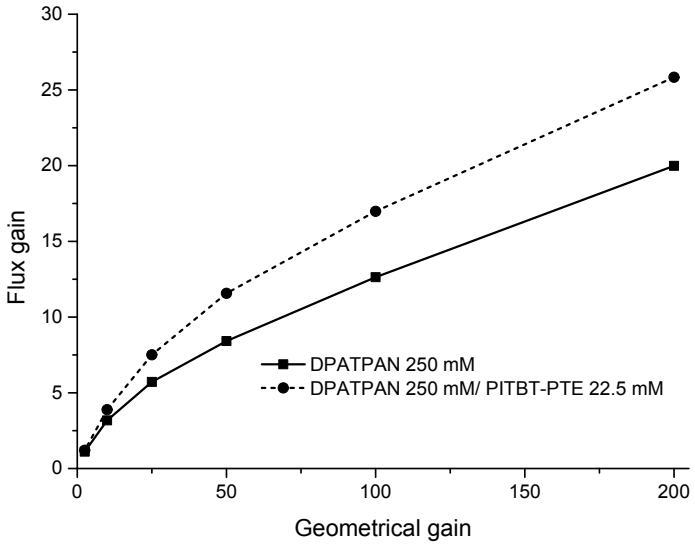

Figure S5 Simulated flux gain of the LSC devices as a function of the geometric gain.

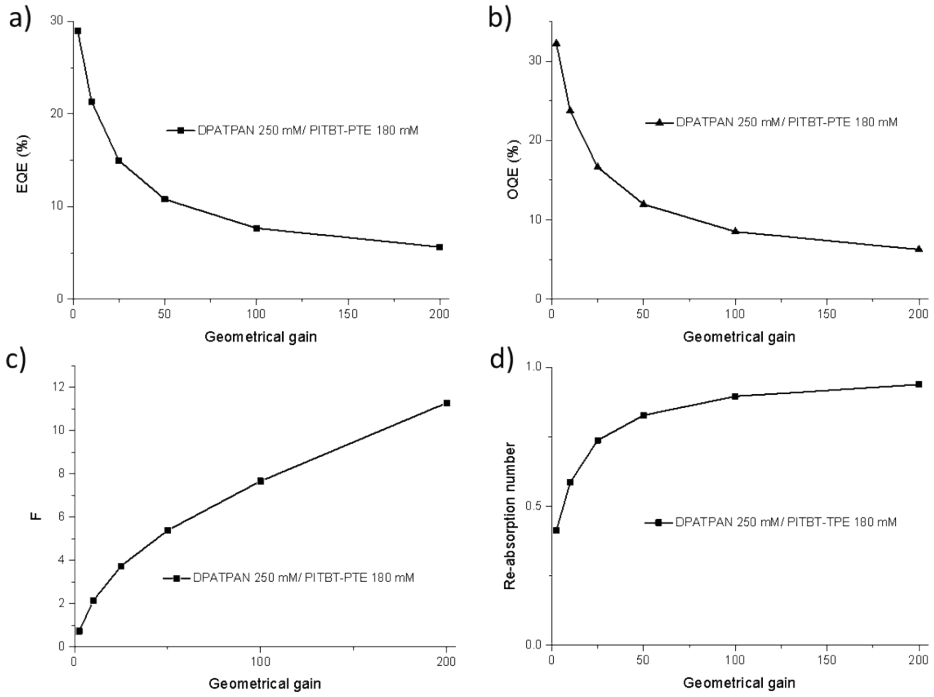

Figure S6 The simulated performance results of LSC devices based on DPATPAN 250 mM and PITBT-TPE 180 mM blend: a) EQE, b) OQE, c) flux gain and d) the re-absorption number.

Reference list:

(1) Gong, Y.; Tan, Y.; Liu, J.; Lu, P.; Feng, C.; Yuan, W. Z.; Lu, Y.; Sun, J. Z.; He, G.; Zhang, Y., *Chemical Communications* **2013,** *49* (38), 4009-4011.

(2) Zhou, J.; He, B.; Xiang, J.; Chen, B.; Lin, G.; Luo, W.; Lou, X.; Chen, S.; Zhao, Z.; Tang , B. Z., *ChemistrySelect* **2016,** *1* (4), 812-818.

(3) (a) Würth, C.; Grabolle, M.; Pauli, J.; Spieles, M.; Resch-Genger, U., *Nature protocols* **2013,** *8* (8), 1535-1550; (b) Porrès, L.; Holland, A.; Pålsson, L.-O.; Monkman, A. P.; Kemp, C.; Beeby, A., *Journal of Fluorescence* **2006,** *16* (2), 267-273.

(4) Wilson, L. R.; Rowan, B. C.; Robertson, N.; Moudam, O.; Jones, A. C.; Richards, B. S., *Applied Optics* **2010,** *49* (9), 1651-1661.

(5) (a) Fluorescence Detection Techniques. In *Introduction to Fluorescence Sensing*, Demchenko, A. P., Ed. Springer Netherlands: Dordrecht, 2009; pp 65-118; (b) Medintz, I. L.; Hildebrandt, N., *FRET - Förster Resonance Energy Transfer: From Theory to Applications*. Wiley: 2013.

(6) Xu, J.; Zhang, B.; Jansen, M.; Goerigk, L.; Wong, W. W. H.; Ritchie, C., *Angewandte Chemie International Edition* **2017,** *56* (44), 13882-13886.

Chapter IV

Molecularly Insulated Donor-emitter Pairs for LSCs

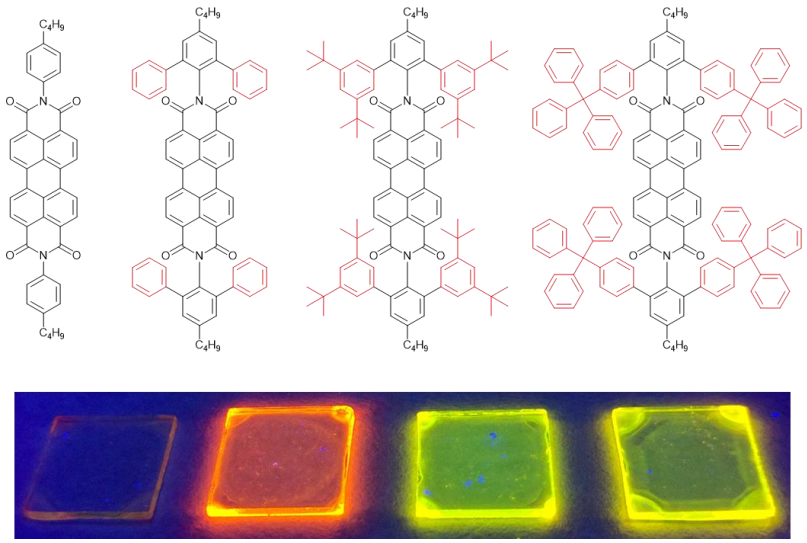

Reprinted with the permission from Ref [4], copyright © 2017 American Chemical Society.

4.1 Preface

As shown in **Chapter III**, the ϕ_{PL} of the AIE fluorophores, PITBT-TPE and DPATPAN, decreased against the increasing concentration in PMMA matrix. The properties of AIE fluorophores can still be affected by aggregation caused quenching (ACQ) in high concentration, particularly in neat solid-state. The ACQ effect will reduce the ϕ_{PL} of the fluorophore when used in high concentration,

leading to a potential limitation to the performance of LSCs. Another approach to avoid the ACQ effect is to introduce bulky-substituents on the fluorophore, which then reduces the chromophore-chromophore interactions when aggregates. This approach has been called molecular insulation in our previous work.[1] The main idea of molecular insulation is to stop the intermolecular π-π stacking of the fluorophores by using bulky substituents.[1] Once the intermolecular π-π stacking is prevented, the ACQ effect on the fluorophores should be reduced in high concentration or even in solid state.

The benefits of the energy migration among molecularly-insulated donors was demonstrated in our group previously.[1] A sterically hindered perylene diimide (PDI) was used as the energy donor material and paired with a commercial PDI-based fluorophore (Lumogen® F Red 305, BASF) to form the donor-emitter pair (Figure 4.1b). To avoid the ACQ effect of the donor in high concentration, four bulky-substituents were installed at the imide-position of the perylene core (Figure 4.1a). The bulky-substituents can help to reduce the intermolecular interactions in the aggregates and retains the photophysical properties of the PDI. Due to the steric hindrance of the bulky substituents, the ϕ_{PL} of the donor PDI was close to unity at 40 mM in PMMA matrix and is still 60% at 120 mM. In addition, when it is blended with the PDI emitter in an optimized ratio, the donor-emitter PDI pair showed an overall ϕ_{PL} of 82% at around 74 mM and the overlap between the absorption and emission spectra was significantly reduced. As a consequence, the power output of the LSC based-on this PDI pair was 1.64 times higher than the emitter-only counterpart device.

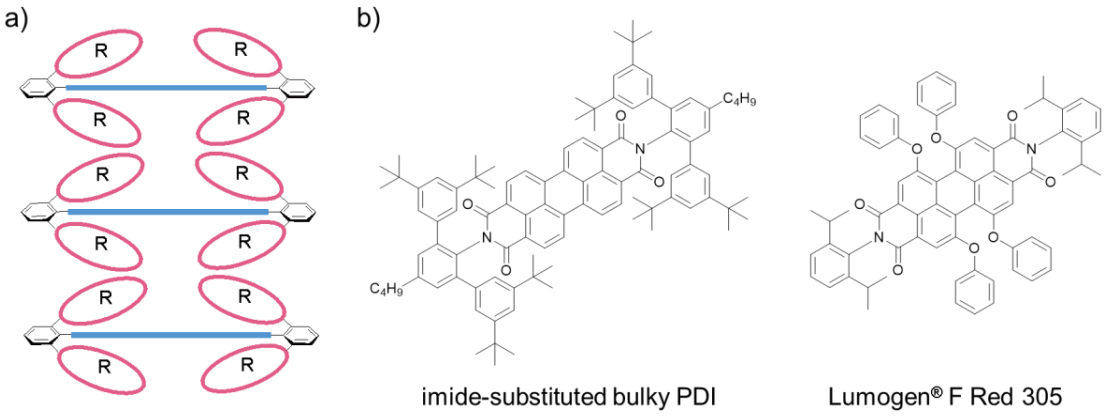

Figure 4.1 a) the bulky-substituents installed at the imide-position of the PDI can effectively reduce the interaction of the perylene cores in aggregates; b) the molecular structure of the donor and the emitter PDIs.

In addition, there are three criteria of the substituents that can influence the photophysical properties of the PDI, namely the shape, the electron density and the location of the substituents. The shape of the bulky-substituents has a direct influence on the π - π interaction of the perylene core in aggregates, leading to the variation of the photophysical properties. The substituents can be installed at the bay-position, ortho-position and imide position of the perylene core (see Figure 1 in the publication in this chapter). The imide-substitution usually shows less influence on the photophysical properties of the PDIs. The electron density of the substituents on the bay or ortho-position can influence the HOMO and LUMO of the PDIs.[2-3] For the purpose of reducing the ACQ effect, we chose to install the bulky-substituents without disturbing the photophysical properties of the PDIs.

Ideally, the influence of intermolecular π-π stacking can be eliminated if the perylene core are fully covered by the bulky substituents R (Figure 4.2). The bulky substituents have to be either non-conjugated structures which have no interaction with the perylene core, or perhaps rigid conjugated groups that have a fixed distance from the core that is out of the range of the π-orbital

interaction. To pursue this concept, two macrocyclic structure designs were examined.

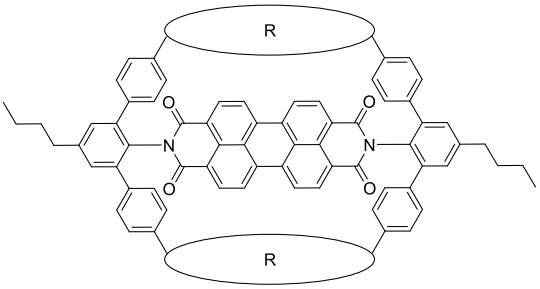

Figure 4.2 The perylene core is protected by two bridging moieties forming a macrocyclic structure.

The first synthesis approach of the macrocyclic PDI (Compound 1) is shown in Figure 4.3. The preliminary molecular models (BioChem3D) showed that such rigid structure may be possible with low calculated strain energy. By this approach, two rigid tether substituents were to be installed on both sides of the tetra-bromo PDI via a Suzuki-coupling reaction to give Compound 1. However, under the difficult macrocyclization conditions, the desired product was not observed in the reaction. A potential reason for the difficulty is that the di-phenyl structure was too rigid. Once the Suzuki-coupling occurred in one side, the rigidity of the bridge would force the other side of the bridge away from the favored reaction configuration.

The second synthesis approach of the macrocyclic PDI (Compound 2) is shown in Figure 4.4. To avoid the synthetic difficulty of the rigid bridge structure, a more flexible bridging moiety was attempted. Four 4-(pent-4-enyloxy)phenyl were added to the tetra-bromo-PDI via Suzuki Coupling to give the precursor of Compound 2. The side-chains in each face of the molecule would be closed by Grubbs reaction (Compound 2). Both the double-bridge product and the single-bridge precursor were observed in the mass spectrum of the crude product (Figure 4.5). However, the double-bridge product could not be isolated.

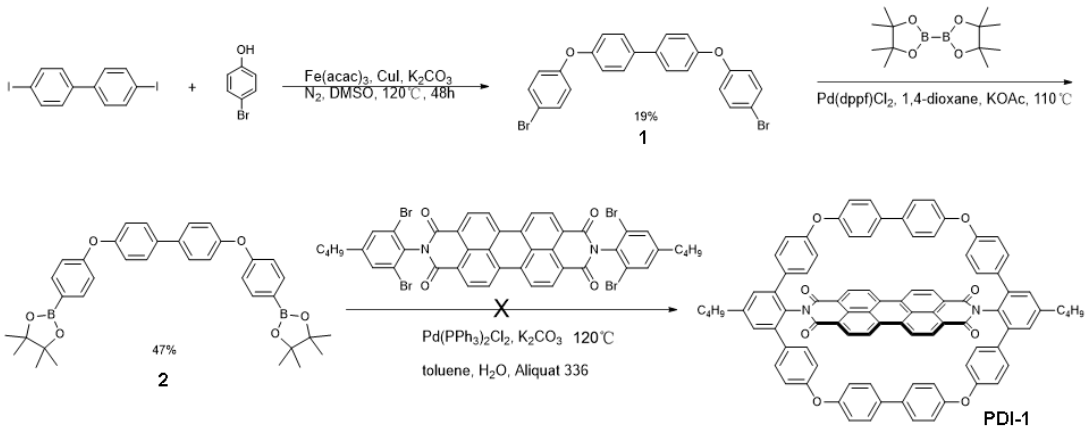

Figure 4.3 The first synthesis process of the double-bridge PDI. The reaction condition and experimental details can be found in the experimental data section.

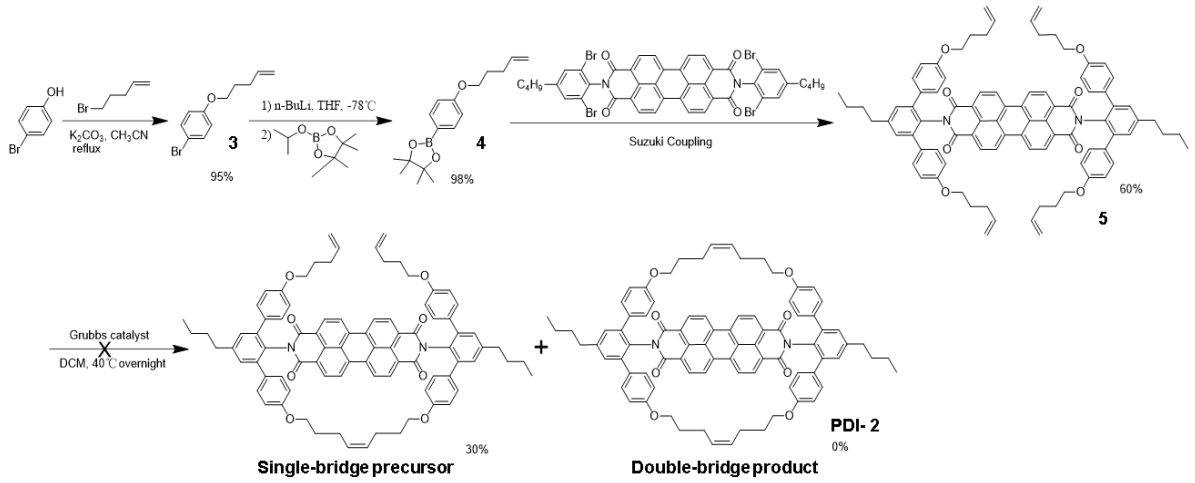

Figure 4.4 The second synthesis process of the double-bridge PDI. The reaction condition and experimental details can be found in the experimental data section.

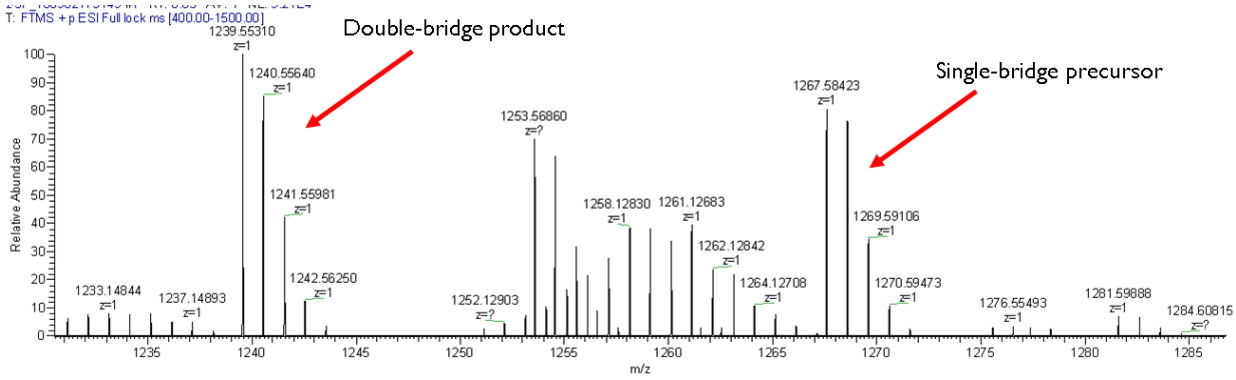

Figure 4.5 The mass spectrum revealed that the crude product of the second synthesis process contains both the target product and the one-side bridge closed precursor.

As it was too difficult to produce the macrocyclic PDI derivatives, synthesis of bulky group substituted PDIs was then considered. In this work, a series of bulky group substituted PDI derivatives (bPDI) were designed and synthesized with their photophysical properties characterized. The bulky substituents were installed at the imide position to avoid influencing the physical/electronic properties of the perylene core. Some bPDIs showed a ϕ_{PL} above 90% at very high concentration in PMMA matrix. The performance of LSCs based-on bPDIs in a donor-emitter fluorophore pair system was examined. The research results were summarized and published in the following article[4]:

Bolong Zhang, Hamid Soleimaninejad, David J. Jones, Jonathan M. White, Kenneth P. Ghiggino, Trevor A. Smith, Wallace W.H. Wong. Highly Fluorescent Molecularly Insulated Perylene Diimides: Effect of Concentration on Photophysical Properties. *Chem. Mater.* **2017**, 29, 19, 8395-8403. DOI: 10.1021/acs.chemmater.7b02968

The experimental details are included in the Supporting Information section following the main manuscript. Reprinted with the permission from Ref [4], copyright © 2017 American Chemical Society.

Contribution of the Candidate:

- Spectroscopy measurements.
- Photoluminescent quantum yield measurements.
- Monte-Carlo ray tracing simulation studies.
- Fabrication of LSC devices.
- Contributing to the writing of drafts of the manuscript.

4.2 Experimental data on initial work

The synthesis details of materials.

1

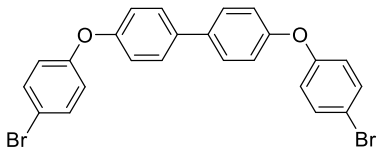

A mixture of diiodo biphenyl (5.0 g, 12.5 mmol), 4-bromo-phenol (4.3 g, 25.0 mmol), $Fe(acac)_3$ (353 mg, 1.0 mmol), CuI (190 mg, 1.0 mmol) and K_2CO_3 (4.1 g, 30 mmol) was dissolved in DMSO (50 mL). The mixture then was degased under N_2 for 30 minutes and stirred under 120 ℃ for 48 hours. The crude product was separated by flash chromatography (SiO_2, cyclohexane: toluene = 7:3) to give the final product (1.2 g, 2.4 mmol) as a white solid with a 19% yield.

^{1}H NMR (500 MHz, $CDCl_3$) δ = 7.54 (d, *J*=8.8, 4H), 7.46 (d, *J*=9.0, 4H), 7.07 (d, *J*=8.8, 4H), 6.94 (d, *J*=9.0, 4H).

^{13}C NMR (126 MHz, $CDCl_3$) δ = 156.43, 156.18, 135.97, 132.73, 128.32, 120.52, 119.25, 115.80.

MS ESI+ (m/z): calcd. for [M^+] $C_{24}H_{16}B_2O_2$, 495.94966; found [M^+], 495.94889.

FT-IR (cm^{-1}, neat): 1602.4, 1519.8, 1481.8, 1257.8, 1166.0, 1072.9, 999.8, 815.0, 772.6.

2

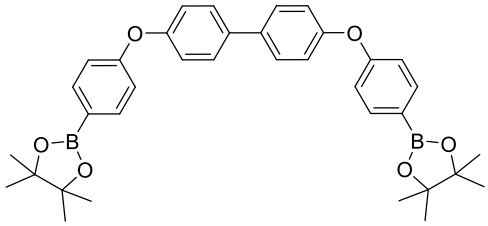

A mixture of 1 (500 mg, 1.0 mmol), bis(pinacolato)diboron (635 mg, 2.5 mmol), $Pd(dppf)Cl_2$ (73 mg, 0.1 mmol) and KOAc (490 mg, 5.0 mmol) was heated at 50 ℃ under vacuum to remove the moisture. The mixture then dissolved in DMF (50 mL) and stirred for 48 hours in 120 ℃ under N_2. The crude product was separated by flash chromatography (SiO_2, from toluene to chloroform) to give the final product (280 mg, 0.47 mmol) as a white solid with a 47% yield.

^1H NMR (400 MHz, $CDCl_3$) δ = 7.80 (d, *J*=8.1, 4H), 7.54 (d, *J*=8.6, 4H), 7.08 (d, *J*=8.6, 4 H), 7.03 (d, *J*=8.3, 4H), 1.35 (s, 24H).

^{13}C NMR (126 MHz, $CDCl_3$) δ = 160.07, 155.97, 136.66, 135.99, 128.24, 119.65, 117.77, 83.75, 24.87.

MS ESI+ (m/z): calcd. for $[M+H^+]$ $C_{36}H_{41}B_2O_6$, 591.30893; found $[M+H^+]$, 591.30890.

FT-IR (cm-1, neat): 2979.4, 1595.3, 1491.5, 1358.8, 1236.3, 1122.7, 960.8, 826.6, 751.5, 653.6.

3

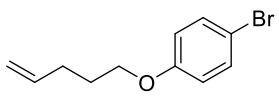

This material is synthesized through the literature reported procedure.[5]

^1H NMR (400 MHz, $CDCl_3$) δ 7.44 – 7.31 (m, 2H), 6.86 – 6.70 (m, 2H), 5.85 (ddt, *J* = 16.9, 10.2, 6.6 Hz, 1H), 5.13 – 4.95 (m, 2H), 3.93 (t, *J* = 6.4 Hz, 2H), 2.31 – 2.15 (m, 2H), 1.88 (dt, *J* = 8.0,

6.6 Hz, 2H).

^{13}C NMR (101 MHz, $CDCl_3$) δ 158.14, 137.63, 132.18, 116.29, 115.29, 112.64, 67.38, 30.03, 28.30.

4

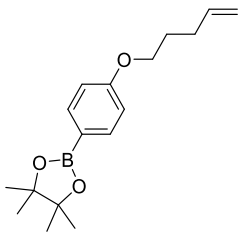

The solution of *n*-BuLi in THF (2.4 M, 11 mmol, 4.6 mL) was dropwisely add to the solution of zbl-52 (1.3 g, 5.5 mmol) in THF (25 ml) under -78℃. The mixture was stirred under -78℃ for 30 minutes and then added isopropoxy bronic acid pinacol ester (2.0 g, 11 mmol). The mixture was kept on stirred in r.t. for 1 hour. After removing the solvent, the crude product was dissolved in toluene and purified by the flush chromatography (SiO_2, toluene) to give the target product (colourless oil, 0.95 g, 60% yield)

^{1}H NMR (400 MHz, $CDCl_3$) δ 7.80 – 7.70 (m, 2H), 6.93 – 6.86 (m, 2H), 5.85 (ddt, *J* = 16.9, 10.2, 6.6 Hz, 1H), 5.13 – 4.93 (m, 2H), 3.99 (t, *J* = 6.5 Hz, 2H), 2.31 – 2.17 (m, 2H), 1.90 (dt, *J* = 8.0, 6.5 Hz, 2H), 1.34 (s, 12H).

^{13}C NMR (101 MHz, $CDCl_3$) δ 161.64, 137.73, 136.48, 115.20, 113.85, 83.49, 66.90, 30.08, 28.37, 24.85.

MS ESI+ (m/z): calcd. for $[M+H^+]$ $C_{17}H_{26}BO_3$, 289.19750; found $[M+H^+]$, 289.19699.

FT-IR (cm^{-1}, neat): 2978.2, 1604.7, 1358.4, 1244.2, 1141.8, 1090.4, 860.3, 830.6, 654.

5

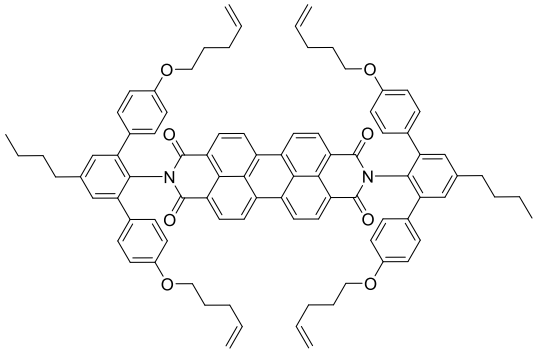

A mixture of tetrabromo-PDI (100 mg, 0.10 mmol), 4 (174 mg, 0.60 mmol) and $Pd(PPh_3)_4$ (30 mg, 0.026 mmol) were dissolved in toluene (8% w/w Aliquate 336, 5 ml) and K_2CO_3 solution (2 M, 1 mL) solution. The solution was sealed under N_2 and then refluxed and stirred 48h. The crude product was purified by flush chromatography (toluene:ethyl acetate 10:1) to give the target product (dark red powder, 77 mg, 60% yield).

^{1}H NMR (400 MHz, Benzene-d_6) δ 8.35 (d, J = 7.9 Hz, 4H), 7.73 – 7.66 (m, 8H), 7.36 (s, 4H), 7.21 (d, J = 8.1 Hz, 4H), 6.69 – 6.63 (m, 8H), 5.53 – 5.30 (m, 4H), 4.82 – 4.64 (m, 8H), 3.35 – 3.25 (m, 8H), 2.53 (t, J = 7.9 Hz, 4H), 1.76 (q, J = 7.2 Hz, 8H), 1.47 (q, J = 8.1 Hz, 4H), 1.35 (dd, J = 9.1, 5.2 Hz, 8H), 1.30 – 1.22 (m, 4H), 0.83 (t, J = 7.4 Hz, 6H).

^{13}C NMR (101 MHz, Benzene-d_6) δ 163.67, 158.58, 143.45, 143.36, 141.72, 137.54, 134.30, 132.46, 130.83, 130.24, 129.90, 129.23, 126.12, 122.69, 122.39, 114.58, 113.86, 66.44, 35.44, 33.28, 29.82, 28.14, 22.62, 13.81.

MS ESI+ (m/z): calcd. for $[M+H^+]$ $C_{88}H_{83}N_2O_8$, 1295.61494; found $[M+H^+]$, 1295.61438.

FT-IR (cm^{-1}, neat): 2927.7, 1701.9, 1662.5, 1593.2, 1509.0, 1341.7, 1241.1, 1175.1, 835.1, 809.9, 745.7.

Reference

1. Banal, J. L.; Soleimaninejad, H.; Jradi, F. M.; Liu, M.; White, J. M.; Blakers, A. W.; Cooper, M. W.; Jones, D. J.; Ghiggino, K. P.; Marder, S. R.; Smith, T. A.; Wong, W. W. H., Energy Migration in Organic Solar Concentrators with a Molecularly Insulated Perylene Diimide. J. Phys. Chem. C 2016, 120 (24), 12952-12958.
2. Lin, M.-J.; Jiménez, Á. J.; Burschka, C.; Würthner, F., Bay-Substituted Perylene Bisimide Dye with an Undistorted Planar Scaffold and Outstanding Solid State Fluorescence Properties. Chem. Commun. 2012, 48 (99), 12050-12052.
3. Chen, Z.; Baumeister, U.; Tschierske, C.; Würthner, F., Effect of Core Twisting on Self-Assembly and Optical Properties of Perylene Bisimide Dyes in Solution and Columnar Liquid Crystalline Phases. Chem. Eur. J. 2007, 13 (2), 450-465.
4. Zhang, B. L.; Soleimaninejad, H.; Jones, D. J.; White, J. M.; Ghiggino, K. P.; Smith, T. A.; Wong, W. W. H., Highly Fluorescent Molecularly Insulated Perylene Diimides: Effect of Concentration on Photophysical Properties. Chem. Mater. 2017, 29 (19), 8395-8403.
5. Li, X.; Huang, Z.; Zavala, R.; Tang, M., Distance-Dependent Triplet Energy Transfer between Cdse Nanocrystals and Surface Bound Anthracene. J. Phys. Chem. Lett. 2016, 7 (11), 1955-1959.

CHEMISTRY OF MATERIALS

Article

pubs.acs.org/cm

Highly Fluorescent Molecularly Insulated Perylene Diimides: Effect of Concentration on Photophysical Properties

Bolong Zhang, Hamid Soleimaninejad, David J. Jones, Jonathan M. White, Kenneth P. Ghiggino, Trevor A. Smith, and Wallace W. H. Wong*

School of Chemistry, Bio21 Institute, The University of Melbourne, Parkville, Victoria 3010, Australia

Supporting Information

ABSTRACT: A series of four perylene diimide (PDI) chromophores were prepared with increasing steric bulk on the imide substituents with the aim of retarding the effect of concentration quenching on photoluminescence, commonly observed with these dyes. Spectroscopic investigations of the compounds in dilute solution confirmed that the photophysical properties of the PDI core chromophore were not perturbed by the bulky substituents. Solid film samples containing the PDI compounds at various concentrations dispersed in a poly(methyl methacrylate) (PMMA) matrix were examined and compared to amorphous neat films as well as crystalline samples. The PDI compounds containing di-*tert*-butylphenyl (bPDI-3) and trityl (bPDI-4) substituents showed near unity photoluminescence quantum yield (PLQY) up to 20 mM in PMMA compared to 10% PLQY for the reference compound (bPDI-1) without molecular insulation. Surprisingly, high concentrations (>40 mM) of a phenyl-substituted PDI compound (bPDI-2) with moderate molecular insulation formed emissive aggregates that showed a higher PLQY compared to the PDI derivatives with greater steric bulk. By examining the molecular structure and solid state packing in conjunction with a series of photophysical measurements, new insights into designing highly fluorescent dyes, particularly in the solid state, were obtained. The trityl-substituted PDI compound (bPDI-4) was used in a luminescent solar concentrator with optical quantum efficiency of 54%, flux gain of 6.4, and geometric gain of 45.

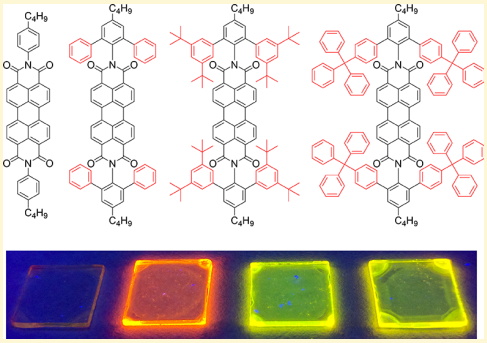

INTRODUCTION

Perylene diimide (PDI) is a polycyclic aromatic chromophore widely used in the dye industry and has been studied as an advanced material with applications in fluorescence labeling,[1] organic semiconducting devices,[2,3] and light harvesting.[4,5] The PDI chromophore can be easily functionalized to achieve derivatives with desired properties including the tuning of photon absorption and emission while maintaining good photo- and thermal stability.[4,6,7] One key feature of PDI compounds is that their conjugated perylene core has a strong tendency to intermolecular $\pi-\pi$ stacking, leading to molecular aggregates. While these aggregates or supramolecular assemblies can lead to desirable materials properties, such as charge transport, photophysical properties of the PDI chromophore can also change significantly.[8−10] Apart from perturbation of the absorption spectrum, a commonly observed characteristic of PDI chromophores is the decrease in photoluminescence quantum yield (PLQY) with increasing concentration.[11] Clearly, this observation is a result of the formation of $\pi-\pi$ stacked PDI dimers and/or larger aggregates. By preventing $\pi-\pi$ interactions between PDI molecules, it is possible to achieve high PLQY at elevated concentrations.[12] The primary goal of this study is to determine the limits of PLQY in passing from dilute solution to the solid state of appropriately designed PDI chromophores.

There are two main approaches to prevent the $\pi-\pi$ stacking in PDI chromophores. One method is to install substituents at the bay region (1, 6, 7, 12-positions) of the perylene core to impart a twist in the normally planar conformation (Figure 1a).[6] By doing so, the tendency of $\pi-\pi$ stacking and intermolecular association is reduced, but not totally eliminated. Bay substitution also significantly alters the photophysical characteristics of the PDI chromophore which may or may not be desirable depending on intended applications.[13−15] Molecular insulation is the other effective approach to reduce the intermolecular $\pi-\pi$ stacking effect in PDI compounds.[12] By positioning substituents (or molecules) around the planar perylene core, one can sterically block $\pi-\pi$ stacking, preventing chromophore−chromophore interactions.[16,17] With this approach, it is possible to eliminate $\pi-\pi$ stacking association between PDI molecules while maintaining the original photophysical characteristics of the individual PDI chromophore.

Covalent substitution is possible through the shoulder (2, 5, 8, 11-positions) of the perylene or through the imides without disturbing the planarity of the PDI core (Figure 1a).[18,19] However, substitution at the shoulder position has a significant

Received: July 14, 2017
Revised: September 5, 2017
Published: September 6, 2017

DOI: 10.1021/acs.chemmater.7b02968
Chem. Mater. 2017, 29, 8395−8403

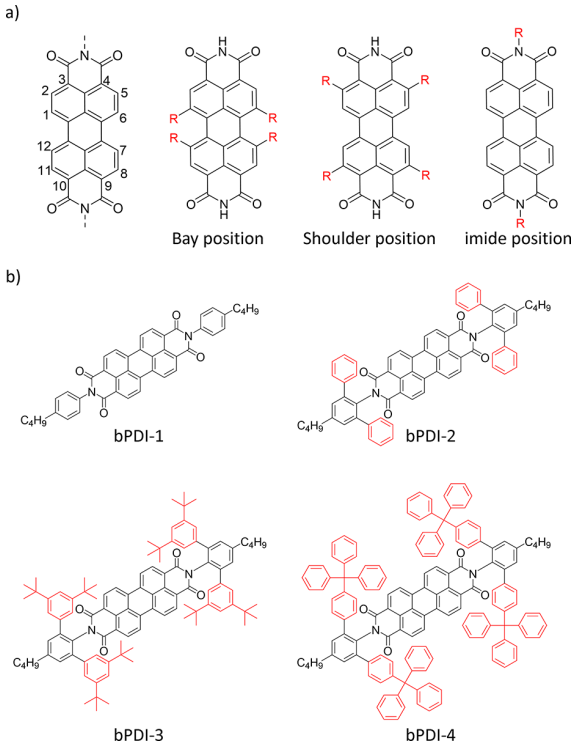

Figure 1. (a) Three potential substituent positions on PDI-type molecules and (b) the structure of four bPDI compounds: bPDI-1, bPDI-2, bPDI-3, and bPDI-4.

impact on the optical and electronic properties of the PDI chromophore.[18,20] As it is important to maintain the original photophysical characteristics of the individual PDI chromophore for our application, *vide infra*, we decided to substitute through the imide positions. It should be noted that it is also possible to achieve supramolecular insulation with one example using cucurbit[8]uril to encapsulate a PDI molecule in water.[21] The PDI–cucurbit[8]uril host–guest association was driven by hydrophobic–hydrophilic interactions in an appropriate solvent environment.

Substituting via the imide positions leaves the perylene core untouched[5,22] and is synthetically more versatile, enabling the creation of a series of compounds. One of our previous articles reported a molecularly insulated PDI molecule with four di-*tert*-butylphenyl groups substituted via the imide position, labeled as bPDI-3 in this work (Figure 1d).[12] This molecule showed near quantitative PLQY in dilute conditions and close to 75% PLQY at a higher concentration (80 mM) dispersed in a thin-film poly(methyl methacrylate) (PMMA) matrix. With such a high PLQY at high concentration, this molecularly insulated PDI was used as a fluorophore in luminescent solar concentrator (LSC) devices, taking advantage of an energy migration and energy trapping strategy (vide infra).[12,23,24]

In this article, four PDI derivatives (bPDI-1, -2, -3, and -4; Figure 1) were synthesized (see Supporting Information for details) with the purpose of studying the correlation between the size of imide moieties and the photoluminescence quantum efficiency at high concentration. The UV–vis absorption and photoluminescence (PL) spectra of the PDI samples were recorded in both solution and solid state under a range of concentrations. The effects of the bulky substituents on the aggregation behavior of the PDI molecules are discussed with reference to the crystallographic data. Absolute PLQYs of PDI molecules dispersed in the PMMA matrix were measured using an integrating sphere to observe the effect of the substituents on photoluminescence quantum efficiency. Finally, the trityl-substituted bPDI-4 was tested in light-harvesting LSC devices as a Förster resonance energy transfer (FRET) donor. In comparison with the previously reported bPDI-3 system,[12] the fully molecularly insulated bPDI-4 demonstrated improvements in both PLQY and performance in LSC devices.

Photophysical Properties of PDI Derivatives. The UV–vis absorption spectra of all four PDI compounds (bPDI-1 to bPDI-4) in dilute solution (2.5×10^{-5} M in $CHCl_3$) are identical to each other (Figure 2). The PL spectrum of the PDI

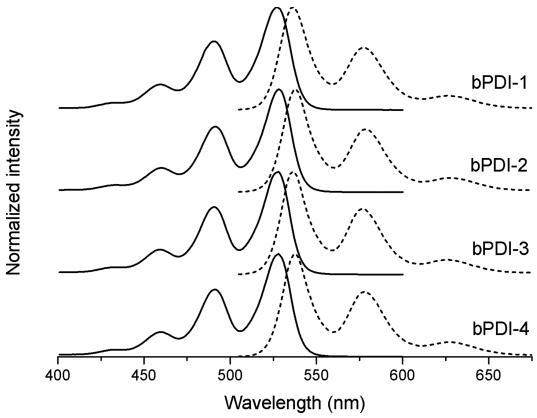

Figure 2. Absorption and emission spectra of all bPDIs in diluted solution.

compounds is also identical in these dilute solution samples. As anticipated, the imide substituents in this compound series did not perturb the photophysical characteristics of the PDI chromophore (i.e., the substituents had no significant conformation or electronic influence). This was further confirmed by frontier orbital energy data obtained in electrochemical experiments (Supporting Information, Table S1). The term "amorphous" used in all figures refers to a noncrystalline thin layer prepared by spin coating the sample solutions onto glass without any PMMA matrix. The term "crystalline" used in all figures refers to ground single-crystal samples loaded on filter paper.

Before discussing the changes in photophysical properties with concentration for the PDI compounds, it is useful to consider their molecular structure. The imide substituents for the PDI compounds consisted of 2,5-substitutions on the 4-butylphenyl unit (Figure 1). Using bPDI-1 as reference, the size of the imide groups increased from phenyl to 3,5-di-*tert*-butylphenyl to 4-trityl for bPDI-2, bPDI-3, and bPDI-4, respectively. From both molecular models (Figure S5) and single-crystal X-ray structure data (Figures 3 to 5), it was evident that the imide substituents provided coverage of the perylene chromophore without perturbation of the planar aromatic core. The perylene π surface of reference compound bPDI-1 is totally exposed (~11 Å), while there is little space for intermolecular π–π association for bPDI-3 and bPDI-4. In the crystal packing diagram, a staggered π–π stacking arrangement was observed for bPDI-2 (Figure 3). This staggered arrangement has been observed previously in a liquid crystalline PDI derivative.[10] Interestingly, no close π–π contact between perylene cores was observed in the crystal packing arrangement

DOI: 10.1021/acs.chemmater.7b02968
Chem. Mater. 2017, 29, 8395–8403

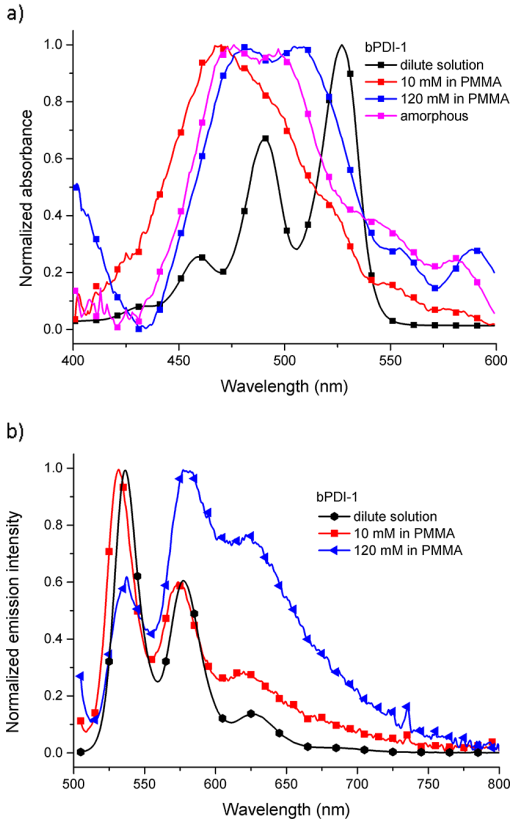

Figure 3. (a) UV–vis absorption and (b) PL spectra of bPDI-1 in various sample preparations.

of bPDI-3 (Figure 4), while some perylene to perylene interactions were apparent for bPDI-4 (Figure 5). These observations will be considered and discussed in the context of the photophysical properties of the materials in the following sections.

Reference Compound bPDI-1. Figure 3 shows the UV–vis absorption and PL spectrum of reference compound bPDI-1 in dilute solution (2.5×10^{-5} M in $CHCl_3$), dispersions in PMMA film, and in an as-cast neat film. It has been observed previously for similar PDI derivatives that aggregation resulting from intermolecular π–π association strongly affects the photophysical properties of the samples with increasing dye concentration.[25] At 10 mM in the PMMA thin film, the absorption spectrum of bPDI-1 shows a significant blue-shift compared with the other conditions, along with a loss of vibronic features, indicative of H-aggregation (Figure 3a).[25] Upon increasing the concentration of bPDI-1 to 120 mM in PMMA and in the neat amorphous thin film, the absorption was more pronounced at lower energies and broader. The PL spectrum of bPDI-1 also varied with concentration (Figure 3b). The relative intensity of the vibronic band at 535 nm decreased with a concomitant emission at higher wavelengths, which may be attributed to emission from excited state aggregates.[25] A marked decrease in the overall fluorescence intensity is also observed with increasing concentration (see below).

Phenyl-Substituted bPDI-2. The changes in photophysical properties with concentration for bPDI-2 (Figure 4) are very different from that of the reference compound bPDI-1. The aggregation of bPDI-2 is not H-aggregate dominated as in the bPDI-1 material. Going from dilute solution to an amorphous neat film, slight shifts in the vibronic bands and broadening of the spectrum are observed. These changes can be attributed to a mixture of molecular aggregates including both H- and J-aggregation. The changes in the PL spectrum of bPDI-2 are more pronounced compared with absorption spectrum changes (Figure 4). With increasing concentration in PMMA, a broad emission band was developed with its maximum at 625 nm, which can be assigned to molecular aggregates. Interestingly, the PL spectrum of the crystalline sample showed clear vibronic features, while the amorphous neat sample only had one broad emission at 625 nm. This indicated that molecular orientation and intermolecular association are very different in the two samples. It should be noted that polarization effects in different media may also contribute to small shifts in the absorption spectra.

3,5-Di-*tert*-butylphenyl-Substituted bPDI-3. The UV–vis absorption spectra of bPDI-3 in the various solution and solid-state preparations were all similar, with clear vibronic features (Figure 5). This suggests that the bulky 3,5-di-*tert*-butylphenyl groups prevent close contact of the perylene chromophores, as intended. However, more marked changes in the PL spectra are observed but with a higher concentration tolerance of aggregation-caused quenching (ACQ) effect than bPDI-2. The dilute solution and 10 mM PMMA spectra were essentially identical. A further increase in concentration in PMMA reveals the development of a red-shifted broad emission that dominated the amorphous neat film spectrum (Figure 5). The origin of the red-shifted broad emission in the neat bPDI-3 sample is unclear as the crystal structure data suggested little chance of close perylene–perylene interaction due to the steric bulk of the substituents. Similar to the bPDI-2 material, the crystalline bPDI-3 spectrum showed clear vibronic features, while the amorphous neat sample exhibited only one broad emission feature. Again, these observations can be attributed to differences in molecular orientation and intermolecular association between the two samples. More intriguing was the observation that the PL spectra of bPDI-2 and bPDI-3 crystalline samples were very similar in profile despite completely different crystal packing arrangements (Figures 4 and 5).

4-Trityl-Substituted bPDI-4. The UV–vis absorption spectra of bPDI-4 in the various solution and solid-state preparations were all very similar to one another in profile, with clear vibronic features (Figure 6). A small 3 nm red-shift of the absorption maximum was recorded when comparing the dilute solution sample to the neat film sample. The crystal packing data indicate the bulky trityl groups sit directly above and below the π surface of the perylene core, and some π–π interaction are possible on the edges of the molecules (3.38 Å). The slight red-shift in absorption spectrum might be related to polarization effect in the solid state (Figure 6d). As with bPDI-3, the PL spectra of bPDI-4 showed the development of a red-shifted emission with increasing concentration to the neat film, indicating the presence of excited state aggregates (Figure 6). A large difference is observed in the PL spectra of the crystalline and amorphous samples again indicative of different molecular arrangement and packing in these samples.

To summarize, the strategy of using sterically bulky groups to prevent close contact of the perylene core chromophores was successful. Less predictable was the excited state properties as observed in the PL spectrum variations. For bPDI-2, -3, and -4, the PL spectrum showed the emergence of a red-shifted broad emission with increasing concentration in PMMA but remained

DOI: 10.1021/acs.chemmater.7b02968
Chem. Mater. 2017, 29, 8395–8403

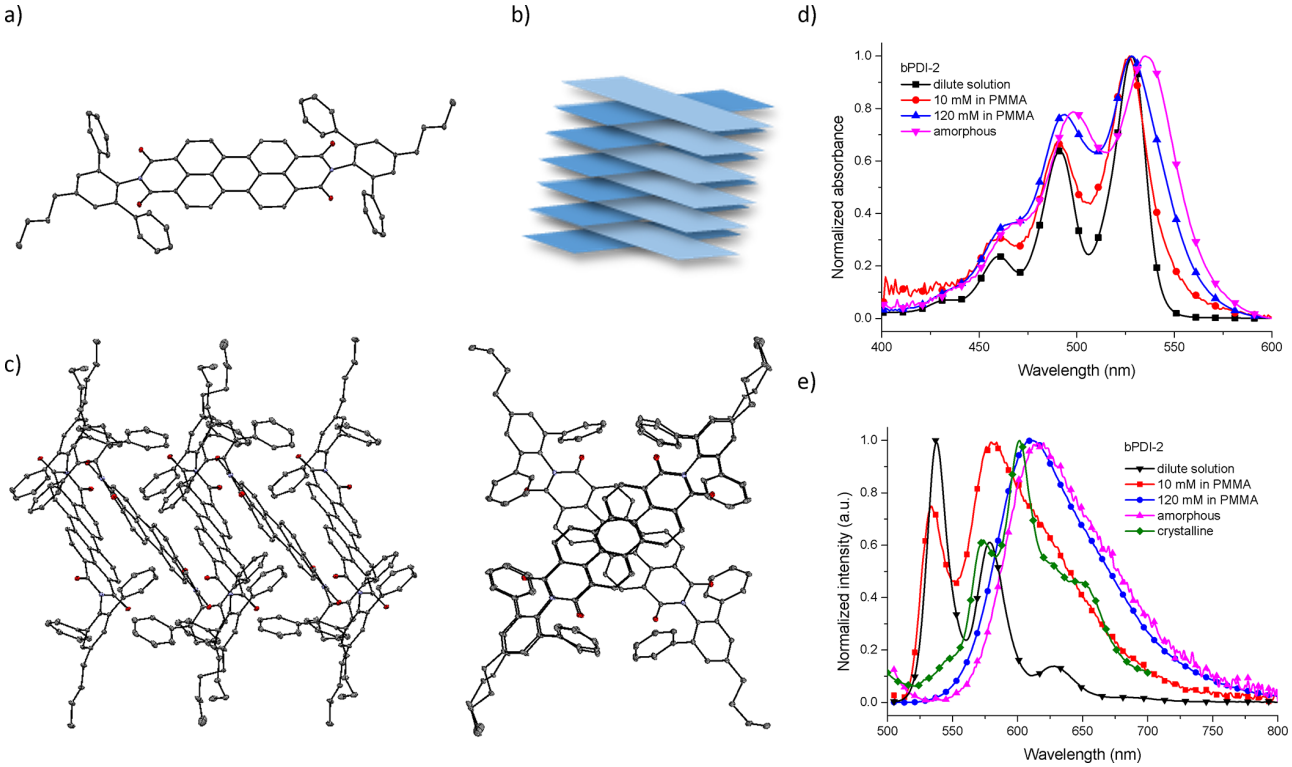

Figure 4. Representations of single-crystal X-ray data of bPDI-2: (a) the thermal ellipsoid illustration of one PDI unit; (b) illustration of crystal packing pattern; (c) the crystal packing diagram from side view and top view of $\pi-\pi$ stacking; (d) UV−vis absorption; and (e) PL spectra of bPDI-2 in various sample preparations.

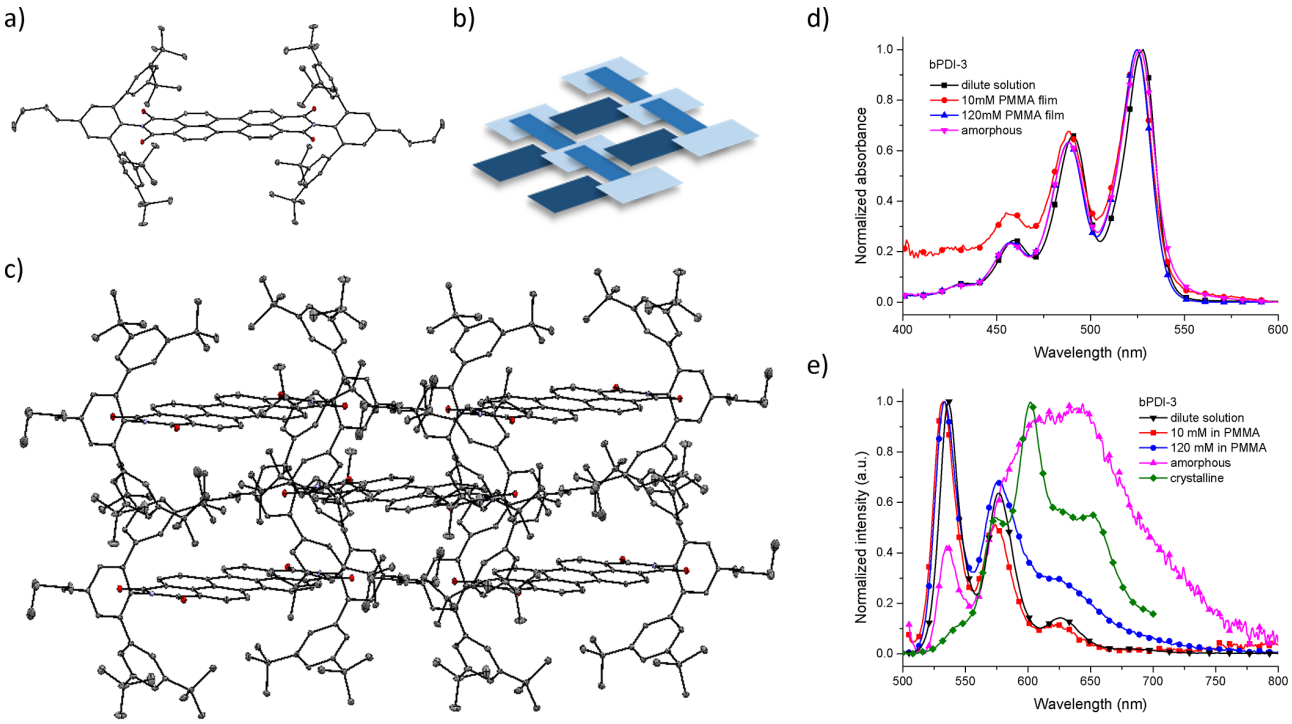

Figure 5. Representations of single-crystal X-ray data of bPDI-3: (a) the thermal ellipsoid illustration of one PDI unit; (b) illustration of crystal packing pattern; (c) the crystal packing diagram; and (d) UV−vis absorption and (e) PL spectra of bPDI-3 in various sample preparations.

emissive (high PLQY) at high concentration. This was in contrast with the reference compound bPDI-1 which showed significant quenching of emission with increasing concentration. The fluorescence decay profiles of bPDI-3 and -4 were

DOI: 10.1021/acs.chemmater.7b02968
Chem. Mater. 2017, 29, 8395−8403

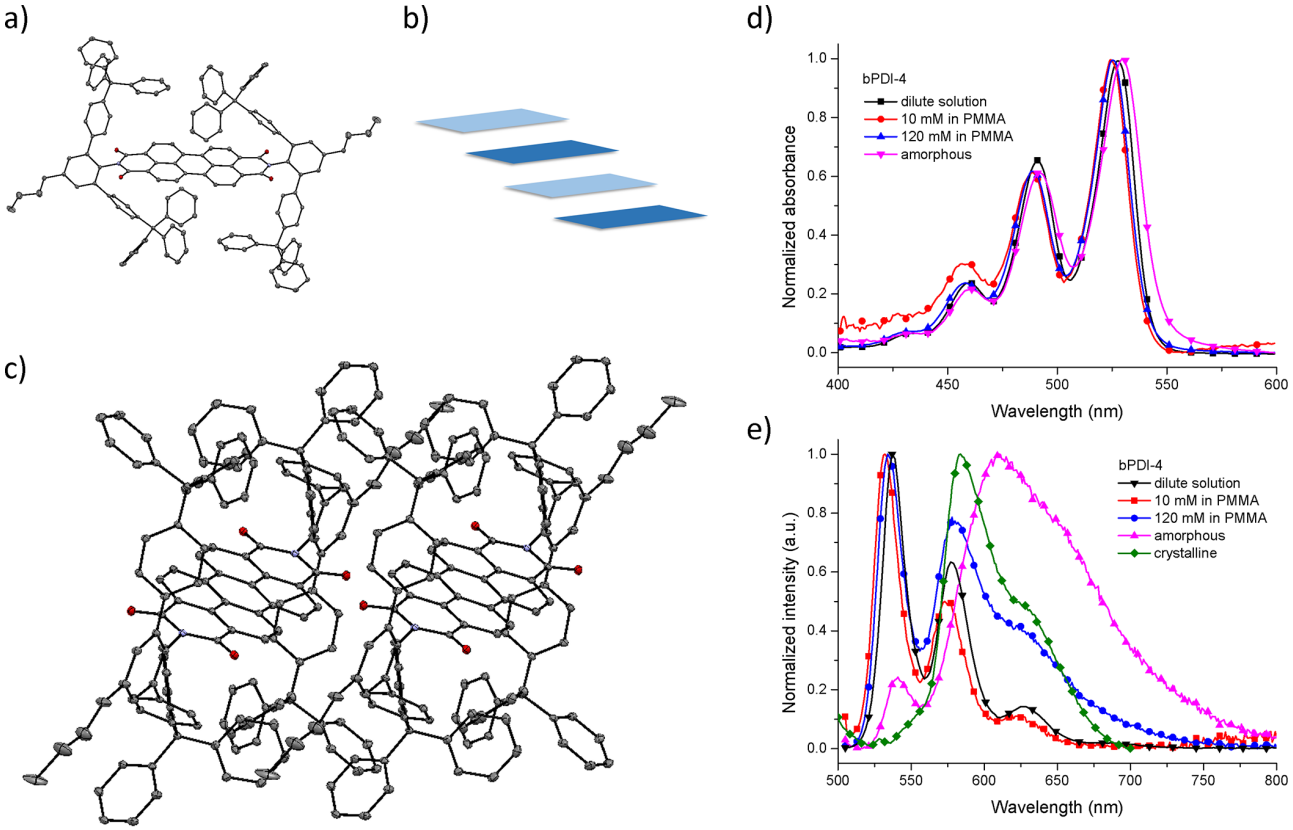

Figure 6. Representations of single-crystal X-ray data of bPDI-4: (a) the thermal ellipsoid illustration of one PDI unit; (b) illustration of crystal packing pattern; (c) the crystal packing diagram, and (d) UV–vis absorption and (e) PL spectra of bPDI-4 in various sample preparations.

recorded at the low wavelength emission band as a function of concentration. These decays cannot be meaningfully interpreted in terms of either discrete decay components or by lifetime distribution analyses. Instead, we have calculated the mean fluorescence lifetimes ($\tau_m = a_1\tau_1 + a_2\tau_2 + ... + a_i\tau_i$, where $a_1 + a_2 + ... + a_i = 1$) as a function of concentration. The τ_m's of these samples were smaller than that of the PDI monomer emission and decrease with increasing concentration (Figure S7). This indicates the presence of emissive excited state aggregates in concentrated samples. With consideration of the data discussed thus far, in the next section we discuss the concentration dependence of the PLQY of the PDI compounds in PMMA.

PLQY of PDI Derivatives. It is clear from the above PL studies that bPDI-2, -3, and -4 are highly emissive at elevated concentration compared to the reference bPDI-1. To quantify the differences, the absolute PLQY of the PDI series dispersed in PMMA at a range of concentrations was measured using an integrating sphere. It is important to note that determining the absolute PLQY measurements, particularly for concentrated samples, was not straightforward. With significant overlap of the absorption and emission spectra for some of these PDI samples, a reabsorption correction must be applied to achieve the true PLQY of the chromophore (see SI for details). Figure 7 summarizes the PLQY values for the four PDI compounds over concentrations ranging from 10 to 120 mM in PMMA.

As expected, the PLQY of the reference compound bPDI-1 was only 21.0 + 0.9% at 10 mM in PMMA which was much lower than the near unity value obtained from typical PDI compounds in dilute solution.[4] This low PLQY is most likely

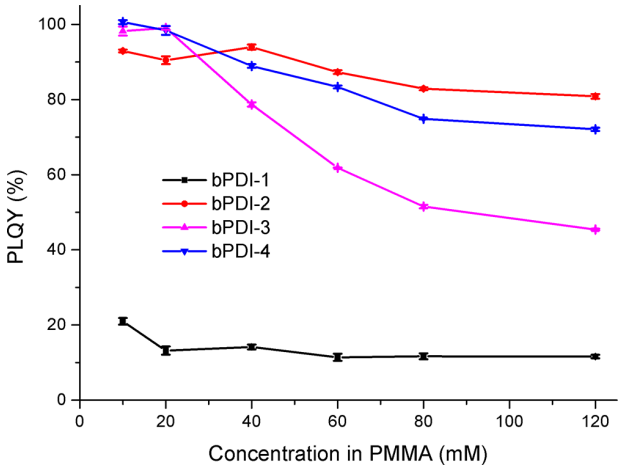

Figure 7. Absolute PLQY of the bPDI derivatives as a function of concentration in PMMA thin films. Reabsorption correction was applied to all data in this figure. Details of the PLQY measurement and the reabsorption correction can be found in the Supporting Information.[29]

the result of aggregation quenching given the strong intermolecular π–π association in such PDI compounds as discussed earlier. On the other hand, the PLQY of bPDI-2 to 4 was above 90% at 10 mM in PMMA with bPDI-4 being the highest at 100% (Figure 7). A high PLQY was maintained up to 40 mM with the values dropping to 80%, 46%, and 72% at 120 mM for bPDI-2, -3, and -4, respectively. As neat films, the

DOI: 10.1021/acs.chemmater.7b02968
Chem. Mater. 2017, 29, 8395–8403

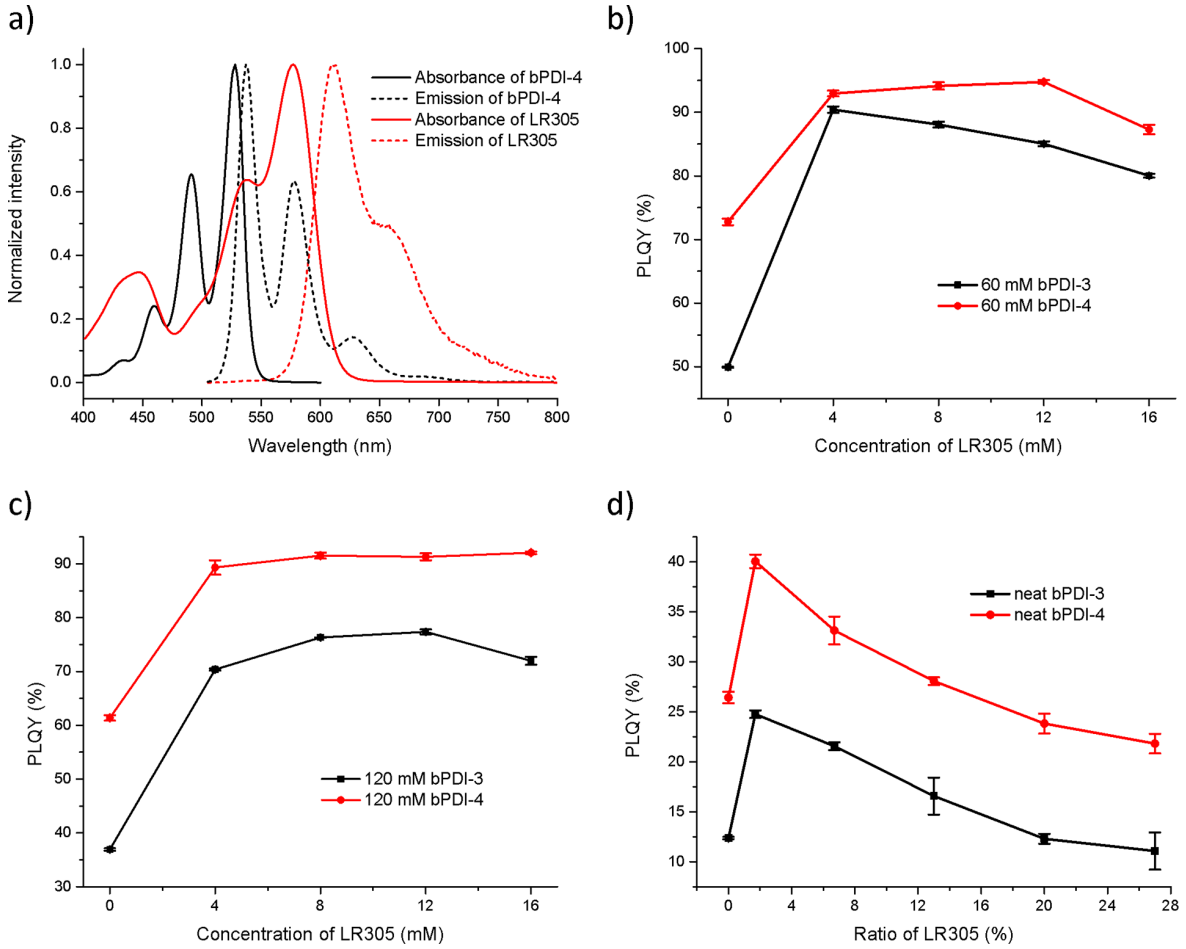

Figure 8. (a) UV−vis absorption and PL spectra of bPDI-4 and LR305. The PLQY variation of the donor−acceptor system against the concentration of LR305 in (b) 60 mM of the donors in PMMA; (c) 120 mM of the donors in PMMA; and (d) amorphous neat films of the donors. All PLQY data here are presented without the reabsorption correction. Therefore the PLQY in 0 mM does not match the data in Figure 7.

PLQY values for bPDI-2, -3, and -4 were 21%, 14%, and 29%, respectively, which are among the highest neat solid state PLQY of PDI-type materials reported.[26−28]

Three main contributions to these PLQY values can be considered: (1) Individual (monomeric) dye emission; (2) aggregate emission; and (3) aggregation-caused quenching. Aggregation-caused quenching is the dominant effect for the bPDI-1 reference compound.[11] For bPDI-2, chromophore aggregation is evident in the absorption spectrum (Figure 4), but the aggregates remain emissive. At 120 mM in PMMA, the PL spectrum of bPDI-2 consists of the red-shifted broad emission with PLQY measured at 80%, which is the highest of the bPDI series at this concentration. Interestingly the PLQY of bPDI-2 even slightly increased after the ground state aggregation at 40 mM. In comparison, the PL of both bPDI-3 and bPDI-4 involves a significant component of individual PDI emission up to very high concentrations (Figures 4 and 5). However, the PLQY decreases more markedly with concentration for bPDI-3 and -4 compared to bPDI-2. This observation suggests that excited state aggregates exist in concentrated samples of bPDI-3 and -4 that are nonemissive despite the separation of the perylene core chromophore by the bulky di-*tert*-butylphenyl and trityl groups. While some of the variations in PLQY were unexpected, the concept of using bulky substituents to maintain the photophysical properties of the perylene chromophore with increasing concentration was successful. The trityl-substituted bPDI-4 shows typical PDI chromophore emission and relatively high PLQY at 120 mM in PMMA, outperforming the di-*tert*-butylphenyl bPDI-3. The energy migration characteristics of bPDI-4 were then investigated and the results discussed below. Using an energy migration and energy trapping approach, the optical quantum efficiency (OQE, definition available in SI) of LSC devices containing bPDI-4 as a FRET donor was compared with devices containing bPDI-3.[12]

Energy Migration and Trapping. In our previous work, an energy migration and trapping strategy was applied to improve the light harvesting performance of PDI-based LSC devices.[12] The di-*tert*-butylphenyl bPDI-3 was used as an energy migration material and FRET donor, while the commercial PDI dye Lumogen F Red 305 (LR305) was incorporated as the energy trap or FRET acceptor. The same spectroscopic experiments as described previously[3] were adopted to examine the trityl-substituted bPDI-4 in this work to compare its performance with bPDI-3.

In energy migration, the excitation energy residing in chromophores can undergo transfer between neighboring molecules of the same type via a FRET process,[30] where the energy migration distance (L_D) is dependent on the concentration of the dye. Apart from concentration, L_D will

DOI: 10.1021/acs.chemmater.7b02968
Chem. Mater. 2017, 29, 8395−8403

depend on the FRET critical radius (R_0), the separation at which energy transfer between chromophores and other intramolecular excited state relaxation processes are equally probable.[31] A good overlap between the UV−vis absorption and PL spectrum of the material is essential for an effective R_0 and an extended L_D. Given the spectral properties of bPDI-3 and bPDI-4, both chromophores are suitable for energy migration.

Using the spectral overlap and PLQY data and the Förster equation, the R_0 of homotransfer within bPDI-3 and bPDI-4 was calculated to be 5.02 and 5.03 nm, respectively (see SI for details). As with our previous study, energy migration in the PDI materials was further investigated using time-resolved fluorescence anisotropy.[12] This technique enabled an alternative determination of R_0 through a Green's function model (see earlier work[3] and SI for details). A R_0 value of 5.0 nm was obtained for both bPDI-3 and bPDI-4, which is in excellent agreement with the values calculated from the Förster equation. The migration distances, L_D, were also obtained from the time-resolved emission anisotropy measurements (see SI for detailed data). At 60 mM in PMMA, the L_D's of bPDI-3 and bPDI-4 were determined to be 23 and 21 nm, respectively. The L_D value was greater than the average intermolecular distance (d) when the concentration exceeded 4 mM (Figure S15c). At 120 mM, the L_D of bPDI-4 reached 35 nm, which is 30 times larger than the average intermolecular distance at this concentration. These results indicate that bPDI-3 and -4 are equally efficient for energy migration.

PMMA films containing a FRET donor, bPDI-4, and a FRET acceptor, LR305, were examined to determine the energy migration and trapping efficiency (Figure 9). LR305 should be an appropriate FRET acceptor for bPDI-4 as there is very good overlap between the PL spectrum of bPDI-4 and the absorption spectrum of LR305 (Figure 8a). The fluorescence quenching of the FRET donor by LR305 was investigated at two concentrations of donor, −60 and 120 mM in PMMA. The fluorescence of the bPDI donor at either concentration was largely quenched by LR305 at 4 mM and completely quenched at 16 mM (Figure S9). For the samples in neat films (in the absence of the PMMA matrix), the emission of both bPDI-3 and bPDI-4 was effectively completely quenched by 1.7 mol % of LR305 (Figure S9). The improvement of the trapping efficiency in neat films is attributed to the increase in L_D in these neat samples and preferential trapping by the LR305.

The PLQYs of these samples indicate that the addition of LR305 to the bPDI donors substantially improved the PLQY value (Figure 8b, c, and d). At 4 mM of LR305, the overall PLQY was close to 90% for both bPDI donors at 60 mM, while 90% PLQY was observed for bPDI-4 at 120 mM. Even in neat films, the PLQY of bPDI-4 improved from 25% to 40% with the addition of 1.7 mol % of LR305. These improvements in PLQY on addition of LR305 can be explained by the proposed energy migration and trapping process (Figure 9). In the samples containing bPDI compounds only, the excitation of the sample results in energy migration and emission from isolated PDI chromophores and/or aggregates depending on the concentration of the dye. As the concentration of PDI is increased, the PLQY value declines with the emergence of the aggregate emission as discussed earlier. By adding LR305, the excitation energy is ultimately trapped by the lower energy LR305 chromophore which exhibits high emission efficiency at the 4−16 mM concentration range (Figure 8).

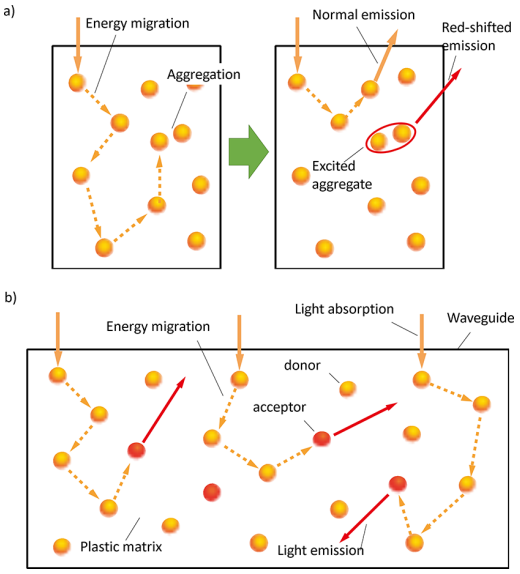

Figure 9. Proposed energy migration process for bPDI-3 and bPDI-4: (a) energy migration followed by trapping by aggregates and (b) the energy migration process followed by trapping by an acceptor.

Apart from high PLQY values, the use of these FRET donor−acceptor dye systems addresses the reabsorption issue that is detrimental to the performance of LSC devices. Monte Carlo ray tracing simulation was performed to predict the performance of the LSCs devices based on bPDI-4 and bPDI-3 with 12 mM LR305 (Figure 10). Since the reabsorption of luminescence in all samples was small, the calculated OQE did not change significantly with increasing geometric gain, G (Figure 10a, definitions of OQE and G in SI). At G = 120, the OQE of devices containing 60 and 120 mM of bPDI-4 were 56% and 54%, respectively. The OQE of devices containing bPDI-3 at 120 mM was significantly lower than that of bPDI-4 primarily because of its lower PLQY value. It is noteworthy that the use of the new trityl bPDI-4 dye would result in 50% reduction in the amount of LR305 in the polymer waveguide without compromising the light-harvesting device performance. The flux gain of LSC devices containing bPDI-4 and LR305 at G = 45 was around 6 which was comparable to the performance of reported benchmark devices (Figure 10b, definition of flux gain in SI).[12,32,33]

CONCLUSION

A series of molecularly insulated perylene diimide derivatives were synthesized and fully characterized. By adding bulky substituents to the imide position, the intermolecular interactions of PDI chromophores were modulated, while the optical properties of the perylene core persisted. In contrast to the reference compound bPDI-1 that exhibits typical aggregation caused quenching of fluorescence with increasing concentration, emissive aggregates were observed for the phenyl-substituted bPDI-2. With the $\pi-\pi$ stacked crystal packing, bPDI-2 is an interesting material for organic light-emitting devices which is currently under investigation in our group. The interchromophore interactions were further reduced for the di-*tert*-butylphenyl-substituted bPDI-3 and the trityl-substituted bPDI-4 leading to isolation of the perylene core, as evident in their UV−vis absorption spectra. While bPDI-3 and bPDI-4 remained highly emissive at high

DOI: 10.1021/acs.chemmater.7b02968
Chem. Mater. 2017, 29, 8395−8403

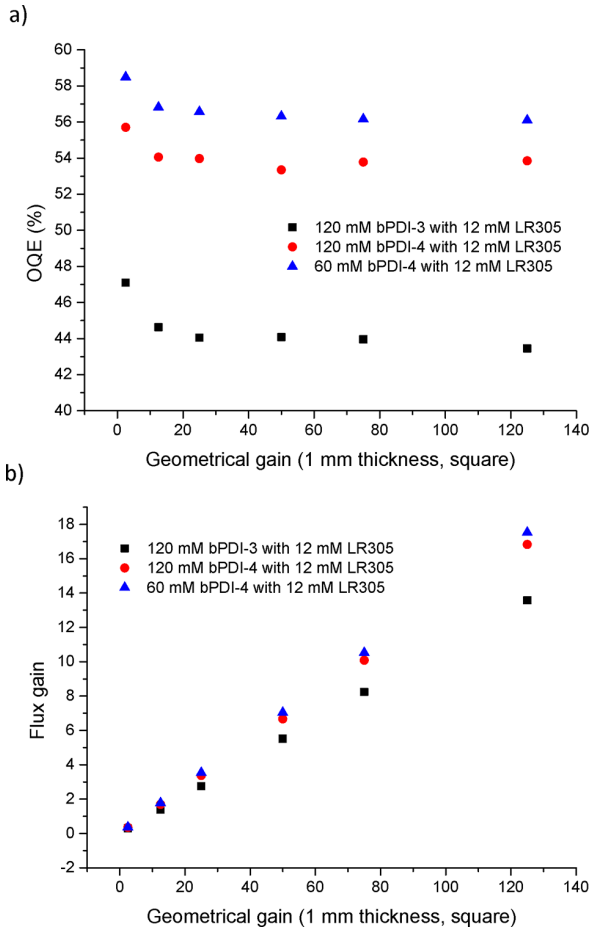

Figure 10. Simulated (a) optical quantum efficiency (OQE) and (b) flux gain of LSC devices based on 120 mM bPDI-4 and bPDI-3 with 12 mM LR305 plotted as a function of the geometric gain on a 1 mm thick square glass waveguide. All samples were excited at 490 nm. The absorbance of all samples was set to 1.0 at 490 nm, and a total of 100 000 photons were used in each simulation.

concentrations in PMMA, a red-shifted broad emission became more prominent with increasing concentration. This suggested the presence of excited state aggregate species even though, from crystal structures, direct $\pi-\pi$ interactions between PDI chromophores must be small. Efficient energy migration was demonstrated in PMMA films containing bPDI-3 and bPDI-4 at high concentrations by time-resolved fluorescence anisotropy experiments with an energy migration distance (L_D) of 35 nm measured for bPDI-4 at 120 mM. Using bPDI-4 (120 mM) as the FRET donor and LR305 (4 mM) as the FRET acceptor in PMMA films, a PLQY of 90% was obtained. With such a high PLQY and reduced reabsorption in this donor−acceptor dye system, light-harvesting LSC devices were investigated giving an optical quantum efficiency of 54% and a flux gain of 6 at geometric gain of 45. This light-harvesting performance is comparable to the state-of-the-art LSCs, and we anticipate that these materials that maintain their high luminescence at high concentrations may find broad applications in large area devices especially on glass.

■ ASSOCIATED CONTENT

Supporting Information

The Supporting Information is available free of charge on the ACS Publications website at DOI: 10.1021/acs.chemmater.7b02968.

Synthesis and characterization of all new compounds, sample preparation for photophysical measurements, additional photophysical characterization data, calculations on energy migration, and Monte Carlo ray tracing simulation (PDF)
CIF file for C68 H50 N2 O4 (CIF)
CIF file for C144 H106 N2 O4 (CIF)
CIF Platon report for C68 H50 N2 O4 (PDF)
CIF Platon report for C144 H106 N2 O4 (PDF)

■ AUTHOR INFORMATION

Corresponding Author

*E-mail: wwhwong@unimelb.edu.au.

ORCID

Hamid Soleimaninejad: 0000-0002-4034-0910
Jonathan M. White: 0000-0002-0707-6257
Kenneth P. Ghiggino: 0000-0001-6621-4448
Wallace W. H. Wong: 0000-0001-7131-8532

Notes

The authors declare no competing financial interest.

■ ACKNOWLEDGMENTS

This work was made possible by support from the Australian Renewable Energy Agency which funds the project grants within the Australian Centre for Advanced Photovoltaics (ACAP). Responsibility for the views, information, or advice expressed herein is not accepted by the Australian Government. WWHW is supported by an ARC Future Fellowship (FT130100500). KPG, TAS, and WWHW are also supported by the ARC Centre of Excellence in Exciton Science (CE170100026). We would like to thank Dr. James Banal for constructive discussions.

■ REFERENCES

(1) Fan, Q.; Cheng, K.; Yang, Z.; Zhang, R.; Yang, M.; Hu, X.; Ma, X.; Bu, L.; Lu, X.; Xiong, X.; Huang, W.; Zhao, H.; Cheng, Z. Perylene-Diimide-Based Nanoparticles as Highly Efficient Photoacoustic Agents for Deep Brain Tumor Imaging in Living Mice. *Adv. Mater.* **2015**, *27*, 843−847.
(2) Li, G.; Zhao, Y.; Li, J.; Cao, J.; Zhu, J.; Sun, X.; Zhang, Q. Synthesis, Characterization, Physical Properties, and OLED Application of Single BN-Fused Perylene Diimide. *J. Org. Chem.* **2014**, *80*, 196−203.
(3) Briseno, A. L.; Mannsfeld, S. C. B.; Reese, C.; Hancock, J. M.; Xiong, Y.; Jenekhe, S. A.; Bao, Z.; Xia, Y. Perylenediimide Nanowires and Their Use in Fabricating Field-Effect Transistors and Complementary Inverters. *Nano Lett.* **2007**, *7*, 2847−2853.
(4) Huang, C.; Barlow, S.; Marder, S. R. Perylene-3,4,9,10-tetracarboxylic Acid Diimides: Synthesis, Physical Properties, and Use in Organic Electronics. *J. Org. Chem.* **2011**, *76*, 2386−2407.
(5) Chen, W.; Yang, X.; Long, G.; Wan, X.; Chen, Y.; Zhang, Q. A Perylene Diimide (PDI)-based Small Molecule with Tetrahedral Configuration as a Non-fullerene Acceptor for Organic Solar Cells. *J. Mater. Chem. C* **2015**, *3*, 4698−4705.
(6) Würthner, F.; Saha-Moller, C. R.; Fimmel, B.; Ogi, S.; Leowanawat, P.; Schmidt, D. Perylene Bisimide Dye Assemblies as Archetype Functional Supramolecular Materials. *Chem. Rev.* **2016**, *116*, 962−1052.

DOI: 10.1021/acs.chemmater.7b02968
Chem. Mater. 2017, 29, 8395−8403

(7) Kozma, E.; Catellani, M. Perylene Diimides based Materials for Organic Solar Cells. *Dyes Pigm.* **2013**, *98*, 160−179.
(8) Yan, P.; Chowdhury, A.; Holman, M. W.; Adams, D. M. Self-organized Perylene Diimide Nanofibers. *J. Phys. Chem. B* **2005**, *109*, 724−730.
(9) Ide, J.; Mereau, R.; Ducasse, L.; Castet, F.; Olivier, Y.; Martinelli, N.; Cornil, J.; Beljonne, D. Supramolecular Organization and Charge Transport Properties of Self-assembled $\pi-\pi$ Stacks of Perylene Diimide Dyes. *J. Phys. Chem. B* **2011**, *115*, 5593−603.
(10) Chen, Z.; Stepanenko, V.; Dehm, V.; Prins, P.; Siebbeles, L. D.; Seibt, J.; Marquetand, P.; Engel, V.; Würthner, F. Photoluminescence and Conductivity of Self-assembled $\pi-\pi$ Stacks of Perylene Bisimide Dyes. *Chem. - Eur. J.* **2007**, *13*, 436−449.
(11) Mei, J.; Leung, N. L.; Kwok, R. T.; Lam, J. W.; Tang, B. Z. Aggregation-Induced Emission: Together We Shine, United We Soar! *Chem. Rev.* **2015**, *115*, 11718−940.
(12) Banal, J. L.; Soleimaninejad, H.; Jradi, F. M.; Liu, M.; White, J. M.; Blakers, A. W.; Cooper, M. W.; Jones, D. J.; Ghiggino, K. P.; Marder, S. R.; Smith, T. A.; Wong, W. W. H. Energy Migration in Organic Solar Concentrators with a Molecularly Insulated Perylene Diimide. *J. Phys. Chem. C* **2016**, *120*, 12952−12958.
(13) Osswald, P.; Würthner, F. Effects of Bay Substituents on the Racemization Barriers of Perylene Bisimides: Resolution of Atropo-enantiomers. *J. Am. Chem. Soc.* **2007**, *129*, 14319−14326.
(14) Osswald, P.; Leusser, D.; Stalke, D.; Würthner, F. Perylene Bisimide based Macrocycles: Effective Probes for the Assessment of Conformational Effects on Optical Properties. *Angew. Chem., Int. Ed.* **2005**, *44*, 250−253.
(15) Ramanan, C.; Smeigh, A. L.; Anthony, J. E.; Marks, T. J.; Wasielewski, M. R. Competition between Singlet Fission and Charge Separation in Solution-Processed Blend Films of 6,13-Bis-(triisopropylsilylethynyl)pentacene with Sterically-Encumbered Perylene-3,4:9,10-bis(dicarboximide)s. *J. Am. Chem. Soc.* **2012**, *134*, 386−397.
(16) Mitsui, M.; Fukui, H.; Takahashi, R.; Takakura, Y.; Mizukami, T. Single-Molecule Fluorescence Spectroscopy of Perylene Diimide Dyes in a gamma-Cyclodextrin Film: Manifestation of Photoinduced H-Atom Transfer via Higher Triplet (n, π^*) Excited States. *J. Phys. Chem. A* **2017**, *121*, 1577−1586.
(17) Takashima, Y.; Fukui, Y.; Otsubo, M.; Hamada, N.; Yamaguchi, H.; Yamamoto, H.; Harada, A. Emission Properties of Cyclodextrin Dimers Linked with Perylene Diimide - Effect of Cyclodextrin Tumbling. *Polym. J.* **2012**, *44*, 278−285.
(18) Nakazono, S.; Easwaramoorthi, S.; Kim, D.; Shinokubo, H.; Osuka, A. Synthesis of Arylated Perylene Bisimides through C-H Bond Cleavage under Ruthenium Catalysis. *Org. Lett.* **2009**, *11*, 5426−5429.
(19) Li, X.; Wang, H.; Schneider, J. A.; Wei, Z.; Lai, W.-Y.; Huang, W.; Wudl, F.; Zheng, Y. Catalyst-free one-step synthesis of ortho-tetraaryl perylene diimides for efficient OPV non-fullerene acceptors. *J. Mater. Chem. C* **2017**, *5*, 2781−2785.
(20) Ma, Y.-S.; Wang, C.-H.; Zhao, Y.-J.; Yu, Y.; Han, C.-X.; Qiu, X.-J.; Shi, Z. Perylene Diimide Dyes Aggregates: Optical Properties and Packing Behavior in Solution and Solid State. *Supramol. Chem.* **2007**, *19*, 141−149.
(21) Biedermann, F.; Elmalem, E.; Ghosh, I.; Nau, W. M.; Scherman, O. A. Strongly Fluorescent, Switchable Perylene Bis(diimide) Host-guest Complexes with Cucurbit[8]uril in Water. *Angew. Chem., Int. Ed.* **2012**, *51*, 7739−7743.
(22) Herrmann, A.; Weil, T.; Sinigersky, V.; Wiesler, U. M.; Vosch, T.; Hofkens, J.; De Schryver, F. C.; Müllen, K. Polyphenylene Dendrimers with Perylene Diimide as a Luminescent Core. *Chem. - Eur. J.* **2001**, *7*, 4844−4853.
(23) Banal, J. L.; Ghiggino, K. P.; Wong, W. W. Efficient Light Harvesting of a Luminescent Solar Concentrator using Excitation Energy Transfer from an Aggregation-induced Emitter. *Phys. Chem. Chem. Phys.* **2014**, *16*, 25358−25363.
(24) Banal, J. L.; Zhang, B.; Jones, D. J.; Ghiggino, K. P.; Wong, W. W. H. Emissive Molecular Aggregates and Energy Migration in Luminescent Solar Concentrators. *Acc. Chem. Res.* **2017**, *50*, 49−57.
(25) Haines, C.; Chen, M.; Ghiggino, K. P. The Effect of Perylene Diimide Aggregation on the Light Collection Efficiency of Luminescent Concentrators. *Sol. Energy Mater. Sol. Cells* **2012**, *105*, 287−292.
(26) Lin, M.-J.; Jiménez, Á. J.; Burschka, C.; Würthner, F. Bay-substituted Perylene Bisimide Dye with an Undistorted Planar Scaffold and Outstanding Solid State Fluorescence Properties. *Chem. Commun.* **2012**, *48*, 12050−12052.
(27) Ramírez, M. G.; Pla, S.; Boj, P. G.; Villalvilla, J. M.; Quintana, J. A.; Díaz-García, M. A.; Fernández-Lázaro, F.; Sastre-Santos, Á. 1,7-Bay-Substituted Perylenediimide Derivative with Outstanding Laser Performance. *Adv. Opt. Mater.* **2013**, *1*, 933−938.
(28) Jiménez, Á. J.; Lin, M.-J.; Burschka, C.; Becker, J.; Settels, V.; Engels, B.; Würthner, F. Structure−Property Relationships for 1,7-Diphenoxy-perylene Bisimides in Solution and in the Solid State. *Chem. Sci.* **2014**, *5*, 608−619.
(29) Wilson, L. R.; Richards, B. S. Measurement Method for Photoluminescent Quantum Yields of Fluorescent Organic Dyes in Polymethyl Methacrylate for Luminescent Solar Concentrators. *Appl. Opt.* **2009**, *48*, 212−220.
(30) Olson, R. W.; Loring, R. F.; Fayer, M. D. Luminescent Solar Concentrators and the Reabsorption Problem. *Appl. Opt.* **1981**, *20*, 2934−2940.
(31) Hildebrandt, N. How to Apply FRET: From Experimental Design to Data Analysis. In *FRET - Förster Resonance Energy Transfer: From Theory to Applications*; Wiley-VCH: 2013.
(32) Erickson, C. S.; Bradshaw, L. R.; McDowall, S.; et al. Zero-reabsorption Doped-nanocrystal Luminescent Solar Concentrators. *ACS Nano* **2014**, *8*, 3461−3467.
(33) Currie, M. J.; Mapel, J. K.; Heidel, T. D.; Goffri, S.; Baldo, M. A. High-efficiency Organic Solar Concentrators for Photovoltaics. *Science* **2008**, *321*, 226−228.

DOI: 10.1021/acs.chemmater.7b02968
Chem. Mater. 2017, 29, 8395−8403

Supporting Information

Highly Fluorescent Molecularly Insulated Perylene Diimides: Effect of Concentration on Photophysical Properties

Bolong Zhang, Hamid Soleimaninejad, David J. Jones, Jonathan M. White, Kenneth P. Ghiggino, Trevor A. Smith, and Wallace W. H. Wong*

Contents

General experimental details

All reagents were used in reactions as received from the suppliers. Dried toluene and tetrahydrofuran were obtained from a glass contour solvent purification system. Flash chromatography purification was performed using standard methods on silica gel (Merck Silica Gel 60, 0.040-0.063 mm, 230-400 mesh ASTM). All reactions were monitored by thin-layer chromatography using silica gel (Merck, Silica Gel 60 F254) coated glass sheets, either examined under UV lamps (254 nm and 365 nm) in a black box or stained by $KMnO_4$/ethanol solution with heat treatment.

The ^{1}H, ^{13}C and COSY NMR spectra were collected using Agilent MR400 (400 MHz), Oxford 500 (500 MHz) or Varian Inova 600 (600 MHz) instruments. All NMR spectra, if not otherwise specified, were measured at 25 °C and calibrated using the residual solvent signals. All HPLC-based analysis and purification were carried out using a standard HPLC system with a UV-Vis detector, FT-IR spectra were provided by a Perkin Elmer Spectrum One FT-IR spectrometer while UV-Vis spectra were recorded using a Cary UV-Vis spectrometer. All high resolution mass spectrometry (HRMS) experiments were conducted with a commercially available hybrid orbital-trap and Fourier-transform ion cyclotron resonance mass spectrometer, equipped with electrospray ionization (ESI). Electrochemical measurements were recorded on a Solartron 1287A Potentiostat/Galvanostat.

bPDI-3 was synthesized according to literature procedure.[1]

Synthesis and characterization details

Tetrabromo-PDI

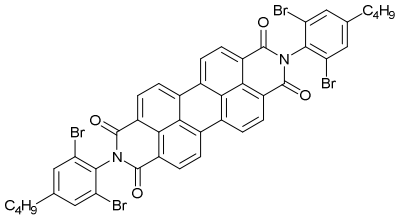

Tetrabromo-PDI was synthesized according to a literature procedure.[1]

bPDI-1

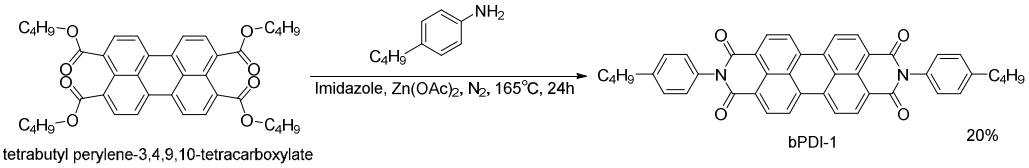

The tetrabutyl perylene-3,4,9,10-tetracarboxylate was synthesized according to a literature procedure.[2, 3]

A mixture of tetrabutyl perylene-3,4,9,10-tetracarboxylate (200 mg, 0.31 mmol), 4-butyl-aniline (62 mg, 0.62 mmol), imidazole (0.5 g) and $Zn(OAc)_2$ (22.4 mg, 0.1 mmol). The mixture was sealed under N_2, heated to 165° C and stirred 24h. The crude product was purified by flash chromatography (petroleum spirit: chloroform 9:1) to give the target product (red powder, 37 mg, yield 18 %).

^{1}H NMR (400 MHz, 1,2-dichloroethene-*d*) δ 8.73 (d, *J* = 7.9 Hz, 4H), 8.70 (d, *J* = 8.2 Hz, 4H), 7.43 (d, *J* = 8.0 Hz, 4H), 7.27 (d, *J* = 8.0 Hz, 4H), 2.76 (t, *J* = 7.8 Hz, 4H), 1.80 – 1.65 (m, 4H), 1.46 (h, *J* = 7.4 Hz, 4H), 1.00 (t, *J* = 7.3 Hz, 6H).

^{13}C NMR (101 MHz, 1,2-dichloroethene-*d*) δ163.5, 143.8, 134.8, 132.2, 131.7, 129.6, 129.3, 128.2, 126.5, 123.4, 123.2, 35.3, 33.3, 22.4, 14.0.

HRMS ESI+ (m/z): calcd. for $[M+H^+]$ $C_{44}H_{35}N_2O_4$, 655.25968; found $[M+H^+]$, 655.25916.

FT-IR (cm^{-1}, neat): 2928, 1705, 1662, 1593, 1361, 1259, 1183, 808, 744.

RF: 0.28 in DCM.

Figure S1. ^{1}H NMR, ^{13}C NMR and mass spectra for bPDI-1.

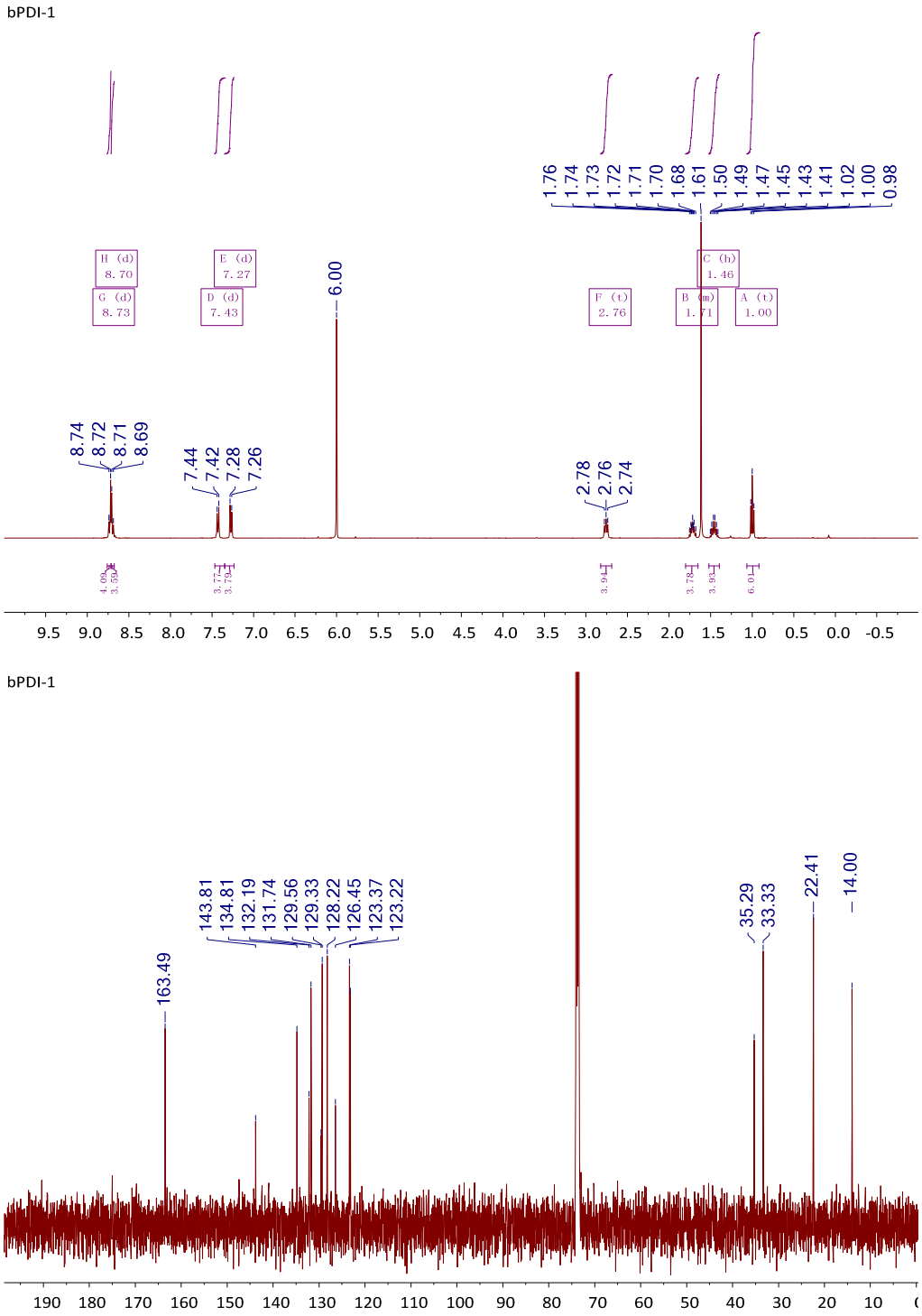

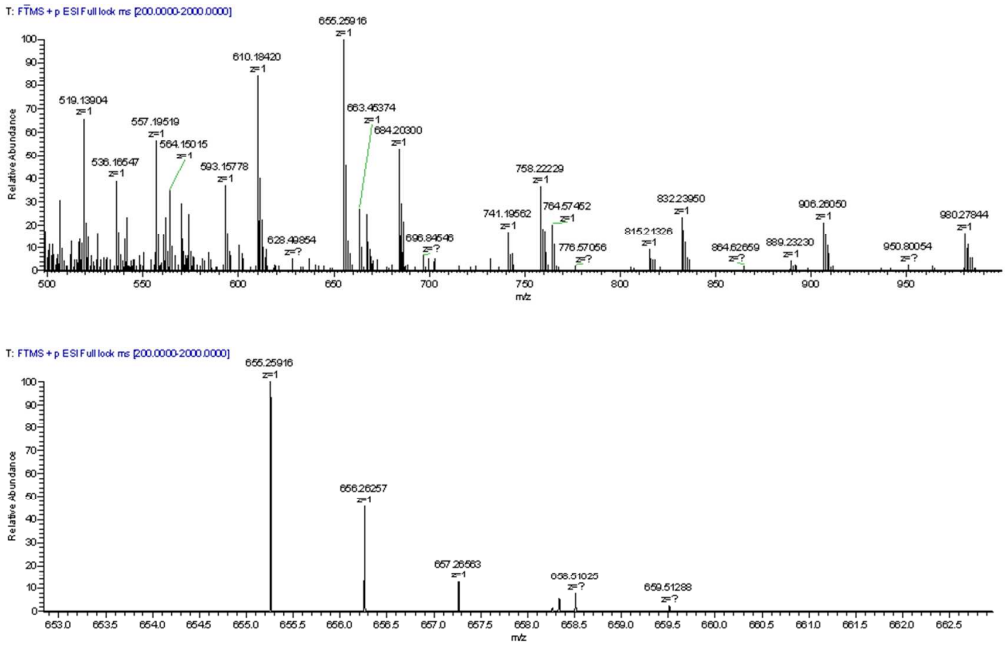

bPDI-2

A mixture of tetrabromo-PDI (50 mg, 0.052 mmol), phenyl bronic acid pinacol ester (80 mg, 0.39 mmol) and $Pd(PPh_3)_4$ (15 mg, 0.013 mmol) were dissolved in toluene (2.5 ml, 8% w/w Aliquate 336) and 2M K_2CO_3 (in water) solution. The solution was sealed under N_2, heated to reflux and stirred for 48h. The organic solvent layer of the crude product was separated and purified by flash chromatography (toluene: ethyl acetate 10:1) and recrystallization (DCM and ethanol) to give the target product (red powder, 42 mg, 0.044 mmol, 84% yield).

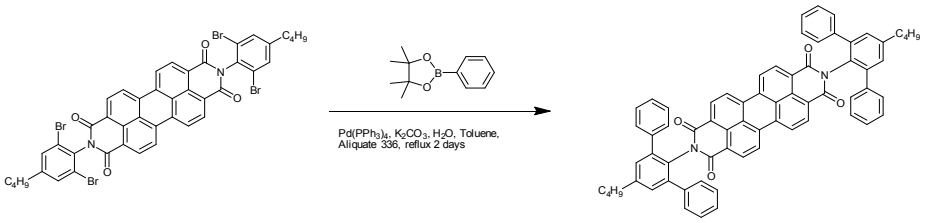

^{1}H NMR (400 MHz, benzene) δ 8.31 (d, *J* = 7.9 Hz, 4H), 7.83 – 7.71 (m, 8H), 7.32 (s, 4H), 7.19 (s, 4H), 7.05 (t, *J* = 7.6 Hz, 8H), 6.94 – 6.83 (m, 4H), 2.59 – 2.44 (m, 4H), 1.47 (tt, *J* = 8.1, 6.3 Hz, 4H), 1.28 (h, *J* = 7.3 Hz, 4H), 0.86 (t, *J* = 7.3 Hz, 6H).

^{13}C NMR (101 MHz, benzene) δ163.6, 143.7, 142.0, 140.3, 134.3, 130.8, 130.3, 129.7, 129.2, 128.9, 127.3, 126.1, 122.6, 122.4, 35.4, 33.3, 22.7, 13.9.

MS ESI+ (m/z): calcd. for $[M+H^+]$ $C_{68}H_{51}N_2O_4$, 959.38488; found $[M+H^+]$, 959.38422.

FT-IR (cm^{-1}, neat):2928, 17028, 1553, 1598, 1403, 1340, 1254, 811, 744, 700.

RF: 0.50 in DCM.

Figure S2. ^{1}H NMR, ^{13}C NMR and mass spectra for bPDI-2.

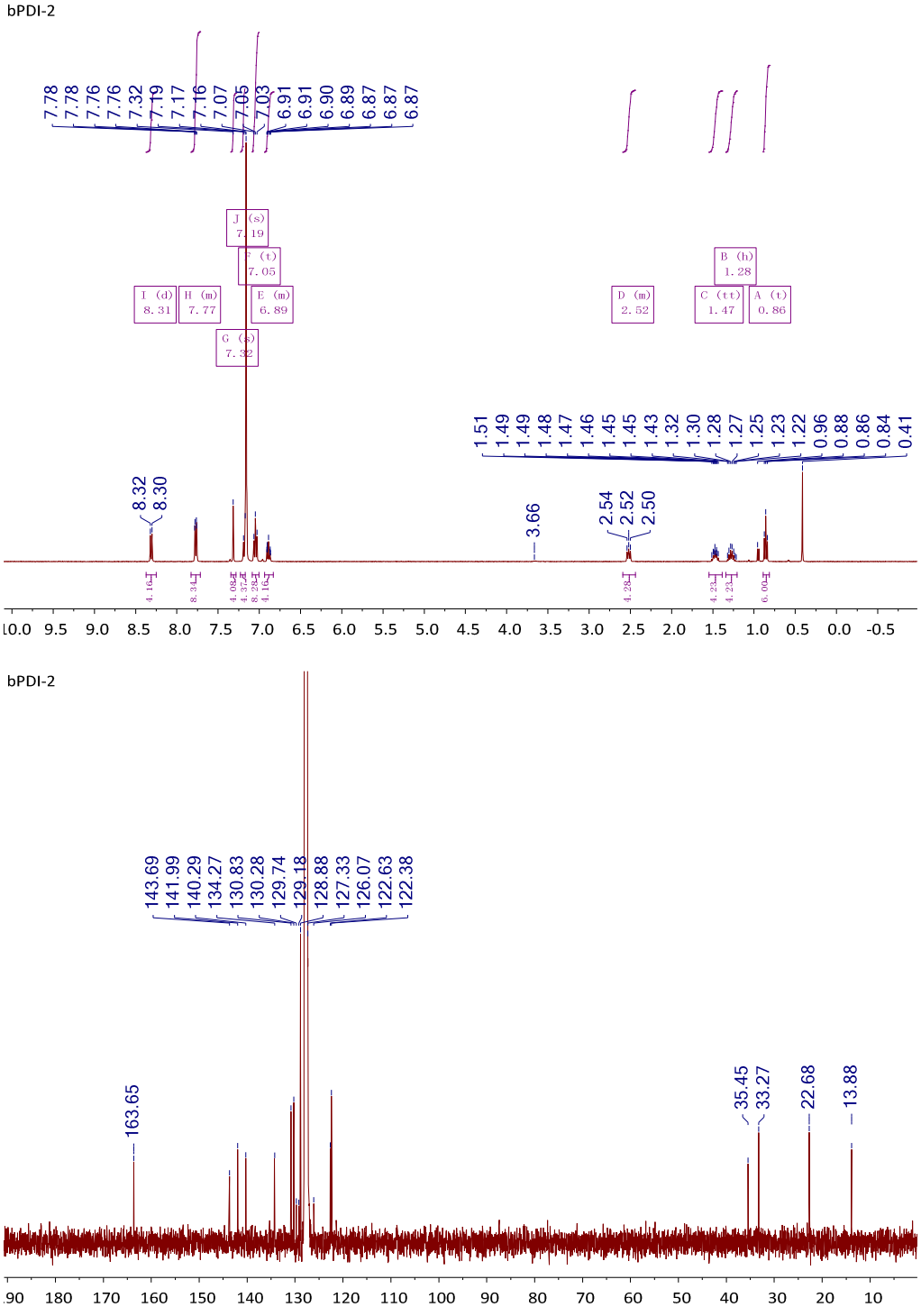

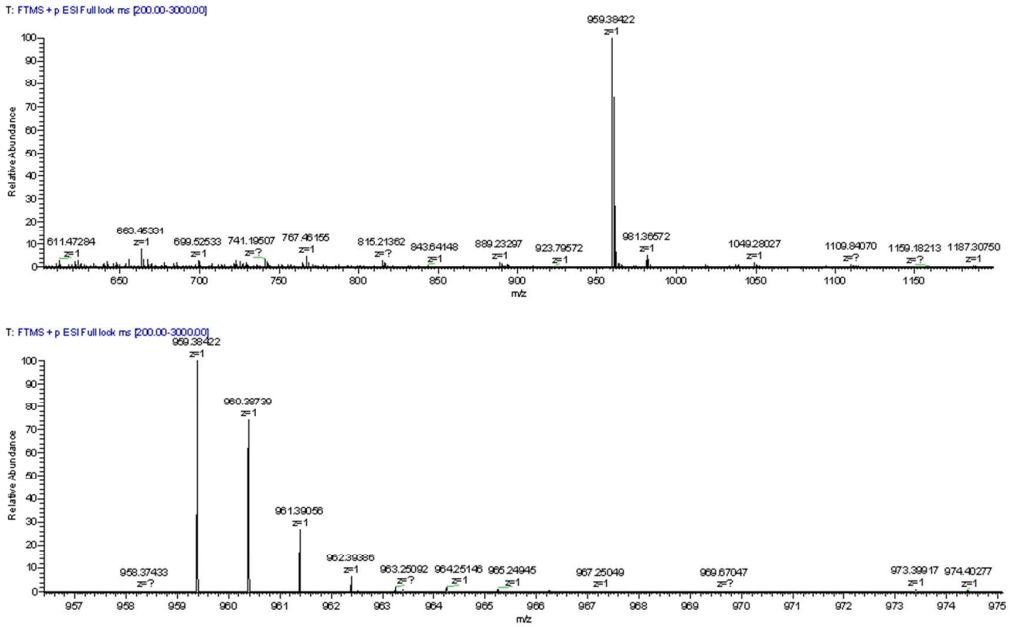

bPDI-3

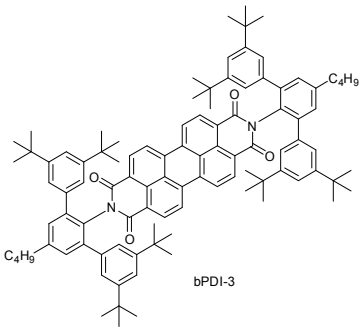

This compound was synthesized according to literature procedure.[1]

4,4,5,5-tetramethyl-2-(4-tritylphenyl)-1,3,2-dioxaborolane

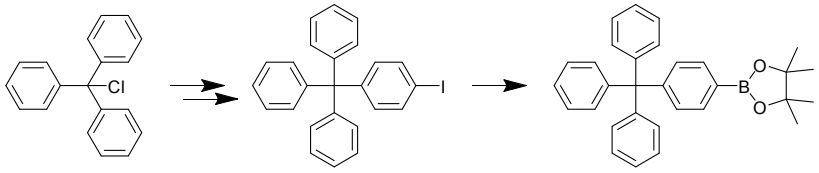

The (4-iodophenyl)methanetriyl)tribenzene was synthesized from trityl-chloride according to a literature procedure.[2, 3]

The solution of *n*-BuLi in THF (2.4 M, 2.15 mmol, 0.9 mL) was added dropwise to the solution of

((4-iodophenyl)methanetriyl)tribenzene (400 mg, 0.9 mmol) in THF (25 ml) at -78 °C . The mixture was stirred at -78 °C for 30 minutes before isopropoxy bronic acid pinacol ester (400 mg, 2.15 mmol) was added. The mixture was stirred at r.t. for a further 1 hour. After removing the solvent, the crude product was dissolved in toluene and purified by the flush chromatography (toluene) to give the target product (faint yellow powder, 180 mg, 45% yield).

^{1}H NMR (400 MHz, $CDCl_3$) δ7.75 – 7.64 (m, 2H), 7.27 – 7.14 (m, 17H), 1.32 (s, 12H).

^{13}C NMR (101 MHz, $CDCl_3$) δ150.1, 146.7, 134.1, 131.3, 130.7, 127.6, 126.0, 83.9, 65.3, 25.0.^{13}C NMR (101 MHz, cdcl$_3$) δ 150.1, 146.7, 134.1, 131.3, 130.7, 127.6, 126.0, 83.9, 65.3, 25.0.

MS ESI+ (m/z): calcd. for [M+H$^+$] $C_{31}H_{32}NO_2$, 447.24954; found [M+H$^+$], 447.24908.

FT-IR (cm^{-1}, neat): 1608.6, 1360.6, 1143.8, 1089.3, 762.0, 749.8, 701.2, 663.6.

RF: 0.62 in toluene.

Figure S3. ^{1}H NMR, ^{13}C NMR and mass spectra for 4,4,5,5-tetramethyl-2-(4-tritylphenyl)-1,3,2-dioxaborolane.

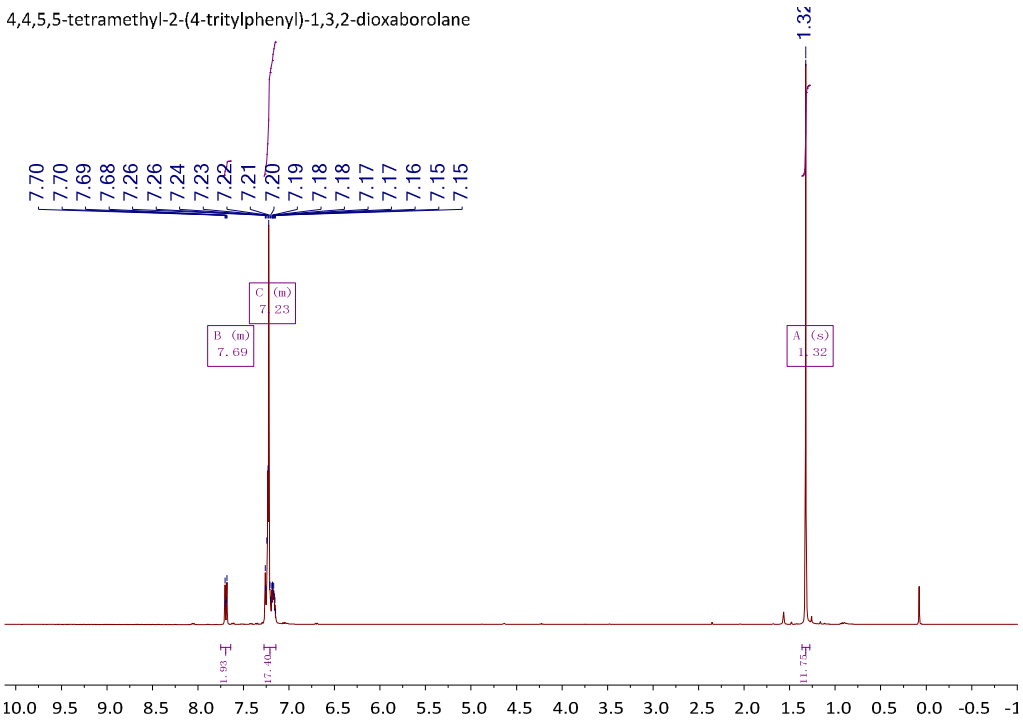

4,4,5,5-tetramethyl-2-(4-tritylphenyl)-1,3,2-dioxaborolane

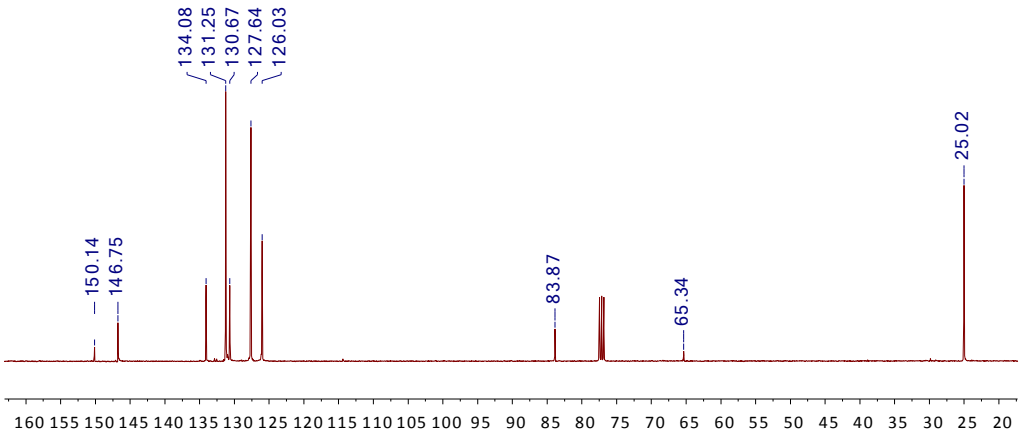

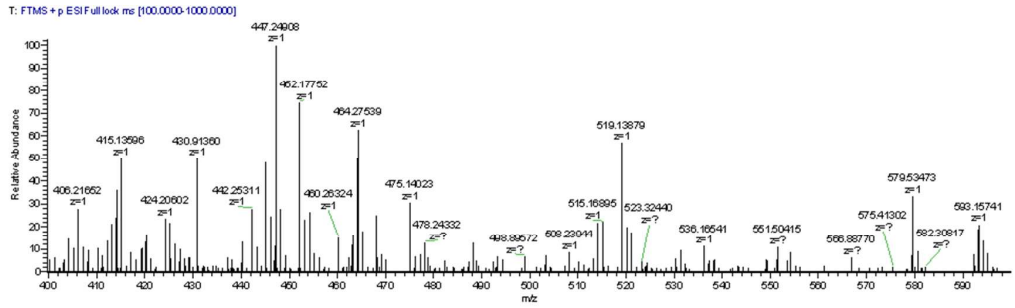

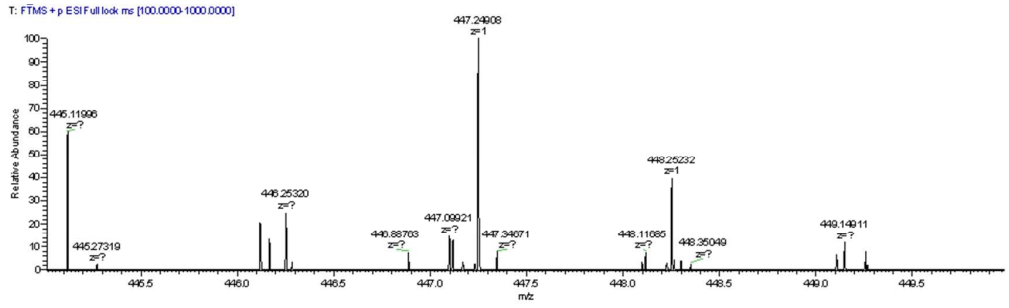

bPDI-4

A mixture of tetrabromo-PDI (40 mg, 0.04 mmol), 4,4,5,5-tetramethyl-2-(4-tritylphenyl)-1,3,2-dioxaborolane (110 mg, 0.24 mmol) and $Pd(PPh_3)_4$ (6 mg, 0.005 mmol) were dissolved in toluene (2.5 ml, 8% w/w Aliquate 336) and 2 M K_2CO_3 (in

water, 0.5 mL) solution. The reaction vessel was sealed under N_2, heated to reflux and stirred for 48h. The organic solvent layer of the crude product was separated and purified by flash chromatography (toluene:ethyl acetate 10:1) and recrystallization (DCM and ethanol) to give the target product (red powder, 57 mg, 72%).

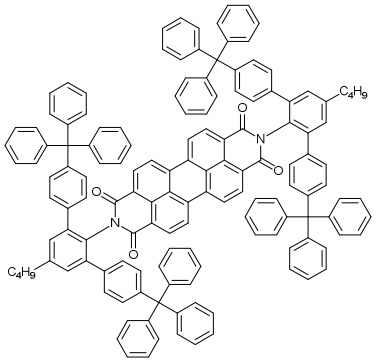

^{1}H NMR (400 MHz, Chloroform-*d*) δ 8.61 (d, *J* = 8.1 Hz, 4H), 8.46 (d, *J* = 7.9 Hz, 4H), 7.36 (s, 4H), 7.22 (d, *J* = 8.1 Hz, 8H), 6.98 (d, *J* = 8.3 Hz, 8H), 6.95 – 6.89 (m, 60H), 2.78 (t, *J* = 7.9 Hz, 4H), 1.75 (t, *J* = 7.8 Hz, 4H), 1.51 – 1.45 (m, 4H), 0.99 (t, *J* = 7.3 Hz, 6H).

^{13}C NMR (101 MHz, cdcl$_3$) δ163.3, 146.6, 145.7, 144.0, 141.0, 137.1, 134.8, 131.7, 131.0, 130.8, 130.0, 129.5, 129.0, 127.5, 127.3, 126.5, 125.8, 123.1, 123.1, 64.7, 35.7, 33.5, 22.8, 14.2.

163.3, 146.6, 145.7, 144.0, 141.0, 137.1, 134.8, 131.7, 131.0, 130.8, 130.0, 129.5, 129.0, 127.5, 127.3, 126.5, 125.8, 123.1, 123.1, 64.7, 35.7, 33.5, 22.8, 14.2.

MS ESI+ (m/z): calcd. for [M+H$^+$] $C_{144}H_{107}N_2O_4$, 1928.82644; found [M+H$^+$], 1928.82605.

FT-IR (cm^{-1}, neat): 1705.1, 1667.1, 1595.0, 1344.0, 1254.7, 812.3, 748.1, 701.0.

RF: 0.78 in DCM.

Figure S4. ^{1}H NMR, ^{13}C NMR and mass spectra for bPDI-4.

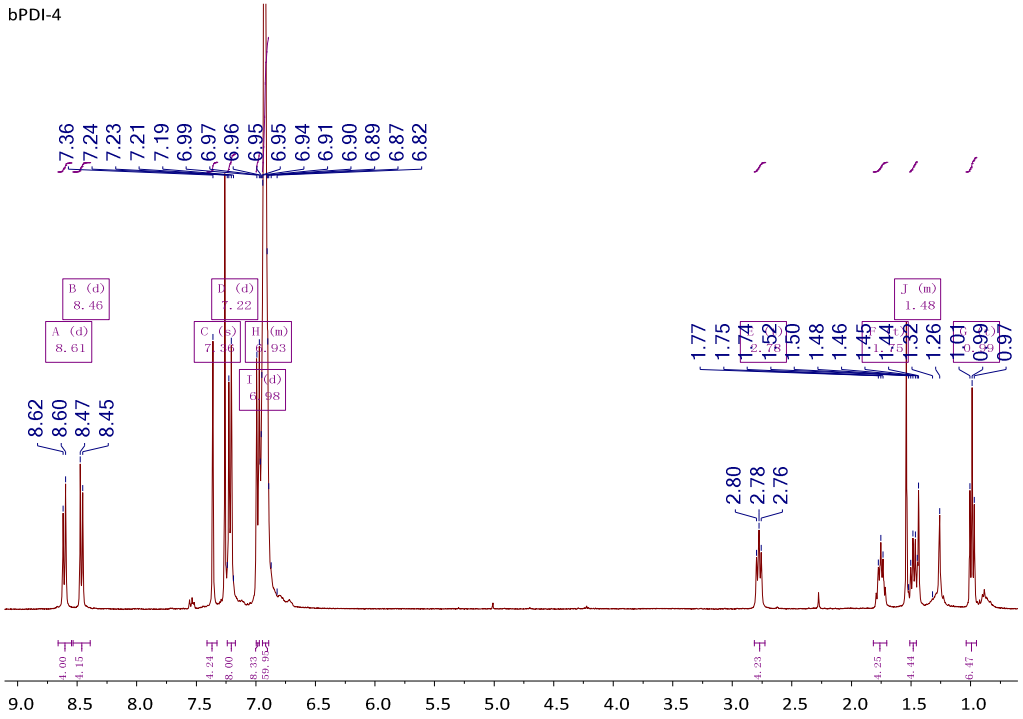

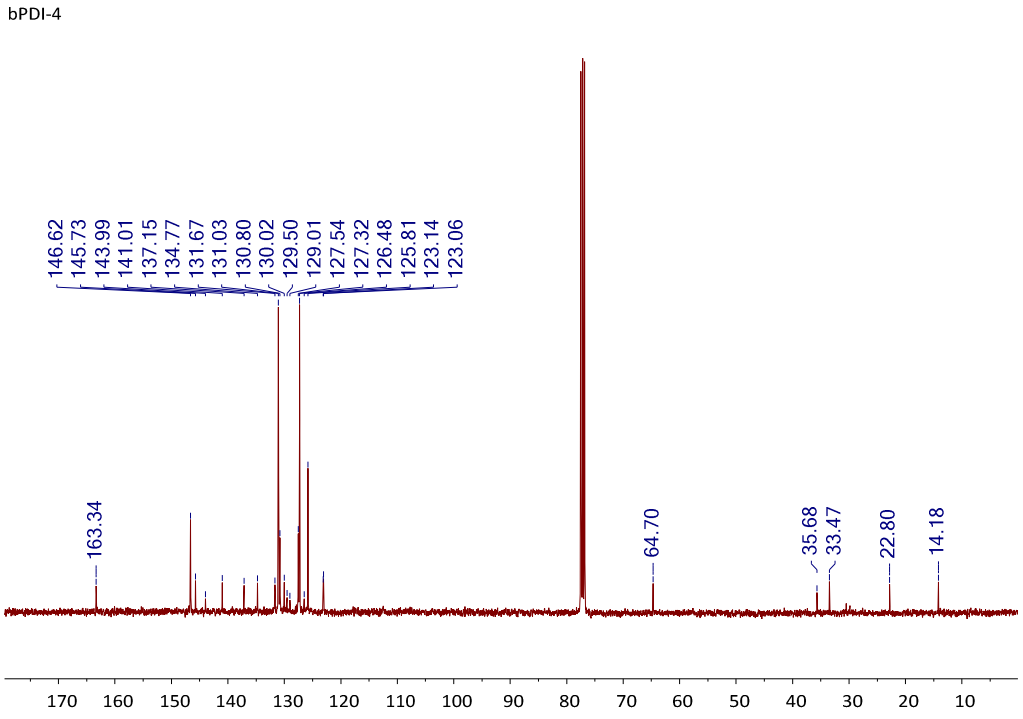

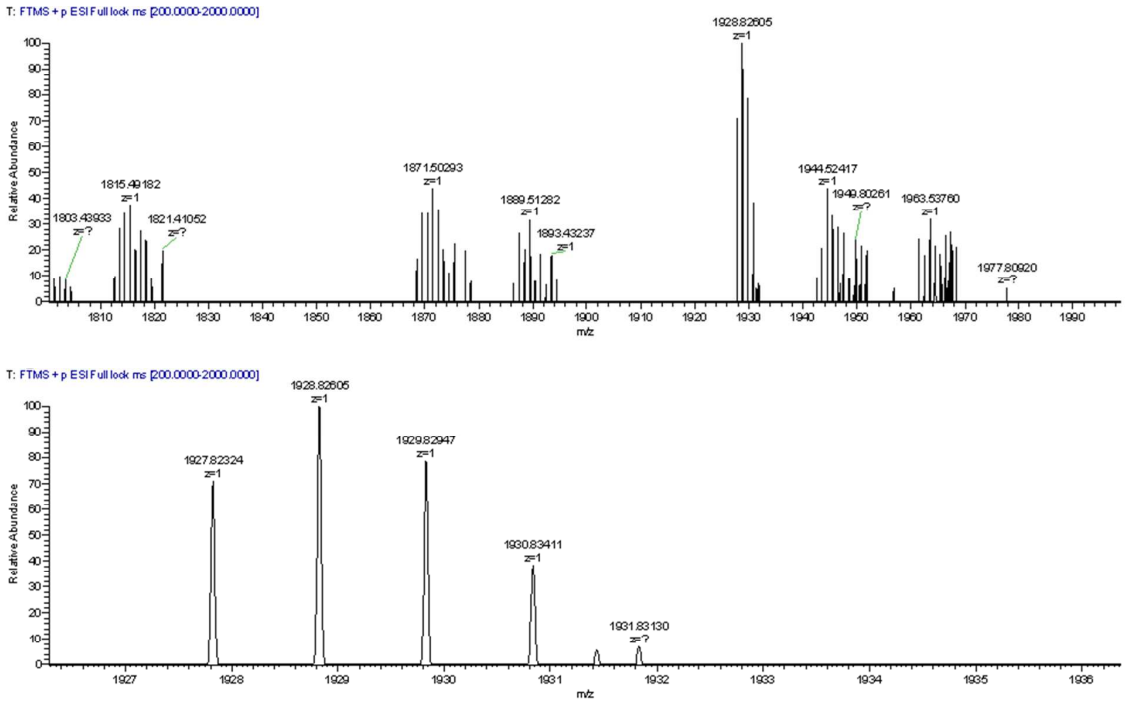

The optimized 3D chemical structure of bPDIs

The perylene core in each bPDI varies from totally exposed to fully covered.

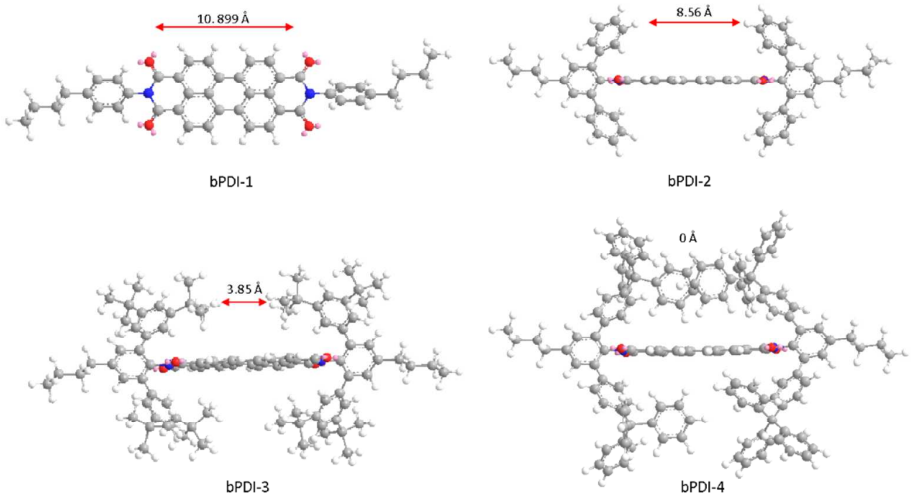

Figure S5. The optimized 3D chemical structures of the studied bPDIs. The gap of the exposed perylene core is shown in Å.

X-ray crystal experimental procedures and data of bPDIs

Intensity data for bPDI-2 and bPDI-3 were collected at 100 K on the MX1 beamline at the Australian Synchrotron[4], bPDI-4 was collected on an Oxford SuperNova CCD diffractometer at 130 K. The structures were solved by direct methods and difference Fourier synthesis. Thermal ellipsoid plots were generated using the program ORTEP-3 integrated within the WINGX suite of programs.

Crystal data for bPDI-2 ($C_{136}H_{100}N_4O_8$). M = 1918.19, T = 100.0(2) K, λ= 0.71073 Å, triclinic, space group P-1, a = 16.945 (3), b = 17.240(3), c = 20.307(4) Å, α = 81.27(3), β= 73.96(3)° γ = 64.79(3). V = 5154.36 Å^3, Z = 2, Dc = 1.236 Mg/m^3, μ(Mo-Kα) 0.076 mm^{-1}, F(000) = 2016, crystal size 0.15 x 0.10 x 0.02 mm^3. 90186 reflections measured to a maximum θ = 33.179°, 28660 independent reflections (R_{int} = 0.0606), the final R was 0.0694 [I > 2σ(I)] and wR(F^2) was 0.2281 (all data).

Crystal data for bPDI-3 ($C_{100}H_{114}N_2O_4$). M = 1407.93, T = 100.0(2) K, λ= 0.71073 Å, monoclinic, space group $P2_1/c$, a = 14.593(3), b = 16.448(3), c = 17.819(4) Å, β= 106.32(3)°. V = 4104.7(15) Å^3, Z = 2, Dc = 1.139 Mg/m^3, μ(Mo-Kα) 0.068 mm^{-1}, F(000) = 1520, crystal size 0.08 x 0.08 x 0.01 mm^3. 81742 reflections measured to a maximum θ = 30.08°, 11995 independent reflections (R_{int} = 0.1018), the final R was 0.070 [I > 2σ(I)] and wR(F^2) was 0.2035 (all data).

Crystal data for bPDI-4 ($C_{144}H_{106}N_2O_4$). M = 1928.3, T = 130.0(2) K, λ= 1.54184 Å, triclinic, space group P-1, a = 9.5089 (6), b = 16.5114(10), c = 18.4177(11) Å, α = 96.813(5), β = 99.765(5)° γ = 93.246(5)°. V = 2820.9(3) Å^3, Z = 1, Dc = 1.135 Mg/m^3, μ(Mo-Kα) 0.517 mm^{-1}, F(000) = 1016, crystal size 0.42 x 0.22 x 0.02 mm^3. 16294 reflections measured to a maximum θ = 67.495°, 10045 independent reflections (R_{int} = 0.0394), the final R was 0.0708 [I > 2σ(I)] and wR(F^2) was 0.2168 (all data).

Spectroscopy results

Table S1. Summary of the photophysical properties of the bPDIs.

Compound	Abs_{max} (Abs_{onset}) nm	$\varepsilon \times 10^4$ $mol^{-1}cm^{-1}$	PL_{max} nm	Stokes shift nm	$\Phi_{PL,PMMA}$ [a] %	$\Phi_{PL,amorphous}$ [b] %
bPDI-1	527 (543)	8.56	536	9	21.0±0.9	N/A
bPDI-2	527 (542)	7.80	538	11	92.9±0.4	21.2±0.8
bPDI-3	528 (541)	8.68	536	9	98.2±1.2	14.6±0.1
bPDI-4	528 (542)	8.48	538	10	100.6±0.5	29.1±0.6

a, PLQY of 10 mM in PMMA thin film samples; b, PLQY of the neat amorphous film samples.

Table S2. Summary of the electrochemical properties of the bPDIs.

Compound	E_{red} [a] eV	E_{LUMO} eV	E_{ox} [a] eV	E_{HOMO} eV	E_{Δ} eV
bPDI-1	-1.03	-4.07	1.25	-6.35	2.28
bPDI-2	-1.00	-4.10	1.26	-6.36	2.26
bPDI-3	-1.11	-3.99	1.23	-6.33	2.34
bPDI-4	-1.05	-4.05	1.22	-6.32	2.27

a, vs Fc/Fc^+

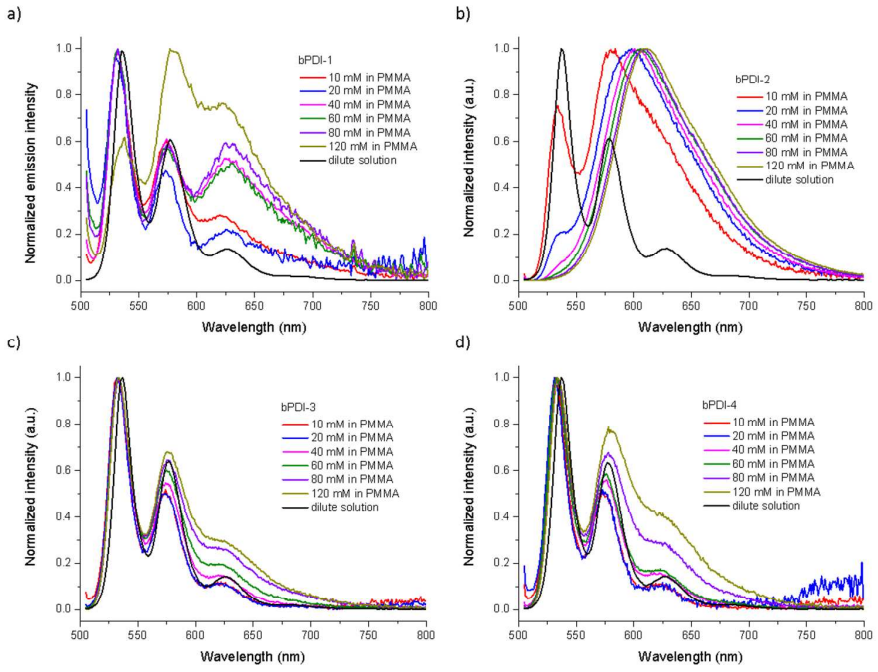

Figure S6. PL spectra of bPDIs as a function of concentration: a) bPDI-1; b) bPDI-2; c) bPDI-3 and d) bPDI-4.

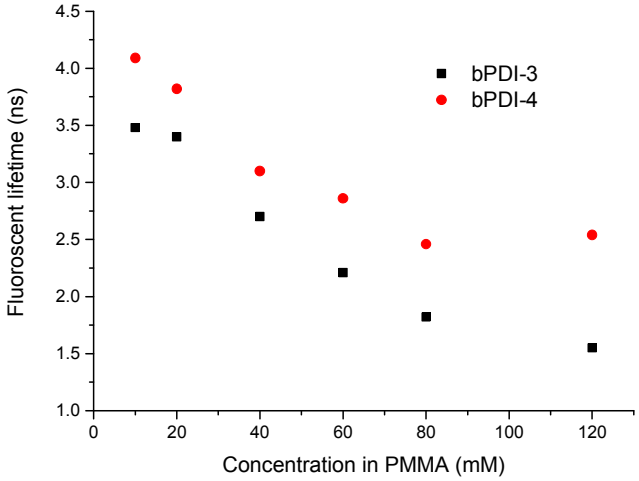

Figure S7. Average fluorescence lifetimes of bDI-3 and bPDI-4 in PMMA thin-film matrix as a function of concentration (λ_{ex}=440nm, λ_{em}=540nm). The maximum uncertainty is ±0.04 ns.

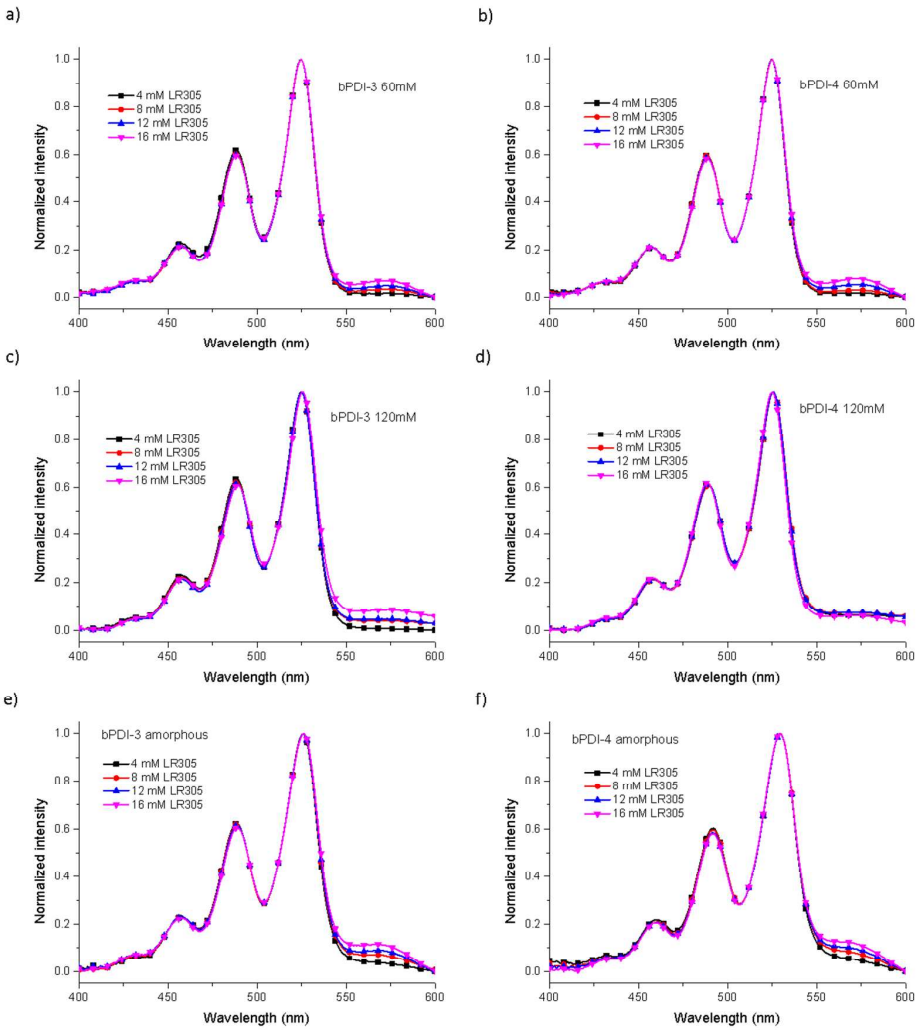

Figure S8. UV-vis absorption spectra of the donor-acceptor system.

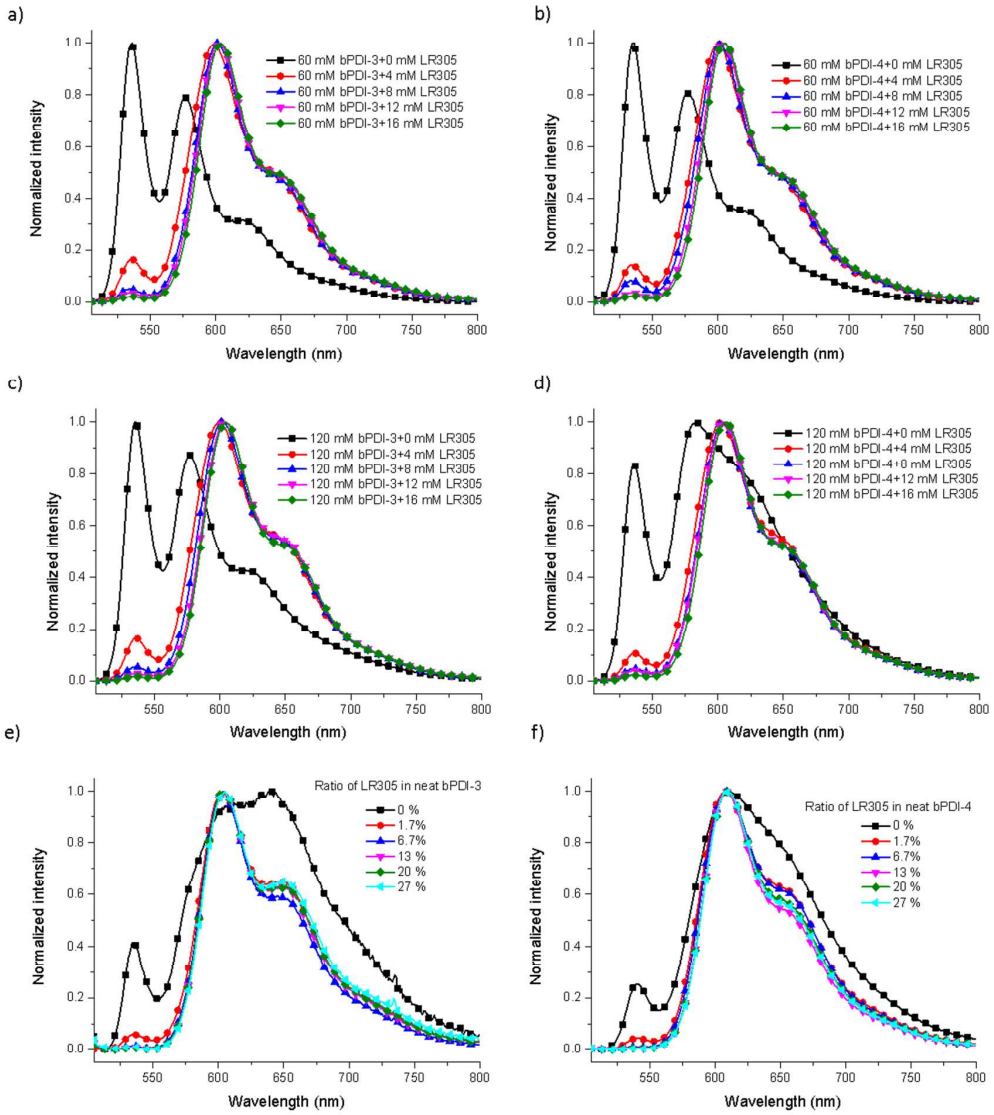

Figure S9. PL spectra of thin-film samples based on the mixture of LR305 as a function of concentration with a) 60 mM bPDI-3 in PMMA, b) 60 mM bPDI-4 in PMMA, c) 120 mM bPDI-3 in PMMA, d) 120 mM bPDI-4 in PMMA, e) neat bPDI-3 and f) neat bPDI-4.

Electrochemical analysis:

All cyclic voltammograms (CV) were acquired in a mixed solution of CH_2Cl_2 and MeCN (9:1 v:v) with 0.1 M TBA PF_6. The reference electrode was Ag/Ag+, the working electrode was glassy carbon and platinum was used as the counter electrode. The CVs were acquired at a scan rate of 50 mV/s and ferrocene was used as the internal reference. Therefore, the LUMO and HOMO energy levels of the samples were calculated (Figure 4.19) based on the following equations[5]:

$$E_{LUMO} = -(5.1 + E_{red})\ eV$$

$$E_{HOMO} = -(5.1 + E_{ox})\ eV$$

The HOMO and LUMO energy level of all four bPDIs were very similar to each other and the energy gap between HOMO and LUMO were determined from their absorption spectra.

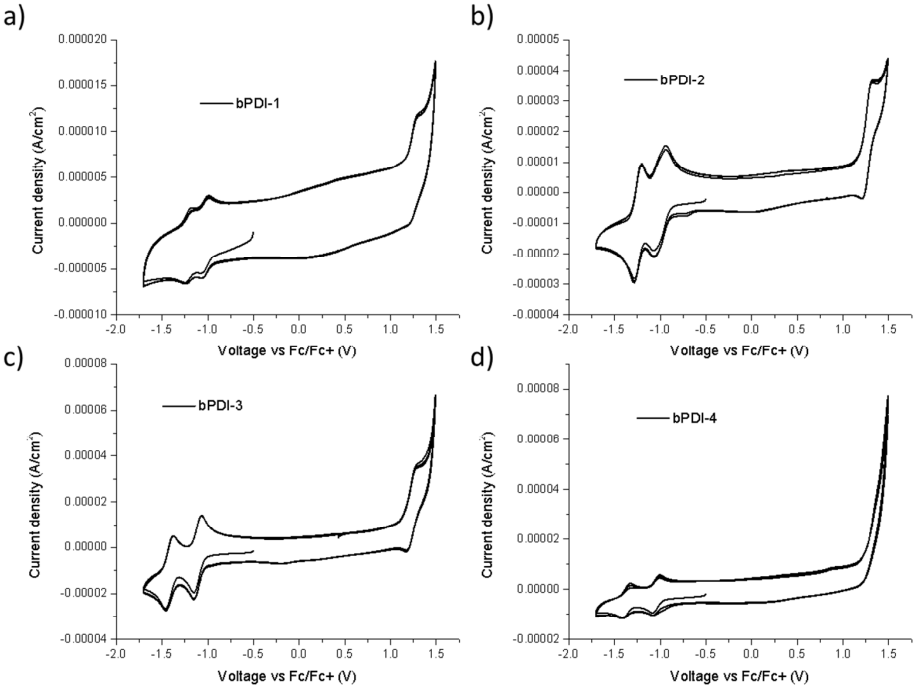

Figure S10. CV curves of the compounds a) bPDI-1, b) bPDI-2, c) bPDI-3 and d) bPDI-4.

Thermal gravimetric analysis (TGA)

TGA of all samples were conducted on a Mettler Toledo TGA/SDTA851e thermogravimetric analyzer heating from 25 °C to 800 °C at a ramp of 10 °C min^{-1} under a flow of nitrogen (30 mL min^{-1}). The temperature of a 5% weight loss for bPDI-1 was at 488 °C, bPDI-2 was at 450 °C, bPDI-3 was at 450 °C and bPDI-4 was at 443 °C.

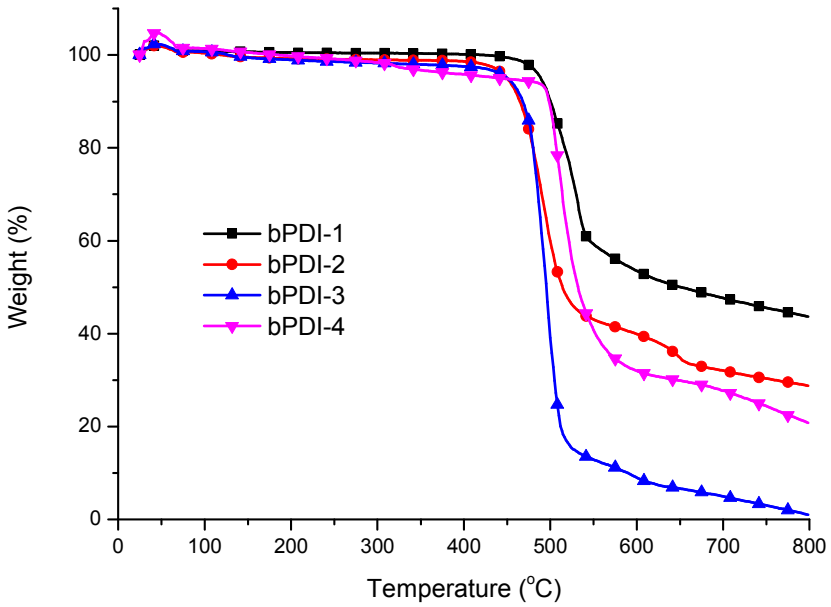

Figure S11. TGA analysis plot of all bPDIs with a 5% weight loss after 450 °C.

Differential scanning calorimetry (DSC)

DSC experiments of all samples were performed on a Perkin-Elmer Sapphire DSC at a ramp rate of 10 °C min^{-1} unless otherwise noted.

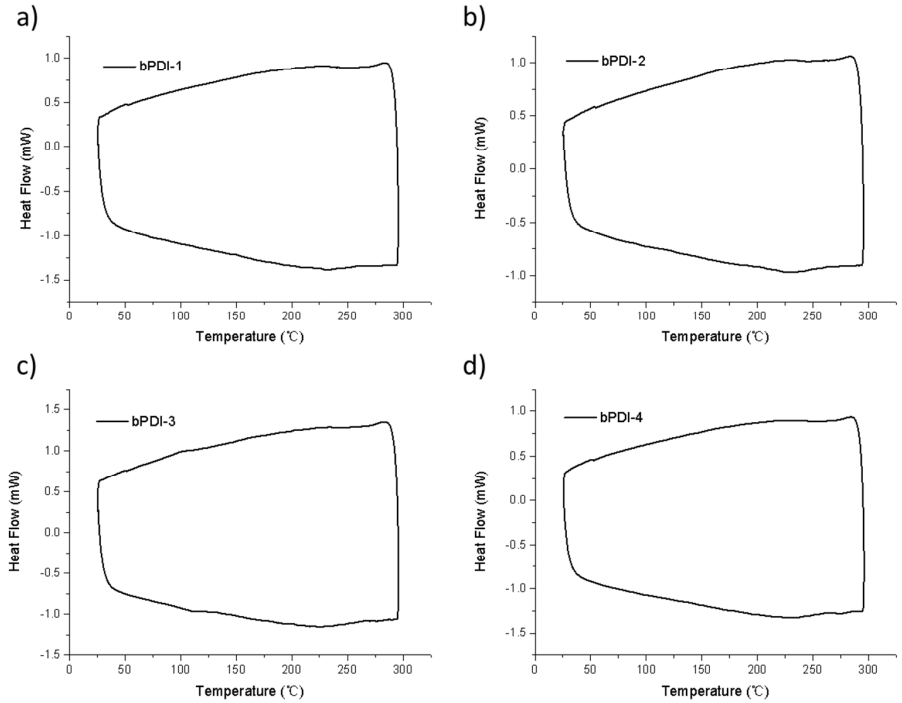

Figure S12. DSC analysis plot of a) bPDI-1, b) bPDI-2, c) bPDI-3 and d) bPDI-4. The plot for bPDI-2 has an endothermic process in the first circle.

Thin-film samples preparation

Thin-film samples preparation for absolute PLQY measurement:

All the glass (MENZEL-GLÄSER Microscope Slides, 76 × 26 mm) and quartz (PST Quartz slide, 76 × 25mm) slides used in the absolute PLQY measurements were cut to 1.25 cm × 1.25 cm × 0.1 cm, cleaned by sonicating sequentially in $CHCl_3$, acetone, NaOH (a.q.), distilled water and isopropanol and dried using a strong flow of N_2.

All the thin film samples for the absolute PLQY measurement were prepared by spin coating 80 µL of a casting solution of the dyes and PMMA on top of the above-mentioned glass or quartz slides. The spin coating speed was from 500 to 800 rpm depending on the absorbance required for the sample and the acceleration was 400 rpm/s. The casting solutions of the dyes and PMMA were prepared by diluting the mixture of the prototypical solution of each dye (5 mM in $CHCl_3$) and the PMMA solution (0.05 g/ml in $CHCl_3$) with $CHCl_3$ to reduce the concentration of PMMA to 1% w/w. The concentration of the dyes in the casting solutions were calculated based on the volume of the solid-state PMMA. After spin coating, the samples were baked at 100°C for 10 min to evaporate the solvent.

Thin-film sample preparation for TCSPC and time-resolved fluorescence anisotropy measurements:

The glass slips (MENZEL-GLÄSER Cover Slips, 22 × 22 × 0.13 mm) were used as received from the supplier without further cleaning in preparing thin-film samples for TCSPC and time-resolved fluorescence anisotropy measurements. All these thin-film samples were prepared by spin coating 180 µL of the above-mentioned casting solution on the above-mentioned glass slips. The spin coating speed was from 500 to 800 rpm depending on the absorbance required and the acceleration was 400 rpm/s. The concentration of the dyes in the casting solutions were calculated based on the volume of the solid-state PMMA (See Figure S7). After spin coating, the samples were baked at 100°C for 30 min to evaporate the solvent.

Absolute PLQY measurements and re-absorption correction

Absolute PLQY measurements of all samples were performed according to the experimental approach described elsewhere[6, 7] using an integrating sphere accessory (F3018, Horiba Jobin Yvon) on a Fluorolog®-3 fluorimeter. The angle of the excitation beam to the normal of the sample surface can be modified using the variable sample holder. All spectra for the absolute quantum yield measurements were corrected for the light source noise, wavelength sensitivity and the transmittance of the filters. The photon counts of all the measurements on the Fluorolog®-3 fluorimeter were within the linear response range of the detector (less than 2×10^6 cps).

The re-absorption correction[8] was used on all donor materials PLQY measurement. The reference emission spectrum for re-absorption correction was recorded from the PLQY sample in the absence of the integrating sphere. For samples with a large absorption and emission spectral overlap (all bPDI-3 and bPDI-4 in PMMA matrix and bPDI-2 at 10 mM and 20 mM), the reference emission spectrum for re-absorption correction was recorded from samples in an ultra-thin PMMA matrix (spin-coating speed at 3000 rpm) to further minimise the re-absorption effect in the reference samples. The PLQYs of all donor-acceptor systems were reported without re-absorption correction (minimal re-absorption).

The definition of OQE, G and flux gain

The OQE and G can be defined as:

$$OQE = \frac{n_{edge}}{n_{abs}}$$

$$G = \frac{S_{surface}}{S_{edge}}$$

where the n_{edge} is the number of the total edge output photon, the n_{abs} is the number of photon absorbed from the surface. S_{edge} and $S_{surface}$ are the area of the edges and surface of the waveguide respectively.

The flux gain can be defined as:

$$flux\ gain = \frac{I_{edge}}{I_{abs}} = \frac{1}{4} OQE \times G$$

where the I_{edge} refers to the intensity of one edge output and I_{abs} is the intensity of the light absorbed.

Time-correlated single photon counting (TCSPC) and time-resolved fluorescence anisotropy measurements

As described previously[1, 9], the excitation source was a mode-locked and cavity dumped Ti:Sapphire laser (Coherent Mira 900F/APE PulseSwitch) pumped by a Coherent Verdi-10 DPSS Nd:YVO_4 laser. The laser output (880 nm wavelength, 5.4 MHz repetition rate) was frequency doubled to provide an excitation wavelength of 440 nm. The individual fluorescence decay curves were collected using the time-correlated single photon counting technique. Synchronization of the laser pulses was achieved using a fast photodiode (Becker & Hickl, PHD-400-N) fed through a nanosecond delay box and constant fraction discriminator (Tennelec TC455) as the stop signal for the time-to amplitude converter (Ortec model 457). The fluorescence decay profiles of the bPDI samples were collected at the magic angle relative to the (vertical) excitation polarization. The fluorescence lifetimes were calculated by FAST software (Edinburgh Instruments Ltd) using exponential components analysis. For anisotropy measurements, the excitation beam passed through a silica double rhomb to select the input (vertical) excitation polarization. The emission was collected at right angles relative to the excitation, first passing through a polarization analyzer mounted on a stage that rotates both the polarizer and collection lens to collect vertically and horizontally polarized emission. The analyzer orientation was driven by a computer controlled stepper motor board (Phidgets 1067). The emission was then passed through a polarization scrambler (ThorLabs DPU-25), spectrally selected using a monochromator (Jobin Yvon, H20), and detected using a single photon counting photomultiplier tube (XP2020Q). The memory of the multichannel analyser (MCA-p7882, Fastcom Tech) was divided into segments in which the various I_{ij} components (i and j are the polarization of the excitation and detection respectively), generated following control of the stepper motors, and the contents saved during each acquisition sequence. Decay profiles were acquired by sequentially toggling between the respective polarisation orientations/memory locations to achieve equal collection conditions for each orientation. The correction for the polarization bias of detection system (G factor) was determined to be very close to unity by both tail-matching the I_{VV} and I_{VH} profiles and the I_{HV}/I_{HH} ratio from the time-resolved fluorescence decays of Coumarin 153 in solution.

Calculation of Energy Migration Distance

TCSPC and time-resolved anisotropy measurements were carried out to further examine the energy migration behavior of bPDI-4.

The Förster resonance energy transfer (FRET) critical radius (R_0, nm) is defined via the following Förster equation[10, 11]:

$$R_0 = 0.02108 \times \left(\frac{\kappa^2 \Phi_{PL} J}{n^4}\right)^{\frac{1}{6}}$$

$$J = \int \varepsilon_A(\lambda) F_D(\lambda) \lambda^4 \, d\lambda$$

where κ^2 is the orientation factor (κ^2=2/3 for random orientation, long lifetime donor and acceptor system), Φ_{PL} refers to the PLQY of the donor fluorophore in the absence of the acceptor, J (nm^4, M^{-1}, cm^{-1}) is a coefficient related to the overlap between the normalized (area) emission spectrum (F_D) of the donor and the absorption extinction coefficient (ε_A) of the acceptor, λ is the wavelength over the full spectrum, and n is the refractive index of the matrix material (n=1.49 for PMMA matrix). The calculated R_0 of bPDI-4 is 5.03 nm, which is very similar to the previously reported R_0 of bPDI-3 (5.2 nm).ref

The energy migration process in a disordered medium can be further described by the Green's function:

$$\ln \mathrm{G^s(t)} = -\mathrm{C_D}\lambda^{-\frac{1}{2}}\Gamma\left(\frac{1}{2}\right)\left(\frac{\mathrm{t}}{\tau}\right)^{\frac{1}{2}}$$

$$C_D = \frac{4\pi\gamma R_0^3\rho}{3}$$

where C_D is the dimension-less donor concentration, γ is the correction factor for static averaging orientation. ρ is the concentration of the fluorophore (nm^{-3}), λ is the scaling factor (λ=2 for energy migration), $\Gamma\left(\frac{1}{2}\right)$ is the incomplete gamma function ($\sqrt{\pi}$), and τ is the fluorescence lifetime of the donor in absence of the acceptor (τ = 4.0 ± 0.2 ns for bPDI-4 at all concentrations used for the time-resolved anisotropy measurements). The time-dependent anisotropy of the donor then can be described in terms of the following function:

$$r(t) = r_0 G^s(t) + r_\infty$$

where r_0 is the initial anisotropy (r_0 = 0.4 based on the anisotropy date at low concentration at t= 0 ns) and r_∞ refers to the residue anisotropy at the point where the value of $G^s(t)$= 0 and it is an individual free parameter for each sample. As shown in Figure S13, the Green's function fits in with the anisotropy decay results very well when $R_0 = 5.14$ nm, which is corresponding to the value of R_0 (5.03 nm) calculated from the Förster equation.

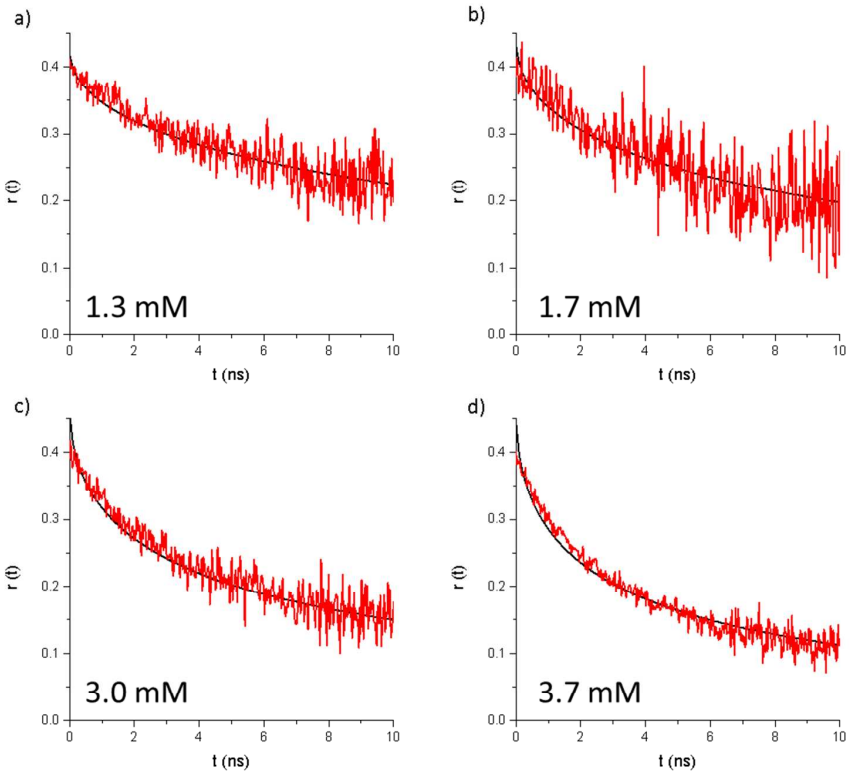

Figure S13. Time-resolved fluorescence anisotropy decays (red) and the theoretical fitting based on the Green's function of bPDI-4 in thin-film PMMA matrix: a) 1.3 mM, b) 1.7 mM, c) 3.0 mM and d) 3.7 mM.

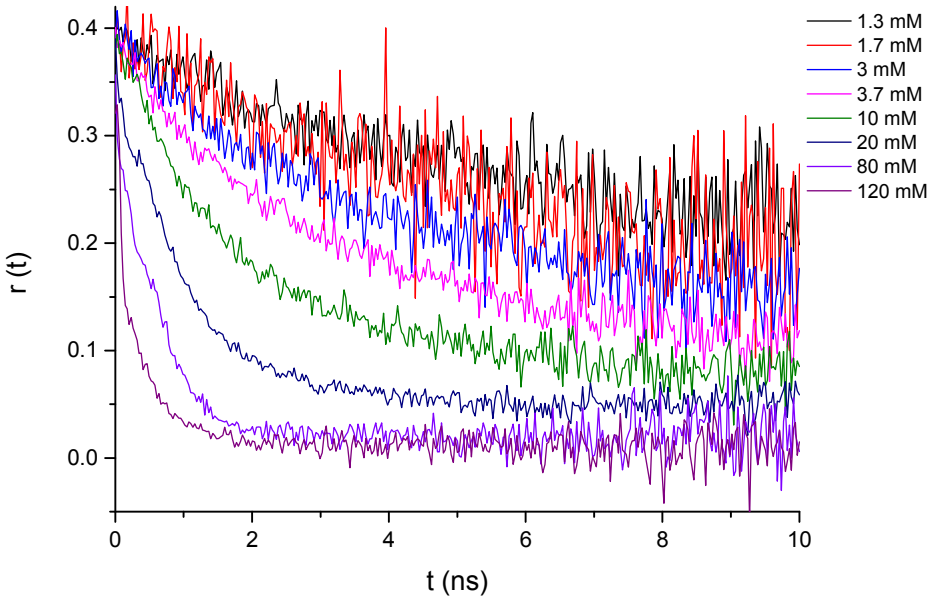

Figure S14. Time-resolved fluorescence anisotropy decays at different concentration of bPDI-4 in thin-film PMMA matrix.

The Laplace transformed mean-squared displacement ($\langle r^2(\varepsilon)\rangle$) of the anisotropy is given by:

$$\langle r^2(\varepsilon)\rangle = \frac{6}{\varepsilon^2} D(0,\varepsilon)$$

$$D(0,\varepsilon) = \frac{\pi C_D R_0^2 \tau^{-1}}{6(2\hat{G}^s(\varepsilon)\tau^{-1})^{1/6}} - \frac{0.02145 {C_D}^2 R_0^2 \hat{G}^s(\varepsilon)^{1/3}}{\tau^{4/3}}$$

$$\hat{G}^s(\varepsilon) = \frac{\tau\left\{\frac{\pi^2 {C_D}^2}{4}\left[1-\sqrt{1+\frac{32}{\pi^2 {C_D}^2}\left(\varepsilon\tau-0.1887 {C_D}^2\right)}\right]+4\left(\varepsilon\tau-0.1887 {C_D}^2\right)\right\}}{4\left(\varepsilon\tau-0.1887 {C_D}^2\right)^2}$$

where the $D(0,\varepsilon)$ stands for the generalized diffusion coefficient, $\hat{G}^s(\varepsilon)$ is the Laplace transformed Green's function and ε is the complex frequency variable in Laplace space. The $\langle r^2(\varepsilon)\rangle$ is then transformed into the mean square displacement of $\langle r^2(t)\rangle$ via the numerical Laplace inversion conducted by the Talbot algorithm.[12-14] The code of the Talbot algorithm calculation program used in this report was developed using MATLAB® code. The $\langle r^2(t)\rangle$ of bPDI-4 as a function of concentration increased linearly with time (Figure S15a).

The diffusion length (L_D) of the energy migration is given by:

$$L_D = \sqrt{D(0,0)\tau}$$

The calculated L_D of bPDI-4 in the concentration of 60 mM is 21 nm, which is very similar to the

previously reported L_D of bPDI-3 (23 nm) (Figure S15b). As shown in Figure S15c, the L_D is greater than the average intermolecular distance (d) when the concentration is exceeding 4 mM. At 120 mM, the calculated L_D of bPDI-4 reaches 35 nm with is 30 times larger than the average intermolecular distance in this concentration.

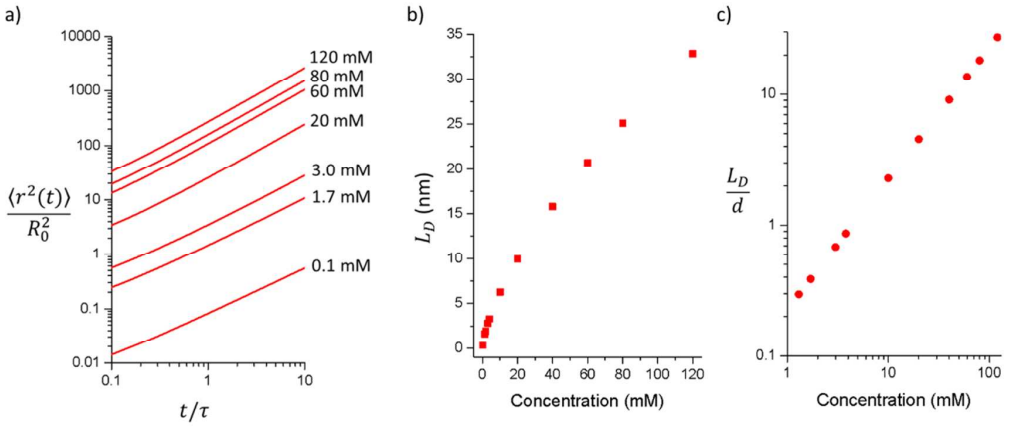

Figure S15. a) the Laplace inverted mean-squared displacement $\langle r^2(t)\rangle$ increases linearly with time with a slope of $6D(0,0)$; b) the L_D of bPDI-4 as a function of the concentration and c) the L_D is greater than d when the concentration of the bPDI-4 in PMMA exceeds 4 mM.

References

1. Banal, J. L.; Soleimaninejad, H.; Jradi, F. M.; Liu, M.; White, J. M.; Blakers, A. W.; Cooper, M. W.; Jones, D. J.; Ghiggino, K. P.; Marder, S. R.; Smith, T. A.; Wong, W. W. H., Energy Migration in Organic Solar Concentrators with a Molecularly Insulated Perylene Diimide. *J. Phys. Chem. C* **2016,** *120*, 12952-12958.

2. Hutchison, J. A.; Uji-i, H.; Deres, A.; Vosch, T.; Rocha, S.; Muller, S.; Bastian, A. A.; Enderlein, J.; Nourouzi, H.; Li, C.; Herrmann, A.; Mullen, K.; De Schryver, F.; Hofkens, J., A Surface-bound Molecule that Undergoes Optically Biased Brownian Rotation. *Nat. Nanotechnol.* **2014,** *9*, 131-6.

3. Verde-Sesto, E.; Pintado-Sierra, M.; Corma, A.; Maya, E. M.; de la Campa, J. G.; Iglesias, M.; Sanchez, F., First Pre-functionalised Polymeric Aromatic Framework from Mononitrotetrakis(iodophenyl)methane and its Applications. *Chem. Eur. J.* **2014,** *20*, 5111-5120.

4. Cowieson, N.; Aragao, D.; Clift, M.; Ericsson, D. J.; Gee, C.; Harrop, S. J.; Mudie, N.; Panjikar, S.; Price, J. R.; Riboldi-Tunnicliffe, A., MX1: A Bending-magnet Crystallography Beamline Serving Both Chemical and Macromolecular Crystallography Communities at the Australian Synchrotron. *J. Synchrotron Radiat.* **2015,** *22*, 187-190.

5. Cardona, C. M.; Li, W.; Kaifer, A. E.; Stockdale, D.; Bazan, G. C., Electrochemical Considerations for Determining Absolute Frontier Orbital Energy Levels of Conjugated Polymers for Solar Cell Applications. *Adv. Mater.* **2011,** *23*, 2367-2371.

6. Porres, L.; Holland, A.; Pålsson, L.-O.; Monkman, A. P.; Kemp, C.; Beeby, A., Absolute Measurements of Photoluminescence Quantum Yields of Solutions using an Integrating Sphere. *J. Fluoresc.* **2006,** *16*, 267-273.

7. Würth, C.; Grabolle, M.; Pauli, J.; Spieles, M.; Resch-Genger, U., Relative and Absolute Determination of Fluorescence Quantum Yields of Transparent Samples. *Nat. Protoc.* **2013,** *8*, 1535-1550.

8. Wilson, L. R.; Richards, B. S., Measurement Method for Photoluminescent Quantum Yields of Fluorescent Organic Dyes in Polymethyl Methacrylate for Luminescent Solar Concentrators. *Appl. Opt.* **2009,** *48*, 212-220.

9. Soleimaninejad, H.; Hong, Y.; Smith, T. A. In *Time-resolved and Polarised Microspectroscopy of Thin Films of Bio-and Nanomaterials*, SPIE Nanoscience+ Engineering, 2016; International Society for Optics and Photonics: 2016; pp 99230M-99230M-9.

10. Fluorescence Detection Techniques. In *Introduction to Fluorescence Sensing*, Demchenko, A. P., Ed. Springer Netherlands: Dordrecht, 2009; pp 65-118.

11. Medintz, I. L.; Hildebrandt, N., *FRET - Förster Resonance Energy Transfer: From Theory to Applications*. Wiley: 2013.

12. Kuhlman, K. L., Review of Inverse Laplace Transform Algorithms for Laplace-space Numerical Approaches. *Numer. Algorithms* **2013,** *63*, 339-355.

13. Abate, J.; Valkó, P. P., Multi-precision Laplace Transform Inversion. *Int. J. Numer. Methods Eng.* **2004,** *60*, 979-993.

14. Abate, J.; Whitt, W., A Unified Framework for Numerically Inverting Laplace Transforms. *INFORMS J. Comput.* **2006,** *18*, 408-421.

Chapter V

A Donor-emitter Fluorophore Pair in a Large-area Printed LSC

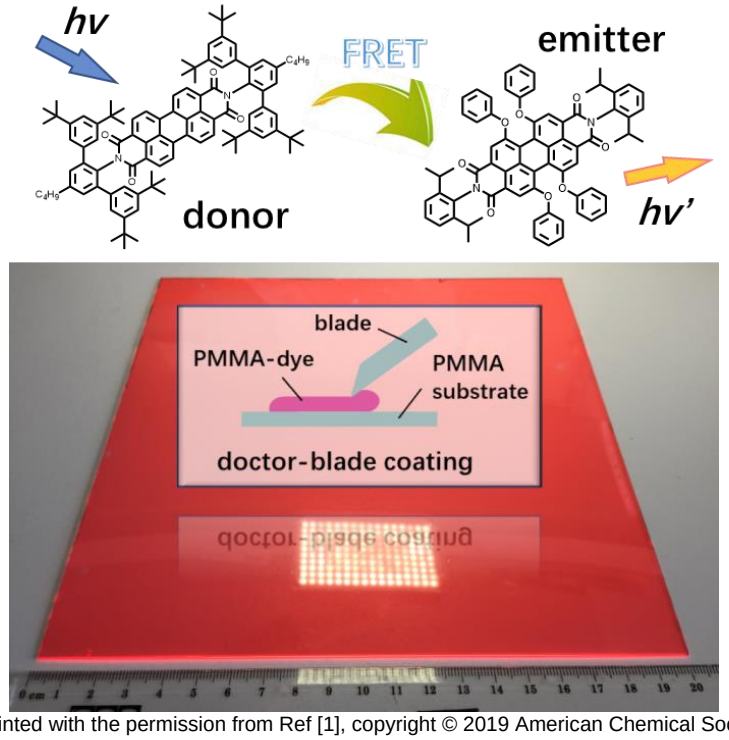

Reprinted with the permission from Ref [1], copyright © 2019 American Chemical Society.

5.1 Preface

Inspired by the promising results from **Chapter IV**, printing a large-area LSC based on the PDI

donor-emitter fluorophore pair system was undertaken. Although the Monte-Carlo ray-tracing simulation suggested the LSC based on the PDI pairs would have high efficiency, the practical difficulties of making a LSC with a large area of 20 cm × 20 cm × 0.1 cm (G = 50) was investigated.

The doctor blading process (Figure 5.1) was used to deposit the thin-layer of PMMA embedded with the PDI donor-emitter fluorophore pair. In most thin-film LSCs, the dye layer was deposited on glass substrates. However, the glass substrates may not be the best choice for the waveguide in practice, as the impurities in glass usually result in some absorbance in the UV and visible range. To demonstrate the influence of the substrate material, the large-area LSCs were fabricated by printing a dye/PMMA layer on both a soda-lime glass substrate and a PMMA substrate, and the performance of the resulting LSCs compared. Besides the substrate materials, the choice of solar cells is also important in designing highly efficient LSCs. Three different types of solar cells were coupled to the LSC and the overall power conversion efficiency of the devices were compared. By optimizing the donor-emitter fluorophore pairs, the waveguide substrate materials and the choice of solar cells, an outstanding LSC device was achieved. Besides the demonstration of the large-area LSC of the donor-emitter fluorophore pair system, the appropriate measurement guidelines of the LSC performance was also considered. The research results were summarized and published in the following article[1]:

Bolong Zhang, Pengjun Zhao, Lachlan J. Wilson, Jegadesan Subbiah, Hanbo Yang, Paul Mulvaney, David J. Jones, Kenneth P. Ghiggino and Wallace W.H. Wong. A High-Performance Large-Area Luminescence Solar Concentrator Incorporating a Donor-Emitter Fluorophore System. *ACS Energy Lett.* **2019**, 4, 1839-1844. DOI: 10.1021/acsenergylett.9b01224

The experimental details were included in the Supporting Information section following the main manuscript. Reprinted with the permission from Ref [1], copyright © 2019 American Chemical Society.

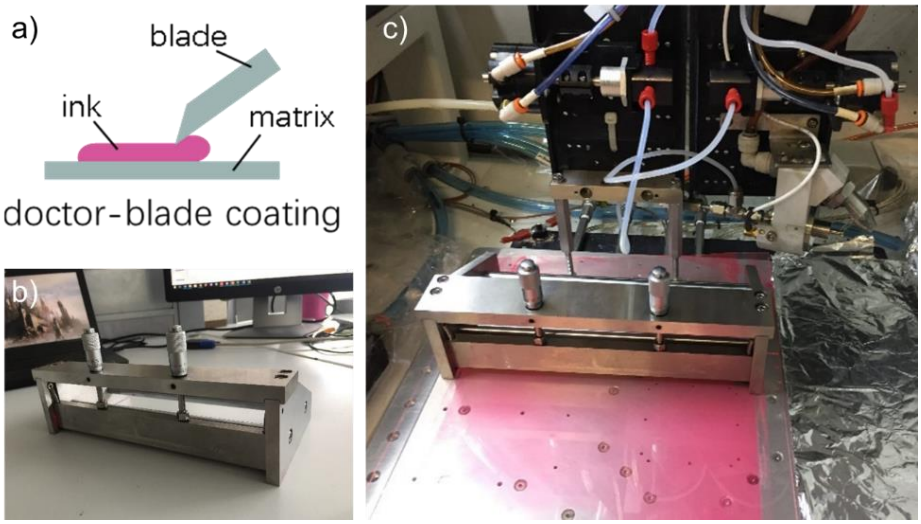

Figure 5.1 a) the scheme for the doctor-blading film deposition process; b) the doctor-blade. The film thickness can be tuned by adjusting the blade height via the Vernier calipers on top of the blade. c) a robot-arm was used to drive the doctor-blade in a steady, uniform movement.

Contribution of the Candidate:

- Donor fluorophore synthesis.
- Fabrication of the LSC devices.
- Characterization and simulations of LSC performance.
- Writing of drafts of the manuscript

Reference:

1. Zhang, B.; Zhao, P.; Wilson, L. J.; Subbiah, J.; Yang, H.; Mulvaney, P.; Jones, D. J.; Ghiggino, K. P.; Wong, W. W. H., High-Performance Large-Area Luminescence Solar Concentrator Incorporating a Donor–Emitter Fluorophore System. *ACS Energy Lett.* **2019**, 1839-1844.

ACS Energy LETTERS

Cite This: ACS Energy Lett. 2019, 4, 1839−1844

http://pubs.acs.org/journal/aelccp

High-Performance Large-Area Luminescence Solar Concentrator Incorporating a Donor−Emitter Fluorophore System

Bolong Zhang,[†,‡] Pengjun Zhao,[‡] Lachlan J. Wilson,[†,‡] Jegadesan Subbiah,[‡] Hanbo Yang,[†] Paul Mulvaney,[†] David J. Jones,[‡] Kenneth P. Ghiggino,[†,‡] and Wallace W. H. Wong*[,†,‡]

[†]ARC Centre of Excellence in Exciton Science, School of Chemistry, The University of Melbourne, Parkville, Victoria 3010, Australia

[‡]Australian Centre for Advanced Photovoltaics, School of Chemistry, Bio21 Institute, The University of Melbourne, Parkville, Victoria 3010, Australia

Supporting Information

ABSTRACT: **A high-performance large-area luminescent solar concentrator (LSC) is demonstrated, fabricated via careful choice of the fluorophore system, waveguide material, and coupled photovoltaic (PV) cells. Doctor-blading was used to deposit a PMMA−dye blend film on the surface of a PMMA planar waveguide to fabricate the large-area LSC with dimensions of 20 × 20 × 0.1 cm^3. A perylene diimide-based donor−emitter fluorophore pair was chosen to both improve the photoluminescent quantum yield and reduce the luminescence reabsorption. Three types of photovoltaic cells were coupled to the LSC to optimize the device output performance. With the combination of the donor−emitter fluorophore pair chosen, the PMMA-based LSC deposition process and coupled perovskite PV cells, the LSC has an experimental flux gain of 7.4 at a geometric gain of 50 (G = 50) under 1 sun irradiation, with a power conversion efficiency of 2.6%.**

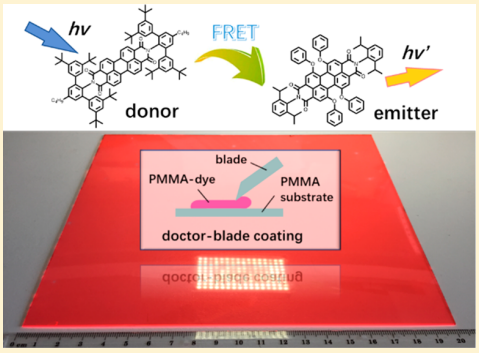

Luminescence solar concentrators (LSCs) are a class of light-harvesting devices that involve a combination of fluorophores and waveguiding matrixes.[1,2] In typical LSCs, fluorophores are dispersed on, or in, planar waveguides, such as glass or plastic substrates. Light incident on the front surface of the LSC is absorbed by the fluorophore, and the photoluminescence is waveguided within the substrate and concentrated at the device edges. In comparison to either silicon photovoltaic (PV) cells or traditional solar concentrators, LSCs can harvest diffuse light, and the absorption profile (i.e., color and transparency) can be tuned by choice of appropriate fluorophores, giving great flexibility. It has been proposed that LSCs are an attractive alternative to traditional PV cells in urban environments, such as roofing on bus stops, building windows, or noise barriers.[3,4] While various fluorophores have been investigated that address LSC limitations such as solid-state emission quenching and luminescence reabsorption, only a few, efficient, large-area LSC devices have been reported to date.[5,6]

The output photon density from the thin edges of an LSC can be amplified in comparison to the incident light on the surface, and this amplification is described by the flux gain (F) of the waveguiding system

$$F = \frac{D_{out}}{D_{in}}$$

where D_{in} and D_{out} refer to the density of the incident and output photons of the LSC, respectively. By increasing the geometric gain (G, where G = waveguide surface area/edge area) of LSCs, one can increase F by concentrating incident light from a larger surface area. However, F is also limited by the external quantum efficiency (EQE) of the devices ($F = G \times$ EQE), which decreases as a function of the increasing size of the LSC. There are four factors that influence the EQE of LSCs: (1) the absorptance of the waveguide, (2) the photoluminescence quantum yield (ϕ_{PL}) of the fluorophores, (3) the waveguide surface loss or escape-cone loss, and (4) the reabsorption of the photoluminescence due to the overlap of fluorophore absorption and emission spectra.[7] The reabsorption effect does not intrinsically cause photon loss in an LSC, but it will increase the loss for a nonunity fluorophore ϕ_{PL}, and it also leads to increases in the escape-cone loss of the

Received: June 6, 2019
Accepted: July 8, 2019
Published: July 8, 2019

DOI: 10.1021/acsenergylett.9b01224
ACS Energy Lett. 2019, 4, 1839−1844

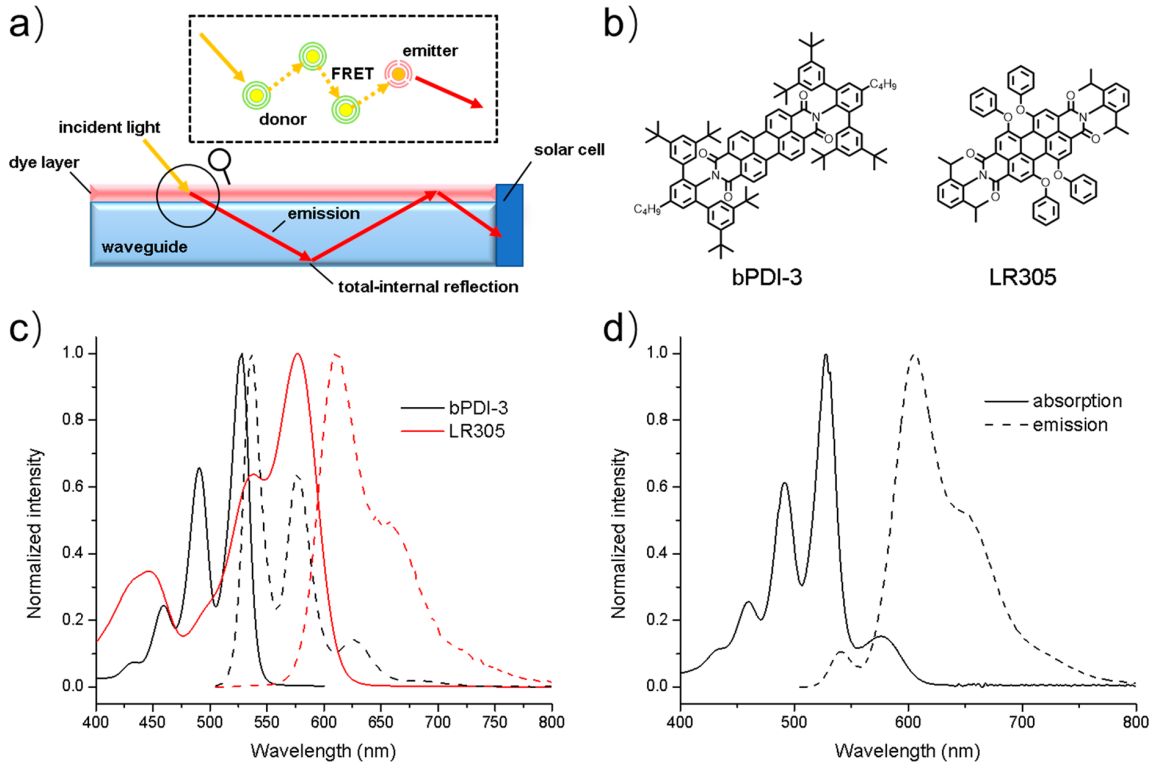

Figure 1. (a) **Structure of a typical thin-film LSC device and energy migration process for a donor−emitter fluorophore pair system; (b) chemical structure of the donor, bPDI-3, and the emitter, LR305; (c) normalized absorption and emission spectra (excitation wavelength = 490 nm) of bPDI-3 and LR305 alone; and (d) absorption and emission spectra for the optimized blend of the donor−emitter mixture in PMMA.**

waveguide.[8,9] As the waveguide size increases, the emitted photons generated from the center of an LSC will be affected most strongly by the reabsorption effect, resulting in higher photon losses. Consequently, the reabsorption effect is geometry-dependent and is magnified in large-scale LSC devices.

Besides the above-mentioned four factors affecting LSC performance, the choice of substrate material can also influence the performance of LSCs due to absorption and scattering by the waveguide matrix. As the emitted light travels through the waveguide (Figure 1a), the matrix material will have a greater attenuation effect as the size of the LSC increases. Consequently, careful selection of the matrix material becomes important for fabricating large-area LSCs. Poly(methyl methacrylate) (PMMA) and glass are the two most frequently used materials for the LSC waveguide matrix, and differences in their transmittance can lead to a significant difference in the performance of large-scale LSCs.

By utilizing fluorescence resonance energy transfer (FRET)[10] for a donor−acceptor dye pair, reabsorption in an LSC can be reduced because of the reduced overlap of the absorption and emission spectra of the dye (Figure 1a).[11,12] Perylene diimide derivatives are suitable fluorophores for LSCs due to their good photo- and thermal stability, large molar absorptivity values, and high ϕ_{PL}. We previously reported a perylene diimide-based donor−emitter fluorophore pair showing improved ϕ_{PL} at high dye concentrations and significantly reduced reabsorption (Figure 1b).[13,14] By carefully tuning the ratio of the donor and emitter in the PMMA matrix, one can create a chromophore combination for which light absorption is predominantly due to the donor (bPDI-3) while fluorescence is almost entirely from the emitter (LR305) and with a ϕ_{PL} close to unity for the overall donor−emitter fluorophore pair system.[13,14] Energy transfer requires close proximity of the donors and emitters, and consequently, a thin-film LSC with high fluorophore concentration was adopted in this study.

To achieve large-area thin films on planar waveguides, doctor-blading was chosen in this work as the deposition method.[6,15] Large-area LSC devices were fabricated by deposition of PMMA−dye blend solutions on both glass and PMMA substrates. Compared to the most common building glass substrates (i.e., soda-lime glass), a PMMA substrate has several advantages, such as a higher transparency in the visible range, a better impact strength, and greater mechanical flexibility. By depositing a PMMA−dye blend on a PMMA matrix, one can reduce the energy loss from the absorbance of the substrate medium and avoid any refractive index mismatch. The donor−emitter fluorophore pair system, bPDI-3 and LR305, was used to make the above-mentioned devices. This is the first time that a doctor-blade thin-film deposition method has been reported for producing a fluorophore/PMMA coating on a PMMA waveguiding matrix for large-area LSCs. A counterpart device was printed on soda-lime glass by the same process. Three different types of photodetectors/PV cells were used to characterize the performance of the LSCs. In addition, we have proposed standard measurement guidelines for characterizing and comparing LSC performance.

The sizes of both the glass-based and PMMA-based LSCs were 20 × 20 × 0.1 cm^3, giving G = 50. LSC devices with a

DOI: 10.1021/acsenergylett.9b01224
ACS Energy Lett. 2019, 4, 1839−1844

gain of G = 50 are rarely reported in the literature, with most studies using simulations to predict device performance at G = 50.[5] The optimized concentrations of the donor and the emitter were 60 and 12 mM respectively, which resulted from a careful balancing of the overall ϕ_{PL}, the material absorbance, the FRET process, and the spectral overlap.[13,14] bPDI-3 was chosen as the donor as it provides the best balance of good solubility and a high ϕ_{PL}. Using the doctor-blade deposition method, LSCs with good surface uniformity and transparency were achieved on both glass and PMMA substrates. The fluorophore layer thickness was adjusted to ∼3 μm to maximize device absorbance (see the Experimental Methods section for details). A photograph of the PMMA device is shown in Figure 2a. It is perhaps surprising that the

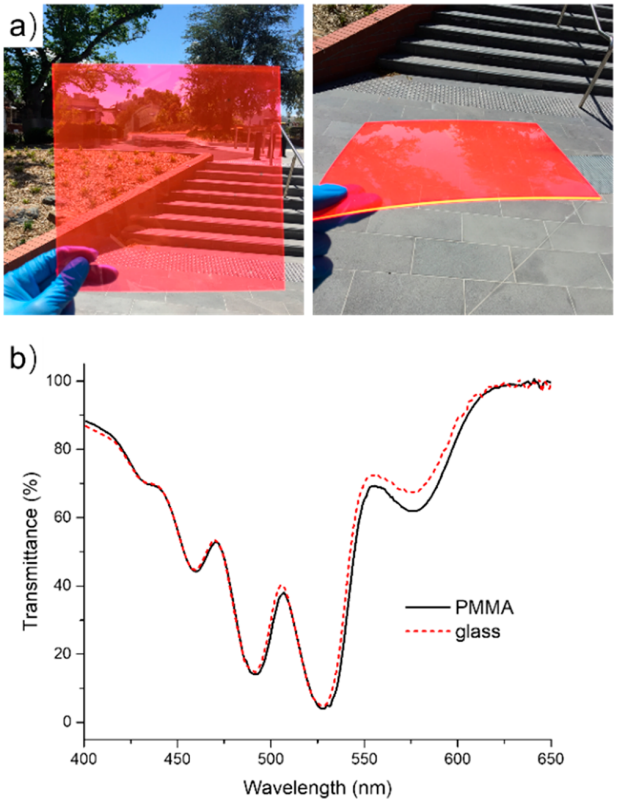

Figure 2. (a) PMMA-based LSC outdoors on a sunny day; (b) transmittance spectra of the PMMA-based and glass-based LSCs.

chlorobenzene solvent used in preparing the PMMA−dye solution, did not adversely affect the transparency of the PMMA substrate. We speculate that any solvent damage at the substrate interface is repaired during the solvent evaporation process of the top PMMA−dye layer. The absorption and emission spectra of the glass-based and PMMA-based LSCs were very similar, indicating that the waveguide substrate materials did not have a significant influence on the thin-film fluorophore layer (Figure S2). In addition, there was no scattering observed in the absorption spectra of both samples, suggesting that thin-film deposition using a doctor-blading process did not cause any optical defects in the devices. The transmittance spectra collected from the surface of both LSC devices (Figure 2b) were also in close correspondence. As the absorption spectrum of LR305 overlaps strongly with the emission spectrum of bPDI-3 (Figure 1c), the FRET process was highly efficient in the donor−emitter fluorophore pair at the concentrations used, leading to the overall emission of the blend being dominated by the emitters (>95%) with the overall ϕ_{PL} enhanced to 97.6 ± 0.3%. The absorption and emission spectral overlap of the donor−emitter blend (Figure 1d) is much smaller compared to that of either the donor or the emitter alone (Figure 1c), indicating that the reabsorption effect can be drastically reduced in the LSCs with this dye combination.

To date, the flux gains, F, of LSCs reported in the literature have been calculated in two different ways, namely, using the optical flux gain (F_{opt}) or the photocurrent flux gain (F_{pc}).[6] F_{opt} is usually obtained by directly measuring D_{out} and D_{in} via a calibrated photodiode or an integrating sphere.[7,16,17] Therefore, F_{opt} is an absolute property of an LSC device but will be affected by the choice of the incident light source, for example, 1 sun AM1.5G conditions or single-wavelength excitation (because the fraction of light absorbed depends on the absorption wavelength). However, the measurement of F_{opt} is not practical when the wavelength responsivity of the detector is unknown or the sample is difficult to measure under the experimental conditions. Consequently, F_{pc} is more often used in practice. The value of F_{pc} is usually measured by PV cells and refers to the photon-current density gain of a PV cell when coupled to the LSC device

$$F_{pc} = \frac{J_{out}}{J_{in}}$$

where J_{out} and J_{in} are the observed photocurrent densities of a PV cell illuminated by the LSC or by the light source, respectively. Because F_{pc} is determined relative to the performance of the PV cell when directly excited by the light source without coupling to the LSC, the value of F_{pc} can vary depending on the type of PV cell used. The EQE calculated based on the F_{pc} (EQE_{PC}) will also depend on the type and performance of the PV cell

$$EQE_{PC} = \frac{F_{pc}}{G}$$

Furthermore, the overall power conversion efficiency (PCE) of the LSC device (PCE_{LCS}) should also be reported along with F_{pc} to reveal the absolute performance of the LSC device when coupled to certain types of PV cells. The value of PCE_{LCS} can be determined from the maximum output power value of the PV cells (P_{max}) when coupled with the LSC and the incident power (P_{in}) amplified by the factor G of the LSC

$$PCE_{LCS} = \frac{P_{max}}{P_{in} \times G}$$

Our LSC devices were initially characterized under a green LED spotlight excitation with a wavelength that closely corresponds to the maximum absorption wavelength (λ_{abs} = 525 nm, λ_{LED}= 516 nm, 0.419 mW/cm^2) of the donor dye. As shown in Figure 3, the F_{opt} of the PMMA-based LSC was much higher than that of the soda-lime glass-based LSC for all G values measured, with the difference increasing with increasing G. Competitive absorption of the LR305 emission by nonemissive impurities in the soda-lime glass was the main reason for the poor performance in the glass-based LSC.[18] When increasing G from 37.5 to 50, the F_{opt} of glass-based LSC increased by only about 3%, indicating that most of the emission originating from the center of the device never

DOI: 10.1021/acsenergylett.9b01224
ACS Energy Lett. 2019, 4, 1839−1844

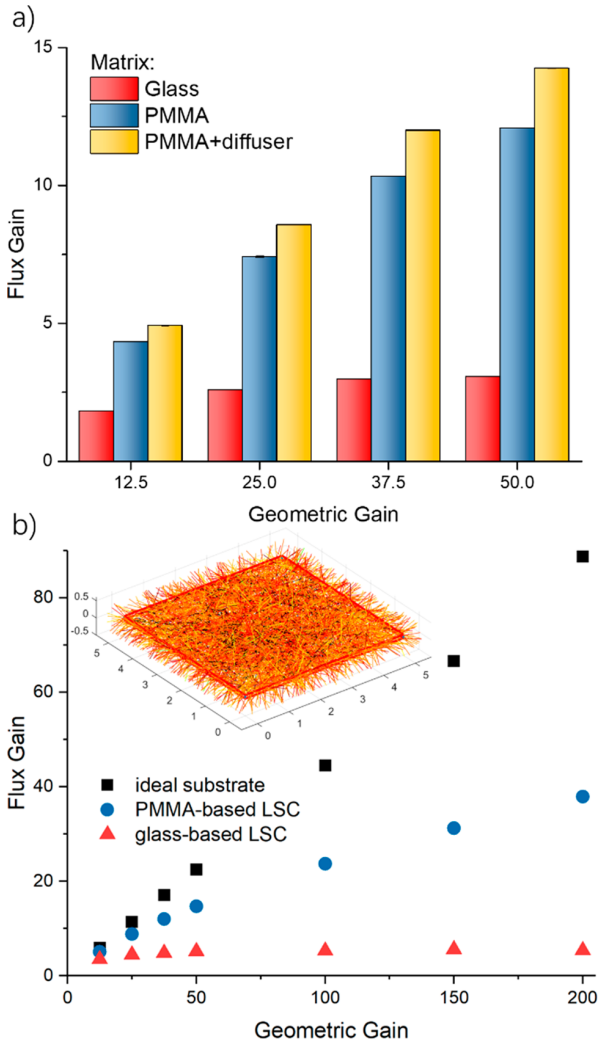

Figure 3. (a) F_{opt} of LSCs based on glass and PMMA waveguide substrates under narrow-wavelength excitation (515 nm) as a function of G measured by the photodiode. Error bars are too small to be shown on the scale. (b) Simulated F_{opt} of LSCs in different waveguide substrates as a function of G under the green LED spotlight excitation. The simulations were based on experimental data from the LSCs, and 100 000 photons were traced in each simulation. The inset illustrates one Monte Carlo ray simulation of an LSC with the ideal substrate at G = 5. Additional information about the Monte Carlo ray tracing simulations can be found in the SI.

reached the waveguide edges at higher G. On the other hand, the increase in F_{opt} with G was much more significant in the PMMA-based device. At G = 50, F_{opt} for the PMMA-based LSC was already 3 times higher than for the glass-based counterpart (Figure 3). The absorption coefficients of the soda-lime glass and the PMMA sheets are 0.11 and 0.00032 cm^{-1}, respectively, at 615 nm. Therefore, the inner transmittance of the glass dropped to 7.9% over half of the LSC length (10 cm), while the transmittance of the PMMA matrix remained at 99% over the same distance, consistent with the observed trend of F_{opt} against G in each device.

A Monte Carlo ray simulation also suggested that absorbance of the waveguide had significant influence on the performance of large-area LSCs.[19−22] The absorbance of PMMA and glass-based waveguides was obtained by measuring the transmittance minus the reflectance, while absorbance of the ideal substrate was set at 0. These absorbance values were used in the simulations. As shown in Figure 3b, F_{opt} had similar values for low G due to the insignificant influence from the waveguide for the small LSCs. However, when G became larger than 50, the value of F_{opt} for the glass-based LSC stopped increasing, which is in agreement with the experimental data presented above. For the PMMA-based waveguide, the increase in F_{opt} slowed after G = 50 but was much greater than that for the glass-based waveguide system. For the simulated ideal substrate, the increase in F_{opt} continued to rise steadily to G = 200. This highlights the fact that the main loss in LSCs is due to substrate absorbance when the device size is large. The huge differences in the simulated F_{opt} for each G of the substrates suggests that the choice of waveguide materials is important in fabricating large-area LSCs. The glass-based device was not examined further, and the focus of the rest of this work is on the PMMA device.

When a white diffuse reflecting layer[23] (white paper) was placed at the back of the PMMA-based LSC, F_{opt} increased by 15% consistently for all G values (Figure 3). As there was a small air gap between the waveguide and the reflecting layer, the total internal reflection of the waveguide was not affected. The 15% increase in F_{opt} is mainly associated with reducing transmission losses from the LSCs (i.e., reflecting transmitted incident light back into the LSC substrate). Although F_{opt} in PMMA-based LSCs increased with G, the rate of increase of F_{opt} slowed. F_{opt} increased by ∼74% from G = 12.5 to 25 but only ∼19% from G = 37.5 to 50. At G = 50, F_{opt} of the LSC without and with the diffuse reflecting layer was 12.1 and 14.2, respectively, with the latter the highest experimental F_{opt} reported to date for an LSC at G = 50.[5] This high F_{opt} can be attributed to the low luminescence reabsorption of the donor−emitter fluorophore system used here and the excellent

Table 1. Summary of LSC Performance Measured under AM1.5G 1 sun Conditions with (w) and without (w/o) a Diffuse Back-Reflector

detector	diffuse reflector	V_{oc} (V)	J_{sc}[a] (mA/cm^2)	FF (%)	P_{max} (mW/cm^2)	PCE_{LSC} (%)	F_{opt}[b]	F_{pc}	EQE_{pc} (%)
photodiode	w/o	0.50 ± 0.004	98 ± 1	34.7 ± 0.4	17.0 ± 0.4	0.34	1.72	3.9	7.8
	w	0.50 ± 0.004	118 ± 1	32.7 ± 0.4	19.3 ± 0.3	0.38	2.07	4.7	9.4
Si PV	w/o	0.64 ± 0.004	123 ± 1	58.1 ± 0.3	45.8 ± 0.4	0.92	1.72	4.7	9.4
	w	0.64 ± 0.004	168 ± 3	50 ± 2	54 ± 2	1.08	2.07	6.4	12.8
perovskite PV	w/o	1.10 ± 0.02	124 ± 4	70 ± 1	95 ± 2	1.90	1.72	5.2	10.4
	w	1.09 ± 0.02	176 ± 3	67 ± 2	130 ± 2	2.59	2.07	7.4	14.8

[a] J_{sc} and P_{max} are determined based on the area of the PV cells. [b] F_{opt} was measured by the photodiode, based on the photon density of 4.3×10^{17} s^{-1} cm^{-2} under AM1.5G 1 sun conditions, regardless the solar cell types.

DOI: 10.1021/acsenergylett.9b01224
ACS Energy Lett. 2019, 4, 1839−1844

intrinsic light transmission properties of the PMMA waveguide.

The PMMA-based LSC was also examined under AM1.5G 1 sun conditions using three different detectors, namely, a photodiode (PIN-RD100A, OSI Optoelectronics) and Si PV and perovskite PV cells (see the SI for the spectral response of these devices). The performance of the LSCs under 1 sun is summarized in Table 1. With all three detectors, the J_{sc} of the device increased by ∼20−40% when using the white diffuse reflector, indicating the benefits of reducing the transmittance loss under 1 sun illumination. The F_{opt} values of the LSC without and with the diffuse reflector were 1.72 and 2.07, respectively, and the former was in agreement with the simulated F_{opt} value of 1.98 of the LSC without the diffuse reflector under 1 sun conditions. The F_{pc} values measured by the photodiode were higher than F_{opt} due to the limited wavelength response of the photodiode to the AM1.5G spectrum. While the value of F_{pc} obtained using the photodiode clearly showed the light concentration effect of the LSC device, low PCE_{LSC} values were measured because of the high inner resistance of the photodiode (Table 1). The fill factors (FFs) of the three detectors all dropped when coupled with the LSC and were even lower with the diffuse reflector layer in place. This was because the charge-carrier recombination rate of the PV cells used increased under higher incident light intensities.[24−26] The FFs of the photodiode and the Si PV cell both decreased more than 25%, while the FF of the perovskite PV cell only decreased a relatively moderate 7%. This data indicated that perovskite PV cells are attractive candidates for integration with LSCs.[27]

F_{pc} values using the different detectors varied from one another due to the performance and the spectral response of the PV cells used. Of the three detectors, the perovskite PV cell coupled LSC showed the highest F_{pc}. When comparing PCE_{LSC} values, the perovskite PV cell-based LSC again had the better performance mainly due to a higher V_{oc} and lower internal resistance. For the perovskite PV cells, the PMMA-based LSC with a diffuse reflector showed the best experimental PCE_{LSC} of 2.6% and F_{pc} of 7.4 at G = 50, which was the highest experimental performance of LSCs at G = 50. As mentioned earlier, F_{opt} is a property of the LSC and is independent of the detector used. The F_{opt} values for the Si and perovskite PV devices were not calculated as their spectral responsivities were not available.

With the experience of measuring large-area LSC devices in this study, we propose that the characterization of LSC performance should include measurement of all three parameters: F_{opt}, F_{pc}, and PCE_{LSC}. Most other LSC performance parameters can be determined from these three parameters. It is important to note that F_{opt} relates to the optical performance of the LSC device and is not dependent on the PV cell coupled to the LSC. F_{opt} can be measured using an integrating sphere for small LSCs or with a photodiode for large LSCs as we have done in this work. The values of F_{opt} and F_{pc} can be compared using the same excitation source to reveal the influence of size (or G) of the LSC, although F_{pc} should only be compared using the same detectors or PV cells. The F_{pc} reveals the performance of the LSC through the detector or PV cell but does not capture the performance of the combined LSC/PV device, which is ultimately provided by the PCE_{LSC} value. The PCE_{LSC} of an LSC/PV device can be compared with the same excitation source and similar G to reveal how different types of solar cells perform, providing a guideline for practical effectiveness. It should also be noted that different dimensions of the LSC can give the same G (e.g., if the thickness of the waveguide is changed and the surface area adjusted), and this can affect luminescence reabsorption and parasitic substrate absorption. The dimensions of the LSC should always be reported.

In conclusion, we demonstrate for the first time a highly efficient, large-area LSC device containing a donor−emitter fluorophore system that was fabricated by doctor-blade thin-film deposition onto a PMMA waveguide substrate. The importance of the waveguide substrate choice was demonstrated by comparing glass-based and PMMA-based LSCs. F_{opt} for G = 50 was 3 times higher for PMMA than that for glass due to the lower absorbance of the PMMA matrix. Three different detectors were used to characterize LSC performance. The best LSC described here showed the highest experimental PCE_{LSC} and F_{pc} at G = 50 reported to date when coupled with a perovskite PV cell. This achievement is due to careful choice of the fluorophores, waveguide substrate materials, and PV cells. Guidelines for measurement and reporting the LSC performance were proposed, which will enable more ready comparison of devices in the future.

EXPERIMENTAL METHODS

The energy donor, bPDI-3, was synthesized using the literature procedure,[13] and the emitter, LR305, was purchased from BASF (IMCD Australia Limited). The bPDI-3 and LR305 were premixed in the optimized ratio (60 and 12 mM, respectively, based on the PMMA volume)[13,14] and dissolved in a PMMA solution (3% by weight in chlorobenzene). The solution (6 mL) was then gently deposited close to one edge of either the PMMA or glass matrix surface. The PMMA thin film was formed by passing the doctor-blade over the solution and across the entire substrate controlled by a robot arm (10 cm/s, blade height 150 μm). The wet PMMA film was then baked at 100 °C for 1 h to remove residual solvent. After baking, the LSC devices were then cut into 20 × 20 cm^2 areas, and the three edges of the devices were covered by black matte paint. We chose 0.1 cm as the thickness of the LSC devices because a smaller thickness increases the difficulty of mounting a PV cell or photodiode on the edges. The fluorophore coating thicknesses of the glass-based and PMMA-based LSCs were 2.6 and 2.7 μm, respectively, calculated based on the transmittance of each sample (Figure 2b).

The performance of the LSCs was measured by a photodiode, Si PV cell (Sliver cell[28]), or perovskite PV cell mounted in the middle of one edge of the final devices. Additional information about the PV cells can be found in the SI. Optical lens immersion oil (Olympus Australian Pty Ltd.) was applied between the LSC edge and the PV cell surface to minimize optical coupling loss. The LSC devices were studied using a narrow-band excitation light source (green LED spotlight, Edmund Optics Inc., λ_{LED}= 516 nm) close to the maximum absorption wavelength of the donor and also under 1 sun AM1.5G conditions (infinityPV ISOSun solar simulator). The F values for the LSCs were measured by mounting three different types of detector on the middle of one edge of the waveguide, while the other three edges were covered with black paint. To measure the performance as a function of G, the 20 × 20 × 0.1 cm^3 LSC devices were masked by a black paper mask to alter the irradiated area.

DOI: 10.1021/acsenergylett.9b01224
ACS Energy Lett. 2019, 4, 1839−1844

■ ASSOCIATED CONTENT

Supporting Information

The Supporting Information is available free of charge on the ACS Publications website at DOI: 10.1021/acsenergylett.9b01224.

Information about instruments used in this work, characterization of the PV cells, and spectra of the LSCs (PDF)

■ AUTHOR INFORMATION

Corresponding Author

*E-mail: wwhwong@unimelb.edu.au.

ORCID

Bolong Zhang: 0000-0002-2955-8409
Paul Mulvaney: 0000-0002-8007-3247
David J. Jones: 0000-0003-1088-7744
Kenneth P. Ghiggino: 0000-0001-6621-4448
Wallace W. H. Wong: 0000-0001-7131-8532

Notes

The authors declare no competing financial interest.

■ ACKNOWLEDGMENTS

This work was made possible by support from the Australian Renewable Energy Agency, which funds the project grants within the Australian Centre for Advanced Photovoltaics (ACAP). K.P.G., P.M., and W.W.H.W. are also supported by the ARC Centre of Excellence in Exciton Science (CE170100026). The Sliver PV cell was provided by Prof. Andrew Blakers, Australian National University. The authors also thank Dr. Hasitha Weerasinghe (CSIRO) for his assistance with the solar simulator measurements.

■ REFERENCES

(1) van Sark, W. G.; Barnham, K. W.; Slooff, L. H.; Chatten, A. J.; Büchtemann, A.; Meyer, A.; McCormack, S. J.; Koole, R.; Farrell, D. J.; Bose, R.; et al. Luminescent Solar Concentrators-A Review of Recent Results. *Opt. Express* **2008**, *16* (26), 21773−21792.

(2) Debije, M. G.; Verbunt, P. P. C. Thirty Years of Luminescent Solar Concentrator Research: Solar Energy for the Built Environment. *Adv. Energy Mater.* **2012**, *2* (1), 12−35.

(3) Meinardi, F.; Bruni, F.; Brovelli, S. Luminescent Solar Concentrators for Building-Integrated Photovoltaics. *Nat. Rev. Mater.* **2017**, *2*, 17072.

(4) Kanellis, M.; de Jong, M. M.; Slooff, L.; Debije, M. G. The Solar Noise Barrier Project: 1. Effect of Incident Light Orientation on the Performance of a Large-Scale Luminescent Solar Concentrator Noise Barrier. *Renewable Energy* **2017**, *103*, 647−652.

(5) Currie, M. J.; Mapel, J. K.; Heidel, T. D.; Goffri, S.; Baldo, M. A. High-Efficiency Organic Solar Concentrators for Photovoltaics. *Science* **2008**, *321* (5886), 226−228.

(6) Wu, K.; Li, H.; Klimov, V. I. Tandem Luminescent Solar Concentrators Based on Engineered Quantum Dots. *Nat. Photonics* **2018**, *12* (2), 105−110.

(7) Tummeltshammer, C.; Taylor, A.; Kenyon, A. J.; Papakonstantinou, I. Losses in Luminescent Solar Concentrators Unveiled. *Sol. Energy Mater. Sol. Cells* **2016**, *144*, 40−47.

(8) Olson, R. W.; Loring, R. F.; Fayer, M. D. Luminescent Solar Concentrators and the Reabsorption Problem. *Appl. Opt.* **1981**, *20* (17), 2934−2940.

(9) Banal, J. L.; Zhang, B.; Jones, D. J.; Ghiggino, K. P.; Wong, W. W. Emissive Molecular Aggregates and Energy Migration in Luminescent Solar Concentrators. *Acc. Chem. Res.* **2017**, *50* (1), 49−57.

(10) Medintz, I.; Hildebrandt, N. *FRET-Förster Resonance Energy Transfer: From Theory to Applications*; John Wiley & Sons: Hoboken, NJ, 2013.

(11) Schiphorst, J. t.; Kendhale, A. M.; Debije, M. G.; Menelaou, C.; Herz, L. M.; Schenning, A. P. H. J. Dichroic Perylene Bisimide Triad Displaying Energy Transfer in Switchable Luminescent Solar Concentrators. *Chem. Mater.* **2014**, *26* (13), 3876−3878.

(12) McKenna, B.; Evans, R. C. Towards Efficient Spectral Converters through Materials Design for Luminescent Solar Devices. *Adv. Mater.* **2017**, *29* (28), 1606491.

(13) Banal, J. L.; Soleimaninejad, H.; Jradi, F. M.; Liu, M.; White, J. M.; Blakers, A. W.; Cooper, M. W.; Jones, D. J.; Ghiggino, K. P.; Marder, S. R.; Smith, T. A.; Wong, W. W. H. Energy Migration in Organic Solar Concentrators with a Molecularly Insulated Perylene Diimide. *J. Phys. Chem. C* **2016**, *120* (24), 12952−12958.

(14) Zhang, B. L.; Soleimaninejad, H.; Jones, D. J.; White, J. M.; Ghiggino, K. P.; Smith, T. A.; Wong, W. W. H. Highly Fluorescent Molecularly Insulated Perylene Diimides: Effect of Concentration on Photophysical Properties. *Chem. Mater.* **2017**, *29* (19), 8395−8403.

(15) Li, H.; Wu, K.; Lim, J.; Song, H.-J.; Klimov, V. I. Doctor-Blade Deposition of Quantum Dots onto Standard Window Glass for Low-Loss Large-Area Luminescent Solar Concentrators. *Nat. Energy* **2016**, *1* (12), 16157.

(16) Verbunt, P. P. C.; Kaiser, A.; Hermans, K.; Bastiaansen, C. W. M.; Broer, D. J.; Debije, M. G. Controlling Light Emission in Luminescent Solar Concentrators through Use of Dye Molecules Aligned in a Planar Manner by Liquid Crystals. *Adv. Funct. Mater.* **2009**, *19* (17), 2714−2719.

(17) Mulder, C. L.; Reusswig, P. D.; Velázquez, A. M.; Kim, H.; Rotschild, C.; Baldo, M. A. Dye Alignment in Luminescent Solar Concentrators: I. Vertical Alignment for Improved Waveguide Coupling. *Opt. Express* **2010**, *18*, A79.

(18) Kastelijn, M. J.; Bastiaansen, C.; Debije, M. G. Influence of Waveguide Material on Light Emission in Luminescent Solar Concentrators. *Opt. Mater.* **2009**, *31* (11), 1720−1722.

(19) Carrascosa, M.; Unamuno, S.; Agullo-Lopez, F. Monte Carlo Simulation of the Performance of Pmma Luminescent Solar Collectors. *Appl. Opt.* **1983**, *22* (20), 3236−3241.

(20) Haines, C.; Chen, M.; Ghiggino, K. P. The Effect of Perylene Diimide Aggregation on the Light Collection Efficiency of Luminescent Concentrators. *Sol. Energy Mater. Sol. Cells* **2012**, *105*, 287−292.

(21) Xu, J.; Zhang, B.; Jansen, M.; Goerigk, L.; Wong, W. W. H.; Ritchie, C. Highly Fluorescent Pyridinium Betaines for Light Harvesting. *Angew. Chem., Int. Ed.* **2017**, *56* (44), 13882−13886.

(22) Gutierrez, G. D.; Coropceanu, I.; Bawendi, M. G.; Swager, T. M. A Low Reabsorbing Luminescent Solar Concentrator Employing Π-Conjugated Polymers. *Adv. Mater.* **2016**, *28* (3), 497−501.

(23) Debije, M. G.; Teunissen, J.-P.; Kastelijn, M. J.; Verbunt, P.; Bastiaansen, C. The Effect of a Scattering Layer on the Edge Output of a Luminescent Solar Concentrator. *Sol. Energy Mater. Sol. Cells* **2009**, *93* (8), 1345−1350.

(24) Chegaar, M.; Hamzaoui, A.; Namoda, A.; Petit, P.; Aillerie, M.; Herguth, A. Effect of Illumination Intensity on Solar Cells Parameters. *Energy Procedia* **2013**, *36*, 722−729.

(25) Kim, J. H.; Moon, K. J.; Kim, J. M.; Lee, D.; Kim, S. H. Effects of Various Light-Intensity and Temperature Environments on the Photovoltaic Performance of Dye-Sensitized Solar Cells. *Sol. Energy* **2015**, *113*, 251−257.

(26) Alnuaimi, A.; Almansouri, I.; Nayfeh, A. Performance of Planar Heterojunction Perovskite Solar Cells under Light Concentration. *AIP Adv.* **2016**, *6* (11), 115012.

(27) Lin, Q.; Wang, Z.; Snaith, H. J.; Johnston, M. B.; Herz, L. M. Hybrid Perovskites: Prospects for Concentrator Solar Cells. *Adv. Science* **2018**, *5* (4), 1700792.

(28) Verlinden, P. J.; Blakers, A. W.; Weber, K. J.; Babaei, J.; Everett, V.; Kerr, M. J.; Stuckings, M. F.; Gordeev, D.; Stocks, M. J. Sliver® Solar Cells: A New Thin-Crystalline Silicon Photovoltaic Technology. *Sol. Energy Mater. Sol. Cells* **2006**, *90* (18−19), 3422−3430.

Supporting Information for

High-Performance Large Area Luminescence Solar Concentrator Incorporating a Donor-Emitter Fluorophore System

*Bolong Zhang [a,b], Pengjun Zhao [b], Lachlan J. Wilson[a, b], Jegadesan Subbiah [b], Hanbo Yang[a], Paul Mulvaney[a], David J. Jones [b], Kenneth P. Ghiggino [a,b] and Wallace, W. H. Wong[*a,b]*

[a.] ARC Centre of Excellence in Exciton Science, School of Chemistry, The University of Melbourne, Parkville, Victoria, 3010, Australia.

[b.] Australian Centre for Advanced Photovoltaics, School of Chemistry, Bio21 Institute, The University of Melbourne, Parkville, Victoria, 3010, Australia.

[*]E-mail: wwhwong@unimelb.edu.au.

General information

bPDI-3 was synthesized via a literature reported procedure.[1]

BASF Lumogen F Red 305 (LR305) was obtained from IMCD Australia Limited.

All other chemicals were used as received from the suppliers. The UV-Vis spectra were recorded using a Cary UV-Vis 50 spectrophotometer. The fluorescence emission spectra of all samples were recorded using a Horiba Jobin Yvon FluorologOR -3 fluorometer. The photon counts of all the measurements on the FluorologOR -3 fluorometer were within the linear response range of the detector (2×10^6 cps).

The colourless PMMA sheets were purchased from YIWU CLOUDZHUO CRAFTS LIMITED, China.

The soda-lime glass sheets were purchased from SHENYANG LONGQIAN GLASS, China.

Photoluminescence quantum yield measurements

Absolute photoluminescent quantum yield measurements of all samples were determined according to the experimental procedure described elsewhere[2] using the integrating sphere accessory (F3018, Horiba Jobin Yvon) for a FluorologOR -3 fluorometer. The angle of the excitation beam to the normal of the sample surface can be modified using the variable sample holder. All spectra for the absolute quantum yield measurements were corrected for the light source noise, wavelength sensitivity and the transmittance of the filters. The photon counts of all the measurements on the FluorologOR -3 fluorometer were within the linear response range of the detector (2×10^6 cps).

PV cell characterization

The photodiode (PIN-RD100A) was produced by OSI Optoelectronics. The Sliver® PV cell was provided by Prof Andrew Blakers, Australian National University. The architecture of the perovskite PV cell was ITO/SnO2/Perovskite/Spiro-oMeTAD/Ag, which was fabricated according to a previous method.[3]

All PV cells were characterized under the infinityPV ISOSun solar simulator (AM 1.5 100mW/cm^2).

Table S1. Summary of PV cells performance in one-sun condition.

Detector	Size (mm)	V_{oc} (V)	J_{sc} (mA/cm^2)	FF (%)	P_{max} (mW/cm^2)
Photo-diode	9.0 X 1.0	0.45±0.02	25.1±0.4	58.4±0.4	6.5±0.3
Sliver® PV cell	20 X 1.0	0.576±0.008	26±1	68.7±0.8	10.4±0.4
Perovskite PV cells	2.0 X 1.0	0.99±0.02	23.6±0.2	74±2	17.4±0.5

Table S2. Summary of LSC performance measured relevant to the surface area.

Detector	Diffuse reflector	V_{oc} (V)	J_{sc}[a] (mA/cm^2)	FF (%)	P_{max} (mW/cm^2)
Photo-diode	w/o	0.50±0.004	1.96±0.02	34.7±0.4	0.34±0.01
	w	0.50±0.004	2.36±0.02	32.7±0.4	0.39±0.01
Si PV	w/o	0.64±0.004	2.46±0.02	58.1±0.3	0.92±0.01
	w	0.64±0.004	3.36±0.06	50±2	1.08±0.04
Perovskite PV	w/o	1.10±0.02	2.48±0.08	70±1	1.90±0.02
	w	1.09±0.02	3.52±0.06	67±2	2.60±0.04

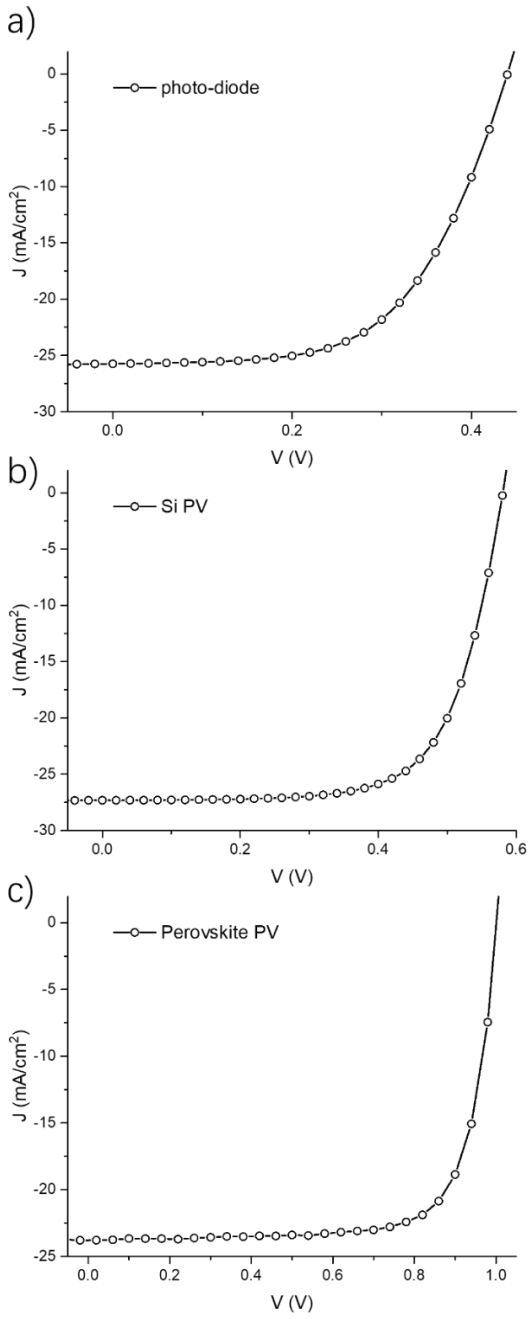

Figure S1. The J-V curve of a) photodiode, b) Sliver® PV cell and c) Perovskite cell under one-sun condition.

UV-Vis Absorption and emission spectrum of LSC devices

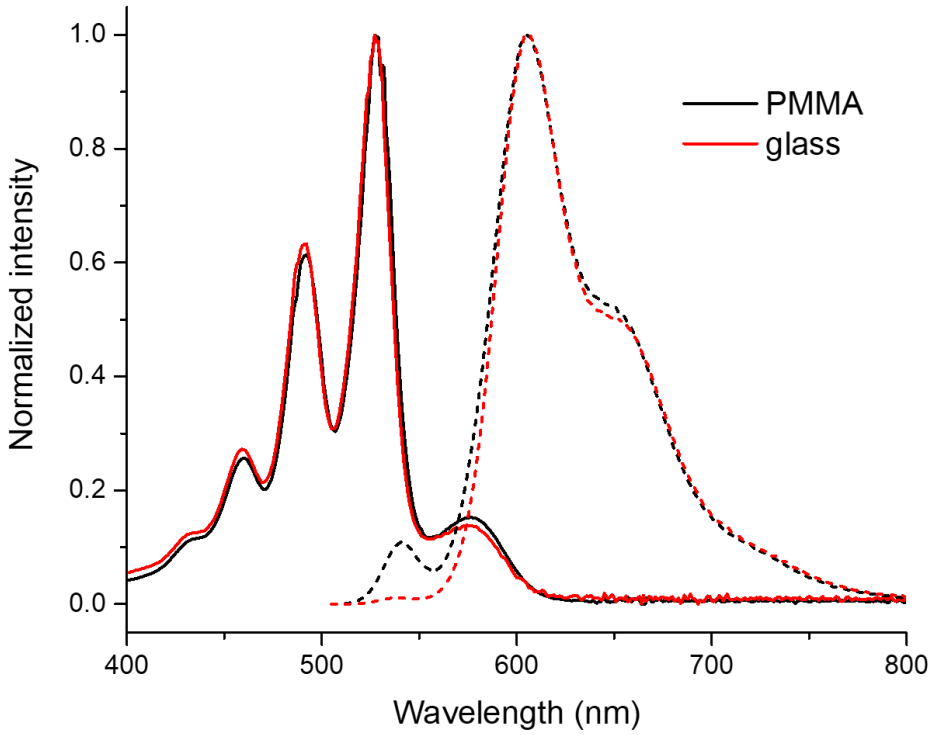

Figure S2. Comparison of the normalized absorption (solid line) and emission (dash line, excitation wavelength = 490 nm) spectra of the PMMA-based and glass-based LSC device. It is interesting to note that the spectrum of the glass and PMMA samples were very similar except for an emission band at 540 nm for the PMMA sample. This 540 nm band can be assigned to the bPDI-3 emission that is not fully quenched by LR305. We speculate that some diffusion of bPDI-3 into the PMMA substrate occurred during thin film deposition. This small amount of bPDI-3 at the thin film-substrate interface undergoes less efficient energy transfer and leads to emission from bPDI-3.

Monte-Carlo ray tracing simulation

Monte-Carlo ray tracing simulation was carried out using MATLAB®. The process of the simulation was described by the flow chart in Figure S3. During the simulation process, all of the events, for example the re-absorption, reflection, escape cone loss, PLQY loss or release from the edges, are recorded for assessing the performance of the waveguide system. The scattering and interface coupling caused losses are not considered in the simulation.

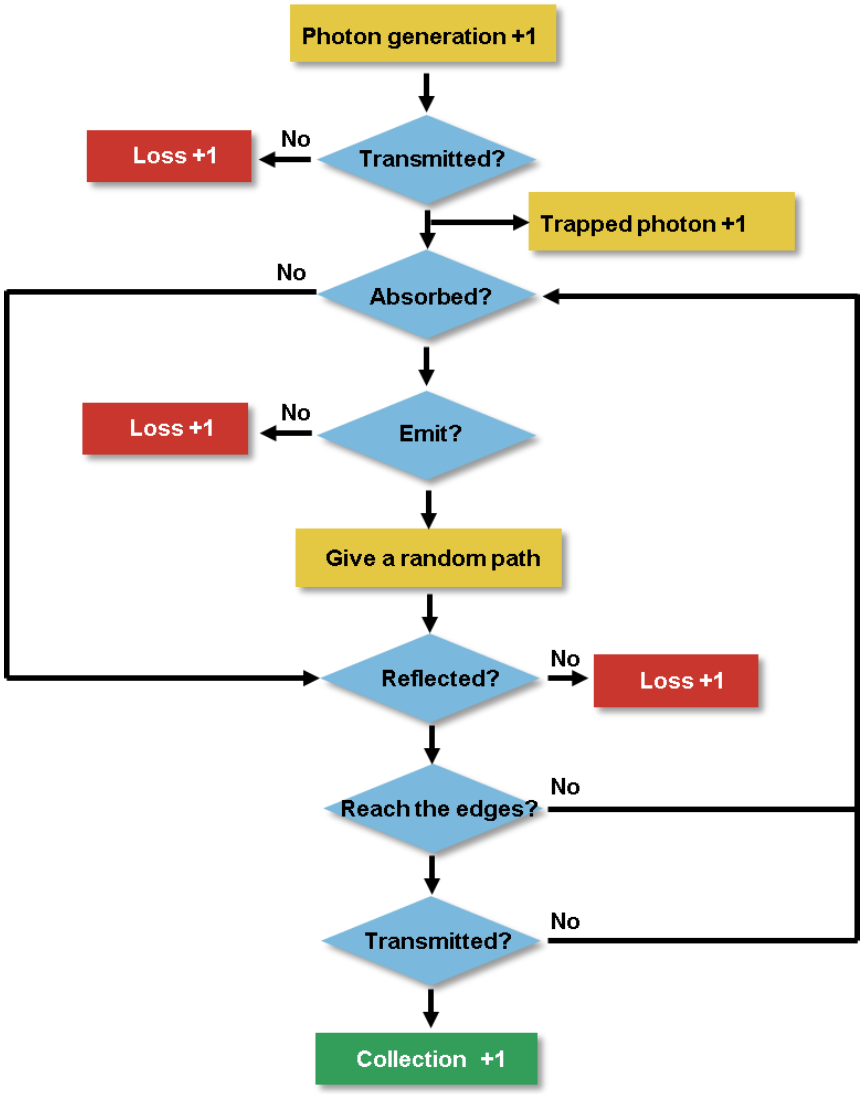

Figure S3. Flow chart of the Monte-Carlo ray tracing simulation process.

LSC device information

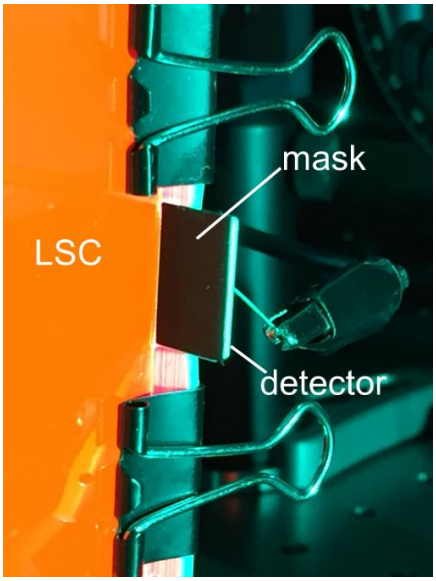

Figure S4. The detector was masked by black duct tape, mounted tightly by paper clips and placed perpendicular to the LSC so only the edge of the LSC was measured. Lens immersion oil was added between the edge of the LSC and the detector surface. The remaining edges of the LSC were covered by the black paint.

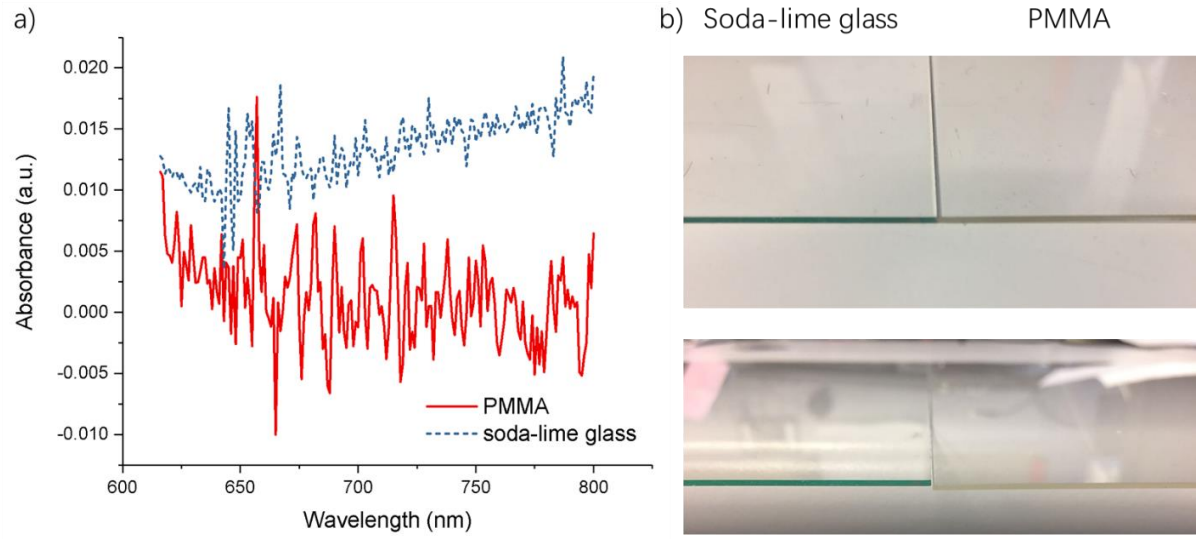

Figure S5. a) the absorption spectra of the PMMA-LSC and glass-LSC in the emission range of the emitter, with the surface reflectance subtracted. b) the top view of both the soda-lime glass and the PMMA sheet are transparent, but the side view of the soda-lime glass appears dark green, indicating some absorbance of visible wavelengths (particularly of red light). The absorbance difference of the glass and PMMA is not obvious visually at a thickness of 1mm, but the overall pathlength of the emitted light in the waveguide can be >100 mm when small absorbance differences will become significant in waveguided light collection.

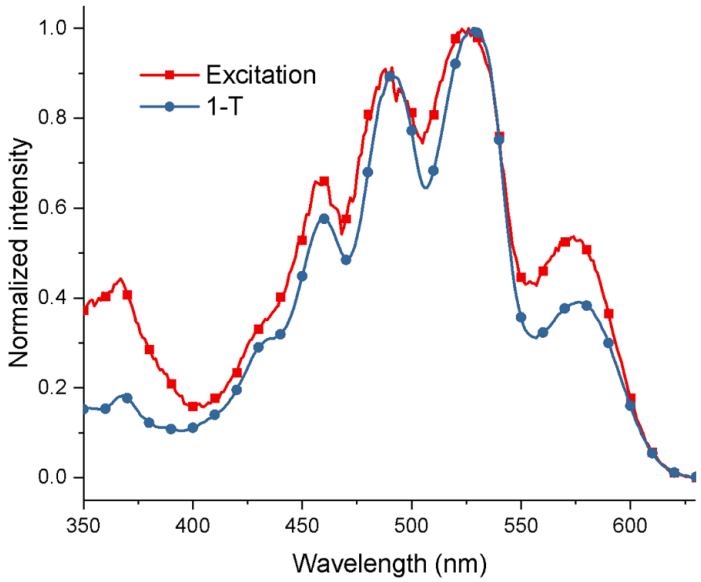

Figure S6. The comparison between the normalized excitation and (1-transmitance) spectra of the PMMA-LSC (60 mM of the donor and 12 mM of the emitter). The good concordance between the two spectra provides evidence for efficient FRET from the donor dye to the emitter .[1, 4]

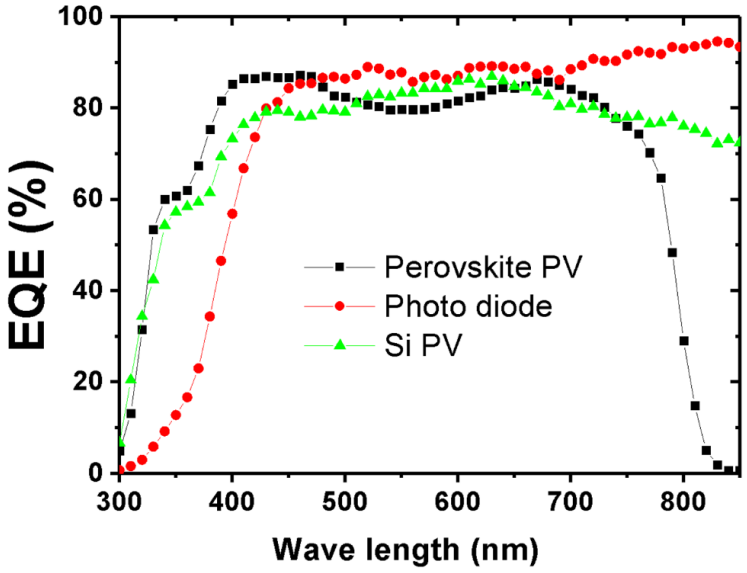

Figure S7. The measured external quantum efficiency (EQE) in the visible range of the Perovskite PV, photo diode[5] and the Si PV[6-7] that were used this work.

References

(1) Banal, J. L.; Soleimaninejad, H.; Jradi, F. M.; Liu, M.; White, J. M.; Blakers, A. W.; Cooper, M. W.; Jones, D. J.; Ghiggino, K. P.; Marder, S. R.; Smith, T. A.; Wong, W. W. H., Energy Migration in Organic Solar Concentrators with a Molecularly Insulated Perylene Diimide. *J. Phys. Chem. C* **2016,** *120* (24), 12952-12958.
(2) Xu, J.; Zhang, B.; Jansen, M.; Goerigk, L.; Wong, W. W. H.; Ritchie, C., Highly Fluorescent Pyridinium Betaines for Light Harvesting. *Angew. Chem. Int. Ed.* **2017,** *56* (44), 13882-13886.
(3) Jiang, Q.; Zhang, L.; Wang, H.; Yang, X.; Meng, J.; Liu, H.; Yin, Z.; Wu, J.; Zhang, X.; You, J., Enhanced Electron Extraction Using Sno2 for High-Efficiency Planar-Structure Hc(Nh2)2pbi3-Based Perovskite Solar Cells. *Nat. Energy* **2016,** *2*, 16177.
(4) Zhang, B. L.; Soleimaninejad, H.; Jones, D. J.; White, J. M.; Ghiggino, K. P.; Smith, T. A.; Wong, W. W. H., Highly Fluorescent Molecularly Insulated Perylene Diimides: Effect of Concentration on Photophysical Properties. *Chem. Mater.* **2017,** *29* (19), 8395-8403.
(5) High Breakdown Voltage, Fully Depleted Series Large Active Area Photodiodes. https://docs-apac.rs-online.com/webdocs/1668/0900766b816684f7.pdf.
(6) Verlinden, P. J.; Blakers, A. W.; Weber, K. J.; Babaei, J.; Everett, V.; Kerr, M. J.; Stuckings, M. F.; Gordeev, D.; Stocks, M. J., Sliver® Solar Cells: A New Thin-Crystalline Silicon Photovoltaic Technology. *Sol. Energy Mater. Sol. Cells* **2006,** *90* (18-19), 3422-3430.
(7) Zhao, J.; Wang, A.; Altermatt, P. P.; Wenham, S. R.; Green, M. A., 24% Efficient Perl Silicon Solar Cell: Recent Improvements in High Efficiency Silicon Cell Research. *Sol. Energy Mater. Sol. Cells* **1996,** *41*, 87-99.

Chapter VI

Selectively Aligned Donor-emitter Pairs in LSCs

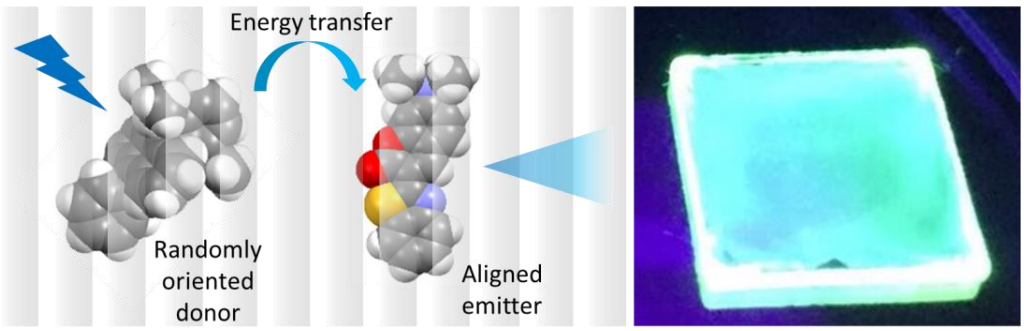

Reprinted with the permission from Ref [2], copyright © 2019 American Chemical Society.

6.1 Preface

As mentioned in the Introduction, there are three major energy loss pathways in LSCs, i.e. the ϕ_{PL} loss, the escape cone loss and the reabsorption effect. So far, in the previous chapters, the donor-emitter fluorophore pair system reported in this thesis demonstrated the effectiveness of enhancing the ϕ_{PL} of the fluorophore system and reducing the reabsorption effect. The escape cone loss of LSCs can also be reduced by using a donor-emitter pair approach as described below.

For a typical LSC device, the transition dipoles of fluorophores are normally oriented isotropically

in the waveguide, leading to the isotropic emission directions. According to Equation 1-15 in **Chapter I**, the maximum trapping efficiency η_{trap} of LSCs will be around 25%, using glass or PMMA based waveguides (n = 1.5). However, for an ideal LSC, the direction of the emitted light is best confined to be parallel to the waveguide surface to reduce the escape cone loss. By aligning the transition dipole of dichroic fluorophores perpendicular to the waveguide surface of LSCs, one can confine the emitted light to be parallel to the waveguide surface and significantly reduce the escape cone loss.

As discussed in **Chapter I**, there were several examples of liquid crystal substrates used as the waveguide matrix for aligning fluorophores in LSCs. In 2008, Baldo et. al. reported an approach to fabricate a LSC[1] by depositing a fluorophore embedded liquid crystal polymer thin-layer on the surface of a glass matrix. They dissolved a rod-shaped fluorophore into the liquid crystal monomer, and then deposited the blend as a thin film on the glass matrix. The liquid crystal monomer was aligned perpendicularly to the glass surface via the self-assembling process, forcing the rod-shaped fluorophore to be aligned in the same direction (Figure 6.1). After the self-assembly, the liquid crystal monomer layer was cured by a UV lamp and the orientation of the fluorophore was permanently fixed. As the transition dipole of the reported fluorophore was parallel to the longer molecular axis, the transition dipole of the molecules was perpendicularly aligned to the waveguide surface. The emission of the fluorophore was thus confined in a direction parallel to the waveguide surface, leading to a decrease to the escape cone losses of the LSC. As mentioned previously, the maximum limit of the OQE is around 75% for a glass matrix-based LSC. By adopting the alignment approach, one can increase the OQE to 81%.

The drawback of perpendicular alignment was that it will lead to a decrease in absorbance of the LSC to the normal incident light, also due to the perpendicularly aligned transition dipole of the fluorophore. To overcome the drawback, a diffuser layer was added on top of the LSC to increase the absorbance of the LSC in the above-mentioned paper. However, the diffuser layer may not

be the ideal solution, as it will also scatter and reflect a fraction of the incident light.

The ideal solution of this problem is to design a selectively aligned donor-emitter fluorophore pair system. In the selectively aligned system, the donor should have an isotropic orientation to harvest incident light as usual, while the emitter should be perpendicularly aligned to confine the emission. To fulfill the selective alignment, a liquid crystal monomer/polymer (UCL-018, DIC Corporation) was chosen to be the aligning waveguide matrix. Once deposited on a glass surface, the liquid crystal monomer will self-assemble perpendicular to the surface, leading to the embedded materials aligning in the same direction. The liquid crystal monomer is then cured by the UV radiation to give a solid liquid crystal polymer layer. The liquid crystal monomer will have a stronger interaction with planar-shape materials than sphere-shape materials. Therefore, the molecular shape of the donor can be designed to have a highly symmetrical configuration to reduce the interaction with the liquid crystal polymer. On the other hand, the emitter should be designed in a rod-shape or planar-shape structure, so that it will be more strongly influenced by the liquid crystal monomer and be perpendicularly aligned. The donor fluorophores will absorb the incident light in random directions while the emission of the acceptor fluorophores will be limited to the direction perpendicular to the aligned orientation. Besides the selective alignment, the donor-emitter fluorophore pairs should be able to also reduce the re-absorption effect and help to increase the overall ϕ_{PL} as described in the previous chapters.

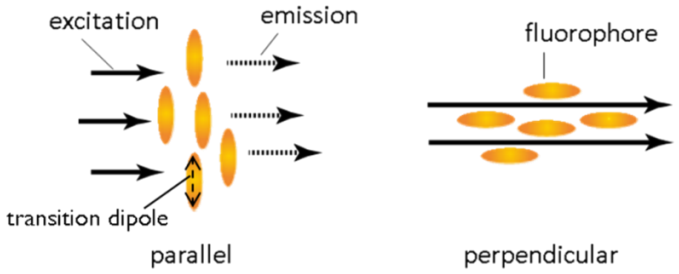

Figure 6.1 The dichroic fluorophore exhibits stronger absorption and emission in the direction perpendicular to its transition dipole.

In this research, a couple of tetrahedral donor molecules were designed and synthesized for the purpose of the selective alignment. As mentioned before, the molecular structure of the donors was required to be bulky enough to avoid the interaction with the liquid crystal monomer. A tetrahedral structure was a first approach. A tetrahedral perylene diimide tetramer (tetra-PDI) was designed and synthesized (Figure 6.2) by installing the functionally desymmetrized bPDI on the tetra(4-nitrobenzene)methane core via the imidazation reaction (see experimental section for details). However, the tetra-PDI was too bulky to disperse in the liquid crystal matrix. Instead, it precipitated from the liquid crystal matrix even in a low concentration. Then a diphenyl anthracene tetramer (tetra-DPA, provided by Dr. Can Gao) was assessed in the liquid crystal matrix (Figure 6.2) as well, but the solubility of tetra-DPA was not sufficient and the compound decomposed under ambient conditions over time. The failure of tetra-PDI and tetra-DPA suggested that a tetrahedron structure may not be the best choice for the donors to disperse in the liquid crystal. Instead, a smaller molecule with bulky-substituents may help to avoid the precipitation from the matrix.

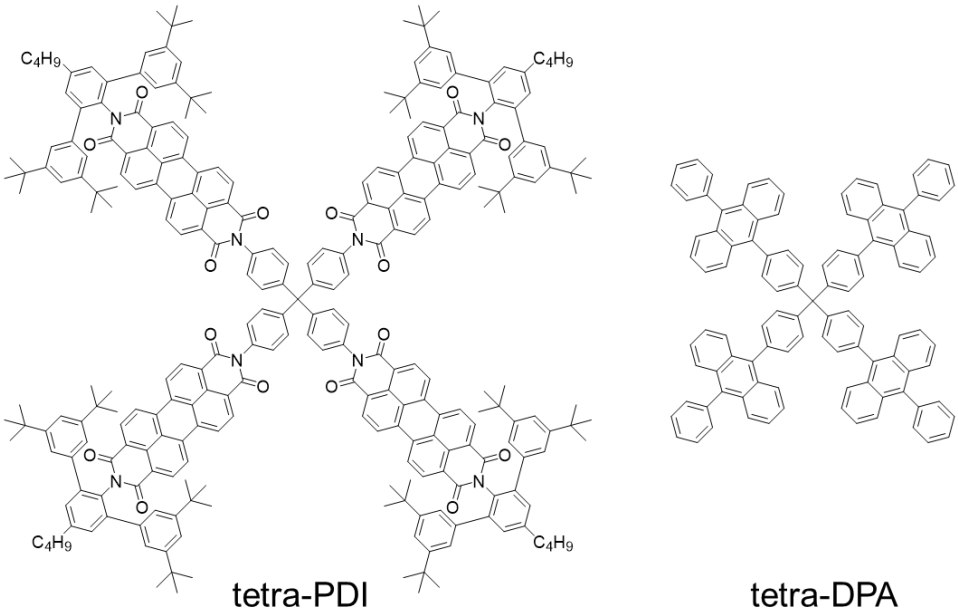

Figure 6.2 The chemical structure of tetra-PDI and tetra-DPA.

Subsequently, two diphenyl anthracene (DPA) derivatives with different molecular shapes were synthesized and investigated as potential light harvesting donors. DPA and these two derivatives were three donors being examined in the project. As the bulkiness of the substituents in each DPA were different, the molecular shapes of the donors vary from planar to ellipsoid to sphere. As expected, the ellipsoid shaped DPA successfully reduced the interaction with the liquid crystal polymer while remaining homogenously dispersed. The selectively aligned donor-emitter fluorophore pair system was prepared by pairing the ellipsoid DPA with a rod-shaped emitter, coumarin 6, in the liquid crystal polymer matrix. The resulting LSCs were examined and showed close to 80% OQE without sacrificing the absorbance of the device. The research results were summarized and published in the following article[2]:

Bolong Zhang, Can Gao, Hamid Soleimaninejad, Jonathan M. White, Trevor A. Smith, David J. Jones, Kenneth P. Ghiggino, Wallace W.H. Wong. Highly Efficient Luminescent Solar Concentrators by Selective Alignment of Donor-Emitter Fluorophores. *Chem. Mater.* **2019**, 8, 3001-3008. DOI: 10.1021/acs.chemmater.9b00647

The experimental details are included in the Supporting Information section following the main manuscript. Reprinted with the permission from Ref [2], copyright 2019 © American Chemical Society.

Contribution of the candidate:

- Fluorophore synthesis and characterization.
- Crystal preparation for x-ray crystallography
- LSC device fabrication.
- Characterization of the LSC performance.

- Writing of drafts of the manuscript

6.2 Experimental data on initial work

The synthesis procedure of tetra-PDI.

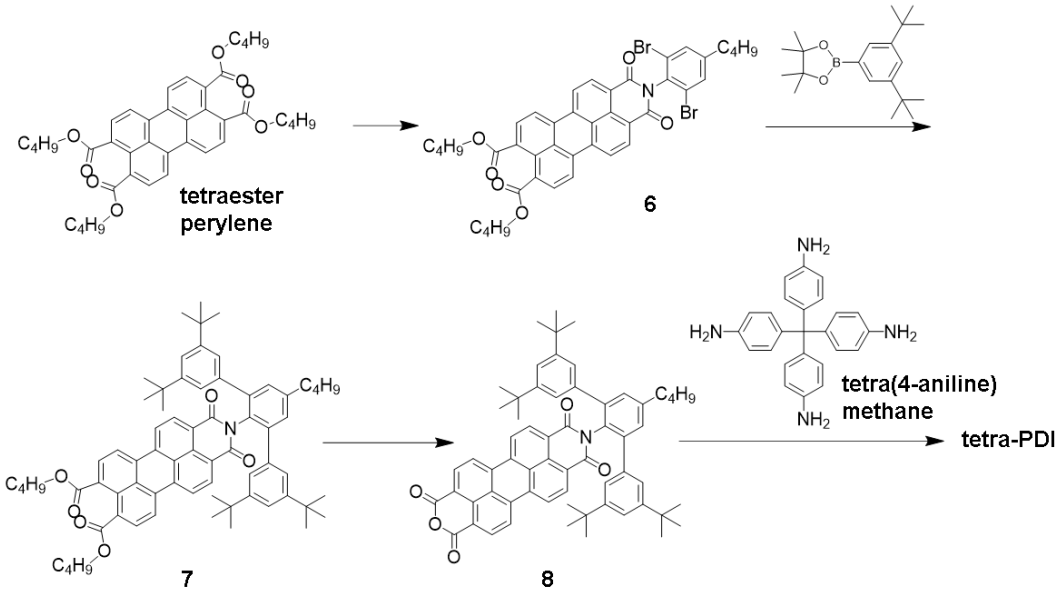

6

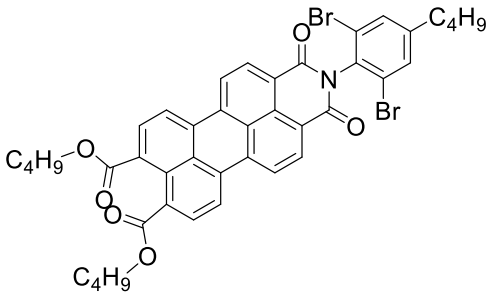

The mixture of tetraester perylene (2.0 g, 3.1 mmol), 2,6-dibromo-4-butylaniline (1.0 g, 3.3 mmol), $Zn(OAc)_2$ (55 mg, 0.3 mmol) and imidazole (5 g) was stirred at 140 ^oC under N_2 atmosphere for 24 hours. The crude product then dissolved in $CHCl_3$ and filtrate to remove the solid impurities. The filtrate then purified by flash chromatography ($CHCl_3$) to yield the target product (red solid,

310 mg, 13 %).

^{1}H NMR (400 MHz, $CDCl_3$) δ 8.69 (d, *J* = 8.0 Hz, 2H), 8.48 (d, *J* = 8.1 Hz, 2H), 8.42 (d, *J* = 8.0 Hz, 2H), 8.09 (d, *J* = 7.9 Hz, 2H), 7.56 (s, 2H), 4.36 (t, *J* = 6.8 Hz, 4H), 2.74 – 2.57 (m, 2H), 1.88 – 1.76 (m, 4H), 1.67 (p, *J* = 7.5 Hz, 2H), 1.55 – 1.47 (m, 4H), 1.47 – 1.37 (m, 2H), 1.05 – 0.91 (m, 9H).

^{13}C NMR (101 MHz, $CDCl_3$) δ 168.22, 162.20, 147.03, 136.24, 132.40, 132.12, 131.98, 130.33, 130.09, 129.14, 129.05, 126.37, 123.67, 122.88, 121.92, 121.78, 65.61, 34.94, 32.90, 30.61, 22.34, 19.25, 13.87, 13.79.

MS ESI+ (m/z): calcd. for $[M+H^+]$ $C_{42}H_{38}Br_2NO_6$, 812.10454; found $[M+H^+]$, 812.10345.

FT-IR (cm^{-1}, neat): 2958.2, 2931.0, 1711.5, 1677.3, 1594.1, 1466.0, 1359.7, 1273.9, 1174.6, 1074.8, 805.6, 748.0

7

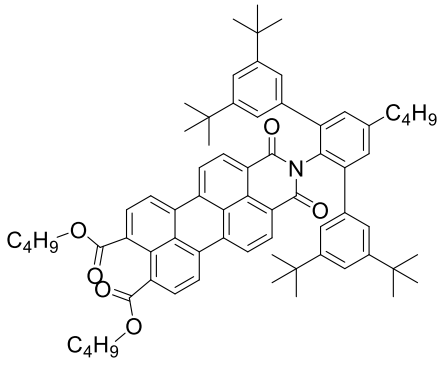

A mixture of **6** (81 mg, 0.1 mmol), 3,5-di-t-butylphenyl bronic acid pinacol ester (95 mg, 0.3 mmol) and $Pd(PPh_3)_4$ (11 mg, 0.01 mmol) were dissolved in toluene (2.5 ml, 8% w/w Aliquate 336) and K_2CO_3 aqueous solution (2M, 0.5 ml). The solution was sealed under N_2, heated to reflux and stirred for 48h. The organic phase from the crude product was separated and purified by flash

chromatography ($CHCl_3$) to give the target product (red powder, 66 mg, 0.064 mmol, 64%).

^{1}H NMR (400 MHz, $CDCl_3$) δ 8.46 – 8.31 (m, 6H), 8.09 (d, *J* = 7.9 Hz, 2H), 7.35 (s, 2H), 7.22 (s, 4H), 7.06 (s, 2H), 4.32 (t, *J* = 6.8 Hz, 4H), 2.78 (t, *J* = 7.9 Hz, 2H), 1.75 (q, *J* = 6.7, 5.9 Hz, 6H), 1.47 (p, *J* = 7.0 Hz, 6H), 1.07 (s, 36H), 1.00 – 0.95 (m, 9H).

^{13}C NMR (101 MHz, $CDCl_3$) δ 168.21, 149.76, 142.06, 138.57, 135.17, 132.34, 131.74, 131.09, 130.32, 129.56, 122.91, 122.42, 122.23, 121.57, 120.50, 65.47, 35.54, 34.63, 33.16, 31.19, 30.57, 22.66, 19.21, 14.01, 13.76.

MS ESI+ (m/z): calcd. for [M+H$^+$] $C_{70}H_{80}NO_6$, 1030.59856; found [M+H$^+$], 1030.59741.

FT-IR (cm^{-1}, neat): 3435.0, 3345.9, 2957.8, 2870.6, 1704.6,1664.3, 1593.5, 1463.5, 1360.6, 1261.5, 1159.6, 879.0, 749.9, 717.4

8

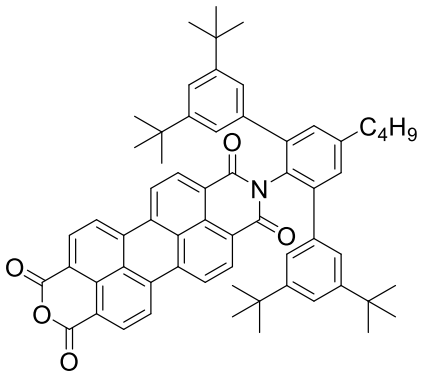

A mixture of **7** (200 mg, 0.19 mmol) and $TsOH.H_2O$ (57 mg, 0.30 mmol) was dissolved in toluene and stirred at 100 ^{o}C overnight under N_2 atmosphere. The crude product was purified by flash chromatography ($CHCl_3$) to give the target product (red powder, 70 mg, 0.08 mmol, 42 %).

^{1}H NMR (400 MHz, $CDCl_3$) δ 8.68 (d, *J* = 8.0 Hz, 2H), 8.59 (d, *J* = 8.1 Hz, 2H), 8.52 (d, *J* = 8.1 Hz, 2H), 8.46 (d, *J* = 8.0 Hz, 2H), 7.36 (s, 2H), 7.21 (d, *J* = 1.8 Hz, 4H), 7.07 (t, *J* = 1.9 Hz, 2H),

2.83 – 2.74 (m, 2H), 1.76 (p, *J* = 7.7 Hz, 2H), 1.48 (dt, *J* = 14.7, 7.4 Hz, 2H), 0.99 (t, *J* = 7.3 Hz, 3H).

^{13}C NMR (101 MHz, $CDCl_3$) δ 159.94, 149.84, 143.77, 142.01, 139.53, 138.46, 136.42, 133.50, 132.16, 131.81, 131.08, 129.62, 129.18, 129.01, 126.28, 123.95, 123.58, 123.10, 122.88, 120.54, 118.92, 35.54, 34.65, 33.16, 31.19, 22.67, 14.00.

MS ESI+ (m/z): calcd. for [M+H$^+$] $C_{62}H_{62}NO_5$, 900.46280; found [M+H$^+$], 900.46143.

FT-IR (cm^{-1}, neat): 2960.2, 2866.5, 1771.4, 1704.9, 1593.6, 1363.4, 1248.8, 1122.3, 811.1, 740.7

tetra-PDI

A mixture of **8** (50 mg, 0.056 mmol), tetra(4-aniline)methane (3.5 mg, 0.0093 mmol), P_2O_5 (25 mg), $Zn(OAc)_2$ (5 mg, 0.028 mmol) and imidazole (1.0 g) was sealed under N_2 atmosphere and stirred at 140 ^{o}C overnight. The crude product was purified by flash chromatography ($CHCl_3$) to give the target product (orange powder, 7 mg, 0.0018 mmol, 20 % to tetra(4-aniline)methane).

^{1}H NMR (500 MHz, $CDCl_3$) δ 8.73 (d, *J* = 7.9 Hz, 2H), 8.62 (d, *J* = 8.2 Hz, 2H), 8.52 (d, *J* = 8.2 Hz, 2H), 8.47 (d, *J* = 8.0 Hz, 2H), 7.67 – 7.58 (m, 2H), 7.43 – 7.34 (m, 4H), 7.24 (d, *J* = 1.8 Hz, 4H), 7.09 (t, *J* = 1.8 Hz, 2H), 2.80 (t, *J* = 8.0 Hz, 2H), 1.83 – 1.72 (m, 2H), 1.49 (dt, *J* = 14.7, 7.4 Hz, 2H), 1.10 (s, 36H), 1.00 (t, *J* = 7.4 Hz, 3H).

^{13}C NMR (151 MHz, $CDCl_3$) δ 163.48, 163.16, 149.81, 146.27, 143.65, 142.04, 138.51, 135.11, 134.20, 133.44, 132.36, 131.78, 131.07, 129.79, 129.60, 129.28, 129.16, 127.91, 126.65, 126.20, 123.41, 123.25, 123.01, 122.95, 122.90, 120.52, 64.68, 35.53, 34.64, 33.15, 31.19, 22.65, 13.99.

MS MALDI+ (m/z): calcd. for [M$^+$] $C_{273}H_{260}N_8O_{16}$, 3907.98444; found [M$^+$], 3907.2.

FT-IR (cm^{-1}, neat): 2954.9, 2865.7, 1706.7, 1667.9, 1593.3, 1403.8, 1342.3, 1249.9, 1195.8, 810.8, 745.1

Reference:

1. Mulder, C. L.; Reusswig, P. D.; Velázquez, A. M.; Kim, H.; Rotschild, C.; Baldo, M. A., Dye Alignment in Luminescent Solar Concentrators: I. Vertical Alignment for Improved Waveguide Coupling. *Opt. Express* **2010,** *18* (9), 90.
2. Zhang, B. L.; Gao, C.; Soleimaninejad, H.; White, J. M.; Smith, T. A.; Jones, D. J.; Ghiggino, K. P.; Wong, W. W. H., Highly Efficient Luminescent Solar Concentrators by Selective Alignment of Donor-Emitter Fluorophores. *Chem. Mater.* **2019,** *31* (8), 3001-3008.

CHEMISTRY OF MATERIALS
Cite This: Chem. Mater. 2019, 31, 3001−3008
Article
pubs.acs.org/cm

Highly Efficient Luminescent Solar Concentrators by Selective Alignment of Donor−Emitter Fluorophores

Bolong Zhang,[†,‡] Can Gao,[†,‡] Hamid Soleimaninejad,[†] Jonathan M. White,[‡] Trevor A. Smith,[†] David J. Jones,[‡] Kenneth P. Ghiggino,[†] and Wallace W. H. Wong*[,†,‡]

[†]ARC Centre of Excellence in Exciton Science, School of Chemistry, and [‡]School of Chemistry, Bio21 Institute, The University of Melbourne, Parkville, Victoria 3010, Australia

Supporting Information

ABSTRACT: Vertically aligning fluorophores to the surface of a waveguide is known to be an effective approach to improve the optical quantum efficiency (OQE) of luminescent solar concentrators (LSCs). While the chromophore alignment assists waveguiding of the emitted photons to the LSC edges, it also significantly reduces the light-harvesting properties of the LSC. We report here a fluorophore pair consisting of a sphere-shaped energy donor and a rod-shaped emitter that was incorporated in LSCs to provide selective fluorophore alignment to address the reduced incident-light absorption issue. A liquid-crystal polymer matrix was used to perpendicularly align the rod-shaped acceptors to a favorable orientation for light guiding, while the sphere-shaped donor was randomly oriented to maintain its light-absorbing properties. The OQE of LSC devices with this selectively aligned donor−acceptor fluorophore system is 78% without significant loss of light-harvesting capability.

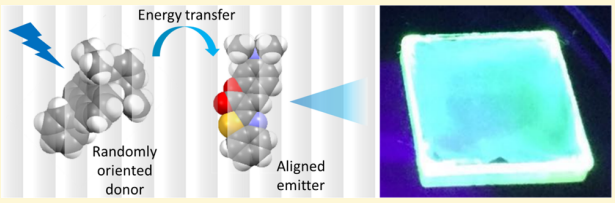

1. INTRODUCTION

A luminescent solar concentrator (LSC) is a light-harvesting device containing fluorophores that absorb light over the large surface area of a planar waveguide. The resulting luminescence is guided to the device edges by total internal reflection, where the concentrated light can be converted to electric current by a photovoltaic cell.[1] The planar geometry, together with the range of colors and transparencies possible, make LSCs particularly attractive for light-harvesting applications in urban environments.[2]

The performance of LSCs is limited mainly by four aspects, namely the transmission loss due to incomplete light absorption by the fluorophores, the photoluminescence quantum yield (ϕ_{PL}) of the fluorophore, the escape cone loss of the waveguide system, and luminescence re-absorption.[1] The transmission loss can be addressed by improving the fraction of incident light absorbed by the fluorophore, by adjusting the fluorophore concentration and/or the thickness of the LSC device. The ϕ_{PL} is related to the photophysical properties of the fluorophore system and our group and others have used a variety of strategies to improve this parameter.[2−4] The escape cone loss refers to the re-emitted photons released from the top and bottom surfaces of the waveguide because of the refractive index change at the interface.[5,6] Escape cone loss can be addressed by using a higher refractive index material as the waveguide, but there is a trade-off with increased reflectance of the incident light from the waveguide surface and the higher cost of high-refractive index materials. The luminescence re-absorption effect does not lead to energy loss directly but adds to the escape cone loss and the ϕ_{PL} loss in systems where there is an overlap of the absorption and emission spectra of the fluorophore.[7−9] Careful selection of a light-harvesting energy donor and a highly emitting energy acceptor (the "emitter") that increases the Stokes shift has been demonstrated to reduce the re-absorption effect and improve the performance of LSCs.[10−13] The concentration of the energy donor materials is usually quite high in this case to capture the incident light, while the concentration of the emitters is adjusted to just sufficiently quench the emission from the donors. Consequently, the overall spectrum of the mixture will be dominated by the donor absorption and the emitter emission spectrum with minimum spectral overlap.

Aligning the emission transition dipole of a molecular fluorophore perpendicular to a plane, defined in Figure 1a, will bias the direction of the emitting light to be within the (x, y) plane. In the context of a LSC, aligning the emission transition dipoles of all the fluorophores perpendicular to the plane of the waveguide (Figure 1) has been shown to reduce the escape cone loss.[14−16] However, in many cases, the absorption transition dipole of the fluorophores is parallel to the emission transition dipole leading to significant decrease in fluorophore absorption ability for light incident from the (z) direction, Figure 1a, resulting in LSC efficiency loss.[17,18] This loss was reduced for a reported vertically aligned dye system using a light diffuser layer on top of the LSC device.[15]

Received: February 14, 2019
Revised: March 28, 2019
Published: March 29, 2019

DOI: 10.1021/acs.chemmater.9b00647
Chem. Mater. 2019, 31, 3001−3008

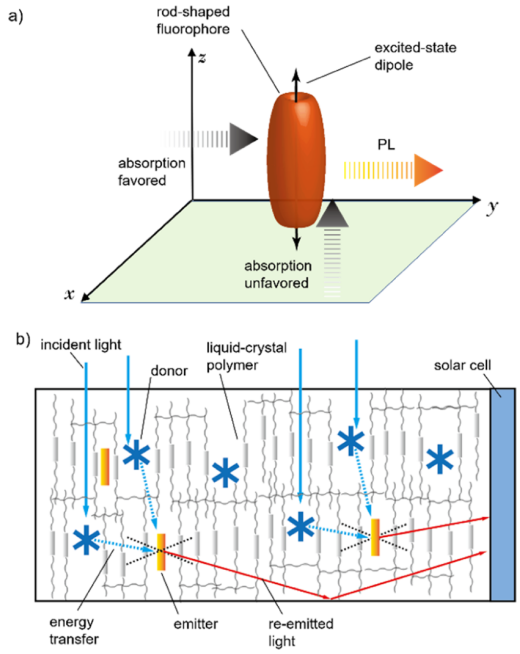

Figure 1. (a) Alignment influences the observed absorption of light and emission intensity in different directions of an aligned fluorophore system; (b) the wave-guiding process in a LSC device containing randomly oriented light-absorbing energy donors and aligned emitters.

Selectively aligning a donor−emitter fluorophore pair is an alternative approach to overcome the drawbacks of aligning a single fluorophore species. The emitter is required to be aligned perpendicular to the plane of the waveguide to confine the re-emitted light within the waveguide, while the energy donor needs to be randomly oriented to maximally harvest the light incident on the surface of the waveguide. To fulfil this approach, two criteria need to be met: a matrix that can align the emitter perpendicular to the plane of the waveguide, but not the donor; and efficient energy transfer from the donor to the emitter (Figure 1b). With an appropriate donor−emitter energy transfer process, the emission from a high concentration of randomly distributed donor molecules can be efficiently quenched by only a small amount of emitter.[3] The high donor to emitter ratio results in a small spectral overlap reducing the luminescence re-absorption effect as discussed earlier. In addition, the low concentration of the emitter also helps to avoid the aggregation-caused quenching effect and improves the effective ϕ_{PL} of the system.[10] In terms of the LSC performance, the selected random donor/aligned-emitter waveguide system should improve the optical quantum efficiency (OQE) of LSCs while retaining good external quantum efficiency (EQE) by minimizing light absorption losses. OQE and EQE are defined here as the percentage of the edge output photons with relation to absorbed photons and incident photons, respectively

$$\mathrm{OQE} = \frac{n_{\mathrm{edge}}}{n_{\mathrm{abs}}} \quad (1)$$

$$\mathrm{EQE} = \frac{n_{\mathrm{edge}}}{n_{\mathrm{incident}}} = \mathrm{OQE} \times A\ \% \quad (2)$$

where n_{edge} is the number of the total edge output photons, n_{abs} is the number of incident photons that are absorbed, n_{incident} refers to the number of photons incident on the waveguide surface, and A % represents the percentage light absorption.

During our studies, a biomimetic light-harvesting funnel system was reported whereby a selectively aligned chromophore pair was investigated.[19] While this work provided a glimpse of this light-harvesting strategy, application in LSC devices was not explored.

In this work, 9,10-diphenylanthracene (DPA) derivatives and coumarin 6 were used as the energy donor and energy acceptor, respectively, in a selectively aligned LSC device. The alignment of coumarin 6 in a self-assembling liquid-crystal polymer (LCP) matrix was reported previously.[15] The rod-shaped molecular structure of coumarin 6 meant that the alignment effect driven by the LCP packing was very strong. Conversely, it was envisaged that spherically shaped molecules would not be aligned in the LCP matrix. DPA derivatives are suitable candidates as energy donor materials because of their high ϕ_{PL}, good spectral overlap with coumarin 6 absorption, and readily modifiable molecular structures. Although the DPA molecule is close to a planar-shaped structure, we proposed to install bulky substituents on the DPA structure to modify the molecular shape into an ellipsoid or even a sphere. In this way, the LCP will only drive the alignment of coumarin 6 while leaving the sphere-shaped DPA derivatives randomly oriented.

Herein, two DPA derivatives, bDPA-1 and bDPA-2, bearing isopropyl substituents on the phenyl rings were synthesized (Figure 2a). Together with DPA, these energy donors were paired with coumarin 6, the rod-shaped emitter, as donor−emitter pairs and incorporated in both poly(methyl methacrylate) (PMMA) and the LCP thin-film waveguide matrix. LSC devices with different combinations of fluorophores and matrices were then examined, revealing benchmark experimental OQEs for the selectively aligned donor−emitter system.

2. RESULTS AND DISCUSSION

The DPA derivatives, bDPA-1 and bDPA-2, were synthesized by the Suzuki−Miyaura coupling of 2,6-diisopropylphenylboronic acid pinacol ester with 9-bromo-10-phenylanthracene and 9,10-dibromoanthracene, respectively (see Supporting Information for details). The absorption and emission spectra of the DPA derivatives in dilute solution were similar to each other except for the more pronounced vibronic structures for bDPA-1 and bDPA-2 (Figure 2b). As the isopropyl substituents block the free rotation of the phenyls, the vibronic structures in the spectrum of bDPA-1 and bDPA-2 were more resolved, indicating a more rigid molecular structure. As required by the donor−emitter energy transfer process, the absorption spectrum of coumarin 6 has a large degree of overlap with the emission spectrum of the DPA derivatives. In terms of reducing the re-absorption effect, the overlap of the absorption and emission spectra of the donor−emitter system was much reduced compared to the donor or emitter on their own (vide infra). The overall Stokes shift of the donor−emitter pair is approximately 75 nm.

The selectively aligned LSC devices were prepared by incorporating the donor and emitter chromophores in a self-assembled LCP matrix obtained from DIC Corporation (material number UCL018; see Supporting Information for sample preparation details). Control devices without dye alignment were fabricated by using PMMA as the polymer

DOI: 10.1021/acs.chemmater.9b00647
Chem. Mater. 2019, 31, 3001−3008

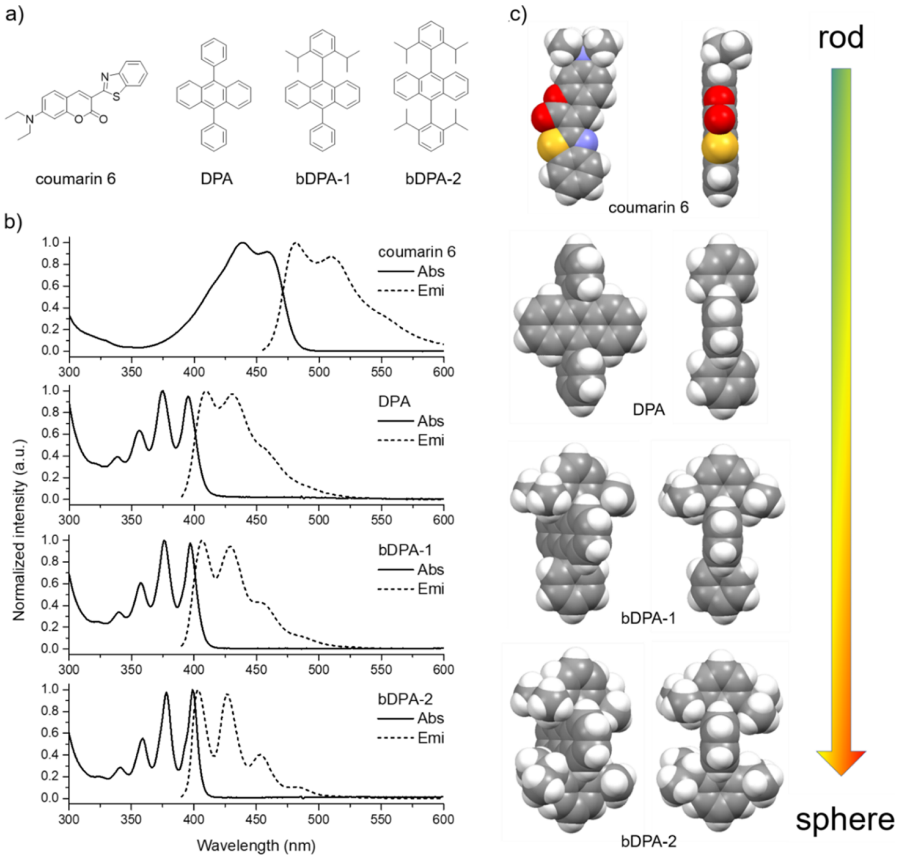

Figure 2. (a) Chemical structures of coumarin 6 and the bDPA series, (b) normalized absorption and emission spectra of the four compounds in dilute solution conditions (10^{-5} M in toluene). Space-filling illustrations of crystal structures of coumarin 6, DPA, bDPA-1, and bDPA-2 in front and side views. The molecular shape changes from rodlike for coumarin 6 to sphere-like for bDPA-2.

matrix instead of the LCP. As mentioned previously, the molecular shape is essential for selective alignment by the LCP matrix. Therefore, the donors and the emitter were all chosen or designed to have distinct molecular shapes. The shape of coumarin 6 is naturally rod-shaped while the shapes of the donors vary from planar to ellipsoid to spherical (Figure 2c). The molecular shape significantly influences the interaction between the LCP matrix and the fluorophores. In the donor−emitter fluorophore pair system, the concentration of the donors needs to be high to capture the incident light. However, the maximum concentration of bDPA-1 that could be included in the LCP matrix was about 50 mM while bDPA-2 precipitated at <10 mM. In contrast, samples with concentrations of up to 100 mM for DPA and coumarin 6 in the LCP matrix were prepared without any observable precipitation. This behavior indicated that the rod-shaped coumarin 6 and planar-shaped DPA interacted favorably with the LCP matrix, while the sphere-shaped bDPA-2 was more easily excluded from the matrix because of shape mismatch. By installing bulky groups only on one end of the DPA molecule, the shape of bDPA-1 (Figure 2c) allowed inclusion into the LCP matrix at a reasonable concentration (50 mM) for assembling a donor−emitter LSC device. Because the achievable concentration of bDPA-2 in the LCP matrix was too low, it was not examined further in this work.

Both the absorption and emission spectra of coumarin 6 showed small red shifts in the LCP matrix compared to the spectra of the PMMA sample (Figure 3a). The spectra of the DPA derivatives also showed a very small red shifts in LCP relative to PMMA (Figure 3b,c). The red shifts indicated a lowering of excited state energy which can be a result of the molecules residing in the more rigid LCP environment or a result of aggregation. A summary of the photophysical properties of the fluorophores in the various matrices is provided in Table 1.

The influence on the effective light absorption ability of aligning the coumarin 6 (as described in Figure 1) in the LCP matrix is shown in Figure 3a. The effective absorption ability (defined as the absorbance per molar per unit thickness) reduced markedly (~60%) in the latter case because of the increased proportion of the chromophores that have their absorption transition dipoles aligned parallel to the direction of the incident light (i.e., perpendicular to the electric field of the incident light). In comparison, the effective absorption ability by DPA and bDPA-1 only dropped by around 20 and 10%, respectively (Figure 3b,c). The two phenyl groups of DPA must be situated out of the plane of the anthracene core, making the molecule more of a thin-ellipsoid rather than planar (Figure 2c). For bDPA-1, the isopropyl substituents made the molecule even more ellipsoidal in shape with less chance of alignment by the LCP matrix. The selectivity of alignment was significant between coumarin 6 and bDPA-1.

The energy transfer between fluorophores that are dispersed in a solid-state matrix can be described by the FRET mechanism.[20] The FRET process requires both dipole−dipole coupling of the fluorophores and a significant spectral overlap

DOI: 10.1021/acs.chemmater.9b00647
Chem. Mater. 2019, 31, 3001−3008

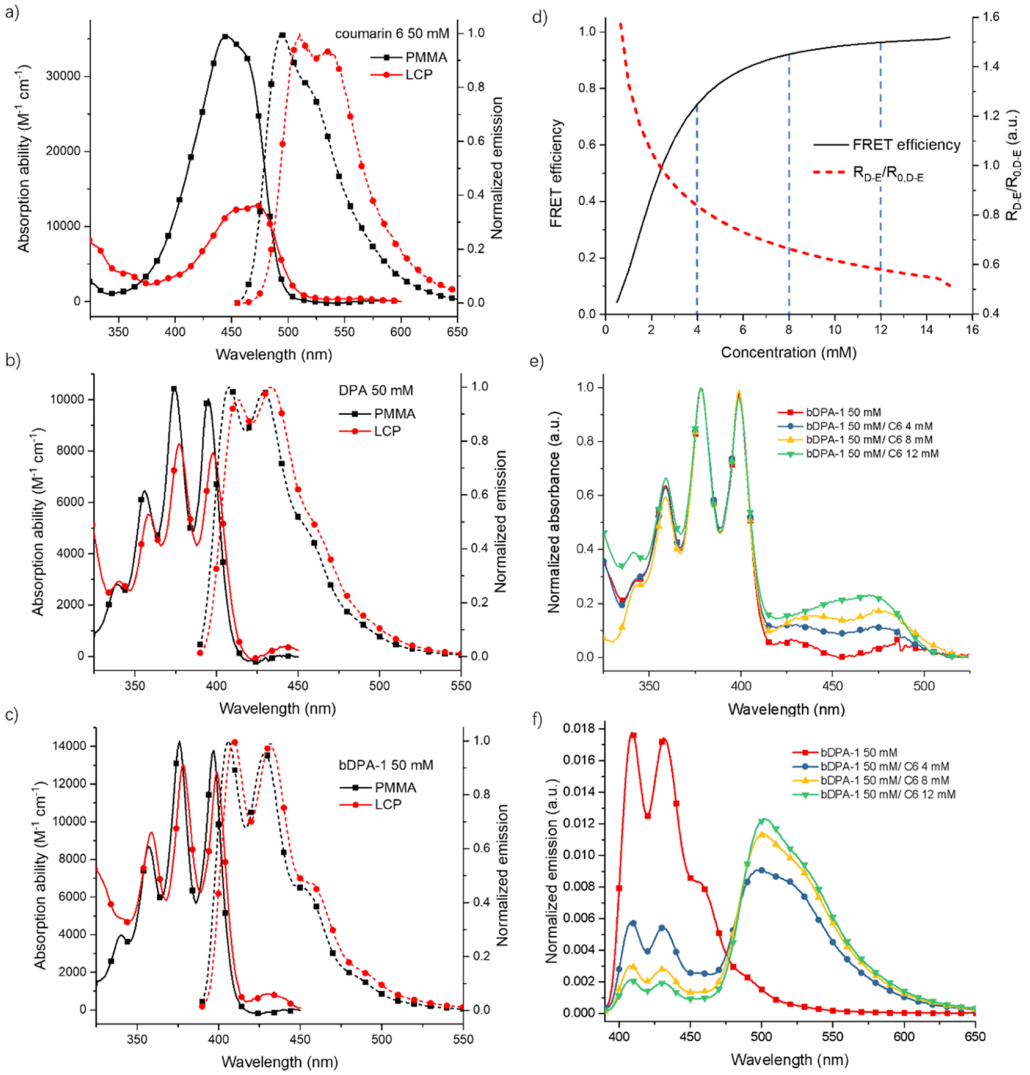

Figure 3. UV−vis absorption spectra (solid lines) showing the observed absorption ability for light incident perpendicular to the plane of the waveguide and emission spectra (dashed) of (a) coumarin 6 (C6), (b) DPA, and (c) bDPA-1 in both PMMA and LCP thin-film matrix at 50 mM. (d) Donor-to-emitter Förster resonance energy transfer (FRET) efficiency (E_{D-E}) and $R_{D-E}/R_{0,D-E}$ as a function of the concentration of coumarin 6, (e) normalized absorption and (f) normalized (by integration) emission spectra (with excitation at 375 nm) of the bDPA-1/coumarin 6 mixture system in the LCP matrix.

of the donor emission and the acceptor absorption. In an isotropic fluorophore system, the electronic coupling of dipoles increases with the fluorophore concentration as the donor−acceptor distance decreases. The emission spectra of all the DPA compounds overlapped significantly with the absorption spectrum of coumarin 6, which enabled efficient donor−emitter energy transfer pairs. The FRET critical distance (R_0, nm; the distance at which the rate for energy transfer is the same as the rate for all other excited donor relaxation processes) can be calculated via the following Förster equation[21,22]

$$R_0 = 0.02108 \times \left(\frac{\kappa^2 \Phi_{PL} J}{n^4} \right)^{1/6} \quad (3)$$

$$J = \int \varepsilon_A(\lambda) F_D(\lambda) \lambda^4 \, d\lambda \quad (4)$$

where κ^2 is the orientation factor ($\kappa^2 = 0.476$ for a randomly oriented, long-lifetime, and nonmobile donor and acceptor system in a rigid matrix[20]), Φ_{PL} refers to the photoluminescence quantum efficiency (PLQY) of the donor fluorophore, J ($nm^4\ M^{-1}\ cm^{-1}$) is the spectral overlap integral involving the area-normalized emission spectrum (F_D) of the donor and the absorption coefficient (ε_A) of the acceptor, λ is the wavelength over the full spectrum, and n is the refractive index of the matrix material (assuming $n = 1.5$ for PMMA and $n = 1.6$ for LCP).

The calculated donor-to-emitter critical distances, $R_{0,D-E}$, are close to 4.4 nm for all donor cases (eqs 3 and 4 and Table 1). In a homogeneously dispersed system, the average intermolecular distance between the donor (high concentration) and emitter (low concentration) (R_{D-E}) is related to the average intermolecular distance of the emitters (R_{E-E}) (eq 5, see the mathematical model in Supporting Information)

DOI: 10.1021/acs.chemmater.9b00647
Chem. Mater. 2019, 31, 3001−3008

Table 1. Photophysical Properties of the Fluorophores in Different matrices[a]

fluorophore	matrix[a]	abs_{max} (nm)	emi_{max} (nm)	$R_{0,D-E}$ (nm)[b]	absorption ability 10^4 (M^{-1} cm^{-1})[c]
coumarin 6	toluene	438	481	n/a	n/a
	PMMA	445	495		3.50 ± 0.08
	LCP	472	510		1.30 ± 0.04
DPA	toluene	375	410	4.41	n/a
	PMMA	374	408		1.04 ± 0.04
	LCP	377	434		0.830 ± 0.005
bDPA-1	toluene	376	407	4.39	n/a
	PMMA	376	409		1.46 ± 0.06
	LCP	378	406		1.30 ± 0.03
bDPA-2	toluene	399	403	4.37	n/a
	PMMA	n/a	n/a		n/a
	LCP	n/a	n/a		n/a

[a]Fluorophore concentration was 10^{-5} M in toluene and 50 mM in the thin-film matrix. [b]$R_{0,D-E}$ is the critical radius of the donor-to-emitter FRET process and was calculated based on solution data. [c]Absorption ability is the effective absorption determined by measurement of the transmission of light incident perpendicular to the waveguide.

$$R_{D-E} = \frac{R_{E-E}}{2\sqrt[3]{\pi/3}} = 0.4924R_{E-E} \tag{5}$$

By using R_{D-E} and $R_{0,D-E}$, one can calculate the efficiency of the FRET process (E) (eq 6)[23]

$$R_{D-E} = R_{0,D-E}\left(\frac{1-E}{E}\right)^{1/6} \text{ or } E = \frac{1}{\left(\frac{R_{D-E}}{R_{0,D-E}}\right)^6 + 1} \tag{6}$$

To experimentally demonstrate the efficiency of the donor-to-emitter energy transfer in the selectively aligned system, a series of samples were prepared consisting of 50 mM of bDPA-1 with varying concentrations of coumarin 6 in the LCP matrix. According to eq 6, the donor-to-emitter FRET efficiency (E_{D-E}) was >75% when the concentration of coumarin was 4 mM, while it increased to above 92% when the concentration reached 8 mM (Figure 3d). As shown in Figure 3e, the absorption band associated with bDPA-1 in the mixtures remained the same, while the absorption band of coumarin 6 rose proportionally with increasing concentration of coumarin 6. In contrast, the normalized emission intensity of the donor dropped dramatically with increasing coumarin 6 concentration along with the appearance of the energy acceptor emission (Figure 3f). With 8 mM of coumarin 6, the donor emission dropped to 17% of the original intensity. By considering the absorbance and emission intensities, 8 mM of coumarin 6 and 50 mM of DPA were found to be close to the optimum in terms of minimizing emission re-absorption.

Apart from donor-to-emitter energy transfer, donor-to-donor energy migration was also an important process in our light-harvesting system. The donor-to-donor energy migration facilitated the transfer of energy from some donor molecules that could not couple directly to emitters under the donor-to-emitter orthogonal transition dipole orientation. At 50 mM of bDPA-1 donor, the donor-to-donor FRET critical distance ($R_{0,D-D}$) was 2.78 nm, which was smaller than the mean donor-to-donor distance (R_{D-D}) of 3.21 nm. This meant that the donor-to-donor FRET efficiency (E_{D-D}) for bDPA-1 was 34%. The residual donor emission in the presence of the 8 mM coumarin emitter can be attributed to this relatively low E_{D-D} (Figure 3f).

LSC devices with coumarin 6, bDPA-1, and the bDPA-1/coumarin 6 mixtures in both PMMA and LCP matrices were fabricated by spin-coating on glass slides (dimensions 1.25 × 1.25 × 0.1 cm) from toluene solutions (Figure 4a, see Supporting Information for fabrication details). The geometric gain (G) of all devices is 3 and the mean film layer thicknesses of the PMMA and LCP are 1.26 ± 0.03 and 1.12 ± 0.02 μm, respectively. The performance of the LSC devices is summarized in Table 2.

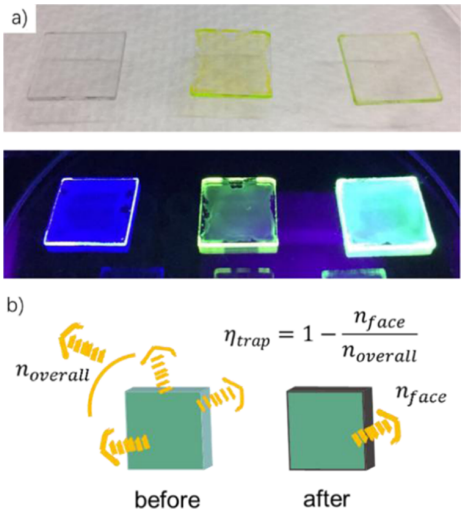

Figure 4. (a) LSC devices (G = 3) fabricated based on bDPA-1, coumarin 6, and the bDPA-1/coumarin 6 mixture (left to right) in the LCP matrix. The devices are exposed to both the ambient light (top) and 365 nm UV light (bottom); (b) η_{trap} of LSC devices was quantified by measuring the integrated emission of devices before and after the edges were covered with black paint. The $n_{overall}$ and n_{face} refer to the photon numbers collected from all the surfaces and edges of the devices or from just the surfaces, respectively.

The G is defined in this work as

$$G = \frac{S_{surface}}{S_{edge}} \tag{7}$$

where S_{edge} and $S_{surface}$ are the area of the edges and surface of the waveguide, respectively.

The donor−emitter fluorophore system was originally designed to increase the Stokes shift and thus minimize the re-absorption effect. By examining the overlap between the absorption spectrum and the emission spectrum (integrally normalized to 1), the re-absorption factor (F_R) of a waveguiding system can be calculated. F_R is defined by eq 8

$$F_R = \int_{\lambda_1}^{\lambda_2} \varepsilon_\lambda PL_\lambda \, d\lambda \tag{8}$$

where ε_λ and PL_λ are the extinction coefficient and the normalized emission intensity at the given wavelength, respectively, and λ_1 and λ_2 define the spectral range.

As shown in Table 2, the F_R of all LCP-based samples was smaller than in the PMMA matrix, mainly because of the red-shifted emission spectrum in the LCP matrix. For the bDPA-1/coumarin 6 mixture in either the PMMA or LCP matrix, F_R was smaller than either the donor and acceptor alone in the

DOI: 10.1021/acs.chemmater.9b00647
Chem. Mater. 2019, 31, 3001−3008

Table 2. Summary of the LSC Device Performance[a]

fluorophores	matrix	F_R	$\phi_{PL,observed}$ (%)[b]	η_{trap} (%)	OQE (%)	EQE[c] (%)
bDPA-1 50 mM	PMMA	1430	87 ± 1	73 ± 2	63 ± 2	9.78
	LCP	880	38 ± 2	70 ± 1	27 ± 2	3.71
coumarin 6 50 mM	PMMA	3030	76 ± 4	73 ± 1	55 ± 4	18.2
	LCP	600	82 ± 1	80 ± 1	66 ± 1	9.21
bDPA-1/coumarin 6 50 mM/8 mM	PMMA	1150	98 ± 1	73 ± 1	72 ± 2	11.2
	LCP	420	98 ± 5	79 ± 1	78 ± 3	10.8

[a]All values in this table are averages of 9 measurements over 3 samples. All samples were measured using an integrating sphere coupled with a fluorometer, with the excitation wavelength of 375 nm for bDPA-1 and 450 nm for coumarin 6. [b]$\phi_{PL,observed}$ values do not include the re-absorption correction. [c]EQE was calculated from OQE based on the absorbance of devices with 1 mm matrix thickness.

same matrix. This indicated that the re-absorption effect was reduced in the donor−emitter fluorophore system.

The ϕ_{PL} of coumarin 6 (50 mM) in the LCP matrix was slightly higher than in PMMA, possibly because of a better molecular dispersion (see Supporting Information for measurement details). On the other hand, the ϕ_{PL} of bDPA-1 was lower in the LCP than in PMMA. As mentioned previously, the molecular shape of bDPA-1 meant that it did not favorably interact with the LCP matrix. At this concentration, some of the bDPA-1 molecules may aggregate and form nonradiative quenching sites in the system. However, the ϕ_{PL} of the bDPA-1/coumarin 6 mixture was 98.4% in both PMMA and the LCP matrices. Compared to bDPA-1 alone, the ϕ_{PL} increase of the donor−emitter mixture was most likely a result of preferential energy trapping by the coumarin 6 emitter over nonemissive aggregate species.[10,24]

The experimental trapping efficiencies (η_{trap}) of all LSCs were determined by comparing the emission intensity of the devices with and without the edges covered with black paint (Figure 4b, See details in the Supporting Information).[1] The η_{trap} of all samples in the PMMA matrix remained at around 72%, which was slightly lower than the theoretical limit of 75%,[6,25] for isotropic waveguide systems with 1.5 refractive index.[26] The η_{trap} of bDPA-1 in the LCP matrix was the same as in PMMA, confirming that the orientation of bDPA-1 was not influenced by the LCP matrix. The η_{trap} values of the donor−emitter mixture and coumarin 6-alone samples in the LCP matrix are 80.4 and 79.3%, respectively. The observation that η_{trap} for these samples is greater than the isotropic limit is direct evidence for the alignment of coumarin 6 in the LCP matrix. Benefiting from the increase in both ϕ_{PL} and η_{trap}, the OQE of the bDPA-1/coumarin 6 mixture in the LCP matrix reached 78.0%, which is amongst the best experimental OQE's reported for an LSC to date.[15,27]

The differences in the absorption and emission spectra of each fluorophore meant that the EQEs of LSCs were not directly comparable. On the other hand, the change in EQE of LSCs with the same fluorophore system but different matrices could be compared (Table 2). The EQE of bDPA-1-only samples dropped by almost two-thirds (9.78 to 3.71%) from PMMA to LCP matrices, mainly because of the lower ϕ_{PL} of bDPA-1 in the LCP matrix. Although the OQE of the perpendicularly aligned coumarin 6-only samples was higher than that of the isotropic samples, the EQE was substantially lower (from 18.2 to 9.21%) because of the lower absorption ability of coumarin 6 in the LCP.

The EQE values of the donor−emitter devices in the two matrices were similar because the improvement in η_{trap} for the LCP sample was negated by the decrease in absorption ability. Among the three LSC device pairs, the selectively aligned donor−emitter system demonstrated a high OQE without significant loss in EQE. Thus, it can be envisaged that selectively aligned donor−emitter systems will be most advantageous in transparent or semitransparent LSC applications requiring limited maximum absorbance, such as windows or tinted polymer/glass roofing. Another possible application is in stacked LSC devices.[19,28] Because transmittance loss drops exponentially with an increase of absorbance according to the Lambert−Beer law,[29] the influence from the absorbance penalty of the perpendicularly aligned system becomes less significant by stacking LSCs (eq 9).

$$T = 0.1^{A} \rightarrow T^{n} = 0.1^{A\times n} \tag{9}$$

The EQE of n stacked layers can be quantified by

$$EQE_n = OQE \times (1 - T^{n}) = OQE \times (1 - 0.1^{A\times n}) \tag{10}$$

where A is the observed absorbance of the devices, T is the percentage transmittance, and n is the number of stacked layers.

By stacking only two layers in the devices, the EQE_2 of bDPA-1/coumarin 6 in the LCP matrix can be predicted to reach 20.6%, which is higher than in the PMMA matrix (20.2%). With the same stacked structure, the EQE_2 of coumarin 6 alone in the LCP matrix (17.2%) is much lower than in the PMMA matrix (30.4%). In other words, the benefits of the selective donor−emitter alignment waveguiding system become more marked after stacking two or more layers.

3. CONCLUSIONS

In conclusion, the selective alignment of donor−emitter fluorophores in LSC devices has been experimentally demonstrated in this work. The η_{trap} of devices is enhanced from 73% for the isotropic fluorophore orientation system to 79.3% for the selective aligned fluorophore system. The resulting absorption penalty in the vertical alignment waveguide is reduced from 60 to 10% because of the presence of the isotropically dispersed bDPA-1 as the donor material. Benefiting from improvements in ϕ_{PL}, η_{trap}, and the re-absorption effect, the LSC with the selectively aligned donor−emitter system showed one of the best experimental OQEs of 78% at G = 3 without any noticeable decrease in EQE.

4. EXPERIMENTAL SECTION

4.1. bDPA-1. A mixture of 9-bromo-10-phenylanthracene (50 mg, 0.15 mmol), 2,6-diisopropylphenyl boronic acid pinacol ester (45 mg, 0.22 mmol), sodium *tert*-butyloxide (43 mg, 0.45 mmol), $Pd(OAc)_2$ (1 mg, 0.004 mmol), and 3-(*t*-butyl)-4-(2,6-dimethoxyphenyl)-2,3-dihydrobenzo[*d*][1,3]oxaphosphole BI-DIME (3 mg, 0.009 mmol)

DOI: 10.1021/acs.chemmater.9b00647
Chem. Mater. 2019, 31, 3001−3008

was dissolved in degassed toluene (2 mL) and stirred at refluxing temperature under the N_2 atmosphere overnight. The crude product was purified by flash chromatography (petroleum spirit 40−60 °C) to obtain the target product (pale powder, 25 mg, 0.06 mmol, 40%). ^{1}H NMR (600 MHz, 1,1,2,2-tetrachloroethane-d_2): δ 7.71 (t, J = 11.9 Hz, 1H), 7.66−7.61 (m, 1H), 7.58 (t, J = 6.5 Hz, 2H), 7.53 (d, J = 8.4 Hz, 1H), 7.42 (d, J = 7.8 Hz, 1H), 7.32 (dt, J = 14.8, 6.5 Hz, 2H), 2.15 (dd, J = 13.3, 6.6 Hz, 1H), 0.92 (d, J = 6.7 Hz, 6H). ^{13}C NMR (101 MHz, chloroform-d): δ 148.45, 139.10, 131.50, 130.36, 129.83, 128.49, 128.29, 127.38, 127.03, 126.97, 125.04, 124.66, 123.17, 30.82, 24.45. FT-IR: 3059.8, 2959.0, 2923.3, 2965.1, 1469.4, 1456.5, 1442.2, 1381.0, 1360.1, 1027.3, 941.2, 806.1, 748.6, 698.0, 664.0. HRMS (m/z): calcd for $C_{32}H_{30}$ [M^+], 414.2348; found, 414.23413.

4.2. bDPA-2. A mixture of dibromoanthracene (250 mg, 0.74 mmol), 2,6-diisopropylphenyl boronic acid pinacol ester (380 mg, 1.84 mmol), sodium *tert*-butyloxide (355 mg, 3.70 mmol), $Pd(OAc)_2$ (5 mg, 0.022 mmol), and 3-(*t*-butyl)-4-(2,6-dimethoxyphenyl)-2,3-dihydrobenzo[*d*][1,3]oxaphosphole BI-DIME (15 mg, 0.045 mmol) was dissolved in degassed toluene (8 mL) and stirred at refluxing temperature under the N_2 atmosphere overnight. The crude product was purified by flash chromatography (petroleum spirit 40−60 °C) to obtain the target product (pale powder, 90 mg, 0.18 mmol, 24%). ^{1}H NMR (400 MHz, chloroform-d_1): δ 7.61−7.50 (m, 3H), 7.41 (d, J = 7.7 Hz, 2H), 7.27 (dd, J = 6.4, 2.6 Hz, 2H), 2.19 (hept, J = 6.6 Hz, 2H), 0.91 (t, J = 9.9 Hz, 12H). ^{13}C NMR (101 MHz, chloroform-d): δ 148.32, 135.45, 134.77, 130.49, 128.44, 127.02, 124.83, 123.08, 30.94, 24.33. FT-IR: 3057.6, 2966.1, 2928.3, 2969.6, 1461.6, 1438.1, 1382.2, 1362.0, 941.3, 801.4, 766.9, 749.8, 673.2. HRMS (m/z): calcd for $C_{38}H_{42}$ [M^+], 498.3286; found, 498.32794.

4.3. X-ray Crystallography. Intensity data for bDPA-1 and bDPA-2 were collected at 100 K on the MX1 beamline at the Australian Synchrotron,[30] bPDI-4 was collected on an Oxford SuperNova CCD diffractometer at 130 K. The structures were solved by direct methods and difference Fourier synthesis. Thermal ellipsoid plots were generated using the program ORTEP-3 integrated within the WINGX suite of programs.

Crystal data for bDPA-1 ($C_{32}H_{30}$): M = 352.49, T = 100.00(10) K, λ = 1.54184 Å, orthorhombic, space group $P\bar{1}$, a = 17.2043(2), b = 8.51290(10), c = 27.5380(3) Å, α = 90°, β = 90°, γ = 90°. V = 4033.17(8) Å^3, Z = 8, D_c = 1.161 mg/m^3, μ(Mo Kα) 0.485 mm^{-1}, F(000) = 1520, crystal size 0.205 × 0.135 × 0.022 mm^3. 49 342 reflections measured to a maximum θ = 78.057°, 4295 independent reflections (R_{int} = 0.1494), the final R was 0.0728 [$I > 2\sigma(I)$] and w$R(F^2)$ was 0.1909 (all data).

Crystal data for bDPA-2 ($C_{38}H_{42}$): M = 498.71, T = 100.00(10) K, λ = 0.71073 Å, triclinic, space group $P\bar{1}$, a = 8.4236(2), b = 8.8483(3), c = 10.6311(3) Å, α = 88.521(2)°, β = 76.573(2)°, γ = 67.212(3)°. V = 708.75(4) Å^3, Z = 1, D_c = 1.168 mg/m^3, μ(Mo Kα) 0.065 mm^{-1}, F(000) = 270, crystal size 0.698 × 0.36 × 0.167 mm^3. 14 483 reflections measured to a maximum θ = 36.968°, 6561 independent reflections (R_{int} = 0.0263), the final R was 0.0532 [$I > 2\sigma(I)$] and w$R(F^2)$ was 0.1643 (all data).

4.4. Thin-Film LSC Device Preparation. Thin-film sample preparation for absolute PLQY measurement: All the glass (MENZEL-GLÄSER Microscope Slides, 76 × 26 mm) slides used in fabricating LSC devices were cut to 1.25 cm × 1.25 cm × 0.1 cm, cleaned by sonicating sequentially in $CHCl_3$, acetone, NaOH (aq.), distilled water, isopropanol, and acetone, and then dried using a strong flow of N_2.

The LSC devices were prepared by spin-coating 20 μL casting solution on top of the abovementioned glass slides. The spin-coating conditions were 2000 rpm (2000 rpm/s) for 1 min to deposit the PMMA thin-film matrix and 1200 rpm (1200 rpm/s) for 15 s to deposit the LCP thin-film matrix. The casting solutions were prepared by dissolving the required quantity of fluorophores in either PMMA solution (8% w/w in toluene) or UCL-018 solution (relative density 1.2, 20% w/w in toluene). The correct quantities of added fluorophores were determined by measuring aliquots from stock solutions (5 mM in toluene) using an automatic pipette, and the solvent was removed using a vacuum-drying oven (60 °C, 35 mbar), before adding to the matrix solution. After spin-coating, the LSC devices were placed in a dry N_2 atmosphere for 1 min and exposed to a UV-lamp (180 nm) for 30 s to cure the LCP matrix.

Absolute PLQY measurements of all samples were performed according to the experimental approach described elsewhere[31,32] using the integrating sphere accessory (F3018, HORIBA Jobin Yvon) for a Fluorolog-3 fluorimeter. The angle of the excitation beam to the normal of the sample surface can be modified using the variable sample holder. All spectra for the absolute quantum yield measurements were corrected for the light source noise, wavelength sensitivity, and the transmittance of the filters. The photon counts of all the measurements on the Fluorolog-3 fluorimeter were within the linear response range of the detector (2×10^6 cps).

The trapping efficiency (η_{trap}) measurements of all samples were performed according to the experimental approach described elsewhere[31,32] using the same conditions described in the absolute PLQY measurement process. The spectra of all samples were recorded with the device edges both covered and not covered with black paint. The η_{trap} can be calculated by the following equation

$$\eta_{trap} = 1 - \frac{PL_{surface}}{PL_0}$$

where $PL_{surface}$ and PL_0 are the integrated emission spectra from the samples with and without the edges being covered with the black paint, respectively. To eliminate the influence of the black paint on the responsivity of the integrating sphere, a white paint was coated over the outside of the black painted surfaces.

■ ASSOCIATED CONTENT

Supporting Information

The Supporting Information is available free of charge on the ACS Publications website at DOI: 10.1021/acs.chemmater.9b00647.

^{1}H and ^{13}C NMR spectra of bDPA-1 and bDPA-2, electrospray mass spectra of bDPA-1 and bDPA-2; summary of definitions of LSC parameters and mean molecular distance; CCDC 1887085, CCDC 1887086, CCDC 1294096, and CCDC 113041 contain the supplementary crystallographic data for this paper (PDF)

■ AUTHOR INFORMATION

Corresponding Author

*E-mail: wwhwong@unimelb.edu.au.

ORCID

Jonathan M. White: 0000-0002-0707-6257
David J. Jones: 0000-0003-1088-7744
Kenneth P. Ghiggino: 0000-0001-6621-4448
Wallace W. H. Wong: 0000-0001-7131-8532

Author Contributions

The manuscript was written through contributions of all the authors. All the authors have given approval to the final version of the manuscript.

Notes

The authors declare no competing financial interest.

■ ACKNOWLEDGMENTS

This work was made possible by support from the Australian Renewable Energy Agency which funds the project grants within the Australian Centre for Advanced Photovoltaics (ACAP). W.W.H.W. was supported by an ARC Future Fellowship (FT130100500). T.A.S., K.P.G., and W.W.H.W. are also supported by the ARC Centre of Excellence in Exciton

DOI: 10.1021/acs.chemmater.9b00647
Chem. Mater. 2019, 31, 3001−3008

Science (CE170100026). The authors are also thankful to Dr Yasuhiro Kuwana, DIC Corporation, for providing the liquid-crystal polymer matrix for this study.

REFERENCES

(1) Tummeltshammer, C.; Taylor, A.; Kenyon, A. J.; Papakonstantinou, I. Losses in Luminescent Solar Concentrators Unveiled. *Sol. Energy Mater. Sol. Cells* **2016**, *144*, 40−47.
(2) Debije, M. G.; Verbunt, P. P. C. Thirty Years of Luminescent Solar Concentrator Research: Solar Energy for the Built Environment. *Adv. Energy Mater.* **2012**, *2*, 12−35.
(3) Banal, J. L.; Zhang, B.; Jones, D. J.; Ghiggino, K. P.; Wong, W. W. H. Emissive Molecular Aggregates and Energy Migration in Luminescent Solar Concentrators. *Acc. Chem. Res.* **2017**, *50*, 49−57.
(4) Meinardi, F.; McDaniel, H.; Carulli, F.; Colombo, A.; Velizhanin, K. A.; Makarov, N. S.; Simonutti, R.; Klimov, V. I.; Brovelli, S. Highly Efficient Large-Area Colourless Luminescent Solar Concentrators Using Heavy-Metal-Free Colloidal Quantum Dots. *Nat. Nanotechnol.* **2015**, *10*, 878−885.
(5) McDowall, S.; Butler, T.; Bain, E.; Scharnhorst, K.; Patrick, D. Comprehensive Analysis of Escape Cone Losses from Luminescent Waveguides. *Appl. Opt.* **2013**, *52*, 1230−1239.
(6) Debije, M. G.; Verbunt, P. P. C.; Rowan, B. C.; Richards, B. S.; Hoeks, T. L. Measured Surface Loss from Luminescent Solar Concentrator Waveguides. *Appl. Opt.* **2008**, *47*, 6763−6768.
(7) Gutierrez, G. D.; Coropceanu, I.; Bawendi, M. G.; Swager, T. M. A Low Reabsorbing Luminescent Solar Concentrator Employing π-Conjugated Polymers. *Adv. Mater.* **2016**, *28*, 497−501.
(8) Olson, R. W.; Loring, R. F.; Fayer, M. D. Luminescent Solar Concentrators and the Reabsorption Problem. *Appl. Opt.* **1981**, *20*, 2934−2940.
(9) Erickson, C. S.; Bradshaw, L. R.; McDowall, S.; Gilbertson, J. D.; Gamelin, D. R.; Patrick, D. L. Zero-Reabsorption Doped-Nanocrystal Luminescent Solar Concentrators. *ACS Nano* **2014**, *8*, 3461−3467.
(10) Zhang, B.; Soleimaninejad, H.; Jones, D. J.; White, J. M.; Ghiggino, K. P.; Smith, T. A.; Wong, W. W. H. Highly Fluorescent Molecularly Insulated Perylene Diimides: Effect of Concentration on Photophysical Properties. *Chem. Mater.* **2017**, *29*, 8395−8403.
(11) Banal, J. L.; Soleimaninejad, H.; Jradi, F. M.; Liu, M.; White, J. M.; Blakers, A. W.; Cooper, M. W.; Jones, D. J.; Ghiggino, K. P.; Marder, S. R.; Smith, T. A.; Wong, W. W. H. Energy Migration in Organic Solar Concentrators with a Molecularly Insulated Perylene Diimide. *J. Phys. Chem. C* **2016**, *120*, 12952−12958.
(12) Currie, M. J.; Mapel, J. K.; Heidel, T. D.; Goffri, S.; Baldo, M. A. High-Efficiency Organic Solar Concentrators for Photovoltaics. *Science* **2008**, *321*, 226−228.
(13) Davis, N. J. L. K.; MacQueen, R. W.; Jones, S. T. E.; Orofino-Pena, C.; Cortizo-Lacalle, D.; Taylor, R. G. D.; Credgington, D.; Skabara, P. J.; Greenham, N. C. Star-shaped fluorene-BODIPY oligomers: versatile donor-acceptor systems for luminescent solar concentrators. *J. Mater. Chem. C* **2017**, *5*, 1952−1962.
(14) MacQueen, R. W.; Cheng, Y. Y.; Clady, R. G. C. R.; Schmidt, T. W. Towards an Aligned Luminophore Solar Concentrator. *Opt. Express* **2010**, *18*, A161−A166.
(15) Mulder, C. L.; Reusswig, P. D.; Velázquez, A. M.; Kim, H.; Rotschild, C.; Baldo, M. A. Dye Alignment in Luminescent Solar Concentrators: I. Vertical Alignment for Improved Waveguide Coupling. *Opt. Express* **2010**, *18*, A79.
(16) Eisfeld, A.; Briggs, J. S. Dye Aggregates in Luminescent Solar Concentrators. *Phys. Status Solidi A* **2018**, *215*, 1700634.
(17) MacQueen, R. W.; Schmidt, T. W. Molecular Polarization Switching for Improved Light Coupling in Luminescent Solar Concentrators. *J. Phys. Chem. Lett.* **2013**, *4*, 2874−2879.
(18) Schiphorst, J. t.; Kendhale, A. M.; Debije, M. G.; Menelaou, C.; Herz, L. M.; Schenning, A. P. H. J. Dichroic Perylene Bisimide Triad Displaying Energy Transfer in Switchable Luminescent Solar Concentrators. *Chem. Mater.* **2014**, *26*, 3876−3878.
(19) Pieper, A.; Hohgardt, M.; Willich, M.; Gacek, D. A.; Hafi, N.; Pfennig, D.; Albrecht, A.; Walla, P. J. Biomimetic Light-Harvesting Funnels for Re-Directioning of Diffuse Light. *Nat. Commun.* **2018**, *9*, 666.
(20) Lakowicz, J. R. *Energy Transfer*; Springer: Basel, 1999; pp 349−367.
(21) Demchenko, A. P. *Introduction to Fluorescence Sensing*; Springer Science & Business Media: Basel, 2008.
(22) Medintz, I.; Hildebrandt, N. *FRET-Förster Resonance Energy Transfer: From Theory to Applications*; John Wiley & Sons: Hoboken, 2013.
(23) Pietraszewska-Bogiel, A.; Gadella, T. W. J. Fret Microscopy: From Principle to Routine Technology in Cell Biology. *J. Microsc.* **2011**, *241*, 111−118.
(24) Zhang, B.; Banal, J. L.; Jones, D. J.; Tang, B. Z.; Ghiggino, K. P.; Wong, W. W. H. Aggregation-Induced Emission-Mediated Spectral Downconversion in Luminescent Solar Concentrators. *Mater. Chem. Front.* **2018**, *2*, 615−619.
(25) Hernandez-Noyola, H.; Potterveld, D. H.; Holt, R. J.; Darling, S. B. Optimizing Luminescent Solar Concentrator Design. *Energy Environ. Sci.* **2012**, *5*, 5798−5802.
(26) Dienel, T.; Bauer, C.; Dolamic, I.; Brühwiler, D. Spectral-Based Analysis of Thin Film Luminescent Solar Concentrators. *Sol. Energy* **2010**, *84*, 1366−1369.
(27) Benjamin, W. E.; Veit, D. R.; Perkins, M. J.; Bain, E.; Scharnhorst, K.; McDowall, S.; Patrick, D. L.; Gilbertson, J. D. Sterically Engineered Perylene Dyes for High Efficiency Oriented Fluorophore Luminescent Solar Concentrators. *Chem. Mater.* **2014**, *26*, 1291−1293.
(28) Carlotti, M.; Ruggeri, G.; Bellina, F.; Pucci, A. Enhancing Optical Efficiency of Thin-Film Luminescent Solar Concentrators by Combining Energy Transfer and Stacked Design. *J. Lumin.* **2016**, *171*, 215−220.
(29) IUPAC. *Compendium of Chemical Terminology (the "Gold Book")*, 2nd ed.; Blackwell Scientific Publications: Oxford, 1997.
(30) Cowieson, N. P.; Aragao, D.; Clift, M.; Ericsson, D. J.; Gee, C.; Harrop, S. J.; Mudie, N.; Panjikar, S.; Price, J. R.; Riboldi-Tunnicliffe, A.; Williamson, R.; Caradoc-Davies, T. Mx1: A Bending-Magnet Crystallography Beamline Serving Both Chemical and Macromolecular Crystallography Communities at the Australian Synchrotron. *J. Synchrotron Radiat.* **2015**, *22*, 187−190.
(31) Porrès, L.; Holland, A.; Pålsson, L.-O.; Monkman, A. P.; Kemp, C.; Beeby, A. Absolute Measurements of Photoluminescence Quantum Yields of Solutions Using an Integrating Sphere. *J. Fluoresc.* **2006**, *16*, 267−273.
(32) Würth, C.; Grabolle, M.; Pauli, J.; Spieles, M.; Resch-Genger, U. Relative and Absolute Determination of Fluorescence Quantum Yields of Transparent Samples. *Nat. Protoc.* **2013**, *8*, 1535−1550.

DOI: 10.1021/acs.chemmater.9b00647
Chem. Mater. 2019, 31, 3001−3008

Supporting Information

Highly Efficient Luminescent Solar Concentrators by Selective Alignment of Donor-Emitter Fluorophores

*Bolong Zhang, Can Gao, Hamid Soleimaninejad, Jonathan M. White, Trevor A. Smith, David J. Jones, Kenneth P. Ghiggino, and Wallace W. H. Wong**

General information

All reagents were used in reactions as received from the suppliers. Dried toluene was obtained from a glass contour solvent purification system. Flash chromatography purification was performed using standard methods on silica gel (Merck Silica Gel 60, 0.040-0.063 mm, 230-400 mesh ASTM). All reactions were monitored by thin-layer chromatography using silica gel (Merck, Silica Gel 60 F254) coated glass sheets, examined under UV lamps (254 nm and 365 nm) in a black box.

The ^{1}H, ^{13}C NMR spectra were collected using Agilent MR400 (400 MHz), Oxford 500 (500 MHz) or Varian Inova 600 (600 MHz) instruments. All NMR spectra, if not otherwise specified, were measured at 25 °C and calibrated using the residual solvent signals. All FT-IR spectra were provided by a Perkin Elmer Spectrum One FT-IR spectrometer while UV-Vis spectra were recorded using a Cary UV-Vis 50 spectrometer. All high-resolution mass spectrometry (HRMS) experiments were conducted with a commercially available hybrid orbital-trap and Fourier-transform ion cyclotron resonance mass spectrometer, equipped with electrospray ionization (ESI).

NMR and HRMS spectra

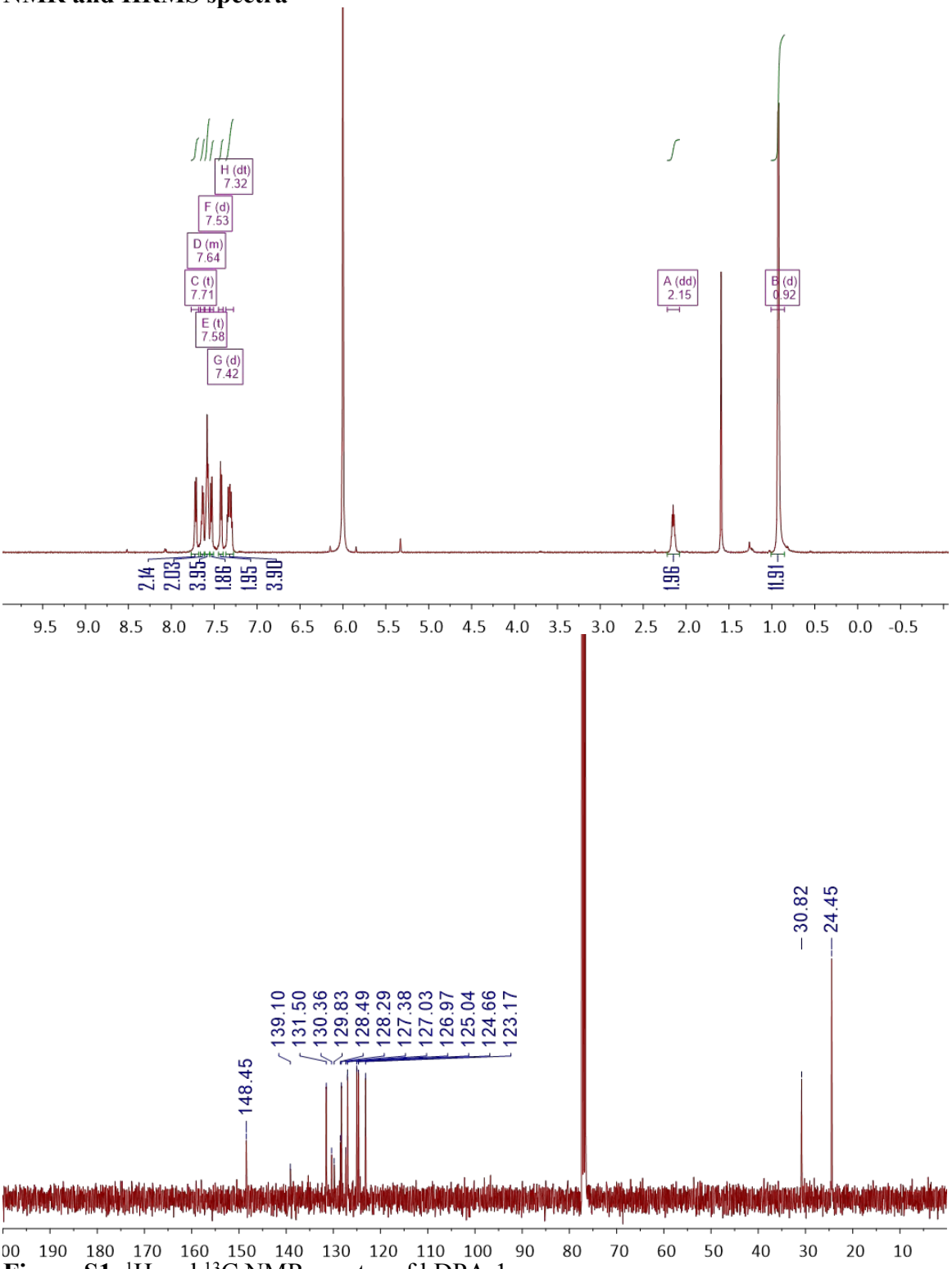

Figure S1. ^{1}H and ^{13}C NMR spectra of bDPA-1.

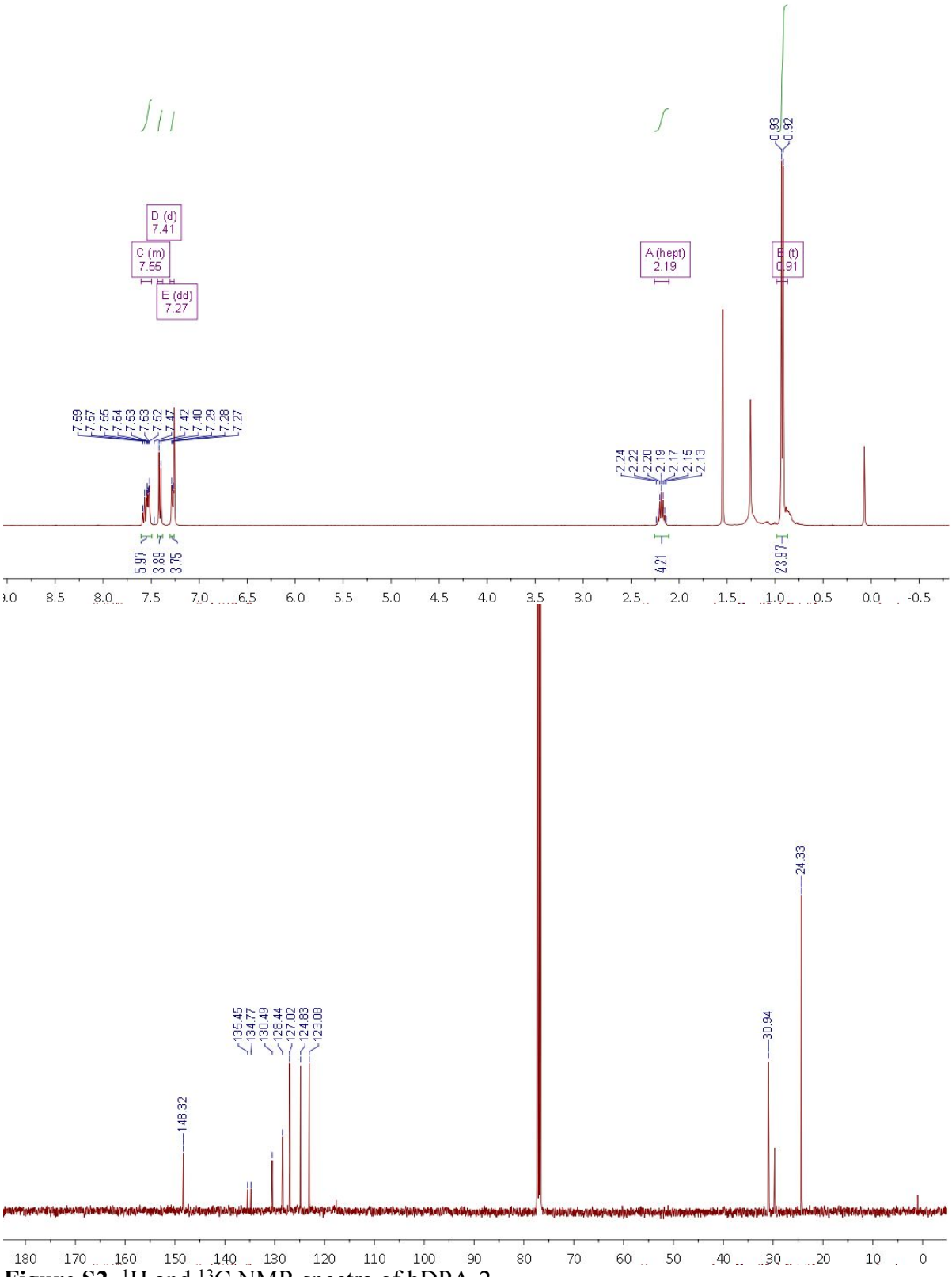

Figure S2. ^{1}H and ^{13}C NMR spectra of bDPA-2.

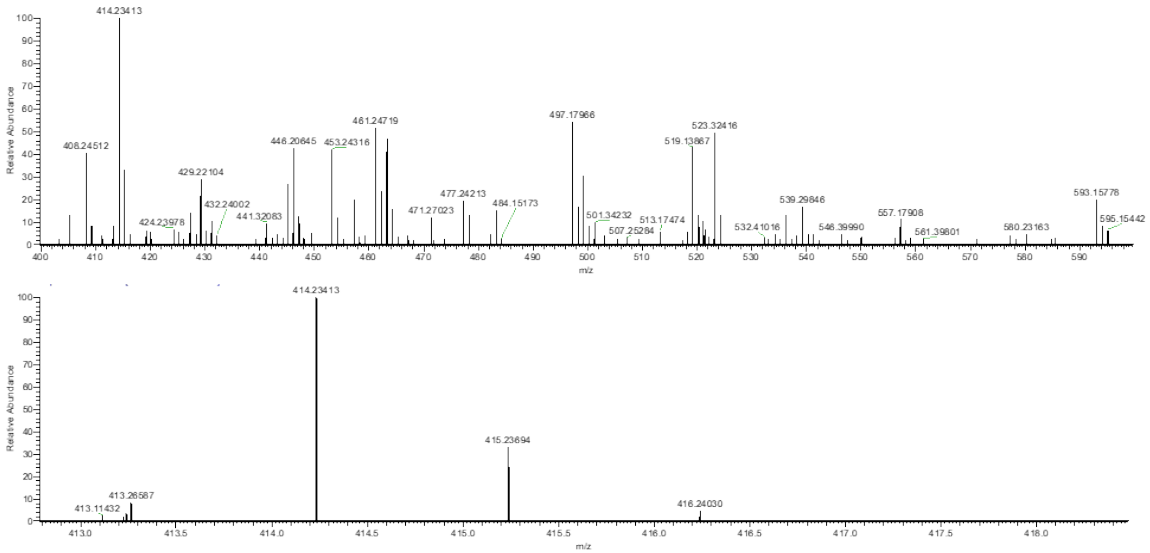

Figure S3. Electrospray mass spectrum of bDPA-1.

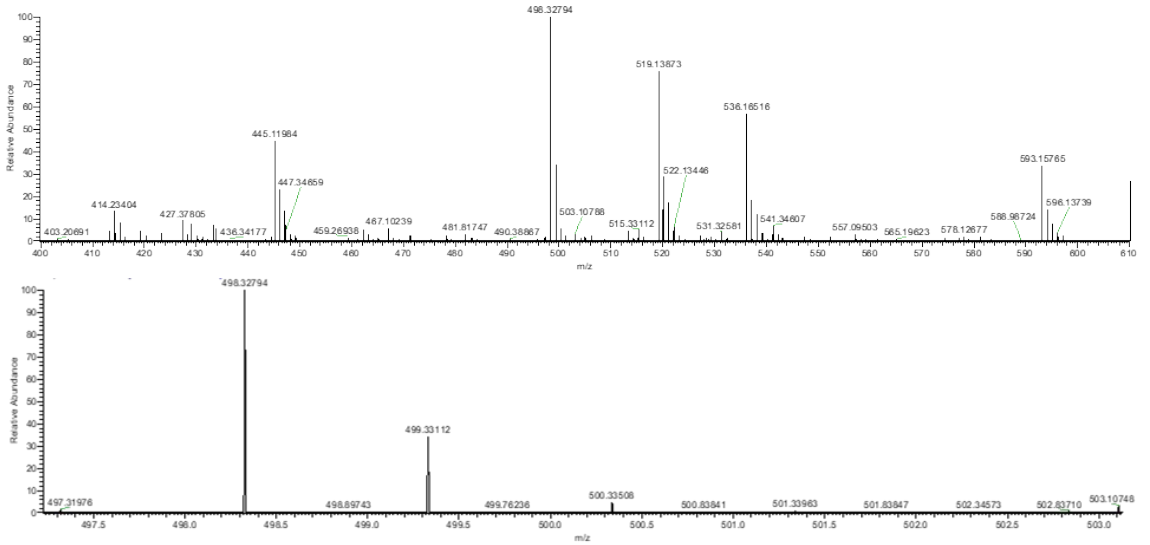

Figure S4. Electrospray mass spectrum of bDPA-2.

The definition of OQE, EQE, G and flux gain

The optical quantum efficiency (OQE), external quantum efficiency (EQE) and geometric gain (G) are defined in this work as:

$$OQE = \frac{n_{edge}}{n_{abs}}$$

$$EQE = \frac{n_{edge}}{n_{incident}} = OQE \times A\%$$

$$G = \frac{S_{surface}}{S_{edge}}$$

where the n_{edge} is the number of the total edge output photons, n_{abs} is the number of incident photons that are absorbed and $n_{incident}$ refers to the number of photons incident on the waveguide surface. $A\%$ stands for absorption rate in percentage. S_{edge} and $S_{surface}$ are the area of the edges and surface of the waveguide respectively.

The flux gain (F) is defined as:

$$F = \frac{I_{edge}}{I_{abs}} = \mathrm{E}QE \times G$$

where the I_{edge} refers to the intensity of one edge output and I_{abs} is the intensity of the incident light.

The definition of mean molecular distance between donor and emitters

For a cubic space containing one centrally located emitter, the red spherical surface defines the boundary where half of the donors are located within the sphere.

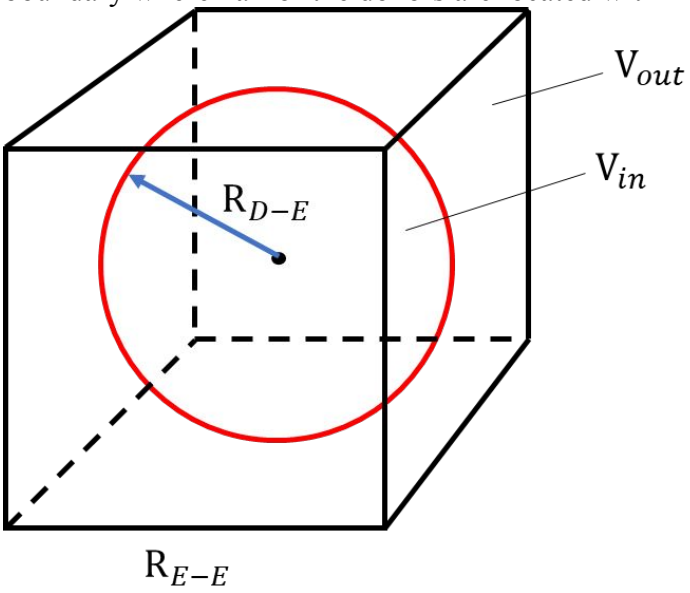

when $V_{out} = V_{in}$

$$\frac{1}{2} R_{E-E}{}^{3} = \frac{4\pi}{3} R_{D-E}{}^{3}$$

$$R_{D-E} = 0.4924\, R_{E-E}$$

Chapter VII

Conclusion and Future Directions

7.1 Conclusion

The objective of this thesis was to investigate the use of donor-emitter pair systems to improve the performance of LSCs. A number of novel fluorophores were designed and synthesized, and their chemical and photophysical properties investigated. The exploitation of these fluorophores revealed new approaches in producing materials with a high ϕ_{PL}, better tolerance to ACQ and other properties. In addition to the fluorophore development, various fabrication approaches were demonstrated in the thesis to produce highly efficient LSC devices. By combining the fabrication approaches and the optimized donor-emitter fluorophore pairs, high performance LSCs were achieved in the thesis.

In **Chapter I**, the Introduction, the background and potential of LSCs were described and the approach of using donor-emitter fluorophore pair systems fully explained.

In **Chapter II**, the general methodology and experimental approaches used/developed in the thesis is described, which includes the information of fluorophore synthesis, devices fabrication and spectroscopy analysis.

In **Chapter III**, to overcome the ACQ effect caused by the required high concentration in the donor-emitter fluorophore pair system, a pair of AIE fluorophores were examined to reveal the influence of the AIE effect to the overall ϕ_{PL} and the spectral overlap of the donor-emitter fluorophore pair. As the AIE effect provided a certain level of resistance to the ACQ effect, the AIE pair retains a high ϕ_{PL} at high concentration in PMMA-matrix. The resulting LSCs based on the AIE pair showed an excellent performance at high fluorophore concentration. On the other hand, the results indicated the AIE molecules were not ideal for LSC applications.

In **Chapter IV**, to further reduce the ACQ effect, a series of PDI derivatives were examined as the energy donor in a donor-emitter pair system. A double-macrocyclic hindered PDI was designed, but the target product was not obtained, due to synthetic difficulties. Instead, a series of bulky substituent PDIs (bPDIs) were prepared, which exhibited an enhanced tolerance to ACQ in high concentration or even in solid state. The optimized donor-emitter pair can retain a ϕ_{PL} at above 90% at very high concentration in the PMMA matrix while minimizing reabsorption effects. Monte-Carlo ray-tracing simulations of the LSC based on the optimized donor-emitter pair indicated the F and EQE of the LSC was comparable with some literature benchmark LSCs.

In **Chapter V**, a large-area LSC (20 cm × 20 cm × 0.1 cm) was fabricated based on the optimized bPDI donor-emitter fluorophore pair via a doctor blade film deposition process on a PMMA substrate. Three types of solar cells/detectors were individually coupled with the LSC and the performance of the LSC was assessed. The LSC achieved an experimental F = 7.4 and PCE = 2.6% at G = 50 which is the highest reported performance for a LSC of this size to-date.

In **Chapter VI**, a selectively aligned donor-emitter fluorophore pair system in a liquid crystal polymer matrix was fabricated to reduce the escape cone loss. By tuning the shape of the molecules, control can be imposed on the interaction between the fluorophore and the liquid crystal polymer matrix, leading to the selective alignment behavior. The emitter was aligned

perpendicularly to the waveguide surface to confine the emitted light to the edges, while the donor remained in a random orientation to harvest the incident light. The resulting LSC achieved an experimental OQE of 79% in a semi-transparent LSC without sacrificing the absorbance of the waveguide.

The work described in this thesis has extended the applications of donor-emitter fluorophore pair systems in the field of LSCs. Several donor-emitter pair systems were designed, synthesized and characterized to reduce the re-absorption effect, develop an approach to selectively align the emitters to direct the emission, and fabricate large-area LSC devices with benchmarked efficiency. Approaches to correctly characterize LSC performance are also proposed. Based on the strategy of a donor-emitter fluorophore pair system key achievements were: (i) an experimental OQE of 79% for a semi-transparent LSC at G = 3 without reduction in absorption behavior, and (ii) experimental values of F = 7.4 and a PCE = 2.6% for a G = 50 large-area printed LSC.

7.2 Future directions:

7.2.1 Organic / inorganic hybrid fluorophore system:

The energy transfer process for molecular fluorophore systems has been very well studied, but the research of the energy transfer between organic-inorganic hybrid systems can still be investigated. LSCs fabricated based-on the organic-inorganic hybrid fluorophore systems are rarely reported. Quantum dot and the perovskite nanocrystals usually show high photo- and thermal stability, high ϕ_{PL} and strong absorption coefficient so are suitable candidates for both energy donor and emitter materials for LSCs. Donor-emitter fluorophore pair systems based on the organic-inorganic hybrid system should be fully investigated, such as the quantum dot / small molecule hybrid or the nanocrystal / small molecule hybrid fluorophore pairs indicated in Figure 7.1.

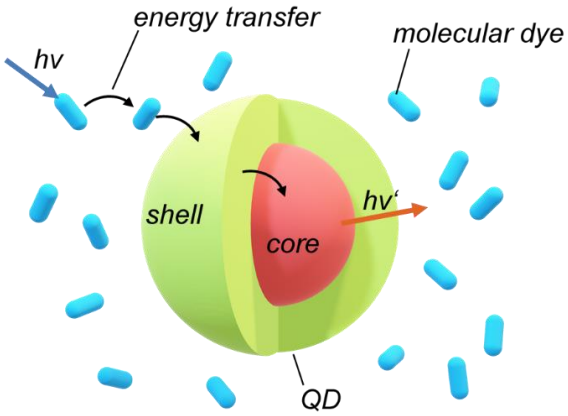

Figure 7.1 Scheme of energy transfer from the small-molecule donor to a QD.

7.2.2 Commercial scale LSC fabrication

While there are many approaches for fabricating large-area LSC waveguides, efficient methods to produce LSCs on an economic commercial scale are yet to be fully developed. Both casting and hot extrusion are the most common methods to produce Perspex industrially and could be adopted in fabricating LSC waveguides. The casting process requires the dissolution of the fluorophores in the monomer and then polymerization in a mold to form the Perspex substrate. The hot extrusion process involves extruding a blend of molten plastic containing the fluorophores into a plastic sheet. The work of this thesis suggests a large-scale doctor blade process might also be exploited on a larger commercial scale.

7.2.3 Commercial LSC electronics

It has been 45 years since the first LSC was made[1], yet the commercialization of LSCs has not been very successful. Inspired by the improvement in performance, as outlined in this thesis, LSC-based electronics or other commercial applications might be considered. The author has successfully built a LSC window (60 cm × 80 cm × 0.8 cm, Figure 7.2) that can generate electricity to power small electronics, such as LED screen, fans, power bank or cellphones, via a USB adaptor. The output working voltage and current are 7.7 V and 55 mA for this device on a sunny

day outdoors. Other applications could include making LSC devices which are sunglasses, included in bus shelters or cellphone cases. The photo- and thermal stability of those LSC devices is also an important aspect that will be investigated in the future.

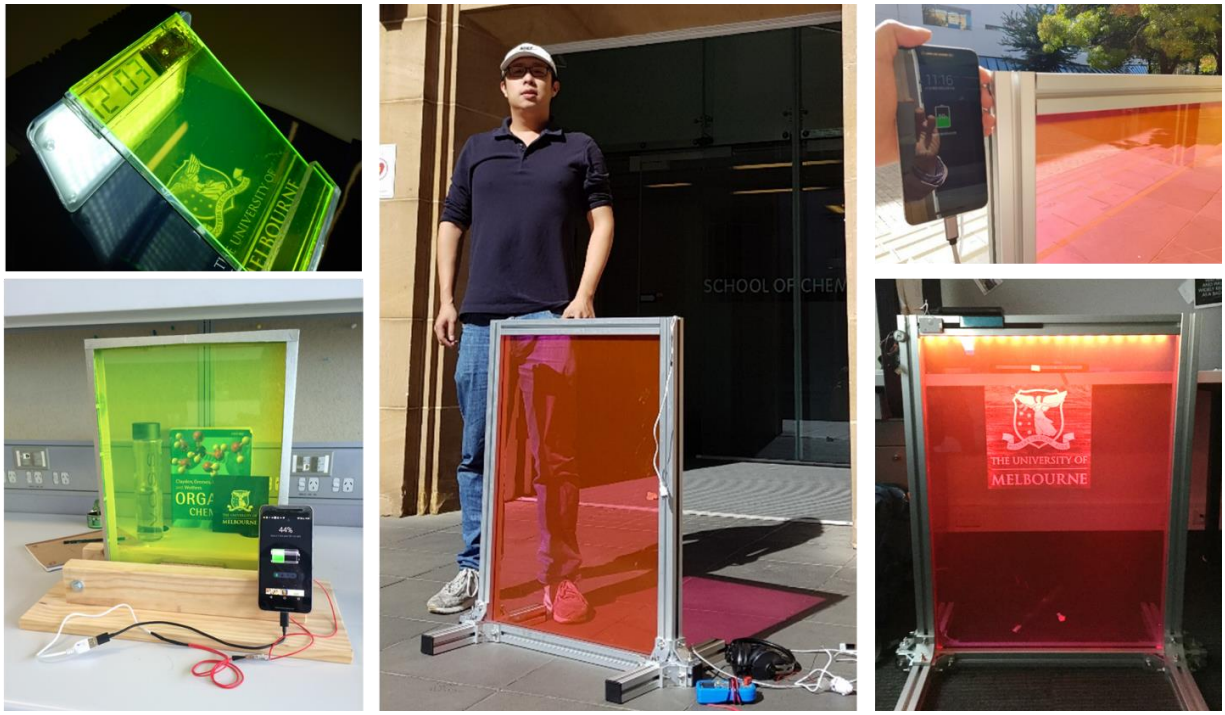

Figure 7.2 The evolution of LSC demonstrators produced by the author.

References:

1. Weber, W. H.; Lambe, J., Luminescent Greenhouse Collector for Solar Radiation. *Appl. Opt.* **1976,** *15* (10), 2299-300.

Appendices:

Co-author authorisation form

THE UNIVERSITY OF MELBOURNE

All co-authors must complete this form. By signing below co-authors agree to the listed publication being included in the student's thesis and that the student contributed greater than 50% of the content of the publication and is the "primary author" ie. the student was responsible primarily for the planning, execution and preparation of the work for publication.

In cases where all members of a large consortium are listed as authors of a publication, only those that actively collaborated with the student on material contained within the thesis should complete this form. This form is to be used in conjunction with the *Declaration for a thesis with publication form.*

Students must submit this form, along with the *Declaration for thesis with publication form*, when the thesis is submitted to the Thesis Examination System: *https://tes.opp.unimelb.edu.au/*

Further information on this policy and the requirements is available at:
gradresearch.unimelb.edu.au/preparing-my-thesis/thesis-with-publication

A. PUBLICATION DETAILS *(to be completed by the student)*

Full title	Aggregation-Induced Emitters in Light Harvesting	
Authors	Bolong Zhang, Can Gao, Nicolau Saker Neto, Wallace W.H. Wong	
Student's contribution (%)	60%	
Journal or book name	Principles and Applications of Aggregation-Induced Emission	
Volume/page numbers	479-504	
Status	☐ Accepted and In-press ☒ Published ☐ In progress	Date accepted/published 10 October 2018

B. CO-AUTHOR'S DECLARATION *(to be completed by the collaborator)*

I authorise the inclusion of this publication in the student's thesis and certify that:

- the declaration made by the student on the *Declaration for a thesis with publication form* correctly reflects the extent of the student's contribution to this work;
- the student contributed greater than 50% of the content of the publication and is the "primary author" ie. the student was responsible primarily for the planning, execution and preparation of the work for publication.

Co-author's name	Co-author's signature	Date *(dd/mm/yy)*
Can Gao	Cangao	18/08/19

Declaration for a thesis with publication

THE UNIVERSITY OF MELBOURNE

PhD and MPhil students may include a primary research publication in their thesis in lieu of a chapter if:

- The student contributed greater than 50% of the content in the publication and is the "primary author", ie. the student was responsible primarily for the planning, execution and preparation of the work for publication
- The student has approval to include the publication in their thesis from their Advisory Committee
- It is a primary publication that reports on original research conducted by the student during their enrolment
- The initial draft of the work was written by the student and any subsequent editing in response to co-authors and editors reviews was performed by the student
- The publication is not subject to any obligations or contractual agreements with a third party that would constrain its inclusion in the thesis

Students must submit this form, along with *Co-author authorisation forms* completed by each co-author, when the thesis is submitted to the Thesis Examination System: *https://tes.app.unimelb.edu.au/*. If you are including multiple publications in your thesis you will need to complete a separate form for each publication. Further information on this policy is available at: *gradresearch.unimelb.edu.au/preparing-my-thesis/thesis-with-publication*

A. PUBLICATION DETAILS *(to be completed by the student)*

Full title	Highly Efficient Luminescent Solar Concentrators by Selective Alignment of Donor-Emitter Fluorophores	
Authors	Bolong Zhang, Can Gao, Hamid Soleimaninejad, Jonathan M White, Trevor A Smith, David J Jones, Kenneth P Ghiggino, Wallace WH Wong	
Student's contribution (%)	60%	
Journal or book name	Chemistry of Materials	
Volume/page numbers	2019, 31, 8, 3001-3008	
Status	☐ Accepted and In press ■ Published ☐ In progress	Date accepted/ published 29-3 月-2019

B. STUDENT'S DECLARATION

I declare that the publication above meets the requirements to be included in the thesis

Student's name	Student's signature	Date *(dd/mm/yy)*
Bolong Zhang	张博隆	23/Jul/2019

C. PRINCIPAL SUPERVISOR'S DECLARATION

I declare that:

- the information above is accurate
- The advisory committee has met and agreed to the inclusion of this publication in the student's thesis
- All of the co-authors of the publication have reviewed the above information and have agreed to its veracity
- 'Co-Author Authorisation' forms for each co-author are attached.

Supervisor's name	Supervisor's signature	Date *(dd/mm/yy)*
Dr. Wallace W.H. Wong		23/Jul/2019

Co-author authorisation form

THE UNIVERSITY OF MELBOURNE

All co-authors must complete this form. By signing below co-authors agree to the listed publication being included in the student's thesis and that the student contributed greater than 50% of the content of the publication and is the "primary author" ie. the student was responsible primarily for the planning, execution and preparation of the work for publication.

In cases where all members of a large consortium are listed as authors of a publication, only those that actively collaborated with the student on material contained within the thesis should complete this form. This form is to be used in conjunction with the *Declaration for a thesis with publication form*.

Students must submit this form, along with the *Declaration for thesis with publication form*, when the thesis is submitted to the Thesis Examination System: *https://tes.app.unimelb.edu.au/*

Further information on this policy and the requirements is available at:
gradresearch.unimelb.edu.au/preparing-my-thesis/thesis-with-publication

A. PUBLICATION DETAILS *(to be completed by the student)*

Full title	Highly Efficient Luminescent Solar Concentrators by Selective Alignment of Donor-Emitter Fluorophores	
Authors	Bolong Zhang, Can Gao, Hamid Soleimaninejad, Jonathan M White, Trevor A Smith, David J Jones, Kenneth P Ghiggino, Wallace WH Wong	
Student's contribution (%)	60%	
Journal or book name	Chemistry of Materials	
Volume/page numbers	2019, 4, 1839-1844	
Status	☐ Accepted and In-press ■ Published ☐ In progress	Date accepted/published: March 29, 2019

B. CO-AUTHOR'S DECLARATION *(to be completed by the collaborator)*

I authorise the inclusion of this publication in the student's thesis and certify that:

- the declaration made by the student on the *Declaration for a thesis with publication form* correctly reflects the extent of the student's contribution to this work;
- the student contributed greater than 50% of the content of the publication and is the "primary author" ie. the student was responsible primarily for the planning, execution and preparation of the work for publication.

Co-author's name	Co-author's signature	Date *(dd/mm/yy)*
Wallace Wong	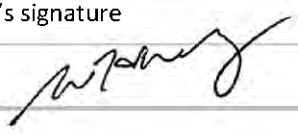	23/07/2019

Co-author authorisation form

THE UNIVERSITY OF MELBOURNE

All co-authors must complete this form. By signing below co-authors agree to the listed publication being included in the student's thesis and that the student contributed greater than 50% of the content of the publication and is the "primary author" ie. the student was responsible primarily for the planning, execution and preparation of the work for publication.

In cases where all members of a large consortium are listed as authors of a publication, only those that actively collaborated with the student on material contained within the thesis should complete this form. This form is to be used in conjunction with the *Declaration for a thesis with publication form*.

Students must submit this form, along with the *Declaration for thesis with publication form*, when the thesis is submitted to the Thesis Examination System: *https://tes.app.unimelb.edu.au/*

Further information on this policy and the requirements is available at:
gradresearch.unimelb.edu.au/preparing-my-thesis/thesis-with-publication

A. PUBLICATION DETAILS *(to be completed by the student)*

Full title	Highly Efficient Luminescent Solar Concentrators by Selective Alignmen	
Authors	Bolong Zhang, Can Gao, Hamid Soleimaninejad, Jonathan M White, Tre	
Student's contribution (%)	60%	
Journal or book name	Chemistry of Materials	
Volume/page numbers	2019, 4, 1839-1844	
Status	☐ Accepted and In-press ■ Published ☐ In progress	Date accepted/published March 29, 2019

B. CO-AUTHOR'S DECLARATION *(to be completed by the collaborator)*

I authorise the inclusion of this publication in the student's thesis and certify that:

- the declaration made by the student on the *Declaration for a thesis with publication form* correctly reflects the extent of the student's contribution to this work;
- the student contributed greater than 50% of the content of the publication and is the "primary author" ie. the student was responsible primarily for the planning, execution and preparation of the work for publication.

Co-author's name	Co-author's signature	Date *(dd/mm/yy)*
Trevor Smith		23/07/19

Co-author authorisation form

THE UNIVERSITY OF MELBOURNE

All co-authors must complete this form. By signing below co-authors agree to the listed publication being included in the student's thesis and that the student contributed greater than 50% of the content of the publication and is the "primary author" ie. the student was responsible primarily for the planning, execution and preparation of the work for publication.

In cases where all members of a large consortium are listed as authors of a publication, only those that actively collaborated with the student on material contained within the thesis should complete this form. This form is to be used in conjunction with the *Declaration for a thesis with publication form*.

Students must submit this form, along with the *Declaration for thesis with publication form*, when the thesis is submitted to the Thesis Examination System: *https://tes.app.unimelb.edu.au/*

Further information on this policy and the requirements is available at:
gradresearch.unimelb.edu.au/preparing-my-thesis/thesis-with-publication

A. PUBLICATION DETAILS *(to be completed by the student)*

Full title	Highly Efficient Luminescent Solar Concentrators by Selective Alignment of Donor-Emitter Fluorophores	
Authors	Bolong Zhang, Can Gao, Hamid Soleimaninejad, Jonathan M White, Trevor A Smith, David J Jones, Kenneth P Ghiggino, Wallace WH Wong	
Student's contribution (%)	60%	
Journal or book name	Chemistry of Materials	
Volume/page numbers	2019, 4, 1839-1844	
Status	☐ Accepted and In-press ■ Published ☐ In progress	Date accepted/published: March 29, 2019

B. CO-AUTHOR'S DECLARATION *(to be completed by the collaborator)*

I authorise the inclusion of this publication in the student's thesis and certify that:

- the declaration made by the student on the *Declaration for a thesis with publication form* correctly reflects the extent of the student's contribution to this work;
- the student contributed greater than 50% of the content of the publication and is the "primary author" ie. the student was responsible primarily for the planning, execution and preparation of the work for publication.

Co-author's name	Co-author's signature	Date *(dd/mm/yy)*
Kenneth P Ghiggino		31/07/19

Co-author authorisation form

THE UNIVERSITY OF MELBOURNE

All co-authors must complete this form. By signing below co-authors agree to the listed publication being included in the student's thesis and that the student contributed greater than 50% of the content of the publication and is the "primary author" ie. the student was responsible primarily for the planning, execution and preparation of the work for publication.

In cases where all members of a large consortium are listed as authors of a publication, only those that actively collaborated with the student on material contained within the thesis should complete this form. This form is to be used in conjunction with the *Declaration for a thesis with publication form*.

Students must submit this form, along with the *Declaration for thesis with publication form*, when the thesis is submitted to the Thesis Examination System: *https://tes.app.unimelb.edu.au/*

Further information on this policy and the requirements is available at:
gradresearch.unimelb.edu.au/preparing-my-thesis/thesis-with-publication

A. PUBLICATION DETAILS *(to be completed by the student)*

Full title	Highly Efficient Luminescent Solar Concentrators by Selective Alignment of Donor-Emitter Fluorophores
Authors	Bolong Zhang, Can Gao, Hamid Soleimaninejad, Jonathan M White, Trevor A Smith, David J Jones, Kenneth P Ghiggino, Wallace WH Wong
Student's contribution (%)	60%
Journal or book name	Chemistry of Materials
Volume/page numbers	2019, 4, 1839-1844
Status	☐ Accepted and In-press ■ Published ☐ In progress
Date accepted/published	March 29, 2019

B. CO-AUTHOR'S DECLARATION *(to be completed by the collaborator)*

I authorise the inclusion of this publication in the student's thesis and certify that:

- the declaration made by the student on the *Declaration for a thesis with publication form* correctly reflects the extent of the student's contribution to this work;
- the student contributed greater than 50% of the content of the publication and is the "primary author" ie. the student was responsible primarily for the planning, execution and preparation of the work for publication.

Co-author's name	Co-author's signature	Date *(dd/mm/yy)*
Jonathan White		25/07/2019

Co-author authorisation form

THE UNIVERSITY OF MELBOURNE

All co-authors must complete this form. By signing below co-authors agree to the listed publication being included in the student's thesis and that the student contributed greater than 50% of the content of the publication and is the "primary author" ie. the student was responsible primarily for the planning, execution and preparation of the work for publication.

In cases where all members of a large consortium are listed as authors of a publication, only those that actively collaborated with the student on material contained within the thesis should complete this form. This form is to be used in conjunction with the *Declaration for a thesis with publication form*.

Students must submit this form, along with the *Declaration for thesis with publication form*, when the thesis is submitted to the Thesis Examination System: *https://tes.app.unimelb.edu.au/*

Further information on this policy and the requirements is available at:
gradresearch.unimelb.edu.au/preparing-my-thesis/thesis-with-publication

A. PUBLICATION DETAILS *(to be completed by the student)*

Full title	Highly Efficient Luminescent Solar Concentrators by Selective Alignment of Donor-Emitter Fluorophores	
Authors	Bolong Zhang, Can Gao, Hamid Soleimaninejad, Jonathan M White, Trevor A Smith, David J Jones, Kenneth P Ghiggino, Wallace WH Wong	
Student's contribution (%)	60%	
Journal or book name	Chemistry of Materials	
Volume/page numbers	2019, 4, 1839-1844	
Status	☐ Accepted and In-press ■ Published ☐ In progress	Date accepted/published: March 29, 2019

B. CO-AUTHOR'S DECLARATION *(to be completed by the collaborator)*

I authorise the inclusion of this publication in the student's thesis and certify that:

- the declaration made by the student on the *Declaration for a thesis with publication form* correctly reflects the extent of the student's contribution to this work;
- the student contributed greater than 50% of the content of the publication and is the "primary author" ie. the student was responsible primarily for the planning, execution and preparation of the work for publication.

Co-author's name	Co-author's signature	Date *(dd/mm/yy)*
Hamid Soleimaninejad	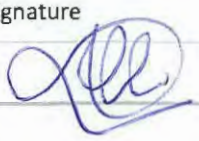	24/7/2019

Co-author authorisation form

THE UNIVERSITY OF MELBOURNE

All co-authors must complete this form. By signing below co-authors agree to the listed publication being included in the student's thesis and that the student contributed greater than 50% of the content of the publication and is the "primary author" ie. the student was responsible primarily for the planning, execution and preparation of the work for publication.

In cases where all members of a large consortium are listed as authors of a publication, only those that actively collaborated with the student on material contained within the thesis should complete this form. This form is to be used in conjunction with the *Declaration for a thesis with publication form*.

Students must submit this form, along with the *Declaration for thesis with publication form*, when the thesis is submitted to the Thesis Examination System: *https://tes.app.unimelb.edu.au/*

Further information on this policy and the requirements is available at:
gradresearch.unimelb.edu.au/preparing-my-thesis/thesis-with-publication

A. PUBLICATION DETAILS *(to be completed by the student)*

Full title	Highly Efficient Luminescent Solar Concentrators by Selective Alignment of Donor-Emitter Fluorophores	
Authors	Bolong Zhang, Can Gao, Hamid Soleimaninejad, Jonathan M White, Trevor A Smith, David J Jones, Kenneth P Ghiggino, Wallace WH Wong	
Student's contribution (%)	60%	
Journal or book name	Chemistry of Materials	
Volume/page numbers	2019, 4, 1839-1844	
Status	☐ Accepted and In-press ☒ Published ☐ In progress	Date accepted/published: March 29, 2019

B. CO-AUTHOR'S DECLARATION *(to be completed by the collaborator)*

I authorise the inclusion of this publication in the student's thesis and certify that:

- the declaration made by the student on the *Declaration for a thesis with publication form* correctly reflects the extent of the student's contribution to this work;
- the student contributed greater than 50% of the content of the publication and is the "primary author" ie. the student was responsible primarily for the planning, execution and preparation of the work for publication.

Co-author's name	Co-author's signature	Date *(dd/mm/yy)*
Dr David Jones	David Jones	31 July 2019

Declaration for a thesis with publication

THE UNIVERSITY OF MELBOURNE

PhD and MPhil students may include a primary research publication in their thesis in lieu of a chapter if:

- The student contributed greater than 50% of the content in the publication and is the "primary author", ie. the student was responsible primarily for the planning, execution and preparation of the work for publication
- The student has approval to include the publication in their thesis from their Advisory Committee
- It is a primary publication that reports on original research conducted by the student during their enrolment
- The initial draft of the work was written by the student and any subsequent editing in response to co-authors and editors reviews was performed by the student
- The publication is not subject to any obligations or contractual agreements with a third party that would constrain its inclusion in the thesis

Students must submit this form, along with *Co-author authorisation forms* completed by each co-author, when the thesis is submitted to the Thesis Examination System: *https://tes.app.unimelb.edu.au/*. If you are including multiple publications in your thesis you will need to complete a separate form for each publication. Further information on this policy is available at: *gradresearch.unimelb.edu.au/preparing-my-thesis/thesis-with-publication*

A. PUBLICATION DETAILS *(to be completed by the student)*

Full title	Highly Fluorescent Molecularly Insulated Perylene Diimides: Effect of Concentration on Photophysical Properties	
Authors	Bolong Zhang, Hamid Soleimaninejad, David J Jones, Jonathan M White, Kenneth P Ghiggino, Trevor A Smith, Wallace WH Wong	
Student's contribution (%)	60%	
Journal or book name	Chemistry of Materials	
Volume/page numbers	2017, 29, 19, 8395-8403	
Status	☐ Accepted and In press ■ Published ☐ In progress	Date accepted/ published 5-9 月-2017

B. STUDENT'S DECLARATION

I declare that the publication above meets the requirements to be included in the thesis

Student's name	Student's signature	Date *(dd/mm/yy)*
Bolong Zhang	张博隆	23/Jul/2019

C. PRINCIPAL SUPERVISOR'S DECLARATION

I declare that:

- the information above is accurate
- The advisory committee has met and agreed to the inclusion of this publication in the student's thesis
- All of the co-authors of the publication have reviewed the above information and have agreed to its veracity
- 'Co-Author Authorisation' forms for each co-author are attached.

Supervisor's name	Supervisor's signature	Date *(dd/mm/yy)*
Dr. Wallace W.H. Wong		23/Jul/2019

Co-author authorisation form

THE UNIVERSITY OF MELBOURNE

All co-authors must complete this form. By signing below co-authors agree to the listed publication being included in the student's thesis and that the student contributed greater than 50% of the content of the publication and is the "primary author" ie. the student was responsible primarily for the planning, execution and preparation of the work for publication.

In cases where all members of a large consortium are listed as authors of a publication, only those that actively collaborated with the student on material contained within the thesis should complete this form. This form is to be used in conjunction with the *Declaration for a thesis with publication form*.

Students must submit this form, along with the *Declaration for thesis with publication form*, when the thesis is submitted to the Thesis Examination System: *https://tes.app.unimelb.edu.au/*

Further information on this policy and the requirements is available at:
gradresearch.unimelb.edu.au/preparing-my-thesis/thesis-with-publication

A. PUBLICATION DETAILS *(to be completed by the student)*

Full title	Highly Fluorescent Molecularly Insulated Perylene Diimides: Effect of Concentration on Photophysical Properties	
Authors	Bolong Zhang, Hamid Soleimaninejad, David J Jones, Jonathan M White, Kenneth P Ghiggino, Trevor A Smith, Wallace WH Wong	
Student's contribution (%)	60%	
Journal or book name	Chemistry of Materials	
Volume/page numbers	2017, 29, 19, 8395-8403	
Status	☐ Accepted and In-press ■ Published ☐ In progress	Date accepted/published 05/Sep/2017

B. CO-AUTHOR'S DECLARATION *(to be completed by the collaborator)*

I authorise the inclusion of this publication in the student's thesis and certify that:

- the declaration made by the student on the *Declaration for a thesis with publication form* correctly reflects the extent of the student's contribution to this work;
- the student contributed greater than 50% of the content of the publication and is the "primary author" ie. the student was responsible primarily for the planning, execution and preparation of the work for publication.

Co-author's name	Co-author's signature	Date *(dd/mm/yy)*
Wallace Wong	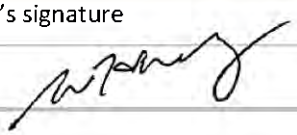	23/07/2019

Co-author authorisation form

THE UNIVERSITY OF MELBOURNE

All co-authors must complete this form. By signing below co-authors agree to the listed publication being included in the student's thesis and that the student contributed greater than 50% of the content of the publication and is the "primary author" ie. the student was responsible primarily for the planning, execution and preparation of the work for publication.

In cases where all members of a large consortium are listed as authors of a publication, only those that actively collaborated with the student on material contained within the thesis should complete this form. This form is to be used in conjunction with the *Declaration for a thesis with publication form*.

Students must submit this form, along with the *Declaration for thesis with publication form*, when the thesis is submitted to the Thesis Examination System: *https://tes.app.unimelb.edu.au/*

Further information on this policy and the requirements is available at:
gradresearch.unimelb.edu.au/preparing-my-thesis/thesis-with-publication

A. PUBLICATION DETAILS *(to be completed by the student)*

Full title	Highly Fluorescent Molecularly Insulated Perylene Diimides: Effect of Co	
Authors	Bolong Zhang, Hamid Soleimaninejad, David J Jones, Jonathan M Whit	
Student's contribution (%)	60%	
Journal or book name	Chemistry of Materials	
Volume/page numbers	2017, 29, 19, 8395-8403	
Status	☐ Accepted and In-press ■ Published ☐ In progress	Date accepted/published 05/Sep/2017

B. CO-AUTHOR'S DECLARATION *(to be completed by the collaborator)*

I authorise the inclusion of this publication in the student's thesis and certify that:

- the declaration made by the student on the *Declaration for a thesis with publication form* correctly reflects the extent of the student's contribution to this work;
- the student contributed greater than 50% of the content of the publication and is the "primary author" ie. the student was responsible primarily for the planning, execution and preparation of the work for publication.

Co-author's name	Co-author's signature	Date *(dd/mm/yy)*
Trevor Smith		23/07/19

Co-author authorisation form

THE UNIVERSITY OF MELBOURNE

All co-authors must complete this form. By signing below co-authors agree to the listed publication being included in the student's thesis and that the student contributed greater than 50% of the content of the publication and is the "primary author" ie. the student was responsible primarily for the planning, execution and preparation of the work for publication.

In cases where all members of a large consortium are listed as authors of a publication, only those that actively collaborated with the student on material contained within the thesis should complete this form. This form is to be used in conjunction with the *Declaration for a thesis with publication form*.

Students must submit this form, along with the *Declaration for thesis with publication form*, when the thesis is submitted to the Thesis Examination System: *https://tes.app.unimelb.edu.au/*

Further information on this policy and the requirements is available at:
gradresearch.unimelb.edu.au/preparing-my-thesis/thesis-with-publication

A. PUBLICATION DETAILS *(to be completed by the student)*

Full title	Highly Fluorescent Molecularly Insulated Perylene Diimides: Effect of Concentration on Photophysical Properties	
Authors	Bolong Zhang, Hamid Soleimaninejad, David J Jones, Jonathan M White, Kenneth P Ghiggino, Trevor A Smith, Wallace WH Wong	
Student's contribution (%)	60%	
Journal or book name	Chemistry of Materials	
Volume/page numbers	2017, 29, 19, 8395-8403	
Status	☐ Accepted and In-press ■ Published ☐ In progress	Date accepted/published 05/Sep/2017

B. CO-AUTHOR'S DECLARATION *(to be completed by the collaborator)*

I authorise the inclusion of this publication in the student's thesis and certify that:

- the declaration made by the student on the *Declaration for a thesis with publication form* correctly reflects the extent of the student's contribution to this work;
- the student contributed greater than 50% of the content of the publication and is the "primary author" ie. the student was responsible primarily for the planning, execution and preparation of the work for publication.

Co-author's name	Co-author's signature	Date *(dd/mm/yy)*
Kenneth P Ghiggino		31/07/19

Co-author authorisation form

THE UNIVERSITY OF MELBOURNE

All co-authors must complete this form. By signing below co-authors agree to the listed publication being included in the student's thesis and that the student contributed greater than 50% of the content of the publication and is the "primary author" ie. the student was responsible primarily for the planning, execution and preparation of the work for publication.

In cases where all members of a large consortium are listed as authors of a publication, only those that actively collaborated with the student on material contained within the thesis should complete this form. This form is to be used in conjunction with the *Declaration for a thesis with publication form*.

Students must submit this form, along with the *Declaration for thesis with publication form*, when the thesis is submitted to the Thesis Examination System: *https://tes.app.unimelb.edu.ou/*

Further information on this policy and the requirements is available at:
gradresearch.unimelb.edu.au/preparing-my-thesis/thesis-with-publication

A. PUBLICATION DETAILS *(to be completed by the student)*

Full title	Highly Fluorescent Molecularly Insulated Perylene Diimides: Effect of Concentration on Photophysical Properties
Authors	Bolong Zhang, Hamid Soleimaninejad, David J Jones, Jonathan M White, Kenneth P Ghiggino, Trevor A Smith, Wallace WH Wong
Student's contribution (%)	60%
Journal or book name	Chemistry of Materials
Volume/page numbers	2017, 29, 19, 8395-8403
Status	☐ Accepted and In-press ☒ Published ☐ In progress
Date accepted/published	05/Sep/2017

B. CO-AUTHOR'S DECLARATION *(to be completed by the collaborator)*

I authorise the inclusion of this publication in the student's thesis and certify that:

- the declaration made by the student on the *Declaration for a thesis with publication form* correctly reflects the extent of the student's contribution to this work;
- the student contributed greater than 50% of the content of the publication and is the "primary author" ie. the student was responsible primarily for the planning, execution and preparation of the work for publication.

Co-author's name	Co-author's signature	Date *(dd/mm/yy)*
Jonathan White		25/07/2019

Co-author authorisation form

THE UNIVERSITY OF MELBOURNE

All co-authors must complete this form. By signing below co-authors agree to the listed publication being included in the student's thesis and that the student contributed greater than 50% of the content of the publication and is the "primary author" ie. the student was responsible primarily for the planning, execution and preparation of the work for publication.

In cases where all members of a large consortium are listed as authors of a publication, only those that actively collaborated with the student on material contained within the thesis should complete this form. This form is to be used in conjunction with the *Declaration for a thesis with publication form*.

Students must submit this form, along with the *Declaration for thesis with publication form*, when the thesis is submitted to the Thesis Examination System: *https://tes.app.unimelb.edu.au/*

Further information on this policy and the requirements is available at:
gradresearch.unimelb.edu.au/preparing-my-thesis/thesis-with-publication

A. PUBLICATION DETAILS *(to be completed by the student)*

Full title	Highly Fluorescent Molecularly Insulated Perylene Diimides: Effect of Concentration on Photophysical Properties	
Authors	Bolong Zhang, Hamid Soleimaninejad, David J Jones, Jonathan M White, Kenneth P Ghiggino, Trevor A Smith, Wallace WH Wong	
Student's contribution (%)	60%	
Journal or book name	Chemistry of Materials	
Volume/page numbers	2017, 29, 19, 8395-8403	
Status	☐ Accepted and In-press ☐ In progress ☐ Published	Date accepted/published 05/Sep/2017

B. CO-AUTHOR'S DECLARATION *(to be completed by the collaborator)*

I authorise the inclusion of this publication in the student's thesis and certify that:

- the declaration made by the student on the *Declaration for a thesis with publication form* correctly reflects the extent of the student's contribution to this work;
- the student contributed greater than 50% of the content of the publication and is the "primary author" ie. the student was responsible primarily for the planning, execution and preparation of the work for publication.

Co-author's name	Co-author's signature	Date *(dd/mm/yy)*
Hamid Soleimaninejad		24/7/2019

Co-author authorisation form

THE UNIVERSITY OF MELBOURNE

All co-authors must complete this form. By signing below co-authors agree to the listed publication being included in the student's thesis and that the student contributed greater than 50% of the content of the publication and is the "primary author" ie. the student was responsible primarily for the planning, execution and preparation of the work for publication.

In cases where all members of a large consortium are listed as authors of a publication, only those that actively collaborated with the student on material contained within the thesis should complete this form. This form is to be used in conjunction with the *Declaration for a thesis with publication form*.

Students must submit this form, along with the *Declaration for thesis with publication form*, when the thesis is submitted to the Thesis Examination System: *https://tes.app.unimelb.edu.au/*

Further information on this policy and the requirements is available at:
gradresearch.unimelb.edu.au/preparing-my-thesis/thesis-with-publication

A. PUBLICATION DETAILS *(to be completed by the student)*

Full title	Highly Fluorescent Molecularly Insulated Perylene Diimides: Effect of Concentration on Photophysical Properties	
Authors	Bolong Zhang, Hamid Soleimaninejad, David J Jones, Jonathan M White, Kenneth P Ghiggino, Trevor A Smith, Wallace WH Wong	
Student's contribution (%)	60%	
Journal or book name	Chemistry of Materials	
Volume/page numbers	2017, 29, 19, 8395-8403	
Status	☐ Accepted and In-press ■ Published ☐ In progress	Date accepted/published 05/Sep/2017

B. CO-AUTHOR'S DECLARATION *(to be completed by the collaborator)*

I authorise the inclusion of this publication in the student's thesis and certify that:

- the declaration made by the student on the *Declaration for a thesis with publication form* correctly reflects the extent of the student's contribution to this work;
- the student contributed greater than 50% of the content of the publication and is the "primary author" ie. the student was responsible primarily for the planning, execution and preparation of the work for publication.

Co-author's name	Co-author's signature	Date *(dd/mm/yy)*
Dr David Jones	David Jones	31 July 2019

Co-author authorisation form

THE UNIVERSITY OF MELBOURNE

All co-authors must complete this form. By signing below co-authors agree to the listed publication being included in the student's thesis and that the student contributed greater than 50% of the content of the publication and is the "primary author" ie. the student was responsible primarily for the planning, execution and preparation of the work for publication.

In cases where all members of a large consortium are listed as authors of a publication, only those that actively collaborated with the student on material contained within the thesis should complete this form. This form is to be used in conjunction with the *Declaration for a thesis with publication form.*

Students must submit this form, along with the *Declaration for thesis with publication form*, when the thesis is submitted to the Thesis Examination System: *https://tes.app.unimelb.edu.au/*

Further information on this policy and the requirements is available at:
gradresearch.unimelb.edu.au/preparing-my-thesis/thesis-with-publication

A. PUBLICATION DETAILS *(to be completed by the student)*

Full title	High-Performance Large-Area Luminescence Solar Concentrator Incorporating a Donor– Emitter Fluorophore System
Authors	Bolong Zhang, Pengjun Zhao, Lachlan J. Wilson, Jegadesan Subbiah, Hanbo Yang, Paul Mulvaney, David J. Jones, Kenneth P. Ghiggino and Wallace W.H. Wong
Student's contribution (%)	60%
Journal or book name	ACS Energy Letters
Volume/page numbers	2019, 4, 1839-1844
Status	☐ Accepted and In-press ■ Published ☐ In progress
Date accepted/published	08/Jul/2019

B. CO-AUTHOR'S DECLARATION *(to be completed by the collaborator)*

I authorise the inclusion of this publication in the student's thesis and certify that:

- the declaration made by the student on the *Declaration for a thesis with publication form* correctly reflects the extent of the student's contribution to this work;
- the student contributed greater than 50% of the content of the publication and is the "primary author" ie. the student was responsible primarily for the planning, execution and preparation of the work for publication.

Co-author's name	Co-author's signature	Date *(dd/mm/yy)*
Hanbo Yang		1/8/2019

Declaration for a thesis with publication

THE UNIVERSITY OF MELBOURNE

PhD and MPhil students may include a primary research publication in their thesis in lieu of a chapter if:

- The student contributed greater than 50% of the content in the publication and is the "primary author", ie. the student was responsible primarily for the planning, execution and preparation of the work for publication
- The student has approval to include the publication in their thesis from their Advisory Committee
- It is a primary publication that reports on original research conducted by the student during their enrolment
- The initial draft of the work was written by the student and any subsequent editing in response to co-authors and editors reviews was performed by the student
- The publication is not subject to any obligations or contractual agreements with a third party that would constrain its inclusion in the thesis

Students must submit this form, along with *Co-author authorisation forms* completed by each co-author, when the thesis is submitted to the Thesis Examination System: *https://tes.app.unimelb.edu.au/*. If you are including multiple publications in your thesis you will need to complete a separate form for each publication. Further information on this policy is available at: *gradresearch.unimelb.edu.au/preparing-my-thesis/thesis-with-publication*

A. PUBLICATION DETAILS *(to be completed by the student)*

Full title	High-Performance Large-Area Luminescence Solar Concentrator Incorporating a Donor– Emitter Fluorophore System	
Authors	Bolong Zhang, Pengjun Zhao, Lachlan J. Wilson, Jegadesan Subbiah, Hanbo Yang, Paul Mulvaney, David J. Jones, Kenneth P. Ghiggino and Wallace W.H. Wong	
Student's contribution (%)	60%	
Journal or book name	ACS Energy Letters	
Volume/page numbers	2019, 4, 1839-1844	
Status	☐ Accepted and In press ■ Published ☐ In progress	Date accepted/ published 8-7 月-2019

B. STUDENT'S DECLARATION

I declare that the publication above meets the requirements to be included in the thesis

Student's name	Student's signature	Date *(dd/mm/yy)*
Bolong Zhang	张博隆	23/Jul/2019

C. PRINCIPAL SUPERVISOR'S DECLARATION

I declare that:

- the information above is accurate
- The advisory committee has met and agreed to the inclusion of this publication in the student's thesis
- All of the co-authors of the publication have reviewed the above information and have agreed to its veracity
- 'Co-Author Authorisation' forms for each co-author are attached.

Supervisor's name	Supervisor's signature	Date *(dd/mm/yy)*
Dr. Wallace W.H. Wong		23/Jul/2019

Co-author authorisation form

THE UNIVERSITY OF MELBOURNE

All co-authors must complete this form. By signing below co-authors agree to the listed publication being included in the student's thesis and that the student contributed greater than 50% of the content of the publication and is the "primary author" ie. the student was responsible primarily for the planning, execution and preparation of the work for publication.

In cases where all members of a large consortium are listed as authors of a publication, only those that actively collaborated with the student on material contained within the thesis should complete this form. This form is to be used in conjunction with the *Declaration for a thesis with publication form*.

Students must submit this form, along with the *Declaration for thesis with publication form*, when the thesis is submitted to the Thesis Examination System: *https://tes.app.unimelb.edu.au/*

Further information on this policy and the requirements is available at:
gradresearch.unimelb.edu.au/preparing-my-thesis/thesis-with-publication

A. PUBLICATION DETAILS *(to be completed by the student)*

Full title	High-Performance Large-Area Luminescence Solar Concentrator Incorporating a Donor– Emitter Fluorophore System	
Authors	Bolong Zhang, Pengjun Zhao, Lachlan J. Wilson, Jegadesan Subbiah, Hanbo Yang, Paul Mulvaney, David J. Jones, Kenneth P. Ghiggino and Wallace WH. Wong	
Student's contribution (%)	60%	
Journal or book name	ACS Energy Letters	
Volume/page numbers	2019, 4, 1839-1844	
Status	☐ Accepted and In-press ■ Published ☐ In progress	Date accepted/published 08/Jul/2019

B. CO-AUTHOR'S DECLARATION *(to be completed by the collaborator)*

I authorise the inclusion of this publication in the student's thesis and certify that:

- the declaration made by the student on the *Declaration for a thesis with publication form* correctly reflects the extent of the student's contribution to this work;
- the student contributed greater than 50% of the content of the publication and is the "primary author" ie. the student was responsible primarily for the planning, execution and preparation of the work for publication.

Co-author's name	Co-author's signature	Date *(dd/mm/yy)*
Wallace Wong	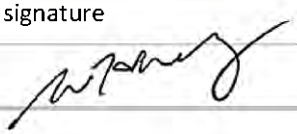	23/07/2019

Co-author authorisation form

THE UNIVERSITY OF MELBOURNE

All co-authors must complete this form. By signing below co-authors agree to the listed publication being included in the student's thesis and that the student contributed greater than 50% of the content of the publication and is the "primary author" ie. the student was responsible primarily for the planning, execution and preparation of the work for publication.

In cases where all members of a large consortium are listed as authors of a publication, only those that actively collaborated with the student on material contained within the thesis should complete this form. This form is to be used in conjunction with the *Declaration for a thesis with publication form*.

Students must submit this form, along with the *Declaration for thesis with publication form*, when the thesis is submitted to the Thesis Examination System: *https://tes.app.unimelb.edu.au/*

Further information on this policy and the requirements is available at:
gradresearch.unimelb.edu.au/preparing-my-thesis/thesis-with-publication

A. PUBLICATION DETAILS *(to be completed by the student)*

Full title	High-Performance Large-Area Luminescence Solar Concentrator Incorporating a Donor– Emitter Fluorophore System	
Authors	Bolong Zhang, Pengjun Zhao, Lachlan J. Wilson, Jegadesan Subbiah, Hanbo Yang, Paul Mulvaney, David J. Jones, Kenneth P. Ghiggino and Wallace WH. Wong	
Student's contribution (%)	60%	
Journal or book name	ACS Energy Letters	
Volume/page numbers	2019, 4, 1839-1844	
Status	☐ Accepted and In-press ■ Published ☐ In progress	Date accepted/published 08/Jul/2019

B. CO-AUTHOR'S DECLARATION *(to be completed by the collaborator)*

I authorise the inclusion of this publication in the student's thesis and certify that:

- the declaration made by the student on the *Declaration for a thesis with publication form* correctly reflects the extent of the student's contribution to this work;
- the student contributed greater than 50% of the content of the publication and is the "primary author" ie. the student was responsible primarily for the planning, execution and preparation of the work for publication.

Co-author's name	Co-author's signature	Date *(dd/mm/yy)*
Pengjun Zhao	Pengjun Zhao	24/07/19

Co-author authorisation form

THE UNIVERSITY OF MELBOURNE

All co-authors must complete this form. By signing below co-authors agree to the listed publication being included in the student's thesis and that the student contributed greater than 50% of the content of the publication and is the "primary author" ie. the student was responsible primarily for the planning, execution and preparation of the work for publication.

In cases where all members of a large consortium are listed as authors of a publication, only those that actively collaborated with the student on material contained within the thesis should complete this form. This form is to be used in conjunction with the *Declaration for a thesis with publication form*.

Students must submit this form, along with the *Declaration for thesis with publication form*, when the thesis is submitted to the Thesis Examination System: *https://tes.app.unimelb.edu.au/*

Further information on this policy and the requirements is available at:
gradresearch.unimelb.edu.au/preparing-my-thesis/thesis-with-publication

A. PUBLICATION DETAILS *(to be completed by the student)*

Full title	High-Performance Large-Area Luminescence Solar Concentrator Incorporating a Donor– Emitter Fluorophore System	
Authors	Bolong Zhang, Pengjun Zhao, Lachlan J. Wilson, Jegadesan Subbiah, Hanbo Yang, Paul Mulvaney, David J. Jones, Kenneth P. Ghiggino and Wallace WH. Wong	
Student's contribution (%)	60%	
Journal or book name	ACS Energy Letters	
Volume/page numbers	2019, 4, 1839-1844	
Status	☐ Accepted and In-press ☐ In progress ☐ Published	Date accepted/published 08/Jul/2019

B. CO-AUTHOR'S DECLARATION *(to be completed by the collaborator)*

I authorise the inclusion of this publication in the student's thesis and certify that:

- the declaration made by the student on the *Declaration for a thesis with publication form* correctly reflects the extent of the student's contribution to this work;
- the student contributed greater than 50% of the content of the publication and is the "primary author" ie. the student was responsible primarily for the planning, execution and preparation of the work for publication.

Co-author's name	Co-author's signature	Date *(dd/mm/yy)*
Lachlan Wilson	Lachlan Wilson	26/07/19

Co-author authorisation form

THE UNIVERSITY OF MELBOURNE

All co-authors must complete this form. By signing below co-authors agree to the listed publication being included in the student's thesis and that the student contributed greater than 50% of the content of the publication and is the "primary author" ie. the student was responsible primarily for the planning, execution and preparation of the work for publication.

In cases where all members of a large consortium are listed as authors of a publication, only those that actively collaborated with the student on material contained within the thesis should complete this form. This form is to be used in conjunction with the *Declaration for a thesis with publication form*.

Students must submit this form, along with the *Declaration for thesis with publication form*, when the thesis is submitted to the Thesis Examination System: *https://tes.app.unimelb.edu.au/*

Further information on this policy and the requirements is available at:
gradresearch.unimelb.edu.au/preparing-my-thesis/thesis-with-publication

A. PUBLICATION DETAILS *(to be completed by the student)*

Full title	High-Performance Large-Area Luminescence Solar Concentrator Incorporating a Donor– Emitter Fluorophore System	
Authors	Bolong Zhang, Pengjun Zhao, Lachlan J. Wilson, Jegadesan Subbiah, Hanbo Yang, Paul Mulvaney, David J. Jones, Kenneth P. Ghiggino and Wallace WH. Wong	
Student's contribution (%)	60%	
Journal or book name	ACS Energy Letters	
Volume/page numbers	2019, 4, 1839-1844	
Status	☐ Accepted and In-press ■ Published ☐ In progress	Date accepted/published 08/Jul/2019

B. CO-AUTHOR'S DECLARATION *(to be completed by the collaborator)*

I authorise the inclusion of this publication in the student's thesis and certify that:

- the declaration made by the student on the *Declaration for a thesis with publication form* correctly reflects the extent of the student's contribution to this work;
- the student contributed greater than 50% of the content of the publication and is the "primary author" ie. the student was responsible primarily for the planning, execution and preparation of the work for publication.

Co-author's name	Co-author's signature	Date *(dd/mm/yy)*
Kenneth P Ghiggino		31/07/19

Co-author authorisation form

THE UNIVERSITY OF MELBOURNE

All co-authors must complete this form. By signing below co-authors agree to the listed publication being included in the student's thesis and that the student contributed greater than 50% of the content of the publication and is the "primary author" ie. the student was responsible primarily for the planning, execution and preparation of the work for publication.

In cases where all members of a large consortium are listed as authors of a publication, only those that actively collaborated with the student on material contained within the thesis should complete this form. This form is to be used in conjunction with the *Declaration for a thesis with publication form*.

Students must submit this form, along with the *Declaration for thesis with publication form*, when the thesis is submitted to the Thesis Examination System: *https://tes.app.unimelb.edu.au/*

Further information on this policy and the requirements is available at:
gradresearch.unimelb.edu.au/preparing-my-thesis/thesis-with-publication

A. PUBLICATION DETAILS *(to be completed by the student)*

Full title	High-Performance Large-Area Luminescence Solar Concentrator Incorporating a Donor– Emitter Fluorophore System	
Authors	Bolong Zhang, Pengjun Zhao, Lachlan J. Wilson, Jegadesan Subbiah, Hanbo Yang, Paul Mulvaney, David J. Jones, Kenneth P. Ghiggino and Wallace WH. Wong	
Student's contribution (%)	60%	
Journal or book name	ACS Energy Letters	
Volume/page numbers	2019, 4, 1839-1844	
Status	☐ Accepted and In-press ■ Published ☐ In progress	Date accepted/published 08/Jul/2019

B. CO-AUTHOR'S DECLARATION *(to be completed by the collaborator)*

I authorise the inclusion of this publication in the student's thesis and certify that:

- the declaration made by the student on the *Declaration for a thesis with publication form* correctly reflects the extent of the student's contribution to this work;
- the student contributed greater than 50% of the content of the publication and is the "primary author" ie. the student was responsible primarily for the planning, execution and preparation of the work for publication.

Co-author's name	Co-author's signature	Date *(dd/mm/yy)*
Jegadesan Subbiah		23/07/2019

Co-author authorisation form

THE UNIVERSITY OF MELBOURNE

All co-authors must complete this form. By signing below co-authors agree to the listed publication being included in the student's thesis and that the student contributed greater than 50% of the content of the publication and is the "primary author" ie. the student was responsible primarily for the planning, execution and preparation of the work for publication.

In cases where all members of a large consortium are listed as authors of a publication, only those that actively collaborated with the student on material contained within the thesis should complete this form. This form is to be used in conjunction with the *Declaration for a thesis with publication form*.

Students must submit this form, along with the *Declaration for thesis with publication form*, when the thesis is submitted to the Thesis Examination System: *https://tes.app.unimelb.edu.au/*

Further information on this policy and the requirements is available at:
gradresearch.unimelb.edu.au/preparing-my-thesis/thesis-with-publication

A. PUBLICATION DETAILS *(to be completed by the student)*

Full title	High-Performance Large-Area Luminescence Solar Concentrator Incorporating a Donor– Emitter Fluorophore System	
Authors	Bolong Zhang, Pengjun Zhao, Lachlan J. Wilson, Jegadesan Subbiah, Hanbo Yang, Paul Mulvaney, David J. Jones, Kenneth P. Ghiggino and Wallace WH. Wong	
Student's contribution (%)	60%	
Journal or book name	ACS Energy Letters	
Volume/page numbers	2019, 4, 1839-1844	
Status	☐ Accepted and In-press ■ Published ☐ In progress	Date accepted/published 08/Jul/2019

B. CO-AUTHOR'S DECLARATION *(to be completed by the collaborator)*

I authorise the inclusion of this publication in the student's thesis and certify that:

- the declaration made by the student on the *Declaration for a thesis with publication form* correctly reflects the extent of the student's contribution to this work;
- the student contributed greater than 50% of the content of the publication and is the "primary author" ie. the student was responsible primarily for the planning, execution and preparation of the work for publication.

Co-author's name	Co-author's signature	Date *(dd/mm/yy)*
Dr David Jones	David Jones	31 July 2019

Declaration for a thesis with publication

THE UNIVERSITY OF MELBOURNE

PhD and MPhil students may include a primary research publication in their thesis in lieu of a chapter if:

- The student contributed greater than 50% of the content in the publication and is the "primary author", ie. the student was responsible primarily for the planning, execution and preparation of the work for publication
- The student has approval to include the publication in their thesis from their Advisory Committee
- It is a primary publication that reports on original research conducted by the student during their enrolment
- The initial draft of the work was written by the student and any subsequent editing in response to co-authors and editors reviews was performed by the student
- The publication is not subject to any obligations or contractual agreements with a third party that would constrain its inclusion in the thesis

Students must submit this form, along with *Co-author authorisation forms* completed by each co-author, when the thesis is submitted to the Thesis Examination System: *https://tes.app.unimelb.edu.au/*. If you are including multiple publications in your thesis you will need to complete a separate form for each publication. Further information on this policy is available at: *gradresearch.unimelb.edu.au/preparing-my-thesis/thesis-with-publication*

A. PUBLICATION DETAILS *(to be completed by the student)*

Full title	Aggregation-induced Emission-mediated Spectral Downconversion in Luminescent Solar Concentrators	
Authors	Bolong Zhang, James L Banal, David J Jones, Ben Zhong Tang, Kenneth P Ghiggino, Wallace WH Wong.	
Student's contribution (%)	60%	
Journal or book name	Material Chemistry Frontiers	
Volume/page numbers	2018, 2, 615-619	
Status	☐ Accepted and In press ■ Published ☐ In progress	Date accepted/ published 24-1 月-2018

B. STUDENT'S DECLARATION

I declare that the publication above meets the requirements to be included in the thesis

Student's name	Student's signature	Date *(dd/mm/yy)*
Bolong Zhang	张博隆	23/Jul/2019

C. PRINCIPAL SUPERVISOR'S DECLARATION

I declare that:

- the information above is accurate
- The advisory committee has met and agreed to the inclusion of this publication in the student's thesis
- All of the co-authors of the publication have reviewed the above information and have agreed to its veracity
- 'Co-Author Authorisation' forms for each co-author are attached.

Supervisor's name	Supervisor's signature	Date *(dd/mm/yy)*
Dr. Wallace W.H. Wong		23/Jul/2019

Co-author authorisation form

THE UNIVERSITY OF MELBOURNE

All co-authors must complete this form. By signing below co-authors agree to the listed publication being included in the student's thesis and that the student contributed greater than 50% of the content of the publication and is the "primary author" ie. the student was responsible primarily for the planning, execution and preparation of the work for publication.

In cases where all members of a large consortium are listed as authors of a publication, only those that actively collaborated with the student on material contained within the thesis should complete this form. This form is to be used in conjunction with the *Declaration for a thesis with publication form*.

Students must submit this form, along with the *Declaration for thesis with publication form*, when the thesis is submitted to the Thesis Examination System: *https://tes.app.unimelb.edu.au/*

Further information on this policy and the requirements is available at:
gradresearch.unimelb.edu.au/preparing-my-thesis/thesis-with-publication

A. PUBLICATION DETAILS *(to be completed by the student)*

Full title	Aggregation-induced Emission-mediated Spectral Downconversion in Luminescent Solar Concentrators	
Authors	Bolong Zhang, James L Banal, David J Jones, Ben Zhong Tang, Kenneth P Ghiggino, Wallace WH Wong.	
Student's contribution (%)	60%	
Journal or book name	Materials Chemistry Frontiers	
Volume/page numbers	2018, 2, 615-619	
Status	☐ Accepted and In-press ■ Published ☐ In progress	Date accepted/published 24/Jan/2018

B. CO-AUTHOR'S DECLARATION *(to be completed by the collaborator)*

I authorise the inclusion of this publication in the student's thesis and certify that:

- the declaration made by the student on the *Declaration for a thesis with publication form* correctly reflects the extent of the student's contribution to this work;
- the student contributed greater than 50% of the content of the publication and is the "primary author" ie. the student was responsible primarily for the planning, execution and preparation of the work for publication.

Co-author's name	Co-author's signature	Date *(dd/mm/yy)*
Kenneth P Ghiggino		31/07/19

Co-author authorisation form

THE UNIVERSITY OF MELBOURNE

All co-authors must complete this form. By signing below co-authors agree to the listed publication being included in the student's thesis and that the student contributed greater than 50% of the content of the publication and is the "primary author" ie. the student was responsible primarily for the planning, execution and preparation of the work for publication.

In cases where all members of a large consortium are listed as authors of a publication, only those that actively collaborated with the student on material contained within the thesis should complete this form. This form is to be used in conjunction with the *Declaration for a thesis with publication form*.

Students must submit this form, along with the *Declaration for thesis with publication form*, when the thesis is submitted to the Thesis Examination System: *https://tes.app.unimelb.edu.au/*

Further information on this policy and the requirements is available at:
gradresearch.unimelb.edu.au/preparing-my-thesis/thesis-with-publication

A. PUBLICATION DETAILS *(to be completed by the student)*

Full title	Aggregation-induced Emission-mediated Spectral Downconversion in Luminescent Solar Concentrators	
Authors	Bolong Zhang, James L Banal, David J Jones, Ben Zhong Tang, Kenneth P Ghiggino, Wallace WH Wong.	
Student's contribution (%)	60%	
Journal or book name	Materials Chemistry Frontiers	
Volume/page numbers	2018, 2, 615-619	
Status	☐ Accepted and In-press ■ Published ☐ In progress	Date accepted/published 24/Jan/2018

B. CO-AUTHOR'S DECLARATION *(to be completed by the collaborator)*

I authorise the inclusion of this publication in the student's thesis and certify that:

- the declaration made by the student on the *Declaration for a thesis with publication form* correctly reflects the extent of the student's contribution to this work;
- the student contributed greater than 50% of the content of the publication and is the "primary author" ie. the student was responsible primarily for the planning, execution and preparation of the work for publication.

Co-author's name	Co-author's signature	Date *(dd/mm/yy)*
James L. Banal	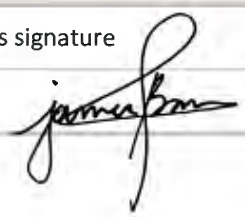	23/07/19

Co-author authorisation form

THE UNIVERSITY OF MELBOURNE

All co-authors must complete this form. By signing below co-authors agree to the listed publication being included in the student's thesis and that the student contributed greater than 50% of the content of the publication and is the "primary author" ie. the student was responsible primarily for the planning, execution and preparation of the work for publication.

In cases where all members of a large consortium are listed as authors of a publication, only those that actively collaborated with the student on material contained within the thesis should complete this form. This form is to be used in conjunction with the *Declaration for a thesis with publication form*.

Students must submit this form, along with the *Declaration for thesis with publication form*, when the thesis is submitted to the Thesis Examination System: *https://tes.app.unimelb.edu.au/*

Further information on this policy and the requirements is available at:
gradresearch.unimelb.edu.au/preparing-my-thesis/thesis-with-publication

A. PUBLICATION DETAILS *(to be completed by the student)*

Full title	Aggregation-induced Emission-mediated Spectral Downconversion in Luminescent Solar Concentrators	
Authors	Bolong Zhang, James L Banal, David J Jones, Ben Zhong Tang, Kenneth P Ghiggino, Wallace WH Wong.	
Student's contribution (%)	60%	
Journal or book name	Materials Chemistry Frontiers	
Volume/page numbers	2018, 2, 615-619	
Status	☐ Accepted and In-press ■ Published ☐ In progress	Date accepted/published 24/Jan/2018

B. CO-AUTHOR'S DECLARATION *(to be completed by the collaborator)*

I authorise the inclusion of this publication in the student's thesis and certify that:

- the declaration made by the student on the *Declaration for a thesis with publication form* correctly reflects the extent of the student's contribution to this work;
- the student contributed greater than 50% of the content of the publication and is the "primary author" ie. the student was responsible primarily for the planning, execution and preparation of the work for publication.

Co-author's name	Co-author's signature	Date *(dd/mm/yy)*
Dr David Jones	David Jones	31 July 2019

Co-author authorisation form

THE UNIVERSITY OF MELBOURNE

All co-authors must complete this form. By signing below co-authors agree to the listed publication being included in the student's thesis and that the student contributed greater than 50% of the content of the publication and is the "primary author" ie. the student was responsible primarily for the planning, execution and preparation of the work for publication.

In cases where all members of a large consortium are listed as authors of a publication, only those that actively collaborated with the student on material contained within the thesis should complete this form. This form is to be used in conjunction with the *Declaration for a thesis with publication form*.

Students must submit this form, along with the *Declaration for thesis with publication form*, when the thesis is submitted to the Thesis Examination System: *https://tes.app.unimelb.edu.au/*

Further information on this policy and the requirements is available at:
gradresearch.unimelb.edu.au/preparing-my-thesis/thesis-with-publication

A. PUBLICATION DETAILS *(to be completed by the student)*

Full title	Aggregation-induced Emission-mediated Spectral Downconversion in Luminescent Solar Concentrators	
Authors	Bolong Zhang, James L Banal, David J Jones, Ben Zhong Tang, Kenneth P Ghiggino, Wallace WH Wong.	
Student's contribution (%)	60%	
Journal or book name	Materials Chemistry Frontiers	
Volume/page numbers	2018, 2, 615-619	
Status	☐ Accepted and In-press ■ Published ☐ In progress	Date accepted/published 24/Jan/2018

B. CO-AUTHOR'S DECLARATION *(to be completed by the collaborator)*

I authorise the inclusion of this publication in the student's thesis and certify that:

- the declaration made by the student on the *Declaration for a thesis with publication form* correctly reflects the extent of the student's contribution to this work;
- the student contributed greater than 50% of the content of the publication and is the "primary author" ie. the student was responsible primarily for the planning, execution and preparation of the work for publication.

Co-author's name	Co-author's signature	Date *(dd/mm/yy)*
Wallace Wong	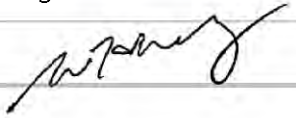	23/07/2019

Declaration for a thesis with publication

THE UNIVERSITY OF MELBOURNE

PhD and MPhil students may include a primary research publication in their thesis in lieu of a chapter if:

- The student contributed greater than 50% of the content in the publication and is the "primary author", ie. the student was responsible primarily for the planning, execution and preparation of the work for publication
- The student has approval to include the publication in their thesis from their Advisory Committee
- It is a primary publication that reports on original research conducted by the student during their enrolment
- The initial draft of the work was written by the student and any subsequent editing in response to co-authors and editors reviews was performed by the student
- The publication is not subject to any obligations or contractual agreements with a third party that would constrain its inclusion in the thesis

Students must submit this form, along with *Co-author authorisation forms* completed by each co-author, when the thesis is submitted to the Thesis Examination System: *https://tes.app.unimelb.edu.au/*. If you are including multiple publications in your thesis you will need to complete a separate form for each publication. Further information on this policy is available at: *gradresearch.unimelb.edu.au/preparing-my-thesis/thesis-with-publication*

A. PUBLICATION DETAILS *(to be completed by the student)*

Full title	Aggregation-Induced Emitters in Light Harvesting	
Authors	Bolong Zhang, Can Gao, Nicolau Saker Neto, Wallace W.H. Wong	
Student's contribution (%)	60%	
Journal or book name	Principles and Applications of Aggregation-Induced Emission	
Volume/page numbers	479-504	
Status	☐ Accepted and In press ■ Published ☐ In progress	Date accepted/ published 10-10 月-2018

B. STUDENT'S DECLARATION

I declare that the publication above meets the requirements to be included in the thesis

Student's name	Student's signature	Date *(dd/mm/yy)*
Bolong Zhang	张博隆	23/Jul/2019

C. PRINCIPAL SUPERVISOR'S DECLARATION

I declare that:

- the information above is accurate
- The advisory committee has met and agreed to the inclusion of this publication in the student's thesis
- All of the co-authors of the publication have reviewed the above information and have agreed to its veracity
- 'Co-Author Authorisation' forms for each co-author are attached.

Supervisor's name	Supervisor's signature	Date *(dd/mm/yy)*
Dr. Wallace W.H. Wong		23/Jul/2019

Co-author authorisation form

THE UNIVERSITY OF MELBOURNE

All co-authors must complete this form. By signing below co-authors agree to the listed publication being included in the student's thesis and that the student contributed greater than 50% of the content of the publication and is the "primary author" ie. the student was responsible primarily for the planning, execution and preparation of the work for publication.

In cases where all members of a large consortium are listed as authors of a publication, only those that actively collaborated with the student on material contained within the thesis should complete this form. This form is to be used in conjunction with the *Declaration for a thesis with publication form*.

Students must submit this form, along with the *Declaration for thesis with publication form*, when the thesis is submitted to the Thesis Examination System: *https://tes.app.unimelb.edu.au/*

Further information on this policy and the requirements is available at:
gradresearch.unimelb.edu.au/preparing-my-thesis/thesis-with-publication

A. PUBLICATION DETAILS *(to be completed by the student)*

Full title	Aggregation-Induced Emitters in Light Harvesting	
Authors	Bolong Zhang, Can Gao, Nicolau Saker Neto, Wallace W.H. Wong	
Student's contribution (%)	60%	
Journal or book name	Principles and Applications of Aggregation-Induced Emission	
Volume/page numbers	479-504	
Status	☐ Accepted and In-press ■ Published ☐ In progress	Date accepted/published 10 October 2018

B. CO-AUTHOR'S DECLARATION *(to be completed by the collaborator)*

I authorise the inclusion of this publication in the student's thesis and certify that:

- the declaration made by the student on the *Declaration for a thesis with publication form* correctly reflects the extent of the student's contribution to this work;
- the student contributed greater than 50% of the content of the publication and is the "primary author" ie. the student was responsible primarily for the planning, execution and preparation of the work for publication.

Co-author's name	Co-author's signature	Date *(dd/mm/yy)*
Wallace Wong		18/08/2019

Co-author authorisation form

THE UNIVERSITY OF MELBOURNE

All co-authors must complete this form. By signing below co-authors agree to the listed publication being included in the student's thesis and that the student contributed greater than 50% of the content of the publication and is the "primary author" ie. the student was responsible primarily for the planning, execution and preparation of the work for publication.

In cases where all members of a large consortium are listed as authors of a publication, only those that actively collaborated with the student on material contained within the thesis should complete this form. This form is to be used in conjunction with the *Declaration for a thesis with publication form*.

Students must submit this form, along with the *Declaration for thesis with publication form*, when the thesis is submitted to the Thesis Examination System: *https://tes.app.unimelb.edu.au/*

Further information on this policy and the requirements is available at:
gradresearch.unimelb.edu.au/preparing-my-thesis/thesis-with-publication

A. PUBLICATION DETAILS *(to be completed by the student)*

Full title	Aggregation-Induced Emitters in Light Harvesting	
Authors	Bolong Zhang, Can Gao, Nicolau Saker Neto, Wallace W.H. Wong	
Student's contribution (%)	60%	
Journal or book name	Principles and Applications of Aggregation-Induced Emission	
Volume/page numbers	479-504	
Status	☐ Accepted and In-press ■ Published ☐ In progress	Date accepted/published 10 October 2018

B. CO-AUTHOR'S DECLARATION *(to be completed by the collaborator)*

I authorise the inclusion of this publication in the student's thesis and certify that:

- the declaration made by the student on the *Declaration for a thesis with publication form* correctly reflects the extent of the student's contribution to this work;
- the student contributed greater than 50% of the content of the publication and is the "primary author" ie. the student was responsible primarily for the planning, execution and preparation of the work for publication.

Co-author's name	Co-author's signature	Date *(dd/mm/yy)*
Nicolau Saker Neto	Nicolau Saker Neto	17/08/16